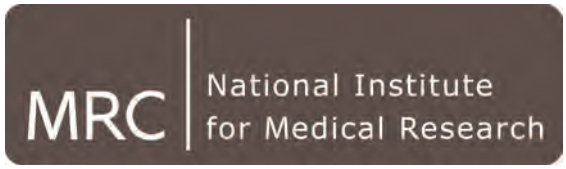

Development of a genetic multicolor cell labeling approach for neural circuit analysis in *Drosophila*

Dafni Hadjieconomou

January 2013

Division of Molecular Neurobiology

MRC National Institute for Medical Research

The Ridgeway

Mill Hill, London

NW7 1AA

U.K.

Department of Cell and Developmental Biology

University College London

A thesis submitted to the University College London

for the degree of Doctor of Philosophy

Declaration of authenticity

This work has been completed in the laboratory of Iris Salecker, in the Division of Molecular Neurobiology at the MRC National Institute for Medical Research. I, Dafni Hadjieconomou, declare that the work presented in this thesis is the result of my own independent work. Any collaborative work or data provided by others have been indicated at respective chapters.

Chapters 3 and 5 include data generated and kindly provided by Shay Rotkopf and Iris Salecker as indicated.

Acknowledgements

I would like to express my utmost gratitude to my supervisor, Iris Salecker, for her valuable guidance and support throughout the entire course of this PhD. Working with you taught me to work with determination and channel my enthusiasm in a productive manner. Thank you for sharing your passion for science and for introducing me to the colourful world of Drosophilists. Finally, I must particularly express my appreciation for you being very understanding when times were difficult, and for your trust in my successful achieving.

Many thanks to my thesis committee, Alex Gould, James Briscoe and Vassilis Pachnis for their quidance during this the course of this PhD.

I am greatly thankful to all my colleagues and friends in the lab. Holger Apitz, Katarina Timofeev, Carole Chotard, Willy Joly, Justine Oyallon, Lauren Ferreira, Emily Richardson, Benjamin Richier, Frederico Rodrigues and Nana Shimosako.

I particularly like to thank Willy Joly for being my teacher in molecular biology techniques and such a fun person to work with. In addition, special thanks to Cyrille Alexandre for all help and fruitful discussions with molecular biology issues that have been raised during the course of this project.

Thanks to the fly community of the NIMR as well as the MNB division. This goes to all past and present members of the Gould, Vincent, Gullemot and Pachnis labs, for providing feedback and technical help and a fantastic working atmosphere. Special, thanks to the CIAL facility and specifically to Donald Bell.

My special thanks go to Holger for being a colleague, a flatmate and a true friend. Your help has been the catalyst for my thesis to progress and eventually close it's cycle. My immense gratitude to Katarina, my PhD buddy for sharing this unique experience with me step by step.

Thanks to Myrto Denaxa, you have been the sunshine in the rainy days of work or life. You sheltered me in your house in difficult times, and you were always there to joke and help. Thank you for your friendship. Thanks to Angeliki Achimastou for being such a generous and patient friend. Thanks Philippos and Maria, Nikos and Gitta for making me laugh out loud.

Thanks to Thomas Brantzos for undertaking the adventure of a scientific life with, me and even though it has been a rocky path remained by my side.

Thanks to Toby Coleman for skipping all the holidays I couldn't make and for always showing me the silver lining of things in life.

Most importantly, thanks to my family. This thesis, I dedicate to you Maria, Andreas and Sophia who make me who I am. Thanks to my parents for supporting my decisions all the way, even if that meant my long absence from our common life. I love you and have no words to express my gratitude towards you. Thanks to my sister, Sofia, that completes and inspires me. You show me how to live the life to its silly and serious moments!

Abstract

The assembly of functional neural circuits during development is pivotal for the ability of the brain to generate complex behaviors. To facilitate the analysis of the underlying molecular mechanisms in *Drosophila*, we have developed a genetic multicolor cell labeling approach called Flybow (FB), which is based on the vertebrate *Brainbow-2* system. FB relies on the stochastic expression of membrane tethered fluorescent proteins (FPs). FP encoding sequences were arranged in pairs within one or two cassettes each flanked by recombination sites. Recombination mediated by an inducible modified Flp/*FRT* system results in both excisions and inversions of the flanked cassettes providing temporal control of FP expression. Moreover, FB employs the GAL4/*UAS* system and hence can be used to investigate distinct cell populations in the tissue of interest.

We have generated three FB variants. FB1.0 consists of one cassette driving expression of either mCherry or V5-tagged Cerulean. FB1.1 contains a second cassette with opposing enhanced green fluorescent protein (EGFP) and mCitrine cDNAs leading to stochastic expression of four FPs. Finally, FB2.0 contains an additional excisable cassette flanked by classical FRT sites to refine transgene expression in specific cell types, in which Gal4 and Flp activities overlap.

The FB approach was validated by investigating neural circuit assembly and connectivity in the visual system. FB makes it possible to visualize dendritic and axonal arborizations of different neuron subtypes and the morphology of glial cells with single cell resolution in one sample. Using live and fixed embryonic tissue, we could show that FB is suitable for studies of this early developmental stage. Additionally, we demonstrated that the approach can be used in non-neural tissues. Finally, combining the mosaic analysis with a repressible cell marker (MARCM) and FB approaches, we demonstrate that our technique is compatible with available *Drosophila* tools for genetic dissection of neural circuit formation.

Table of contents

List of figures and tables

Abbreviations

2D	Two dimensional
3D	Three dimensional
3L	Third instar larval stage
3’	Three prime
5’	Five prime
A	Anterior
aa	Amino acid
AEL	After egg laying
APF	After puparium formation
BSA	Bovine serum albumin
bp	Base pair
CadN	N-Cadherin
cDNA	Complementary deoxyribonucleic acid
CFP	Cyan fluorescent protein
CNS	Central nervous system
DNA	Deoxyribonucleic acid
dNTP	Deoxyribonucleotide triphosphate
EGFP	Enhanced green fluorescent protein
Ey	Eyeless
FB	Flybow
FP	Fluorescent protein
GPC	Glia precursor cell
IPC	Inner proliferation center
IPTG	Isopropyl β-D-1-thiogalactopyranoside
kDa	Kilo-dalton
La	Lamina
Ln	Lamina neurons

M	Medulla layer
MARCM	Mosaic analysis with a repressible cell marker
Me	Medulla
Mn	Medulla neurons
n	Number of independent samples
NB	Neuroblast
O/N	Overnight
OPC	Outer proliferation center
P	Posterior
PBS	Phosphate buffer saline
PBT	PBS/ Triton or Tween
PCR	Polymerase chain reaction
PFA	Paraformaldehyde
PNS	Peripheral nervous system
R-cells	Photoreceptor cells
RNAi	Ribonucleic acid interference
ROI	Region of interest
SD	Standard deviation
SDS	Sodium dodecyl sulphate
TAE	Tris/Acetate/EDTA
UAS	Upstream activating sequence
UK	United Kingdom
USA	United States of America
UTR	Untranslated region
UV	Ultraviolet
VNC	Ventral nerve cord
X-gal	Bromo-chloro-indolyl-galactopyranoside

mm, μm	Millimetre, micrometre
g, mg, μg, ng	Gram, milligram, microgram, nanogram
ml, μl	Millilitre, microlitre
M, mM, μM	Molar, millimolar, micromolar
V	Volt
U	Unit
°C	Celsius degree
’,’’	Minute, second

Chapter 1

Introduction

1.1 Cells in the nervous system entwine to form complex networks

1.1.1 Lessons from history

In 1862, Edwin Smith bought in Luxor what perhaps is the oldest surgical document to date. Within this early manuscript evidence illustrating the importance of brain function can be found portrayed, and date back as far as the 17th century BC in ancient Egypt. During the 5th century BC, Hippocrates describes the brain as the organ that "…exercises the greatest power in the man… The eyes, ears, the tongue and the hands and legs are able to act only because the brain carries the knowledge…". Thus, Hippocrates believed the brain is responsible for our understanding of the world by computation of sensory stimuli from the environment. It is the brain that enables humans to acquire knowledge and eventually wisdom.

"Κατὰ ταῦτα νομίζω τὸν ἐγκέφαλον δύναμιν πλείστην ἔχειν ἐν τῷ ἀνθρώπῳ· …. Οἱ δὲ ὀφθαλμοὶ καὶ τὰ οὔατα καὶ ἡ γλῶσσα καὶ αἱ χεῖρες καὶ οἱ πόδες οἷα ἂν ὁ ἐγκέφαλος γινώσκῃ, τοιαῦτα πρήσσουσι…. Ἐς δὲ τὴν ξύνεσιν ὁ ἐγκέφαλός ἐστιν ὁ διαγγέλλων·…"

Ever since, scientists and philosophers aimed to uncover the ways, by which the nervous system is set up to deliver its complicated functions. Nevertheless, the intricate mechanisms involved in its development and function largely remained *terra incognita* until the groundbreaking work of Santiago Ramón y Cajal in the 19th century. Cajal established that neurons are individual units interrelating in a diverse manner, through specialized contact points to form complex networks, through which electrical signals are transduced. These findings led him to formulate the neuron doctrine and the law of dynamic polarization (Cajal, Nobel Lecture, 1906, reviewed in (Agnati et al., 2007)). These scientific paradigms lasted through time and formed the foundation of modern neuroscience. Importantly, Cajal's work chronologically coincided with developments in other scientific disciplines resulting in an array of tools for investigations of cell anatomy with higher quality. Amongst them were advances in microscopy (immersion lenses), tissue handling (paraffin embedding, and microtome sectioning), fixation

protocols, coloring methods and microphotography (Lopez-Munoz et al., 2006). Key to his important discoveries was the use and improvement of the Golgi method, developed by his scientific adversary Camillo Golgi (Golgi, 1873, reviewed (De Carlos and Borrell, 2007)). This histological staining method was based on randomized silver impregnation of individual neurons that led to sparse cell labeling. Neural cells were labeled in their entirety from the soma to the axonal terminals. Cajal worked tirelessly and produced detailed anatomical maps of neural networks found in different locations of the nervous system from a variety of species.

A lot can be said about Cajal and his contribution to the advances of modern day neuroscience; in direct relevance to this thesis, he has beautifully illustrated the following:

1) The importance of in depth understanding of the anatomical features of the system under investigation and how informative this can prove in understanding some of its functional aspects (Agnati et al., 2007; De Carlos and Borrell, 2007; Lopez-Munoz et al., 2006).

2) The wealth of information retrieved from the study of neural networks of evolutionary "lower" organisms, such as invertebrates, and how this can answer questions about neural network function of "higher" organisms. He has clearly noted that the nervous system is built using three laws of optimization: space optimization, packing compactness and matter optimization. Each element must be the right size, and conduction time must be optimal (Llinas, 2003).

3) The significance in studying neuronal networks, as they develop. This was central to Cajal's understanding of neuron individuality. Moreover, he discovered and named the growth cone, a specialized motile structure at the leading edge of developing axons, and key to the way a neuron is guided to its appropriate target. Noteworthy is the fact that Cajal and Tello had already observed neurons stalling at decision points and change, their growth cone morphology until they remobilize to reach their final targets (de Castro et al., 2007).

4) The importance of incorporating advances in technical methodologies to understand basic biological processes.

1.1.2 Wiring diagrams can be used to decode the complexity of neural network functions

Cajal provided insights on the identification of different cell types, their distribution in different brain structures and their potential ways of communication. Subsequently, the work of the physiologist Charles Scott Sherrington introduced the term "synapse", to describe the manner by which nerve cells connect with each other, and therefore how signals are propagated (Colon-Ramos, 2009). Additionally, owing to Sherrington's work inhibition was established as an active process within the nervous system (Douglas and Martin, 2007). Thus, the efforts of Cajal and Sherrington laid the foundation of what is now known as circuit neuroscience. Circuit neuroscience is by definition the scientific field that aims to fully untangle the computational abilities of neuronal networks, by establishing clear links between network structure and functional output (Yuste, 2008). As elegantly reviewed by Rafael Yuste, one could sum up the efforts of scientists within this field as branching out into four categories:

1) Anatomy of a cell: Identification of different cells within a network remains a major challenge due to their incredible diversity.
2) Anatomy of a circuit: Understanding the way cells within a network interconnect by mapping the synaptic locations used for signal transmission.
3) Computation of a circuit: Generation of anatomical maps can provide information about potential structural connectivity. However, our understanding of the logic of computational routines for information processing remains limited. Thus, comparisons of circuit function**,** from different parts of the nervous system, different individuals and species, are needed to unravel modes of information propagation and processing across different circuits.
4) Exploring the inherent temporal dynamics intrinsic to neural networks: Neural circuits similar to their electrical counterparts linearly transform information from the provided input (i.e. sensory stimulus) to an output (i.e. generation of behavior); or in other words, use predetermined routes on the wiring map. However, it is evident that across species, biological circuits make use of organized spontaneous activity in their function. Consequently, it is important to understand circuit dynamics as a whole.

Information about network anatomy derived from work on these first two categories can be combined and used for assembly of simplified schematic representations of the nervous system. Wiring diagrams are illustrative descriptions of connections between elements within a complex system (Erickson, 2000). They have been predominately used to describe electrical circuits and thus suffice for the description of neural networks, which in essence constitute biological paradigms of electrical systems. Using these diagrams, predictions can be made for the flow and importantly the output of signals manifesting as specific tasks of the system under examination (i.e. light ON in an electronic device or extension of the leg flexor muscle) (Figure 1). To draw such diagrams information on different levels is required, including the identification of the elements comprising the system followed by representation of the modes, in which they interconnect. Consequently, for the generation of neural network diagrams, detailed descriptions of individual cell types as well as their connection modes (axon: soma, axon: axon, axon: dendrite) are central (DeFelipe, 2010).

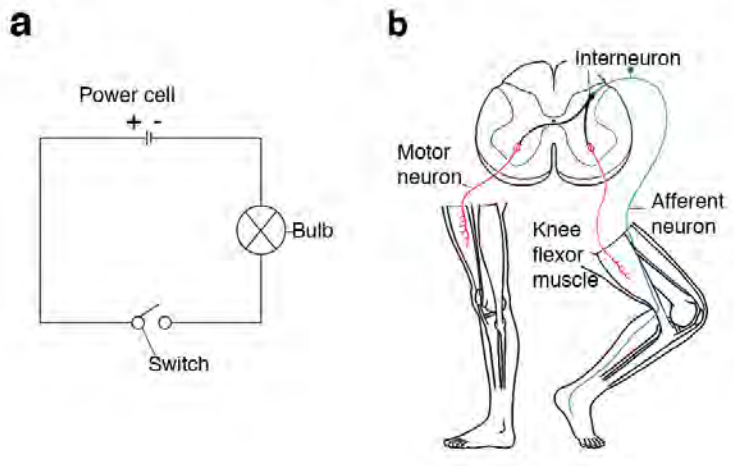

Figure 1. Two simple wiring diagrams.
Common representation of a switch-regulated light bulb electrical circuit (a). Schematic representation of the simple flexor reflex and crossed extensor reflex (b). Adapted from Gray's Anatomy 39e.

1.1.3 The concept of the "connectome"

Envisioning the brain (human and otherwise) as the assemblage of interrelating neuronal networks has in recent years given rise to the concept of "connectomics" (Sporns et al., 2005). Under this term, one can summarize the joined effort of researchers to generate a comprehensive wiring diagram of the nervous system, highlighting its individual cell types and the way they connect to each other. Different levels of studying structural connectivity exist and therefore different versions of wiring diagrams can be generated. As introduced by Olaf Sporns, three scales can be used for structural description of a connectome, and specifically the human connectome; namely the micro-, meso- and macroscale (DeFelipe, 2010; Sporns, 2011; Sporns et al., 2005). Microscale approaches aim to identify single neurons and locations of their synapses and thus make use of light, super-resolution and electron microscopy. Studies at the mesoscale level have the aim to map circuitry within primary processing units, such as columns, and use microscopy together with histological sectioning. Finally, macroscale studies have the goal to uncover connections between discrete parts of the brain and use lower resolution imaging methodologies such as post mortem tracing (using carbocyanine dye staining) or non invasive approaches including diffusion tensor imaging (DTI) or functional magnetic resonance imaging (fMRI). These attempts generate large-scale data sets, requiring thorough computer based analysis, with the goal to piece together parts of the nervous system jigsaw, specifically in the case of higher organisms with larger and more complicated brains (Kaiser, 2011). It thus becomes apparent that information at all these three levels is required for the generation of complete connectome atlases and that the undertaking of the task to "solve" the human connectome could only be achieved relying on scientific cooperation similar to the one shown in the case of the human genome project (Lichtman and Sanes, 2008). Mapping entire genome sequences at base pair resolution with the aim to understand the function of individual genes serves as a direct parallel to connectomic approaches (Lichtman and Sanes, 2008; Sporns, 2011). Nevertheless, additional challenges exist when producing connectomic maps. Neural maps are in contrast to their genomic counterparts structurally plastic. They undergo constant

modifications over time; such as maturation of the circuit from the developing to the adult state, experience induced changes, including memory formation, and degeneration through injury or ageing (Meunier et al., 2009; Sporns, 2011). In addition, interindividual neural circuit variability is present to some extent, both macroscopically (amongst brain areas) and at the microscopic level (main processes of neurons) (Hall and Russell, 1991; Lichtman and Sanes, 2008; Sporns, 2011). Interestingly, this variability can be detected even when comparing individuals with isogenic backgrounds. Studies in the visual system of the crustacean, *Daphnia magna* (Macagno et al., 1973), and the posterior nervous system of the nematode, *Caenorhabditis elegans* (Hall and Russell, 1991), postulate that this could be attributed to developmental noise. Noteworthy is that cell body position and synaptic pairing generally appears to be hardwired; nevertheless, branching patterns are significantly divergent. Concomitantly, the numbers of synapses forming are variable and the strength of interaction significantly different. Thus, it is obvious that different types of connectome maps could arise depending on the individual considered. Finally, a recent report in the mouse olfactory system has shown that neural networks themselves contribute to the generation of diversity within anatomically similar neurons (Angelo et al., 2012; Urban and Tripathy, 2012). Taking all of the above into consideration, the need for wiring diagrams of neural networks that can lead to a better understanding of their function becomes imperative. These could catalyze our better understanding of behavior, since stereotypic behaviors or their alterations, can be considered as finely orchestrated events occurring either simultaneously or sequentially within different parts of such diagrams.

As nicely exemplified by the work in *Daphnia magna,* and *Caenorhadbitis elegans* the model organism, for which a complete connectome exists (White et al., 1986), studies using less complex invertebrate systems are highly informative. In this case, 302 neurons of the worm nervous system are connected via approximately 7000 synapses (Varshney et al., 2011; White et al., 1986). Thus, a different approach to solving the intricate connectomes is trying to focus on mapping invertebrate networks (Kohl and Jefferis, 2011; Lichtman and Sanes, 2008). Experience acquired in this manner (choice of methodology and development of

neuroinformatic tools) could tremendously accelerate the pace, by which the more complex connectomes can be mapped. Finally, a new way to achieve map connectivity information in high throughput fashion has been recently proposed (Zador et al., 2012). This method makes use of advances in the field of DNA sequencing, as well as the currently available tools for studying neural circuitry at the single cell level. Thus, initially individual neurons must be tagged with unique sequences of nucleotide "barcodes" that confer identity. Next, to uncover synaptic pairs, viruses engineered to carry genetic material transsynaptically must be employed (Ekstrand et al., 2008; Wickersham et al., 2007). These need to include another unique bar code that will subsequently be integrated into the genome of the recipient cell; thus marking synaptic connections. Finally, following high throughput DNA sequencing, wiring maps of connectivity between interrelated neurons can be assembled. While it remains unknown if this approach will be applied, it promises a new way of thinking about solving connectivity that importantly overcomes the disadvantages of similar attempts that employ microscopy.

1.1.4 Generation of network components during development

Processes achieving high reproducibility amongst individuals (Sanchez-Soriano et al., 2007) regulate wiring in both vertebrates and invertebrates. Although the precise mechanisms differ amongst species, the key steps appear to be conserved. Network formation includes distinct interconnected processes. First, different cell types involved in circuit assembly are generated through processes grouped as neurogenesis and gliogenesis; for neuron and glial cell types, respectively (Brand and Livesey, 2011; Chotard and Salecker, 2007; Egger et al., 2008; Mao et al., 2012). Next, different cell types are specified and differentiate largely as a result of interactions amongst complex transcription gene regulatory networks (Davidson and Levine, 2008; Guillemot, 2007; Jessell, 2000). Subsequently, neurons extend their axons in a process called axon outgrowth, and navigate through stereotypic pathways to locate and specifically select their targets areas. Next, having identified their respective targets, neurons form synapses at specific target cellular subdomains (Tessier-Lavigne and Goodman, 1996). These steps are employed repeatedly across the nervous system and give rise to organizing units with

characteristic structures at the macroscopic level, such as glomeruli in the olfactory system or columns in the visual system. These very different structures constitute examples of distinct neural circuit organization and are divided in two main categories, discrete and topographic map respectively (Luo and Flanagan, 2007). Moreover, they are further organized into layers, within which synaptic contacts occur and thus forming a striated neuropil that allows parallel information processing. Individual cells within a circuit employ autonomous developmental programs dictated by the tight regulation of molecular mechanisms underlying each of the aforementioned steps. Consequently, different questions about cell or circuit intrinsic mechanisms need to be addressed to further understand the basic principle of neural circuit function that is inter-neuronal communication. Importantly synapse formation requires accurate matching of the pre- and postsynaptic neurons; so how do these neurons find each other, given the variety of options available?

Neurons and glia actively interact with their extracellular environment and are guided to their appropriate locations within the circuit. Neurons utilize their unique structure, the growth cone, identified by Cajal, to scan through their extracellular environment for cues (Dent et al., 2011; Tessier-Lavigne and Goodman, 1996) (Figure 2). Thus, they precisely maneuver the outgrowing axon towards the appropriate trajectories and turn at correct decision points. Growth cones contain different cytoskeletal elements including actin filaments and microtubules that polymerize or dissociate to achieve tremendously dynamic motility (Dent and Gertler, 2003). Based on its cytoskeletal element composition, the growth cone can be divided into three areas: namely the peripheral, transition and the central domains. In the peripheral zone, actin filaments form projections extending from the cell surface. These resemble wand-like structures and are called filopodia. Additionally, sheet-like configurations, named lamellipodia, extend between filopodia in the same region containing criss-crossing actin bundles (Dent et al., 2011; Lowery and Van Vactor, 2009). Microtubules reside mostly in the central zone, where they form stable bundles extending into the axon shaft. Some microtubules can be also observed alongside filopodia in the peripheral region. Finally, the transition zone, which resides between the other

two domains, consists of filamentous actin arcs oriented perpendicular to the filopodia axis. The underlying structural variability within these three regions owes to the discrete functional requirements of each respective domain in propagating axon outgrowth. These domains are only temporary and they evolve from one to the other as axons travel to their target areas (Dent et al., 2011). The process of axon outgrowth can be subdivided in four key steps: substrate recognition, protrusion, engorgement and finally consolidation (Dent and Gertler, 2003; Lowery and Van Vactor, 2009) of the growth cone. Constant interaction of the growth cone with substrates in their environment provides the signals to these cytoskeletal elements and they in turn provide the mechanical forces for the axon to grow along its correct trajectory. Intricate signaling pathways that include major cytoskeletal regulators, lie downstream of the activation of surface receptors in the growth cone (Huber et al., 2003; Killeen and Sybingco, 2008).

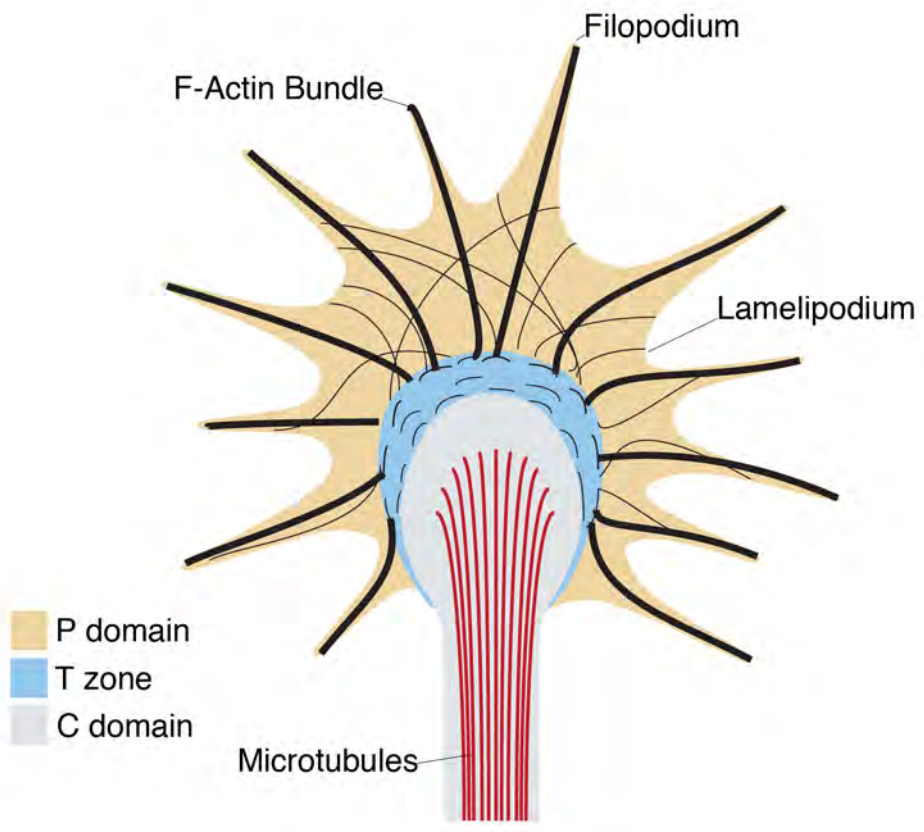

Figure 2. Schematic representation of the growth cone.
The growth cone can be subdivided into three domains: peripheral (P), transition (T), and central domains. Adapted from (Lowery and Van Vactor, 2009).

Growth cones receive a series of attractive and repulsive cues during the different stages of axon outgrowth, pathfinding and targeting. Therefore guidance forces determine the path, in which axons grow to find their targets. The numerous neurons within a network, including comparatively simpler invertebrate neural circuits, establish high numbers of synaptic connections with their targets. Therefore, it becomes evident that an outgrowing axon is faced with a daunting task, when making trajectory choices from its place of birth to its distant target area. However, developmental mechanisms are in place to ensure that axon targeting proceeds accurately and leads to highly stereotyped choices, leading to correct synapse formation between afferent axons and specific target neurons. First, pioneer neurons navigate through the emerging embryonic neural tissue and pattern it, by designating the first axonal trajectories (Bate, 1976b). Next, newly generated neurons, "followers", extend their axons and fasciculate together with pioneer axons and form mature bundles. Pioneer neurons comprise a unique cell population as they can play roles in the correct pathfinding process of the follower neurons by providing local guidance cues (Hidalgo and Brand, 1997). Finally, follower axons reach their respective targets and further follow their autonomous fates (Tessier-Lavigne and Goodman, 1996).

Axon trajectories that can be several soma diameters long are in essence segmented into smaller distances (Tessier-Lavigne and Goodman, 1996). In this manner, axon guidance decisions are subdivided into several steps. Growth cones rely on diffusible molecules, often provided by cells that serve as guidepost cells or intermediate targets; these are positioned in designated areas within the tissue and mediate distinct steps of targeting (Bate, 1976a; Chao et al., 2009; Dickson, 2002; Tessier-Lavigne and Goodman, 1996). As proposed by Cajal, optimization of packing represents another shaping force employed within the developing nervous system. Such an example is highlighted by the recent study in the vertebrate brain, neurites are also organized in grid-like structures formed by parallel sheaths of axons. In this way, the axon trajectory choices are restricted to only four orthogonal routes (Wedeen et al., 2012).

Guidance cues can be attractive or repulsive and can act either at short or long range (Dickson, 2002; Tessier-Lavigne and Goodman, 1996). Short-range guidance systems are employed when the molecule that mediates guidance, acts in close proximity to its release source. Conversely, concomitant to Langley's postulation of chemical relations and Sperry's chemoaffinity hypothesis (Sperry, 1963); long-range mechanisms can be mediated leading to the activation of receptors that are located distant to the source of the guidance cue. Additionally, contact-mediated guidance systems such as cell surface and extra cellular matrix molecules are in place to further guide axons towards or away from guidepost cells.

Importantly, while some molecules can be classified as purely attractive or repulsive, several molecules have been shown to mediate both attraction and repulsion. Studies focusing on the processes involved in midline guidance in the central nervous system have been crucial to our current understanding of guidance systems. Different mechanisms mediating axon guidance representing all these categories have been identified and are found to be highly evolutionary conserved. These molecules are now considered classical guidance systems and include four main families, the ephrins, netrins, semaphorins and slits (Dickson, 2002; Huberman et al., 2010).

1.1.5 Netrins guide axons by both attraction and repulsion

Netrins constitute a family of predominantly secreted proteins, with an established function in axon guidance, whose role is highly conserved across species (Dickson, 2002; Huberman et al., 2010; Lai Wing Sun et al., 2011; Tessier-Lavigne and Goodman, 1996). They have been shown to play a pivotal role in guiding axons at the midline. The sole *C. elegans* family member, *uncoordinated-6* (Unc-6), was discovered in a randomized mutagenesis screen aiming to identify genes that interfere with the smooth sinuous movement of worms on agar plates, using phenotypic analyses (Brenner, 1974). Moreover, this analysis of approximately 400 mutant phenotypes led to the discovery of *unc-40* and *unc-5*. Following their original discovery, these together with *unc-6*, were shown to control ventral-dorsal axon guidance at the worm midline

(Hedgecock et al., 1990; Ishii et al., 1992). In this paradigm, Unc-6 provides positional information by creating a concentration gradient (Wadsworth et al., 2002) (Ogura et al., 2012).

These proteins have been subsequently studied in vertebrates, where highly insightful findings were gained concerning their discrete functions. The first vertebrate orthologues were discovered in the chick in experiments that used spinal cord explants. Commissural axons, included in this tissue preparation, showed extensive outgrowth in the presence of floor plate cells (Serafini et al., 1994). Next, screening for factors that could mediate the attractive force responsible for this behavior, uncovered a previously unidentified guidance molecule. This protein was named Netrin using the Sanskrit prefix "netr" that means "the one who guides" (Kennedy et al., 1994; Serafini et al., 1994). Two homologues were identified in the chick and thus named Netrin-1 and Netrin-2, respectively (Serafini et al., 1994). Subsequently, different studies have identified Netrin-1 orthologues in all vertebrate model organisms (mouse, rat, zebrafish, frog) as well as humans (Lai Wing Sun et al., 2011). Netrin-2 appears less conserved with a single orthologue recovered in zebrafish (Park et al., 2005). Importantly, Netrins in all bilaterally symmetrical animals mediate conserved roles in axon guidance of the developing nervous system. In mammals, both secreted and membrane tethered Netrins have been discovered (Lai Wing Sun et al., 2011). Secreted Netrins functions in different parts of the nervous system during development and in the adult. In addition, they have been reported to have roles in tissues beyond the nervous system, such as the developing internal organs and the mammary gland (Lai Wing Sun et al., 2011). In *Drosophila*, two members Netrin-A and Netrin-B were identified (Harris et al., 1996; Mitchell et al., 1996) to play roles in the guidance of axons at the ventral nerve cord midline. These and subsequent studies in the fly have elucidated modes, by which Netrins function and thus have additionally provided substantial insights on the mechanisms via which these molecules work to mediate guidance.

Netrins were initially identified for their ability to elicit attractive responses of growth cones, but have later been shown to also mediate repulsion depending on the receptor they interact with. In *C. elegans* Unc-40 constitutes the attractive receptor for Unc-6 (Chan et al., 1996). Orthologues of this receptor have been discovered in vertebrates, Deleted in Colorectal

Cancer (DCC), and in *Drosophila*, Frazzled (Fra) (Fazeli et al., 1997; Keino-Masu et al., 1996; Kolodziej et al., 1996). Unc-5 and its orthologues in both *Drosophila* and vertebrates mediate repulsion when activated by Netrins (Keleman and Dickson, 2001; Leonardo et al., 1997; Leung-Hagesteijn et al., 1992; Wadsworth et al., 1996). The Down syndrome cell adhesion molecule (Dscam) protein was originally discovered as a potential gene linked to Down syndrome (Yamakawa et al., 1998), and more recently has been reported to function as an attractive Netrin receptor (Andrews et al., 2008). Dscam orthologues play central roles in the developing spinal cords of vertebrates, as well as at the *Drosophila* CNS midline (Andrews et al., 2008; Liu et al., 2009; Ly et al., 2008).

Netrin proteins are composed of approximately 600 amino acids (aa). They are related to laminins due to their domain similarity (Harris et al., 1996; Ishii et al., 1992; Kennedy et al., 1994; Lai Wing Sun et al., 2011; Serafini et al., 1994). They consist of a laminin-like domain, three epidermal growth factor (EGF) domains (Yurchenco and Wadsworth, 2004), and a C-terminal domain (domain C). Distinct laminin-like domains have been shown to mediate receptor binding for both DCC and Unc-5 receptors (Geisbrecht et al., 2003; Kruger et al., 2004; Lim and Wadsworth, 2002). Based on the observation, that they can mediate guidance at long-range, they have been typically considered as diffusible molecules. Netrins have a high affinity for cell membranes and the extra-cellular matrix, in particular heparan sulphate proteoglycans (HSPGs) and integrins, and a potential Netrin gradient has been suggested but not yet visualized *in vivo*. In the *Drosophila* embryonic central nervous system, Frazzled has been shown to control Netrin distribution and localization (Hiramoto et al., 2000). Membrane-tethered NetB can substitute endogenous Netrin for the guidance of commissural axons at the midline (Brankatschk and Dickson, 2006), indicating that Netrins can act as short-range cues in some systems.

Both Frazzled and Unc-5 belong to the immunoglobulin (Ig) superfamily. Fra consists of four Ig domains and six fibronectin type III (FN3) domains, followed by a single transmembrane domain and three conserved intracellular domains (P1-P3). Unc-5 has two Ig domains, two thrombospondin type I domains, a single TM domain, followed by an intracellular

domain consisting of a ZU-5 domain, a DCC-binding (DB) motif, and a death domain (DD). Netrin-1 has been shown to interact with discrete subdomains of DCC and Unc-5. It binds the fourth and fifth FN3 domain of DCC, and both Ig domains are required for binding to Unc-5. How do the different structures of the two Netrins receptors translate into their opposing effects on the response of the growth cone? One explanation is that the differential intracellular responses might solely be due to the differential composition of their intracellular domains. This is supported by experiments testing growth cone responses to Netrins when chimeric receptor proteins are expressed in which the extra- and intracellular domains of DCC and Unc-5 have been swapped (Hong et al., 1999; Keleman and Dickson, 2001). In addition, the differences in their extracellular domains may point to possible differential recruitments of co-receptors after binding to Netrins and consequently to either attractive or repulsive responses. Notably, Unc-5 repulsion depends in some instances on the co-expression of DCC (Hong et al., 1999; Keleman and Dickson, 2001).

Netrins have been also have been implicated in processes in addition to axon guidance within the nervous system, such as dendritic growth (Brierley et al., 2009), neuron precursor cell and glial cell migration, axon branching and synapse formation. Finally, Netrins have been shown to mediate migration and cell-cell adhesion; for instance in the developing heart and lung, they have been reported to participate in mechanisms resulting in blood vessel formation (Adams and Eichmann, 2010) and lung branching (Liu et al., 2004).

1.1.6 The Robo/Slit system prevents ipsilateral axons from crossing and commissural axons from re-crossing the midline

The Robo/Slit pathway is known as a key player in the decision of an axon on whether to cross or not the midline of the *Drosophila* embryo (Dickson, 2002). A conserved function of Robo/Slit signaling in vertebrate midline commissural axonal guidance has been described (Long et al., 2004). *slit* mutants have been originally identified in the eminent mutagenesis screens for *Drosophila* embryonic pattern formation (Anderson and Nusslein-Volhard, 1984). In *slit* mutants, CNS axons enter the midline and remain there, thus leading to a fusion of

connectives and the loss of commissures. Slit is expressed and secreted by midline glial cells (Brose et al., 1999; Rothberg et al., 1988) and it acts as a short-range repellent for growth cones at the midline (Battye et al., 1999; Brose et al., 1999; Kidd et al., 1999). Roundabout (Robo) is a guidance molecule of the immunoglobulin superfamily that has been identified in a screen for genes required for the crossing of axons at the embryonic midline (Seeger et al. 1993; Kidd et al., 1998). Subsequently, Robo has been found to be the receptor that mediates short-range repulsion by Slit (Brose et al., 1999; Kidd et al., 1999).

Axon crossing is achieved by intracellular downregulation of Robo by Commissureless (Comm) in commissural growth cones. Comm is a short transmembrane protein that is expressed in commissural neurons and midline cells. Two distinct models have been reported for the regulation of Robo surface levels by Comm in commissural neurons (Georgiou and Tear, 2002, 2003; Keleman et al., 2002; Keleman et al., 2005; Myat et al., 2002). After crossing the midline commissural axons express high levels of Robo in order to prevent recrossing. Ipsilateral axons express high levels of Robo from the outset (Kidd et al., 1998). Interestingly, Fra has been suggested to activate *comm* transcription (Yang et al., 2009), linking Netrin-mediated attraction to the suppression of Slit-mediated repulsion of commissural axons. In *Drosophila*, two additional Slit receptors have been identified, Robo2 and Robo3 (Rajagopalan et al., 2000a; Schimmelpfeng et al., 2001; Simpson et al., 2000b). Robo2 cooperates with Robo to control midline crossing (Rajagopalan et al., 2000a; Simpson et al., 2000b). Additionally, the three Robo proteins function in the patterning of longitudinal axon tracts in response to a long-range Slit signal (Rajagopalan et al., 2000b; Simpson et al., 2000a). In this case, differential expression of Robo receptors provides a combinatorial code for axons, which longitudinal pathway to choose. Interestingly, the lateral positioning depends solely on the differential expression levels and not on structural differences between the Robo receptors, as shown in an impressive set of *robo* swap experiments (Spitzweck et al., 2010). In contrast, structural features of Robo and Robo2 account for their role in commissure formation, revealing that while Robo mediates repulsion, Robo2 promotes axons crossing (Spitzweck et al., 2010). Aside from its function in axonal guidance the Robo/Slit pathway has also been shown to be involved in

guidance of dendrites (Kim and Chiba, 2004) and in migration of sensory neurons and support cells in the *Drosophila* PNS (Kraut and Zinn, 2004). In tissues other than the CNS, Slit has not only been shown to act as a repellent but also as an attractive signal. Robo2 mediates an attractive response of trachae to Slit (Englund et al., 2002), while both Robo and Robo2 mediate chemoattraction of muscles to Slit-expressing epidermal attachment sites (Kramer et al., 2001).

In *Drosophila*, postembryonic functions of the Robo/Slit pathway have been described in the development of the giant fiber system (Godenschwege et al., 2002) and of the olfactory system (Jhaveri et al., 2004). Recently, it has been shown that the Robo/Slit pathway acts during *Drosophila* visual system development: Robo and Slit proteins are required for the maintenance of the compartment boundary between lamina and lobula cortex (Tayler, et al., 2004).

Additional guidance systems have been identified to play crucial roles in discrete steps of neural circuit formation in different model organisms. Amongst them two guidance mechanisms that can be categorized as classical, the Eph/Ephrin and Semaphorin guidance systems.

1.1.7 Ephrin and Semaphorin guidance system provide repulsive guidance cues in the midline

Eph receptors constitute the largest family of receptor tyrosine kinases, with 14 distinct members in vertebrates (Klein, 2012; Triplett and Feldheim, 2012). Eph receptors are subdivided into two classes, namely A and B. Similarly, the ephrin ligands are also categorized as members of A or B classes. Eight ephrins exist in vertebrates, members of the class A are linked to the membrane via a glycophosphatidylinositol (GPI) anchor, whereas class B Ephrins are transmembrane (TM) proteins. *In vitro* assays indicate that all class A Eph receptors can bind to all class A ephrins, and all class B Eph receptors bind all class B ephrins, with little interactions between the different classes. Noteworthy for Eph/ephrin signaling is that the Eph receptor and ephrin ligands are membrane-anchored thus signaling is specifically localized to the site of cell-cell contact. In addition, signaling is induced in both Eph and ephrin expressing cells and the signal therefore bidirectional.

Eph/ephrins have been implicated in controlling various developmental processes in the formation of different tissues, and have been intensely studied in the context of neural circuit formation. In this system, Eph/ephrin singaling has been shown to mediate both axon attraction and repulsion. Especially the role of Eph/ephrin signaling in topographic map formation in the tectum of lower vertebrates has received considerable attention. In this case, Eph and ephrins are expressed in a complementary gradient fashion, in the retina and the tectum, establishing a cartesian map paradigm for the maintenance of retinotopy (Triplett and Feldheim, 2012). Furthermore, Eph/ephrin signaling is required for cell migration, segregation and positioning; and axon guidance of, e.g., limb-innervating motor axons in vertebrates (Klein, 2012). *Drosophila* has a single Eph receptor and a single ephrin. Interestingly, removal of the single Eph receptor or ephrin uncovered a very specific role of Eph/ephrin signaling in mushroom body development of *Drosophila* (Boyle et al., 2006). Nevertheless, despite indications from earlier reports using a knock down approach (Bossing et al., 2002) (Dearborn et al., 2002), the current understanding is that removal of the Eph/ephrin signaling in the embryonic CNS and the larval visual system causes only minor axon guidance defects.

Semaphorins are a large family of membrane-associated and secreted proteins that consist of 21 members in vertebrates (Pasterkamp, 2012). They have been originally identified as repulsive axon guidance cues, but several other roles have been uncovered ever since, including neuronal polarization, topographic mapping, axon sorting, axonal pruning, and synapse formation (Pasterkamp, 2012; Yoshida, 2012). However, semaphorins have been also shown to mediate attractive responses. Semaphorins signal predominantly through receptors of the plexin and neuropilin families. Nine plexins have been identified in vertebrates and in flies five semaphorins and two plexins have been identified. A great diversity of potential interactions between semaphorins and their receptors has been reported, with signaling properties depending on the expression of co-receptors, as well as interactions between secreted semaphorins acting as ligands for transmembrane semaphorins. Remarkably, transmembrane semaphorins and plexins are able to induce bidirectional signaling similar to Eph/ephrins.

Recently, semaphorins and plexins have been described to function as repellent guidance cues in the establishment of laminar stratification in the inner plexiform layer of the mammalian retina (Matsuoka et al., 2011). In addition, they are employed for the formation of discrete neural maps in vertebrates and invertebrates (Pasterkamp, 2012).

1.2 The visual system of *Drosophila* as a model to study neural circuit formation

1.2.1 Visual systems comprise good models for circuit studies

The visual system of *Drosophila* consists of circuits organized into reiterated columns and parallel layers and provides an excellent model to study neural network formation and connectivity (Hadjieconomou et al., 2011a). Interestingly, Cajal used the visual system of bigger flies to study the information flow in a sensory system paradigm, assuming it would be a simpler one compared to the vertebrate retina (Cajal, 1915; Sanes and Zipursky, 2010). Strikingly, this work uncovered the inherent complexity of insect visual systems circuits that show both high levels of cell diversity and packing optimization (K.-F Fischbach, 1989; Sanes and Zipursky, 2010). In *Drosophila,* following to the zealous effort that resulted in the production of anatomical atlases, there is a good understanding of the various neuron classes innervating the visual system, but information about their respective connectivity is limited to a still small number of neuron subtypes (Hadjieconomou et al., 2011a; K.-F Fischbach, 1989; Meinertzhagen and Sorra, 2001; Morante and Desplan, 2008). Moreover, the evident variability amongst specific subtypes, for instance in the medulla can, to a certain level, model the heterogeneity of neurons belonging to the same subgroup found in the human cortex (Sanes and Zipursky, 2010). Finally, the visual system is suited for the application of behavioral tests that can be scored reliably, and thus studies on its circuit formation can be linked to network function data (Sanes and Zipursky, 2010).

The *Drosophila* visual system is made up from approximately of 70,000 neurons that form distinct networks within two bilaterally distributed anatomical structures, named optic lobes (Hadjieconomou et al., 2011a). Optic lobes in turn comprise four highly complex neuropils that have been used for elucidating mechanisms of axonal pathfinding and synaptic

connectivity (Clandinin and Feldheim, 2009) (Hadjieconomou et al., 2011a). They are composed of a large number of different neuronal cell types, approximately 113, that are identifiable owing to their shape and position inside the adult optic lobes (K.-F Fischbach, et al., 1989). Interestingly, this number directly compares to the number of neurons identified in primate eyes, 100 distinct neuron types (Dacey and Packer, 2003). A remarkable difference, however, is noticeable when comparing the vertebrate and fly nervous system's glia to neuron distribution. In vertebrates this ratio is approximately 10:1 whereas the opposite ratio is observed in flies (Venken et al., 2011) (Meinertzhagen and Lee, 2012). Three classes of neurons can be distinguished based primarily on the orientation of their neurites: the columnar, tangential and amacrine neuron types. Columnar neurons project transversely into the neuropils thus establishing the retinotopic maps within the neuropils. Tangential elements are oriented perpendicularly to the columns in specific layers of the neuropils and they can span across the entire columnar neuron projection field. Finally, amacrine cells project locally within the neuropil they innervate and relay information in nearby formed circuits. These highly organized neuropils assemble during development, with neurons being born at larval stages and synaptogenesis occurring from mid-pupation onwards (Meinertzhagen, 1993).

1.2.2 Anatomy of the fly visual system

The adult visual system consists of two anatomical structures, the compound eye and the optic lobe. The *Drosophila* eye contains approximately 750 ommatidia or single eyes. Each ommatidium comprises eight photoreceptor cells (R-cells, R1-R8). R-cells extend their axons into their target area, the optic lobe, that is subdivided into of four different neuropils: lamina, medulla and the lobula complex, consisting of lobula plate and lobula (Figure 3). R1-R6 axons terminate in the lamina, while R7 and R8 axons target deeper in the optic lobe in two distinct layers in the medulla, M6 and M3, respectively. R1-R6 cells in one ommatidium have different optical axes, but share the same axis with R-cells from neighbouring ommatidia. R-cells with the same optical axis project to the same postsynaptic targets in the lamina, a phenomenon called neural superposition (Hadjieconomou et al., 2011a). A retinotopic map is thus formed

from the compound eye through the process of neural superposition in the lamina and through the columns of the medulla and lobula complex. Along this way axons project through two chiasms reversing the visual field: the outer chiasm is located between lamina and medulla, the inner chiasm between medulla and lobula complex.

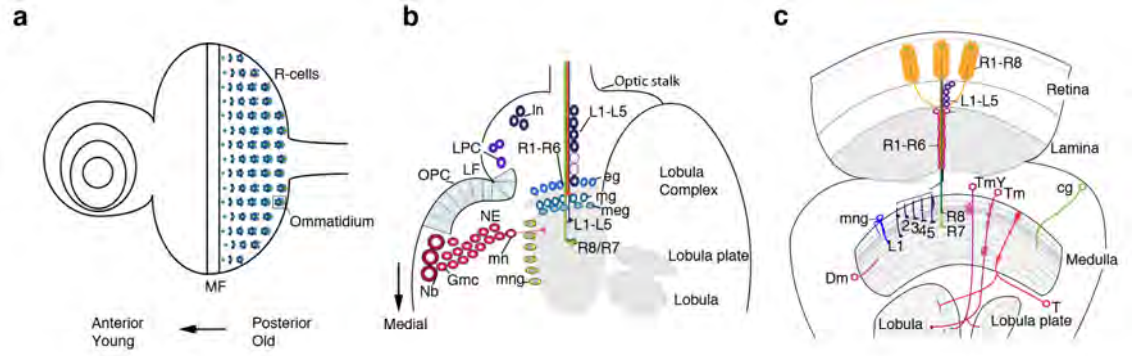

Figure 3. Development and structure of the *Drosophila* visual system.
(a-b) At the third instar larval stage, R-cells differentiate in the eye imaginal disc posterior to the morphogenetic furrow (a, MF) and extend their axons into the target area, the optic lobe (b). R1-R6 axons terminate in the lamina. R7 and R8 send their axons deeper into the medulla neuropil. Neuroepithelial (NE) cells within the outer proliferation center (OPC) medially give rise to medulla neuroblasts (Nb); laterally, adjacent to the lamina furrow (LF) they give rise to lamina precursor cells (LPCs). LPCs undergo a final division and differentiate to lamina neurons (ln). (c) In the adult visual system, R1-R6 axons and processes of lamina neurons L1-L5 form synapses in specialized structures called lamina cartridges. R7 and R8 terminals innervate the medulla neuropil layers M6 and M3, respectively. Both lamina and medulla neurons form elaborate axonal and dendritic arborizations in the medulla creating a complex synaptic network. cg, cortex glia, eg, epithelial glia, GMCs, gangion mother cells, meg, medulla glia, mg, marginal glia, mn, medulla neuron, mng, medulla neuropil glia.

1.2.3 Visual information is processed in parallel pathways within the medulla neuropil

Visual information is processed in parallel pathways beginning in the first neuropil of the optic lobes, the lamina. As an example, both motion detection and color vision require the comparison of at least two R-cell inputs. R1-R6 cells express the same light-sensitive Rhodopsin (Rh1) that detects visible light, and project to the lamina (Meinertzhagen and Sorra, 2001; Ostroy et al., 1974). This input is known to mediate motion detection (Rister et al., 2007). R7 and R8 cells express specific combinations of Rhodopsins that show different spectral sensitivity. R7 cells express Rh3 and Rh4, which detect light in the ultraviolet (UV) part of the

spectrum, and finally R8 cells express Rh5 and Rh6 that are sensitive to light in the green and blue range (Montell et al., 1987; Papatsenko et al., 2001; Salcedo et al., 1999; Zuker et al., 1987). This makes the input from R7 and R8 cells the main source of information for the processing of color information in the medulla. Serial electron microscopy (EM) in combination with molecular as well as genetic approaches provided first insights into the neural substrates of discrete circuits in the visual system, that mediate specific aspects of the computations required for the processing of motion detection (Rister et al., 2007)(Takemura, et al., 2011) or color vision (Gao et al., 2008).

1.2.4 Cell diversity in the *Drosophila* visual system

An astonishing level of cell diversity of distinct cell subtypes is found within the *Drosophila* optic lobes. Their cell bodies are located in the cortex that surrounds the neuropils, into which neurons and glia extend their processes. Neuron subtypes in the fly visual system are classified based on their morphology. Thus, their projections to the different neuropils and their specific arborization patterns restricted to one or spanning several layers or columns, determine their identity.

The lamina neuropil is subdivided into repeated columnar synaptic units, called lamina cartridges that are closely associated with the R-cell axon bundles. Lamina cartridges are innervated by five lamina neurons, L1-L5, the centrifugal cells C1, C2, and the T1 cells. In electron microscopic (EM) studies L1-L3 have been found to be postsynaptic to R1-R6 axons (Meinertzhagen and O'Neil, 1991)(Meinertzhagen, et al., 2001). Lamina neurons connect the lamina with the medulla. The synaptic connections of these neurons, as well as R7 and R8 axons have been studied at the EM level (Takemura, et al., 2008)(Gao et al., 2008), but the circuits that are formed between these neurons and medulla neurons, as well as medulla neurons and neurons of the lobula complex are still largely unexplored.

The medulla neuropil is further subdivided into 10 layers with the distal medulla composed of layers M1-M6, followed by the serpentine layer M7, and layers M8-M10 in the proximal medulla. Medulla neurons appear to be the most divergent cell population within the

optic lobe. More than 60 types of columnar neurons have been identified (K.-F Fischbach, 1989; Morante and Desplan, 2008) with at least 35 neurons estimated to innervate a single column (Meinertzhagen, et al., 2001). Intrinsic medulla neurons (Mi) connect the distal with the proximal medulla; transmedulla neurons (Tm) connect the medulla with the lobula; transmedulla Y-cells (TmY) connect the medulla with the lobula and lobula plate. Several columnar neurons are found with their cell bodies adjacent to the lobula plate: T2 and T3 cells connect the medulla and lobula, T4 connect the proximal medulla to the lobula plate, and T5 connect lobula plate and lobula. In addition to columnar neurons, there are many tangential neurons that extend over several columns in particular layers of each neuropil (Figure 3).

1.2.5 Subtypes of neurons in the fly visual system are generated using distinct mechanisms

The optic lobe is derived from the optic lobe placode, a group of neuroepithelial cells generated during embryogenesis (Green et al., 1993). During early larval development, the pool of progenitor cells is amplified by symmetric neuroepithelial cell divisions (Egger et al., 2007). These neuroepithelial cells are located in two different neurogenic areas within the optic lobe, the outer and inner proliferation centers (OPC and IPC). Thus, OPC and IPC give rise to the different subtypes of optic lobe neurons. Neurogenesis within the optic lobe is well understood for the OPC in contrast to the IPC, for which very little is known. However, exiting new insights have been recently uncovered by ongoing work by Holger Apitz in our laboratory. The OPC employs two distinct mechanisms for generating neurons. The first mode of neurogenesis at the OPC is portrayed by the events resulting to the generation of lamina neurons. In this case, the OPC gives rise to lamina precursor cells (LPC) posteriorly to the lamina furrow. Next, ingrowing R-cell axons release two signals, Hedgehog (Hh) and Spitz (Spi), required for a final division of LPCs and their differentiation into lamina neurons (Chotard et al., 2005; Huang and Kunes, 1996, 1998). In this manner, lamina neuron development and is linked to R-cell differentiation in the eye. In contrast, the second mechanism of OPC neurogenesis is independent of R-cell innervation and generates medulla neurons. At the medial edge of the OPC, neuroepithelial cells gradually transform into neuroblasts (NB) during third instar larval

development (Egger et al., 2007). These NBs undergo asymmetric cell division to generate another NB and a ganglion mother cell (GMC). Finally, GMCs undergo symmetric division and form two medulla neurons. Mechanisms that regulate the differentiation of these neurons to obtain the great diversity of medulla neurons subtypes, as well as lamina neurons L1-L5 are still poorly understood. New insights into medulla neuron development have been provided by the recent findings that medulla neuron identity is specified by the expression of at least four transcription factors; namely Drifter, Runt, Homeothorax and Brain-specific homeobox (Hasegawa et al., 2011). These are expressed in discrete domains, forming concentric zones within the optic lobe at larval stages. A single NB produces progeny forming a cylindrical row. New cells are added in a series of sequential divisions. Thus, the older neurons are proximal to the center of the medulla, and younger neurons are positioned close to the periphery and the neuroepithelium. This row of cells is oriented linearly and radially towards the center of the emerging medulla. Thus, younger neurons will express different combinations of the four transcription factors when compared to older neurons. In this manner, different medulla neurons express characteristic combinations of transcription factors, which determine their subtype identity and reflects their birth order. These concentric zones of expression disappear at 12 hours after puparium formation (APF) and substantial cell migration leads to mixing of cell bodies within the medulla cortex. Importantly, further experiments included in this study show that cell body distribution in the adult is not random but determined according to cell type identity. This work has provided significant insights into the underlying developmental programs of medulla neurons. Future experiments can uncover more molecules, perhaps expressed in overlapping expression domains that can further refine neuron identity and localization within the circuit.

1.2.6 Different glia subtypes are found within the *Drosophila* optic lobes

Based on their morphology and cell body position, different types of glial cells have been identified in the developing optic lobes at the third instar larval stage (Chotard and Salecker, 2007). Interestingly, four groups of glia have been identified that are associated or in close

proximity with the optic lobe neuropils. At the third instar larval stage, two rows of glial cells can be observed in developing lamina plexus. The distally located subgroup of glia is called epithelial glia and the proximally positioned marginal glia. An additional row of glia, the medulla glia is located at the lamina-medulla boundary. Finally, a fourth population, thus named medulla neuropil glia surrounds the emerging medulla neuropil. The origin, clonal relationships, as well as the morphological development of these cells in the optic lobe is poorly understood (Chotard and Salecker, 2007; Edwards and Meinertzhagen, 2010; Hasegawa et al., 2011). A notable exception is however the lamina glial cells population. These cells originate from a region located at the surface of the optic lobe in the dorsal and ventral tips of the outer proliferation centre (OPC), named the glia precursor cell (GPC) area. Following their generation, they migrate towards their final position in the lamina, where they serve as intermediate targets for ingrowing R1-R6 axons (Poeck et al., 2001). Little is known about the functions of the other types of glia during development and in the adult. Moreover, it is possible that their true heterogeneity has yet to be fully comprehended. Epithelial glial cells in the adult are known to be required for the uptake and recycling of histamine, the neurotransmitter employed by R-cells. They form characteristic invaginations called capitate projections into R1-R6 terminals in the lamina (Chotard and Salecker, 2007; Prokop and Meinertzhagen, 2006). Inportantly, capitate projections have been also identified in proximity to the R7 and R8 terminals within the medulla (Prokop and Meinertzhagen, 2006). Thus, medulla neuropil glia, which extend processes in the medulla could play the same role in histamine recycling (Chotard and Salecker, 2007). In ongoing studies in our laboratory, Benjamin Richier has methodically worked towards the characterization of medulla neuropil glia morphologies in the adult with the aim to identify the so far unknown biological processes, in which they are involved. Finally, other types of glia found in the optic lobes are not related with the neuropils. For instance, they generate boundaries to compartmentalize the optic lobe and prevent cells of different origins to mix (Chotard and Salecker, 2007; Fan et al., 2005; Tayler et al., 2004).

1.2.7 Neurons and glia are implicated in neural network assembly of *Drosophila* optic lobes

Neural circuit formation in the *Drosophila* visual system has been studied predominately with the focus on R-cell pathfinding and targeting. At the third instar larval stage, R1-R6 axons project into the lamina plexus where they terminate in-between two rows of glial cells, namely the epithelial and marginal glia. While the role of glial cells as intermediate targets has been well documented, the putative stop signal emitted by glial cells remains elusive. At around 42 hours APF, R1-R6 axons in the lamina project to their correct synaptic partners in neighbouring cartridges to establish the precise connectivity associated with the phenomenon of neural superposition. R8 and R7 axons extend axons through the lamina and terminate at two distinct temporary layers in the medulla; R8 axons terminates at the border of the medulla neuropil and R7 terminals are located just beneath (Bazigou et al., 2007; Ting et al., 2005). During mid-pupal development, R-cell axons start to regrow towards their correct target neurons. Slightly later, R7 and R8 growth cones leave their temporary layers in the medulla to target to their final layer M6 and M3, respectively. For both processes, several molecular factors have been identified that regulate target selection of R-cell axons (Astigarraga et al., 2010; Clandinin and Zipursky, 2002; Hadjieconomou et al., 2011a; Mast et al., 2006). One important guidance cue for layer-specific targeting is N-Cadherin (CadN). CadN is widely expressed in the developing visual system and plays a role in the precise targeting of all R-cell axons (Lee et al., 2001; Petrovic and Hummel, 2008; Prakash et al., 2005; Ting et al., 2005). Importantly, CadN is the only guidance cue identified so far required for layer-specific targeting of optic lobe neurons. Lamina neurons L1-L5 terminate and arborize in specific layers in the distal medulla. Removal of CadN in lamina neurons results in stereotypical phenotypes: L1 mistarget to medulla layer M10 instead of M5, L3 to M5 and M6 instead of M3, and L4 in M2 or M8 instead of M4. In addition, L5 fail to extend their characteristic branches from M1 to M2 (Nern et al., 2008).

1.2.8 Molecular and other mechanisms involved in network formation

A significant number of molecular cues are shared amongst vertebrates and insects in the processes involved in neural network assembly. The nervous system remains an exceptional tissue, as it functions by allowing a constant flow of electricity through its different parts. In this manner, information can be relayed and appropriate responses to external (sensory) or internal (homeostatic) cues can be propagated. Importantly, in addition to the role in information relay, neuronal activity has been reported to facilitate network formation and refinement in different vertebrate model systems (Shatz, 1996; Yoshida et al., 2009; Yu et al., 2004). Nevertheless, in *Drosophila,* it has yet to be clarified as to whether activity can be considered as driving force in network formation. Experimental evidence from work in the lamina neuropil of the fly visual system so far indicates that activity does not play a role and network assembly is genetically hardwired (Hiesinger et al., 2006). Nevertheless, this has not been explored for other parts of the visual system including the highly innervated medulla neuropil. A recent study in the larval antennal lobe shows that spontaneous patterns of electrical currents contribute in restricting olfactory sensory neurons to specific glomerular territories (Prieto-Godino et al., 2012) at early developmental stages. In view of these exciting insights, similar questions remain to be addressed for the visual system.

1.3 Approaches to understand the connectivity and development of neural circuits

The previous sections have highlighted the importance of elucidating neural network assembly and function with particular emphasis in the use of model organisms, that are genetically amenable. In the subsequent sections, I will focus on the means, by which these studies can be carried out. Genetic engineering has played a pivotal role in providing neurobiologists with a versatile array of tools to study the biology of the nervous system (Meinertzhagen and Lee, 2012; Venken et al., 2011). In addition to the increasing number of these genetic methodologies, novel immunohistochemistry approaches, as well as advances in microscopy and image processing have greatly facilitated the visualization and manipulation of cell populations (Denk et al., 2012; Kleinfeld et al., 2011). Genetic tools can be divided according to their scope into

two major categories: 1) tools to study gene function, by altering the dose of a gene product in the nervous system and 2) tools to study individual subsets of neurons, by altering the properties of a specific neuron subtype, for instance by changing its electrophysiological properties, to understand their individual function within a circuit.

1.3.1 Genetic approaches to manipulate genes in circuits in *Drosophila*

Visualizing or manipulating the behavior of specific cell types can be achieved by ectopic expression of reporter or effector genes, within the cellular subpopulation of interest. For this purpose, transgenes have been engineered that include identified tissue-specific regulatory elements and mediate expression of the genes under their control. The yeast derived Gal4/*UAS* has been successfully adopted for heterologous function in a variety of experimental models and has revolutionized the versatility of the aforementioned approach. This binary system consists of the Gal4 transactivator that binds *Upstream Activating Sequences* (*UAS*) to mediate transcription of downstream genes in organisms such as *Drosophila* (Brand AH, 1993; Fischer et al., 1988). The advantage of binary systems is based on their versatility by combining different sets of tissue-specific Gal4 drivers with different *UAS* responder lines. The Gal4/*UAS* system has been originally developed as a tool for gain-of-function studies (Brand AH, 1993). In addition, by the recent creation of several large *UAS*-RNA interference (RNAi) collections tissue-specific loss-of-function studies for virtually every gene can be undertaken (Dietzl et al., 2007; Ni et al., 2009; Ni et al., 2011). Furthermore, several *UAS* transgenes have been developed for interference with neuronal activity to study the function of particular neurons within specific neuronal circuits (Venken et al., 2011). In the past twenty years, many different Gal4 driver collections have been established, including large enhancer trap Gal4 collections, e.g. (Hayashi et al., 2002) and extensive Gal4 transgene constructs driven by short enhancer fragments (Jenett et al., 2012; Pfeiffer et al., 2008). Many additions have been made to improve the spatiotemporal control of the Gal4/*UAS* system. These include the employment of the Gal4 repressor Gal80 (Lee and Luo, 1999), either by expression in a defined overlapping subset of neurons or by controlling the function of a temperature-sensitive Gal80 repressor at particular

developmental stages (McGuire et al., 2003). Alternatively, time- and tissue-specific control can be achieved by using Gal4 lines that are activated by various drugs (Han et al., 2000; Osterwalder et al., 2001; Roman et al., 2001).

In addition to the Gal4/*UAS* system, several other binary systems have been developed for application in *Drosophila*. The first approaches were based on the tetracycline system (Bello et al., 1998; Bieschke et al., 1998; Stebbins et al., 2001; Stebbins and Yin, 2001), but these tools have not been developed further within the *Drosophila* community. In contrast, the introduction of the LexA system (Lai and Lee, 2006; Szuts and Bienz, 2000; Yagi et al., 2010) and the Q system (Potter et al., 2010) to the *Drosophila* toolbox has resulted in the generation of numerous driver and responder lines establishing both as highly valuable approaches complementary to the Gal4/*UAS* system. For example, two binary systems driving different reporter genes in distinct neuronal subpopulations can be combined as intersectional strategies for the visualization of overlapping neuron subsets (Potter et al., 2010). Other intersectional strategies are the split-Gal4 (Luan et al., 2006; Pfeiffer et al., 2010) and split-LexA systems (Ting et al., 2011). In these systems, the transactivator is split into two halves and expressed in distinct neuronal subpopulations. Only in the case, in which the expression of the two driver lines overlap, a functional transactivator will be reconstituted to mediate reporter gene expression in a small subset of neurons.

Complementary to binary expression systems, fly geneticists have greatly benefited from the introduction of the Flp/*FRT* system to *Drosophila* (Golic and Lindquist, 1989). Site-specific recombinases, such as the *S. cerevisiae* derived Flp, recognize specific short DNA sequences or target sites. Recombination is mediated in discrete steps; first the enzyme catalyzes the cleavage at the target site and subsequently DNA strands are re-ligated. Depending on the inherent directionality of the *FRT* target sites, this can result in excision and insertion, as well as inversion, translocation and cassette exchange (Golic and Lindquist, 1989). The Flp/*FRT* system has been widely used for the generation of genetic mosaics by the integration of *FRT* sites near the centromeres of chromosomal arms using homologous recombination. Upon controlled Flp expression, this results in mitotic recombination of whole chromosome arms and

allows the generation of homozygous mutant clones in heterozygous animals (Xu and Rubin, 1993). Using this strategy, mutant cells are typically marked by the absence of a fluorescent protein.

The invention of the MARCM (mosaic analysis with a repressible cell marker) approach greatly facilitated mosaic analysis in the nervous system (Lee and Luo, 1999). In this case, mutant cells are labeled by the expression of membrane tagged GFP (*UAS-cd8-GFP*), therefore, allowing visualization of the morphology of mutant neurons. This is achieved by the loss of the Gal80 repressor in homozygous mutant cells upon Flp/*FRT* system induced mitotic recombination in animals expressing Gal4 in specific neuron subpopulations. Variations of the MARCM approach have been developed for the Q system (Q-MARCM; (Potter et al., 2010)). To simultaneously visualize both wild type and mutant progeny after mitotic recombination, the twin-spot MARCM technique has been added (Yu et al., 2009).

In addition to the Flp/*FRT* system, several other site-specific recombination systems have been introduced to *Drosophila*. These include the Cre/*LoxP* system (Siegal and Hartl, 1996) and the ϕC31 integrase (Bischof et al., 2007; Groth et al., 2004). The use of the Cre/*LoxP* system in *Drosophila* has been limited due to the toxic effects caused by high levels of Cre recombinase expression (Heidmann and Lehner, 2001). In contrast, the ϕC31 integrase system has established itself as the standard approach for site-specific introduction of transgenes into the *Drosophila* genome. Furthermore, four different site-specific recombinase systems derived from yeast (KD, B2, B3, and R) have been very recently developed to *Drosophila* (Nern et al., 2011).

1.3.2 Genetic markers allow neuron labeling within a network in *Drosophila*

Using fluorescent proteins (FPs) as genetic markers is nowadays an inseparable part of the daily routine of scientists in most life sciences laboratories; nevertheless, it is hard to imagine that this has only been the case for just the recent past. Green Fluorescent Protein (GFP), the most commonly used member of this protein family, was isolated from the bioluminescent jellyfish *Aequorea victoria,* by the inquisitive chemist Osamu Shimomura in the early 1960s almost

serendipitously (Shimomura et al., 1962). Following, the work of Douglas Prasher and Martin Chalfie resulted in successful sequencing, cloning and GFP transgenes expression in heterologous prokaryotic (*E. coli*) and eukaryotic (*C. elegans*) systems (Chalfie et al., 1994; Prasher et al., 1992). This proved that GFP could serve as an exceptional tool enabling direct visualization of individual structures and processes within living tissues without interfering with their canonical functions using a genetically encoded marker. Thereafter, a great variety of naturally occurring fluorescent proteins were isolated from different species (Chudakov et al., 2010; Shaner et al., 2007). Noteworthy is that the highest degree of naturally occurring color diversity of fluorescent proteins can be observed amongst the *Anthozoan* taxa (Chudakov et al., 2010; Matz et al., 1999). It is important to highlight two properties of GFP that led to its wide use as an experimental tool; namely:

1) Autocatalytic nature of its fluorescent properties since it does not require any co-factors or enzymes aside molecular oxygen for its function in living organisms. This feature is shared amongst the other protein family members and can be attributed to their structure.
2) Oligomerization state, as GFP is a monomeric protein (unless expressed in extremely high levels where it can form a weak dimer). This is a crucial asset for a genetically encoded marker, especially when placed in frame with a coding sequence of interest to produce chimeric proteins. A GFP monomer placed in the NH_2- or COOH- end of a protein of interest is less likely to interfere with its function. Thus, it can serve as a means to mark the biological changes the protein of interest undergoes including its localization, movement, turnover or interaction with other proteins. The oligomerization status differs significantly amongst fluorescent protein members and often polymeric members have proven deleterious *in vivo* as they tend to form aggregates.

The structure of the GFP protein and of the other members of this protein superfamily is key to their biological function. They are normally comprised of 220-240 aa that fold and form a β-barrel. Eleven β-sheets are typically included in the fluorescent protein barrel and a chromophore group is formed in its interior by an autocatalytic posttranslational modification. This includes cyclization of the key three amino acid residues at positions 65-67 (Ser-Tyr-Gly)

followed by the dehydrogenation of the tyrosine with molecular oxygen. The latter leads to the formation of a two-ring structure that is large, polarized and planar to an adequate level as to absorb and emit light within the visible range (Chudakov et al., 2010; Zacharias and Tsien, 2006). Interestingly, the Serine residue at position 65 can vary amongst protein members, while positions 66 and 67 appear completely conserved amongst the naturally occurring GFP-like variants. Thus, the chromophore is embedded within the protected core of the β-barrel where solvents from different cellular environments are not able to come in contact and interfere with its excitation and emission properties, rendering these bioluminescent molecules highly photostable.

Following the isolation of the original GFP, an extensive effort by Roger Tsien resulted in the generation of bioengineered proteins with improved properties. These included: oligomerization state; photostability; brightness, importantly, the brighter the fluorescent proteins the lesser the dose of light required for excitation thus the lower the overall phototoxicity in an experimental paradigm; pH insensitivity, thus fluorescent proteins can survive well in different cellular enviroments; spectral range; and maturation rate, reaching optimum times for live experiments that range between 40 minutes to -1-2 hours (Chudakov et al., 2010; Matz et al., 1999; Shaner et al., 2007; Shaner et al., 2005).

Thus, protein engineering alongside the isolation of naturally occurring protein members have created a wide palette of fluorescent proteins. Four classes can be identified within the GFP-like family: green, yellow, blue-cyan and orange-red. The first three are all derivatives of the wild type GFP protein, whereas the red derivatives were isolated after the original discovery of a red fluorescent protein from the *Discoma* reef coral (Matz et al., 1999). Recent studies have provided the field with proteins of improved properties such as enhanced GFP (EGFP), mCitrine, mCherry, TagRFP-T, Cerulean and mTurquoise (Goedhart et al., 2012; Griesbeck et al., 2001; Rizzo et al., 2004; Shaner et al., 2004; Shaner et al., 2007). Additionally, reversibly photoactivatable fluorescent protein along with split variants have been developed for use in a variety of divergent biological contexts. One very promising prospect is the development of enhanced phototoxic fluorescent proteins and methodologies that can find

therapeutic applications (i.e. cancer) (Chudakov et al., 2010). With the continuous development of improved fluorescent protein variants an experimentalist should keep in mind that no variant can constitute a golden solution and each of them should be carefully chosen for use according to its desired application (Chudakov et al., 2010; Shaner et al., 2005).

1.3.3 Advanced genetic strategies combined with imaging approaches to study connectivity

The axiom for connectivity studies aiming at uncovering synaptic contacts between interrelated neurons within the nervous system remains serial-section electron microscopy (ssEM; (Meinertzhagen and Lee, 2012). This method has proven its value in different parts of the nervous system such as the vertebrate retina (Briggman et al., 2011) and the fly medulla (Takemura et al., 2008). Unfortunately however, high throughput usage of this technique is currently limited by technical challenges (Meinertzhagen and Lee, 2012). To visualize neural circuit connectivity using light microscopy resolution, several genetic approaches have been successfully applied in *Drosophila,* mainly by sparsely labeling cells in samples. In this manner, potential connectivity can be estimated by revealing single cell morphology of neuron subtypes using the MARCM approach. Aligning different neuron subtypes to a standard brain (Jefferis et al., 2007; Jenett et al., 2012; Peng et al., 2011) may then indicate possible synaptic contacts by proximity. Nonetheless, these approaches need to be examined with care as data about potential synaptic partners are pieced together using different samples. Evidence for synapse formation between two neuron subtypes can be revealed by GRASP (GFP reconstitution across synaptic partners; (Feinberg et al., 2008; Gordon and Scott, 2009)). In this technique, two complementary GFP fragments are expressed in two distinct neural populations. Upon close membrane contact, the two GFP fragments reconstitute a functional GFP protein and therefore visualize the potential presence of pre- and postsynaptic sites. Similarly, expression of photoactivatable GFP in neural subpopulations that are potentially connected to a given neuron type can reveal close proximity and therefore potential connectivity of neurons (Datta et al., 2008; Ruta et al., 2010). The generation of novel fluorescent protein members that would be better suited for super-resolution microscopy experiments and the constant advance of these

microscopy methods (i.e. PALM) provide another optimistic look in the future of solving efficiently connectomes. Nonetheless, light microscopy remains the sole good compromise between single cells, time efficiency and optical resolution for such everyday experiments.

1.3.4 Randomized multicolor cell labeling

Studies of the nervous system would greatly benefit from methods positively that can mark multiple neurons within one sample. Using light microscopy in combination with single marker labeling prevents reconstruction of morphologies from overlapping neurites. Thus, a new approach named Brainbow was developed and has overcome this limitation. The ingenious concept of this method developed by Jean Livet and colleagues brought the use of fluorescent proteins in combination of DNA recombinases to new heights for studies of neuronal connectivity in mice (Livet, et al., 2007) (Lichtman, et al., 2008). The *Brainbow* approach uses Cre/*lox(P)* mediated site-specific recombination, to stochastically drive the expression of one of three to four fluorescent proteins in a genetically determined cell population. In addition, independent combinatorial expression of fluorescent proteins from multiple transgene copies placed in tandem within the genome can lead to the labeling of individual neurons in more than one hundred different hues. Importantly, this method has enabled the tracking of individual neurons based on a distinct color profile. *Brainbow-1* constructs rely on recombination of incompatible pairs of *lox* sites leading to excision of fluorescent protein encoding sequences. Recombination occurs only, when *loxP* pairs are of the same sequence but different *lox(P)* variants cannot be combined to induce recombination. Three *lox(P)* variant pairs were employed, along with four different fluorescent proteins. Excision of the flanked sequences led to three different color outcomes according to the fluorescent proteins positioned immediately downstream of the promoter. A fourth color was observed in the case recombination did not occur. By contrast, *Brainbow-2* variants use inversions and excision of fluorescent protein encoding sequences of *loxP* sites facing in the same or opposite directions, respectively. Upon Cre expression the cassettes can spin numerous times but get stabilized in one of the two orientations, when Cre is removed. Two spinning cassettes, each containing two different

fluorescent proteins were placed in tandem. The fluorescent proteins in each cassette were positioned in a face-to-face orientation, thus only one of them could be expressed at a time, depending on the orientation of the cassette. Additionally, excision events could still occur resulting in four fluorescent protein expression possibilities. Brainbow transgenes were placed under a *Thy1* promoter to drive expression in the majority of the neuron subtypes as well as glia in the brain. Brainbow strains were subsequently used to address connectivity in the specific brain areas of the CNS, e.g. the cerebellum. Additionally, three-dimensional reconstructions of individual neurons were produced using specialized computer software such as attributing a color identity to each cell and, in this manner, facilitating the tracing process on a single cell level. In addition, glial cells could be also labeled providing information about their anatomical relationships with interconnecting neurons or other glial cells.

Following to its introduction Brainbow found applications in different studies and new adaptations of the approach have been generated already for its application beyond the nervous system in the mouse. These include the Confetti (Snippert et al., 2010) and Rainbow (Tabansky et al., 2012) transgenic lines which I will further discuss in section 7.2. Furthermore this method has been adapted for use in different model organisms, for instance in zebrafish (Gupta and Poss, 2012). However, this approach had not been developed for use in *Drosophila*.

1.4 Aims of the work undertaken to complete this thesis

To advance our understanding of the mechanisms that underlie neural circuit connectivity and development, our laboratory uses the *Drosophila* visual system as a model network. Work in this field has so far focused on understanding the connectivity and molecular mechanisms involved in the development of the individual local circuits using a R-cell axon centered bias. Thus, information about the connectivity of higher order neurons, such as the approximately 60 different medulla neuron subtypes, has so far been limited. The medulla shows the greatest level of anatomical complexity amongst the visual system neuropils, thus making its study a very demanding task. Consequently, there is a lack of available tools suitable for its in depth study. Understanding the numerous mechanisms involved in medulla circuit assembly and function will provide new insights into the general biological aspects of neuron circuit assembly.

This thesis describes my PhD work focused on generating a genetic tool that is suitable for facilitating the study of the intricate morphologies of insect neurons with the scope to obtain further insights on the connectivity of the medulla neuropil. I have focused on the development of a novel genetic tool for randomized multicolor cell labeling in flies based on the vertebrate *Brainbow-2* approach (Livet et al., 2007).

Chapter 3 describes the conceptual design involved in adapting the tool for *Drosophila*, which we named "Flybow". We planned to develop three variants of the Flybow approach, namely *FB1.0*, *FB1.1* and *FB2.0*. This chapter includes the experiments that led to the successful generation of these three different FB constructs. Additionally, this chapter also includes methodologies used to obtain Flybow transgenic lines. Chapter 4 provides a proof of principal that all the components of our system work *in vivo,* while also uncovering the suboptimal performance of the Cerulean fluorescent protein. Chapter 5 describes experiments that demonstrate the functionality of *FB1.1* and *FB2.0* approaches in the visual system and beyond for the analysis of single cell morphologies in developing and adult tissues. Moreover, it includes the first application of Flybow in our study aiming at uncovering the role of Netrins in the fly visual system. Finally, Chapter 6 provides experimental proof that Flybow can be used together with MARCM to facilitate gene function studies.

Chapter 2

Materials and Methods

2.1 Genetics

2.1.1 Fly Stocks

Drosophila melanogaster stocks were raised and maintained in vials or bottles containing standard cornmeal/agar medium at 25 ºC. Crosses were carried out at 25 ºC. The fly lines used in this study are shown in Table 1.

Genotype	Use	Origin
vas-ϕC3/zh11	transgenesis	K. Basler
attP^{260b}	transgenesis	S. Rotkopf and B. Dickson
attP^{49b}	transgenesis	S. Rotkopf and B. Dickson
attP^{57b}	transgenesis	S. Rotkopf and B. Dickson
yw^{1118}	transgenesis	lab stock
ey-Flp	generation of modified Flp/*FRT*	S. Rotkopf and B. Dickson
ey-mFlp4	generation of modified Flp/*FRT*	S. Rotkopf and B. Dickson
ey-mFlp5	generation of modified Flp/*FRT*	S. Rotkopf and B. Dickson
ey-mFlp6	generation of modified Flp/*FRT*	S. Rotkopf and B. Dickson
ey-mFlp7	generation of modified Flp/*FRT*	S. Rotkopf and B. Dickson
act5C FRT≥αtub 3'UTR FRT≥nuclear lacZ	generation of modified Flp/*FRT*	S. Rotkopf and B. Dickson
act5C-mFRT11≥αtub 3'UTR mFRT11≥nuclear lacZ	generation of modified Flp/*FRT*	S. Rotkopf and B. Dickson
act5C-mFRT71≥αtub 3'UTR mFRT71≥nuclear lacZ	generation of modified Flp/*FRT*	S. Rotkopf and B. Dickson
act5C-mFRT11-71≥αtub 3'UTR mFRT11-71≥nuclear lacZ	generation of modified Flp/*FRT*	S. Rotkopf and B. Dickson
hs-mFlp5/Gla Bc; TM2/TM6B	heat-shock controlled expression of modified Flp	S. Rotkopf and B. Dickson
y w: CyO/Gla Bc; hs-mFlp5/TM2	heat-shock controlled expression of modified Flp	Generated in the lab for the purpose of this study
y w hs Flp^{1}; Adv/Gla Bc; TM2/TM6B	canonical Flp source	Bloomington
elav-Gal4^{c155}	neuronal marker	Bloomington
pGMR-Gal4	R-cell marker	lab Stock
MzVum-Gal4;UAS-cd8GFP	medulla neuron subtype marker	M. Landgraf

MzVum-Gal4	medulla neuron subtype marker	I. Miguel-Aliaga
repo-Gal4	glial cell marker	K. Sepp and V. Auld
en-Gal4	wing disc posterior compartment marker	J.P. Vincent
dpp-Gal4	wing disc anterior-posterior compartment border marker	J.P. Vincent
NP4151-Gal4	marker for netrin expressing neurons	Kyoto
NP1522-Gal4	marker for Netrin expressing neurons	Kyoto
elav-Gal4^{c155};hs-mFlp5/CyO	marker combined with modified Flp	generated in the lab for the purpose of this study
pGMR-Gal4/CyO;hs-mFlp5/TM6B	marker combined with modified Flp	generated in the lab for the purpose of this study
MzVum-Gal4;hs-mFlp5/CyO	marker combined with modified Flp	generated in the lab for the purpose of this study
hs-mFlp5/CyO;repo-Gal4/TM6B	marker combined with modified Flp	generated in the lab for the purpose of this study
en-Gal4/Gla Bc;hs-mFlp5/TM6B	marker combined with modified Flp	generated in the lab for the purpose of this study
hs-mFlp5/Gla Bc; dpp-Gal4/TM6B	marker combined with modified Flp	generated in the lab for the purpose of this studv
NP4151-Gal4; hs-mFlp5/CyO	marker combined with modified Flp	generated in the lab for the purpose of this study
NP1522-Gal4; hs-mFlp5/CyO	marker combined with modified Flp	generated in the lab for the purpose of this study
UAS-cd8-mCherry^{260b}	red fluorescent protein reporter	generated in the lab for the purpose of this study
UAS-cd8-mCherry^{57b}	red fluorescent protein reporter	generated in the lab for the purpose of this study
UAS-pm-mCitrine^{260b}	yellow fluorescent protein reporter	generated in the lab for the purpose of this study
UAS-pm-mCitrine^{49b}	yellow fluorescent protein reporter	generated in the lab for the purpose of this study
UAS-FB1.0 ^{260b}	Flybow 1.0 version	generated in the lab for the purpose of this study
UAS-FB1.0^{49b}	Flybow 1.0 version	generated in the lab for the purpose of this study
UAS-FB1.1 ^{260b}	Flybow1.1 version	generated in the lab for the purpose of this study
UAS-FB1.1^{49b}	Flybow 1.1 version	generated in the lab for the purpose of this study
UAS-FB2.0 ^{260b}	Flybow 2.0 version	generated in the lab for the purpose of this study
UAS-FB2.0^{49b}	Flybow 2.0 version	generated in the lab for the purpose of this study
y w hs-Flp^{1};UAS-FB2.0 ^{260b}	combination of canonical Flp and FB2.0	generated in the lab for the purpose of this study
y w hs-Flp^{1};UAS-FB2.0^{49b}	combination of canonical Flp and FB2.0	generated in the lab for the purpose of this study
FRT40A;TM2/TM6B	combination of MARCM and FB approaches	lab stock

elav-Gal4^{c155} hs-Flp^{1};tubP-Gal80 FRT40A/Gla Bc	combination of MARCM and FB approaches	generated in the lab for the purpose of this study
elav-Gal4^{C155} hs-FLP^{1}; FRT40A tub-Gal80/CyO; hs-mFLP5/TM2	combination of MARCM and FB approaches	generated in the lab for the purpose of this study
FRT40A;UAS-FB1.1^{49b}/TM6B	combination of MARCM and FB approaches	generated in the lab for the purpose of this study
CadN^{M19} FRT40A/Gla Bc; TM3/TM6B	combination of MARCM and FB approaches	lab stock
CadN^{M19} FRT40A/Gla Bc;UAS-FB1.1^{49b}/TM6B	combination of MARCM and FB approaches	generated in the lab for the purpose of this study

Table 1. Fly stocks.

2.1.2 Transgenesis using the *attP*/*attB* system

Transgenic flies were generated using a standard injection protocol summarized in Figure 4. The *attB*-site containing constructs, *UAS-cd8-mCherry, UAS-pm-mCitrine, FB1.0, FB1.1* and *FB2.0* were inserted into specific *attP*-site containing loci on the second and third chromosomes using the ϕC31 system. Virgin females from stocks carrying the germ-line specific transgene *vas-ϕC31* (*vas-ϕ–C31-zh2A*) on the X chromosome (Groth et al., 2004) were crossed with males from $attP^{260b}$ (2L), $attP^{49b}$ (3R) or $attP^{57b}$ (3R) stocks, respectively (K. Keleman and B.J. Dickson, (Dietzl et al., 2007) and unpublished). Fertilized eggs were injected before cellularization with 500-600 ng DNA of *attB* containing plasmids. The injected embryos were grown until adult stages. All survivors, males and females were collected and crossed with yw^{1118} virgins or males respectively. Next, single males were selected and crossed with virgins containing the balancer chromosomes on the second or the third chromosome. To establish individual lines, males and females from the same cross were used.

The *ey-mFlp 4-7* stocks were generated using a P element-based approach in B. Dickson's laboratory. Coding regions of wild-type *Flp*, *mFlp4*, *mFlp5*, *mFlp6* and *mFlp7* were amplified by PCR, adding 5' NotI and 3' KpnI sites. These PCR products were subcloned as NotI-Asp718 fragments into a *pCarnegie20*-based vector that includes the 4x 258 bp *eyeless* enhancer and a SV40 polyadenylation signal. The *act5C* stop cassette constructs were generated by PCR amplification of a *a-tubulin* 3'UTR fragment using primers that included the sequences of wild type or modified *FRT* sites and a KpnI site. This insert was subcloned into the KpnI site of a vector containing the *act5C* enhancer upstream of *nlacZ*. *ey-mFlp5* transgenic lines were re-established by a new injection round in our laboratory. Plasmids were co-injected into *w* or *y w* embryos together with a *Δ2-3* transposase-expressing plasmid.

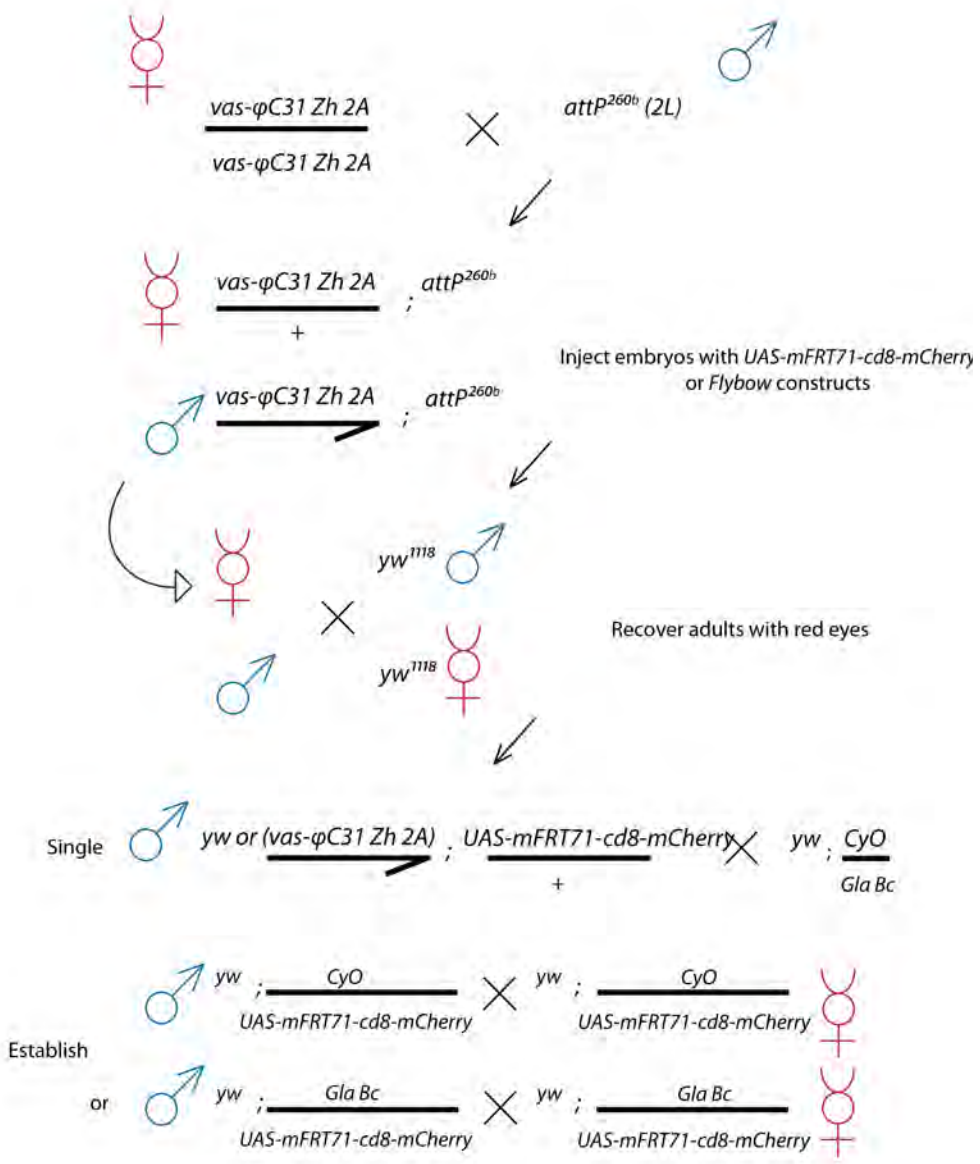

Figure 4. Schematic of genetic crosses to obtain e.g. *UAS-cd8mCherry* transgenic lines.

2.1.3 Clone induction

Female adult flies not older than 4 days were used for genetic crosses since the efficiency of *hs-mFlp5* induced recombination events decreased with the age of the parental stocks. Flies of a given cross were daily transferred into fresh vials for seven days. Developmental stages and lengths of heat shocks (hs) of 24 hour embryo collections in a 37 ºC water bath were adjusted for each combination of FB transgenes and Gal4 drivers as well as the examined tissue. The time points of heat shocks were defined as hours past the egg-

laying window (after egg laying, AEL). Tissues of interest were then dissected and prepared for imaging from flies at third instar larval and adult stages. The optimized conditions for the different experiments are shown in Table 2. FB experiments at embryonic stages were conducted by exposing grape juice agar plates with a 14-hour over-night collection of eggs sealed with Parafilm to heat shock in a 37 ºC water bath. About 7-11 hours later, selected stage 15/16 embryos were analyzed live or prepared for dissections.

Gal4 driver	Number of hs	Developmental stage of hs	Duration of hs	Flybow transgene	Tissue
elav-Gal4^{c155}	one	Embryonic stages 1-14	60 min	FB1.1	embryos stage 15/16
elav-Gal4^{c155}	one	48 h AEL	45 min	FB1.0	eye-brain complex
elav-Gal4^{c155}	one	48 h AEL	45 min	FB1.0	ventral nerve cord
elav-Gal4^{c155}	one	48 h AEL	45 min	FB1.1	eye-brain complex
elav-Gal4^{c155}	two	48 h & 72 h AEL	30 min	FB1.1	eye-brain complex
elav-Gal4^{c155}	three	48 h, 72 h & 96 h AEL	30 min	FB1.1	eye-brain complex
GMR-Gal4	one	72 h AEL	45 min	FB1.1	eye
GMR-Gal4	two	72 h & 96 h AEL	30 min	FB1.1	eye
MzVum-Gal4	two	48 h & 72 h AEL	90 min	FB1.1	eye-brain complex
repo-Gal4	one	48 h AEL	45 min	FB1.1	eye-brain complex
repo-Gal4	two	48 h &72 h AEL	30 min	FB1.1	eye-brain complex
en-Gal4	one	72 h AEL	45 min	FB1.1	wing imaginal disc
dpp-Gal4	info missing	info missing	info missing	FB1.1	wing imaginal disc
elav-Gal4^{c155}	one	48 h AEL	45 min	FB2.0	eye-brain complex
elav-Gal4^{c155}	one	48 h AEL	90 min	FB2.0	eye-brain complex
elav-Gal4^{c155}	two	48 h &72 h AEL	90 min	FB2.0	eye-brain complex
elav-Gal4^{c155}	one	48 h AEL	45 min	MARCM/FB1.1	optic lobe
elav-Gal4^{c155}	one	48 h AEL	90 min	MARCM/FB1.1	optic lobe
elav-Gal4^{c155}	two	48 h &72 h AEL	90 min	MARCM/FB1.1	optic lobe

Table 2. Clone induction in distinct genetic backgrounds.

2.2 Molecular biology

2.2.1 Standard PCR

PCR was performed to amplify the encoding sequences of: a) *cd8* and *2xlyn* membrane tags, b) *hsp70* and *SV40* polyadenylation stop sequences, c) *EGFP*, *mCherry*, *mCerulean*, *mCitrine* fluorescent proteins and d) *wtFRT-lamin-HA-hsp70Ab/hsp27-wtFRT* cassette. The PCR mix contained 1 µl of 50 ng/µl template DNA, 1 µl of 5' hybridizing primer (100 µM), 1

μl of 3' hybridizing primer (100 μM), 5 μl of 10x PCR Buffer, 1 μl of dNTPs (10 mM), 0.8 μl Taq Polymerase (High Fidelity PCR system by Roche™, Platinum Taq DNA polymerase by Invitrogen™). The reaction was performed as follows:

1) Initial denaturation step at 94 °C for 5 minutes;

30 cycles of steps 2) - 4);

2) Denaturation at 94 °C for 1 minute;

3) Primer annealing at 65 °C for 30 seconds;

4) Elongation at 72 °C for 1 minute (68 °C when Platinum Taq was used);

5) Final elongation step for 10 minutes to terminate the reaction.

5 μl of the PCR products were analyzed by electrophoresis on a 1% agarose gel stained with ethidium bromide.

2.2.2 Gel electrophoresis

Gel electrophoresis was used to allow separation and identification of nucleic acids, based on charge migration. Migration of nucleic acids in a field is determined by size and conformation, allowing nucleic acids of different sizes to be separated. Gels were prepared by dissolving 1-2% (w/v) agarose, depending on the size of DNA to be resolved, in 1X TAE (20 mM TRIS acetate, 1 mM $Na_2EDTA\ 2H_20$, pH 8.5) with 1 mg/ml ethidium bromide. Samples were mixed with 10X Buffer (10X TAE, 50% v/v Glycerol, 0.2% w/v bromophenol blue) and loaded onto the gel alongside a 1kb or 100bp ladder (New England Biolabs) and run at *5-20V/cm-gel length*. Nucleic acids stained by ethidium bromide were visualized with a UV lamp ($\lambda \approx 302$ nm).

2.2.3 PCR on bacterial colonies

The 1.1X ReadyMix™ PCR Master Mix (1.5 mM $MgCl_2$) kit by Thermo Scientific was initially used to screen bacterial colonies according to the manufacturer's instructions. In

parallel, a "PCR on colonies" protocol was established, as follows: Single colonies were selected from the bacterial plate using a sterile inoculation needle. Next, the colonies were suspended in 10 μl of sterile water, by steering with the needle. 5 μl were used in the PCR reaction as template DNA whereas 2 μl of the remaining dilution were streaked out on a new Luria Bertani-ampicillin (LBamp) agar plate. The PCR mix was prepared as described in the 2.2.1 section with the addition of 2 μl of 0.1% Tween20. Finally, the PCR reaction was performed as described in 2.2.1 with the only difference being that an initial denaturation step at 94 °C was carried out for 15 minutes. PCR products were analyzed by electrophoresis of a 1% agarose gel stained with ethidium bromide.

2.2.4 Annealing oligonucleotides

To generate double stranded DNA of a) the modified multicloning site (mMCS) for *pTRCHisB* and *pKC26*, b) the *mFRT71* site and c) the 2xV5 tag the following protocol was performed: An annealing mix was prepared that contained 5 μl of NaCl (5 M), 0.6 μl Tris-HCl (1 M, pH 7.0), 0.87 μl $MgCl_2$ (1 M), 25 μg of each of the oligonucleotides and sterile dH_20 to reach a final volume of 100 μl. The reaction was carried out in a PCR machine under the following conditions: Initial denaturation at 95 °C for 10 minutes, one cycle at 65 °C for 10 minutes, one cycle at 60 °C for 10 minutes, one cycle at 55 °C for 10 minutes, one cycle at 50 °C for 10 minutes, one cycle at 25 °C for 10 minutes. Alternatively, a heat block was used at 75 °C for 10 minutes and then switched off to gradually reach room temperature. Subsequently, 2 ng of the hybridized oligonucleotides were used for ligation with the linearized vector of interest.

2.2.5 PCR and gel band purification

DNA purification from PCR reactions was conducted using the QIAquick PCR Purification kit (Qiagen). In addition, DNA band isolation from an agarose gel was carried out using the QIAquick Gel Extraction Kit (Qiagen) according to manufacturer's guidelines.

2.2.6 DNA quantification

The DNA concentration was determined using a Nanodrop Spectrophotometer to measure the optical density ($Abs_{260/280}$) in the final volume of 1 μl from any given sample.

2.2.7 DNA modifications

2.2.7a Restriction endonuclease digestion of DNA

DNA was digested using restriction endonucleases for use in subsequent cloning steps. This yielded DNA fragments of appropriate size for downstream manipulations. A variety of restriction endonucleases was used from New England Biolabs (NEB) and Roche as described in the Results sections, following manufacturer's guidelines.

2.2.7b DNA ligation

To subclone new plasmids, digested DNA fragments were combined and treated with DNA ligase. The products of the ligation mixture were introduced into competent *E. coli* cells and transformants were identified by appropriate genetic selection. For ligation of DNA fragments, T4 DNA ligase from NEB or Roche was used, according to the manufacturer's guidelines.

2.2.7c DNA dephosphorylation

To prevent linearized DNA vectors from self-ligation and to improve ligation efficiency, phosphatases were used. 5' phosphates from DNA vectors were removed by using calf intestinal phosphatase (CIP) from Roche or antartic phosphatase (AP), according to manufacturer's instructions.

2.2.8 Molecular cloning

Standard cloning methodology was used for the assembly of Flybow constructs as described in Chapter 3. Materials used for cloning are summarized in Table 3 and Table 4 (see appendix). Plasmid purification was performed in each step from liquid bacterial cultures grown at rotating incubators at 37 °C. For screening purposes, the following protocol has been used:

Initially, the bacterial cultures were centrifuged at 5,000 rpm for 5 minutes and the supernatant was aspirated. The pellet was resuspended in 100 µl of P1 Buffer (50 mM Tris-Cl, pH 8.0; 10mM EDTA; 100 µg/ml RNase A); 200 µl P2 Buffer (200 mM NaOH, 1% SDS (w/v)) were added to the mix and incubated for 5 minutes at room temperature, finally 150 µl of P3 Buffer (3.0 M potassium acetate, pH 5.5) were added and the mix was centrifuged at 13,000 rpm for 10 minutes at 4 °C. The supernatant was transferred into a new tube, 900 µl of 100% ethanol (EtOH) were added and the tubes were placed at -20 °C for 30 minutes for precipitation. Samples were centrifuged at 13,000 rpm for 30 minutes at 4 °C. The supernatant was aspirated, 700 µl of 70% EtOH were added and centrifuged for 10 minutes at 13,000 rpm. The supernatant was aspirated and the pellets were left to dry completely. The DNA was resuspended in 50 µl of TE buffer and 5 µl were further used for digestions. Next, when the DNA was used for further cloning steps, sequencing and transfection experiments, protein extraction or fly injections; plasmids were purified using the Mini and Midi Qiaprep Kits (Qiagen) following manufacturer's protocols.

2.2.9 Protein expression in bacteria

A 2 ml liquid culture was grown over-night in a shaking incubator at 225 rpm at 37 °C. 25 µl of the overnight culture were inoculated in 1 ml of LBamp and incubated in the shaker for 90 minutes at 37 °C. Next, Isopropyl-D-1-thiogalactopyranoside (IPTG) was added to a final concentration of 0.1 mM and the culture was incubated for an additional 4 hours. Finally, in the case of fluorescence proteins, 10 µl were placed on a cover slip to visualize fluorescence under a dissecting microscope.

2.2.10 Western blot analysis

Bacterial cultures for the *pTRCHisB-mMCS-1xV5-Cerulean* plasmid were grown as discussed in 2.2.8. Next, the cultures were centrifuged, the supernatant aspirated, the pellet resuspended in 150 µl of the lysis buffer (NuPAGE LDS Sample Buffer (4X), Invitrogen™) and

kept at -20°C overnight. The following day, the lysate was denatured at 95 °C on a thermal block for 5 minutes and DTT was added to a final 1X concentration. Protein extracts were separated by 4-12% SDS-PAGE (NuPAGE Novex Bis-Tris gels, Invitrogen™), transferred on a PVDF membrane (Immobilon-P, Millipore), blocked in 5% low fat milk for 1 hour at room temperature and incubated overnight with anti-V5-HRP antibody (1/5000, Invitrogen P/N 46-0708). Bands were visualized using the ECL™ Western Blotting System (Amersham).

2.2.11 Transient transfection of S2 cells

The plasmids used for transfections of Schneider 2 receptor plus (S2 R+) cells were *pMT/V5-HisA-cd8EGFP-SV40* and *pMT/V5-HisA-cd8-mCitrine-hsp70*. Those were generated by directionally cloning *cd8-EGFP-SV40* and *cd8-mCitrine-hsp70* using KpnI and NotI into the *pMT/V5-HisA* cloning vector.

2.2.11a Culture conditions

Schneider 2 receptor plus (S2 R+) cells were transfected using the Effectine Transfection Reagent (Qiagen). All experiments were performed in 35 mm cell culture plates. $4x10^6$ cells were seeded with standard media in a final volume of 2 ml. Subsequently, 3 round coverslips were placed in each well, and the cells were left to grow for 24 hours in a humidified chamber. A transfection mix was prepared according to the manufacturer's protocol. 1 μg of DNA was initially mixed with 75 μl of EC buffer and 8 μl of enhancer, and incubated for 5 minutes at room temperature. 8.3 μl of Effectine Transfection Reagent was added to the mix and further incubated for 10 minutes at room temperature. Finally, 500 μl of Schneider's *Drosophila* medium (containing 500ml of standard Schneider's medium, 10% fetal calf serum (heat-inactivated), 50 μg/ml Penicillin/Streptomycin and 2mM L-glutamine) was added to the mix and applied to the cells. The cells were incubated with the transfection mix for 24 hours. Expression was induced with 500 μM (final concentration) of $CuS0_4$ 12-24 hours post transfection..

2.2.11b Fixation of cells

Medium was removed and the cells were fixed for 12 minutes in 4% parafomaldehyde (PFA) at room temperature. The cells were then washed with PBS, quenched for 10 minutes in NH_4Cl/PBS and permeabilized with 0.1% TritonX-100/PBS for an additional 10 minutes. Finally, cells were washed 4 times with PBS for 5 minutes. Subsequently, the cells were incubated with TOTO3 (Invitrogen) reagent to stain the nuclei for 15 minutes at room temperature. The cover slips were rinsed with dH_2O and mounted using Mowiol mounting medium.

2.2.12 Immunohistochemistry

Eye-brain complexes of wandering third instar larvae and adult brains were dissected alongside with embryonic and larval ventral nerve cords (VNCs) in phosphate-buffered saline (PBS). Next, they were fixed with 2% paraformaldehyde (PFA), in 0.1M containing L-Lysine monohydrochloride (Sigma), 0.05M sodium phosphate containing buffer (PLP) of pH 7.4 for 1 hour at room temperature and washed 3 times in 0.5% Triton X-100/PBS (PBT). The samples were pre-incubated in 10% normal goat serum (NGS) in PBT for 15 minutes at room temperature and then incubated with the primary antibody (mAb24B10 1:75, anti-V5 antibody 1:500) diluted in PBT, 10% NGS at 4°C overnight. Next, the samples were washed in PBT for 15 minutes, incubated with the secondary antibody for 2.5 hours at room temperature, washed twice in PBT and twice in PBS before embedding in Vectashield (Vector Laboratories).

Embryos from an over-night egg collection at 25 ºC were transferred into a mesh basket and washed with distilled water. Subsequently, they were dechorionated by submerging the basket into undiluted sodium hypochloride solution for 2 minutes and washed thoroughly in distilled water for an additional minute. Live preparations were processed in PBS at this stage. For flat preparations, the dechorionated embryos were transferred into a petri dish with PBS 0.1% Triton X-100. Stage 15-17 embryos were isolated form the collection using gut morphology criteria and dissected with sharpened tungsten needles. The dissection was carried

out using a double-sided adhesive tape dipped in PBS. Next the embryos were transferred onto polylysine-coated slides and incubated for 25 minutes in 4% formaldehyde fixative. Finally, the samples were washed 3 times with PBT and incubated in primary antibody (anti-V5 1:500) diluted in PBT, 10% NGS at 4°C overnight. Following a wash with PBT samples were incubated with secondary antibody for at least 2 hours.

Primary antibodies used in this study were: mAb24B10 (1:75; Developmental Studies Hybridoma Bank), mouse anti-β-Galactosidase (1:1000; Promega) and mouse-anti V5 (1:500; Invitrogen). AlexaFluor® 546 conjugated goat-anti mouse IgG (H+L)(1:500; Invitrogen) and goat anti-mouse F(ab')2 fragments coupled to Cy5 (1:200; Jackson ImmunoResearch Laboratories) were used as secondary antibodies.

2.3 Image acquisition and analysis

2.3.1 Confocal microscopy

Samples generated using *FB1.0* transgenes were imaged with an upright Zeiss/Radiance 2100 confocal laser-scanning microscope. A 40x oil immersion objective with digital zoom of 1.7 was used to collect all the data. Images were acquired using a 543 nm argon laser line to image mCherry (laser power ~60%) and a 633 nm laser (laser power 100%) to image V5 tagged-Cerulean visualized with anti-V5 primary and Cy5-coupled secondary antibodies. Images were acquired at 1024x1024 pixel resolution and averaged 3 times.

All other images were acquired using a Leica TCS SP5 upright confocal microscope equipped with a resonance scanner. The lenses used in this confocal set up were a 20x (0.7 NA) air objective or 40x (1.25 NA) and 100x (1.46 NA) oil objectives. Digital zoom was applied when necessary. Stacks of images were collected using: a 488 nm argon laser line for EGFP (acousto-optical beam splitter [AOBS] setting: 490-515 nm), a 514 nm argon laser line for mCitrine (AOBS settings: 525-565 nm), a 561 nm DPSS laser for mCherry (AOBS settings: 572-639 nm), and a 633 nm HeNe laser for V5 tagged-Cerulean visualized with anti-V5 primary and Cy5-coupled secondary antibodies (AOBS settings: 650-711 nm). Endogenous Cerulean fluorescence was tested with 405 nm DPSS and 457 nm argon laser lines. mCitrine

and Cerulean-V5 channels were imaged simultaneously, while signals of EGFP and mCherry channels were collected sequentially. Details of the sequential scanning set up are summarized in Table 5. Imaging of all samples was performed using these conditions; however adjustments to the laser power were necessary at times, depending on the strength of the *Gal4* driver used or the sample quality. Although not essential, the use of the resonance scanner helped to increase the speed of image acquisition of large z stacks and to minimize photobleaching. All samples were averaged 96 times when using the resonance scanner and the images were acquired at the fixed speed of 8 kHz.

Image acquisition set up	Laser lines	AOBS settings	Detector
Scan 1	514 (25%)	525-565 nm	PMT2
	633 (25%)	674-735 nm	PMT4
Scan 2	561 (25%)	572-639 nm	PMT4
Scan 3	488 (20%)	490-515 nm	PMT1

Table 5. Image acquisition set up. A sequential scanning method was used to collect the signals from all fluorophores.

2.3.2 Channel separation and image processing

Images were subjected to the Leica LAS AF suite channel separation tools to further separate the spectra of the four fluorescent proteins. Reference points of the collected signal for each of the four channels were allocated manually. Caution was taken when assigning the true signal reference points in order to maintain a good saturation/mean intensity balance. Finally, the software provided separated fluorescent signal, for each of the four fluorescent proteins. Volocity (Improvision PE) and ImageJ (Fiji) software were used to analyze or project images within z-stacks of confocal images to facilitate the tracing of neurons and glial cell processes. EGFP, mCitrine, mCherry and Cerulean-V5 were displayed in green, yellow, red and blue, respectively.

2.4 Quantifications

Cell bodies of neurons expressing the four FPs were counted using the ImageJ (Fiji) software counting tools. Total numbers of neurons per fluorophore were obtained after summing up the number of cells in three non-consecutive z sections of 10 optic lobes.

Fluorescence intensity measurements were performed using ImageJ (Fiji) software, Measurements were obtained form identical surface areas, using the area selection tools of the software. Background fluorescence signal was measured similarly. Values for the highest and mean intensity values were obtained. True signal measurements were retrieved by subtracting measurement for background signal, from the equivalent signal measurements we obtained for the individual fluorescent protein.

Values for standard deviation (SD), standard error of the mean (SEM), two-tailed t-test, and confidence interval (CI) were calculated for each data set using Excel (Microsoft Office Suite).

Chapter 3

Building “Flybow”

3.1 Introduction

To facilitate our studies of the molecular mechanisms that direct formation of neural networks, we generated a new genetic approach, called Flybow (FB). FB is based on the second variant of the "Brainbow System", *Brainbow-2* (Livet et al., 2007). Similar to the vertebrate approach, this tool uses DNA recombination to achieve stochastic expression of fluorescent proteins with distinct spectral properties. Brainbow employs the binary Cre/*loxP* system to induce recombination events. Site-specific tyrosine DNA recombinases, such as Cre and Flp characteristically mediate their action by successively binding, nicking, exchanging and re-ligating their target sequences (Anastassiadis et al., 2010; Branda and Dymecki, 2004; Coates et al., 2005) (section 1.3). *Brainbow-2* transgenes make use of the inherent ability of Cre recombinase to catalyze different outcomes according to the orientation of the *loxP* sites (Branda and Dymecki, 2004; Coates et al., 2005) (section 1.3.3).

3.2 Adapting the tool for *Drosophila*

Flybow was designed for use in *Drosophila* studies and, thus, should preferably take advantage and complement the array of available genetic tools. Our approach employs the binary *Gal4/UAS* system (Brand and Perrimon, 1993) for transgene expression. Therefore, Flybow can be combined with the plethora of available *Gal4* lines and should find applications in genetically accessible subpopulations of cells in any tissue of interest. The Cre/*loxP* system was used successfully to induce recombination of *Brainbow* transgenes. The same binary system is available in *Drosophila* (Siegal and Hartl, 1996) and has been reported to induce recombination events very efficiently. High levels of recombination using Cre recombinase have however been shown to cause toxicity partly due to recognition of cryptic *loxP* sites found endogenously in the fly genome (Heidmann and Lehner, 2001). In contrast, the yeast-derived Flp/*FRT* system has revolutionized fly genetics in the last (nearly two) decades (Golic and Lindquist, 1989; Lee and Luo, 1999). Importantly, using a heat-shock promoter provides the system with tightly regulated spatio-temporal control of expression. Finally, taking also into consideration that only a few inducible Cre lines are available, we chose to base Flybow on a Flp/*FRT* recombination

system. Collaborating with Shay Rotkopf and Barry Dickson we aimed to develop a modified Flp/*FRT* system that would show similar efficiency of recombination and minimal cross-reactivity with the classical system. In this way, our approach will still be able to be combined with other Flp/*FRT* based tools and facilitate gene functional studies.

3.3 Choosing a modified Flp/*FRT* system

Shay Rotkopf tested four novel Flp recombinases in combination with three pairs of modified *FRT* variants. These enzymes were engineered to recognize optimally modified target sequences as previously shown in bacterial assays (Voziyanov et al., 2003) (Voziyanov et al., 2002). He further sought to verify that the modified systems preserve their specificity when used in *Drosophila*. The three pairs of altered *FRT* sites namely *mFRT11*, *mFRT71* and *mFRT11-71,* include single mutations at positions 1 and 7 or both respectively (Figure 5). Four modified Flp variants containing different amino acid changes (Figure 5e) were named mFlp4, 5, 6 and 7. The coding sequences of the classical and the new Flp recombinases were placed under the control of the eye-specific enhancer fragment of the *eyeless* (*ey*) gene (4 copies of a 258bp sequence; nucleotides 2549-2806) (Newsome et al., 2000). The specificity and efficiency of recombination events were determined in third instar larval eye discs using Flp-out transgenes expressing nuclear β-Galactosidase under the control of the *act5C* enhancer. A *α-tubulin 3'UTR* stop cassette was flanked by pairs of wild type or modified *FRT* sites. All twenty combinations of a recombinase with *FRT* sites were examined. Monitoring of β-Galactosidase-positive areas showed that the wild-type Flp recombinase catalyzes specific recombination of *FRT* sites with 100% efficiency, but does not recognize any of the modified *FRT* sites (Figure 5e). The only modified pair showing both high recombination efficiency and specificity, and no cross reactivity with wild type FRT, consisted of mFlp5 and *mFRT71*. Hence, the mFlp/*FRT* system can be employed for the FB strategy and at the same time combined with canonical Flp/*FRT*-based genetic approaches. The *hs-mFlp5* construct was assembled using a vector containing the heat-inducible *hsp70Aa* promoter and transgenic flies were established.

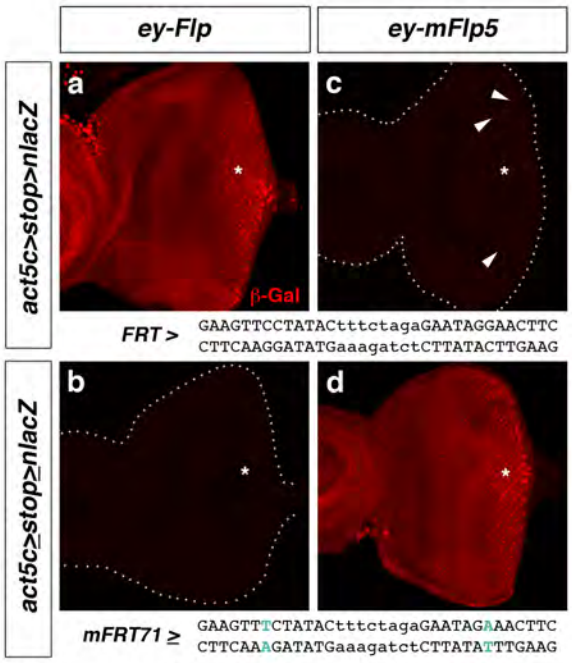

e % recombination efficiency

	Flp	mFlp4 K82Y, V226A	mFlp5 R281V	mFlp6 A36T, T50A K82Y, G109N E150G, R281V	mFlp7 A36T, T50A K82Y, G109N T176A, R281V
FRT	100	28.3 ± 3.6	0.7 ± 1.5	0.2 ± 0.4	0
mFRT11	0	100	0	0	0
mFRT71	0	0	100	0.9 ± 1.1	8.0 ± 6.7
mFRT11-71	0.03 ± 0.07	0	0	17.4 ± 8.6	67.2 ± 9.2

n = 5-8/genotype

Figure 5. Recombination specificity and efficiency of the mFlp5/*mFRT71* system.

Flies expressing new modified versions of Flp recombinase (mFlp4-7) and the wild-type Flp were placed under the control of the *eyeless* (*ey*) enhancer and crossed to *act5c>α-tub 3'UTR >nlacZ* lines. These stop cassettes were flanked either by pairs of wild-type or modified *FRT* sites (*mFRT11*, *mFRT71* and *mFRT11-71*). Inverted repeats are shown in upper case and asymmetric spacer regions in lower case letters. Single base pair changes are highlighted in blue. The orientation of symbols > and ≥ indicate the polarity of wild-type *FRT* and *mFRT71* sites, respectively. Third instar larval eye imaginal discs were labeled with anti-β-Galactosidase (β-Gal, red). Asterisks indicate the eye field. Flp efficiently excises the stop cassette flanked by wild-type *FRT* sites (a and e), but does not recognize *mFRT71* sites (b and e), mFlp5 mediates very low levels of recombination between wild-type *FRT* (arrowheads) (c and e), but is highly efficient for *mFRT71* sites (d and e). Summary of recombination efficiency of wild-type and modified Flp proteins tested with four different pairs of *FRT* sites (e) Data provided by S. Rotkopf and B. Dickson.

3.4 General features of Flybow variants – an overview

Target sequences for Flp recombinases typically include two 13 bp inverted repeats separated by an asymmetric 8 bp spacer (Figure 5). The spacer establishes the inherent directionality of the *FRT* sites. As we chose to base Flybow on the Brainbow-2 approach we aimed at using repeats of a single type of recombination site. Therefore, direct repeats of m*FRT71* sequences located on the same chromosome would lead to excisions of the flanked sequences, whereas inverted repeats should lead to inversions. Fluorescent protein encoding sequences were arranged in opposing orientations in pairs. Each pair constituted a cassette flanked by inward facing *mFRT71* sites (Figure 6a) and could therefore be inverted, (invertible cassette). Placing two cassettes directly after one another, excision cassettes could also be formed (flip-out cassette) because of *mFRT7*1 sites facing in the same direction (Figure 6b and c). Two different polyadenylation signals (*SV40* and *hsp70Ab*) followed each of the fluorescent protein cDNAs within the invertible cassette. As a result, only the fluorophore's coding sequence found closest to the *UAS*-sequence can be expressed.

The final constructs were subcloned into the *pKC26* (Dietzl et al., 2007) vector. This vector contains 10 UAS sites for stronger Gal4 induced expression instead of the commonly used 5 UAS sites. In addition, *pKC26* includes an *attB* recombination site that allowed us to use the site-specific ϕC31 integrase for inserting the transgenes into precise genomic loci on the second or third chromosomes. These loci have been used to generate transgenic lines that only show transgene expression in the presence of Gal4 (B.J. Dickson, Vienna collection and (Dietzl et al., 2007). Moreover, *pKC26* also contains the 5' part of the *mini-white* sequence instead of the full *mini-white* gene. At the same time, the *attP* docking site containing vector (*pKC43 attP202 w*3'), used to generate the transgenic lines, includes the 3' part of the *mini-white* sequence. Therefore, only the accurate integration of the *pKC26* plasmid can reconstitute the *mini-white* coding sequence and result in the characteristic dark red eye pigmentation. In this manner, transformants can be rapidly identified. Making use of the "split-white" approach (Bischof et al., 2007) *pKC26* remains small in size and suitable for cloning large DNA fragments and for fly transgenesis. To facilitate the generation of Flybow containing plasmids we modified the multiple cloning site of *pKC26* (see section 3.5.1).

Four fluorescent proteins were chosen for use based on their previously reported properties (Rizzo et al., 2004; Shaner et al., 2004; Shaner et al., 2007; Shaner et al., 2005) that enhance their fluorescence properties. Similarly to Brainbow-2, members of the green, yellow, red and cyan fluorescent proteins were selected: namely, enhanced GFP (EGFP), monomeric (m) Citrine, mCherry and Cerulean. Endogenous expression of all proteins could be visualized. However, Cerulean showed low levels of fluorescence intensity and was therefore tagged with a V5 epitope for signal amplification after immunostaining (see section 4.3). Making the tool optimal for visualization of delicate structures such as neurite extensions and filopodia, we aimed to attach all four proteins to the membrane. Two different membrane anchors were chosen: the Cd8a (cd8) (Liaw et al., 1986) or the Lyn kinase derived palmitoylation-myristoylation (Zacharias et al., 2002) (pm) localization signal

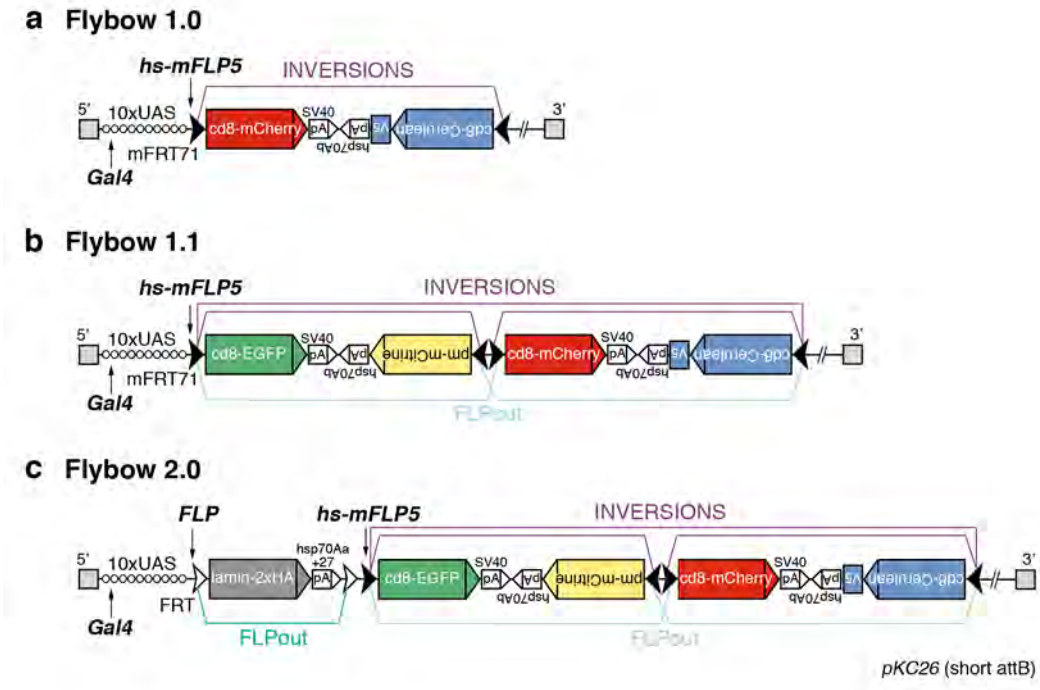

Figure 6. Schematic of *Flybow* variants.

Pairs of fluorescent protein (FP) encoding cDNAs are arranged in opposing orientations and flanked by *mFRT71* sites (black arrowheads). FPs were tethered to the membrane using either a Cd8a (cd8) or the myr/palm (mp) sequence of Lyn kinase. FP sequences are followed by *SV40* and *hsp70Ab* polyadenylation (pA) signals. Constructs were subcloned into a modified *pKC26 UAS*-vector, which contains 10 *UAS* sites and a short *attB* recognition sequence. mFlp5 under the control of the *heat shock*

promoter (*hs-mFlp5*) induces inversions of DNA cassettes by recombining m*FRT71* sites in opposing orientations, or excisions (Flp-out) by recombining *mFRT71* sites in the same orientation. (a) *Flybow 1.0* consists of one invertible cassette encoding two FPs (*mCherry* and *Cerulean*). (b) *Flybow 1.1* contains two invertible cassettes, each encoding two FPs (*EGFP* and *mCitrine*; *mCherry* and *Cerulean* tagged with V5). (c) *Flybow 2.0* contains an additional stop cassette, flanked by canonical *FRT* sites (white arrowheads) facing in the same orientation, which can be excised by wild-type Flp. The stop cassette consists of *lamin* cDNA, followed by two *HA* tag sequences and *hsp70Aa* and *hsp27* polyadenylation signals.

Flybow 1.0 (*FB1.0*) was primarily designed for testing as to whether inversions of sequences flanked by inward facing *mFRT71* sites could be mediated by mFlp5. This transgene consists of a single cassette and includes the encoding sequences for mCherry and Cerulean-V5 placed in opposing orientations (Figure 6a). **Flybow 1.1** (*FB1.1*) contains an additional cassette located closest to the 3' end of the *UAS* sites and comprises the coding sequences for EGFP and mCitrine. Finally, **Flybow 2.0** (*FB2.0*) includes an extra stop cassette to the *FB1.1* version, that consists of *lamin* cDNA followed by polyadenylation signals and was built in the B. J. Dickson laboratory. This cassette is flanked by a pair of canonical *FRT* sites and can only be excised in the presence of the widely used canonical Flp recombinase.

3.5 The cloning strategy

3.5.1 Building the modified vectors

Key to the planned strategy was to build four basic modules (see section 3.5.2) that could serve as unique interchangeable units. These would then be subcloned sequentially into the *pKC26* vector in a defined order for the assembly of the final Flybow transgenes. The *pTRCHisB* vector (Invitrogen™) was chosen as the starting vector for cloning of the basic modules, a plasmid used to express high levels of recombinant proteins (Pfeiffer et al., 2002) kindly provided by Willy Joly. However, the existing multicloning site (MCS) of both *pTRCHisB* and *pKC26* vectors were not suitable for the specific needs of our planned cloning strategy. To overcome this limitation, we designed new MCSs and exchanged them with the existing ones. The new

mMCS of *pTRCHisB* consisted of the following series of enzyme restriction sites along with the *mFRT71* sequence: NheI, BglII, KpnI, XhoI – *mFRT71* – SpeI, BamHI, AvrII, NotI, SacI, HindIII (Figure 7). Similarly, a succession of target sequences for selected restriction enzymes constituted the new MCS in the case of the *pKC26* vector as follows : EcoRI, NheI, BglII, SacI, KpnI, NotI, XhoI, XbaI (Figure 7b). Both new MCSs were generated by annealing complementary oligonucleotides to obtain double-stranded DNA fragments with 5' phosphorylated overhangs.

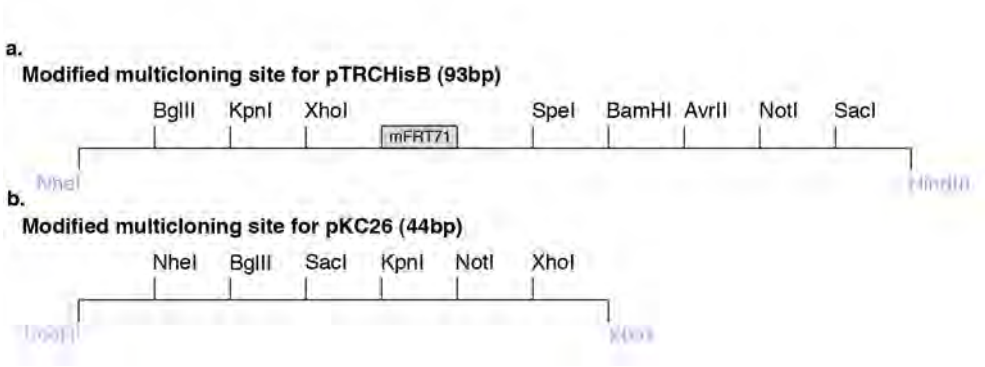

Figure 7. Modified multiple cloning sites for *pTRCHisB* and *pKC26* vectors.
(a) NheI and HindIII were used for digestion of *pTRCHisB* vector to remove the original MCS. The newly generated 93 bp double stranded sequence constituting the mMCS, contained 5' phosphorylated overhangs that could be directly ligated into the linerized *pTRCHisB* plasmid. (b) EcoRI and XbaI were used in the same manner to linearize the *pKC26* vector. Ligation of the 44 bp long double stranded sequence resulted in the generation of the modified *pKC26* vector suitable for assembling *Flybow* constructs.

While subcloning the modified MCSs into their respective vectors (resulting vectors: *pTRCHisB-mMCS* and *pKC26-mMCS*), several problems were successfully resolved. The mMCS for the *pTRCHisB* vector contained tandem palindromic sequences due to the presence of the *mFRT71* site, likely causing the recombination of secondary DNA structures. Initial attempts of cloning therefore yielded faulty mMCSs with numerous gaps and nucleotide changes. Better results were obtained by adjusting the parameters of the annealing protocol, i.e. the concentration of oligonucleotides and vector, annealing buffers, and the temperature steps used for denaturation and subsequent annealing of oligonucleotides. Although some gaps were found throughout the mMCS, they were most frequently located within the *mFRT71* sequence. Sequencing analysis of one of the clones showed that all the restriction enzymes recognition

sites within the mMCS were correct, nevertheless gaps were still present within the *mFRT71* site. Making use of this plasmid, digestion by XhoI and SpeI (Figure 7a) removed the mutated *mFRT71* sequence. A new set of primers (*FB26* and *FB27*, Table 3) containing only the *mFRT71* sequence flanked by the XhoI and SpeI recognition sites was generated. These primers were annealed using the previously optimized annealing protocol and then subcloned into the *pTRCHisB* vector to replace the incorrect *mFRT71*. An additional difficulty was that the insertion efficiency was extremely low. Thus, a high number of bacterial colonies were screened to identify the ones, in which the mMCS fragments were correctly inserted into the plasmids (28 of approximately 1300 screened colonies, 2.1% success rate). Identification of such colonies was accelerated by using direct PCR amplification on bacterial colonies, instead of plasmid purification from liquid mini-cultures, grown over-night and verification with restriction enzyme digests (see section 2.2.3). Although inserted mMCSs were eventually confirmed as correct using restriction enzyme digests for all sites, sequencing results indicated that there were still point mutations and single nucleotide gaps present within the *mFRT71* locus. However, these defects were eventually attributed to errors caused by the applied standard sequencing conditions, and were overcome by making use of protocols adapted to sequence DNA with secondary structures provided by Cogenics™and Geneservice™.

3.5.2 Building the basic modules

Each of the basic modules includes the *mFRT71* site, a coding sequence of one of two membrane anchors (Cd8a (Liaw et al., 1986; Zamoyska et al., 1985): amino acids 1-220; or the pm signal of Lyn kinase: MGCIKSKRKDNLNDDE, (Zacharias et al., 2002), one of four FP encoding sequences (*EGFP*, *mCitrine*, *mCherry* and *Cerulean*) and one of two polyadenylation stop signals (*SV40*: bp 4751-5601 from *pUAST* (Brand AH, 1993); *hsp70Ab*: bp 44-472 from *pCasPeR-hs* (Figure 8). All individual fragments were amplified by PCR using primers that added the 5' and 3' restriction enzyme sites required for cloning. Next, the amplicons were inserted into the *PCRII* or *PCR 2.1-TOPO* vectors (Invitrogen™) by TA cloning. This intermediate step was used to generate plasmids (*PCR-TOPO-cd8a, -pm, -EGFP*, *-mCitrine*, -

mCherry, *-Cerulean, -SV40, -hsp70*) that could serve as stable sources of the fragment of interest for future cloning. Finally, the different inserts were subcloned into the modified MCS of the *pTRCHisB* vector in three successive steps. These included subcloning (1) of sequences encoding a membrane tag (2) of polyadenylation signal sequences and (3) of sequences encoding the four fluorescent proteins.

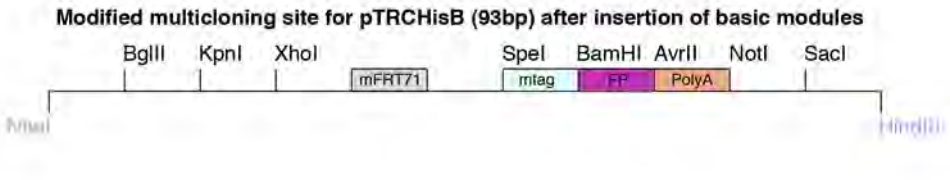

Figure 8. Basic sequence modules used to build *Flybow* transgenes.
Each basic module included one of two sequences encoding a membrane localization signal (mtag) illustrated by the cyan box. SpeI and BamHI were used to directionally subclone (5'-3') mtags into *pTRCHisB-mMCS*. The ochre box represents polyadenylation sequences (one of two) subcloned using AvrII and NotI restriction endonucleases (5'- 3'). Sequences encoding fluorescence proteins (FP, one of four) shown as the magenta box were inserted into respective vectors using BamHI and AvrII.

Sequences encoding membrane anchors were placed into the *pTRCHisB-mMCS* vector using SpeI and BamHI (resulting vectors: *pTRCHisB-mMCS-cd8* and *pTRCHisB-mMCS-mp*). In my initial strategy, the same membrane tag was used in all four modules and, therefore, they were all built using the Cd8a anchor. However, due to cloning difficulties discussed below (section 3.8), the palmitoylation-myristoylation signals for membrane anchoring were used in the case of the mCitrine module instead. The use of the same membrane anchor in all four modules was not possible likely because the similarities of the reiterated sequences caused recombination events in different bacterial strains tested for cloning; these included TOP10, DH5α, Stbl2, SURE, IVaF'.

The polyadenylation signals were inserted using AvrII and NotI (resulting vectors: *pTRCHisB-mMCS-cd8-SV40* and *pTRCHisB-mMCS-cd8-hsp70*). Finally, FP sequences were

added using BamHI and AvrII resulting vectors: *pTRCHisB-mMCS-cd8-EGFP-SV40*, *pTRCHisB-mMCS-cd8-mCitrine-hsp70*, *pTRCHisB-mMCS-cd8-mCherry-SV40, pTRCHisB-mMCS-cd8-Cerulean-hsp70*). An additional step was required for the completion of the Cerulean expressing module. The planned strategy included the addition of two C-terminal V5 tags to the Cerulean protein. This proved to be challenging and three different cloning approaches were employed for its successful completion (Figure 9). Initially, *Cerulean* cDNA was amplified by PCR using primers (*FB19*/*FB20* and *FB21*, Table 3) that introduced a PstI enzyme restriction site at the 3' end of the sequence. After cloning this fragment into the modified *pTRC* vector, PstI would then be used with AvrII for inserting the coding sequence of the 2xV5 tag. Subcloning this amplicon into the *pTRCHisB-mMCS-cd8-hsp70* vector, as well as TA cloning was attempted unsuccessfully. Next, we designed a new strategy that used a new primer (*FB28*, Table 3) for PCR. This primer (5'->3') comprised the 24bp at the 3'end of *Cerulean* cDNA followed by a V5 coding sequence and an AvrII restriction site. The desired fragment was successfully amplified and used for TA cloning. However, none of the screened bacterial colonies contained the correct construct. In addition, we attempted direct subcloning of the amplicon into the *pTRCHisB-mMCS-cd8-hsp70* vector. Restriction enzyme digest patterns indicated that a positive clone was obtained using this strategy. However, sequencing revealed 6 single nucleotide mutations when compared to the expected sequence. Finally, the third strategy required the design of three new primers (*FB29, FB30, FB31*, Table 3). *Cerulean* was amplified by PCR using *FB15* and *FB29*. *FB29* recognizes the 3' end of *Cerulean*, introduces a 3' AvrII recognition site and also removes the stop codon. The PCR product was successfully inserted into the *TOPO2.1* vector and was further subcloned directionally using BamHI and AvrII into the *pTRCHisB-mMCS-cd8a-hsp70*. Next, the resulting vector was linearized using the AvrII restriction enzyme. At the same time, a single V5 tag was generated by annealing two highly complementary oligonucleotides (*FB30* and *FB31*). The resulting double stranded DNA included single stranded overhands able to ligate to the linearized *pTRCHisB-mMCS-cd8-cerulean-hsp70* vector. The 5' AvrII site was mutated and therefore destroyed upon ligation, while the 3' AvrII site remained intact. Finally, to verify that one V5 epitope is sufficient for recognition using the anti-V5 antisera, recombinant protein was purified from bacterial lysate

and used in a western blot experiment. This analysis confirmed that the anti-V5 antibody (Invitrogen™) can recognize specifically a single V5 epitope (Figure 10).

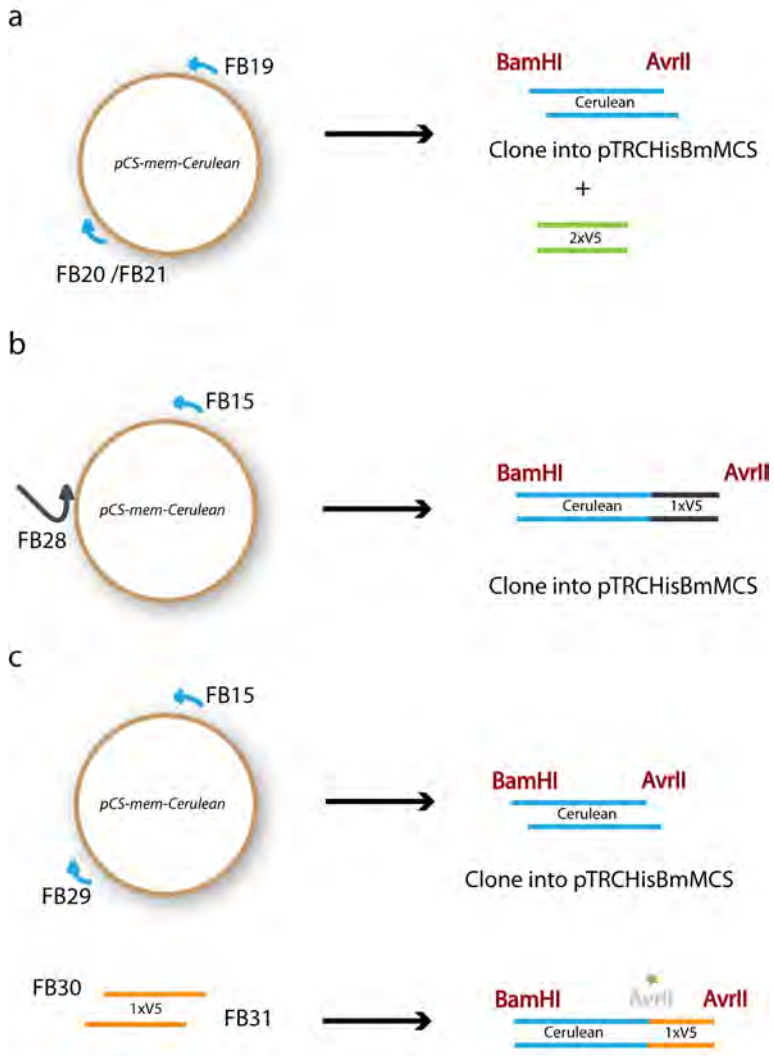

Figure 9. Strategies used to complete the Cerulean expressing module.

Schematic drawing summarizing the three strategies employed to generate the *pTRC-mMCS-cd8a-Cerulean-V5-hsp70* module (a-c).

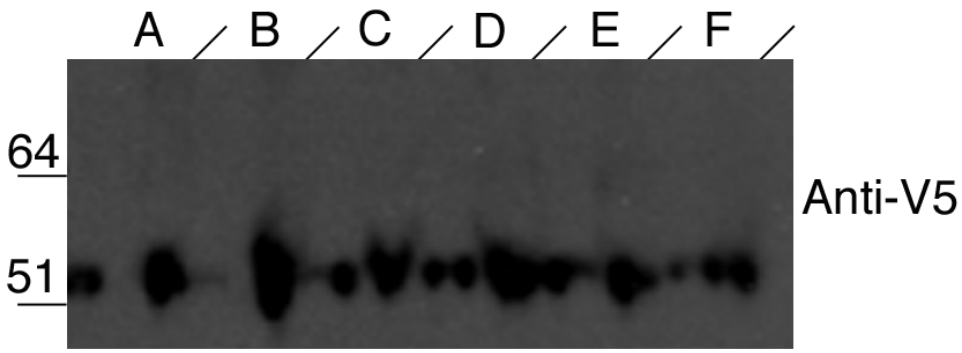

Figure 10. Western blot analysis for Cerulean fusion-protein.
Six lanes (A-F) were loaded with the cd8-Cerulean-1xV5 recombinant protein isolate from bacterial lysates. The single V5 epitope was specifically recognized by a HRP conjugated anti-V5 antibody (Invitrogen™). Predicted bands of approximately 52 kDa were visible using 15 minutes exposure of the film.

3.6 Expression of individual membrane-tethered fluorescent proteins in bacteria

To ascertain that recombinant fluorescent proteins are functional, bacterial strains bearing the constructs of individual modules were cultured in the presence of Isopropyl β-D-1-thiogalactopyranoside (IPTG) to induce expression. The *pTRCHis* vector allowed us to directly evaluate the quality of constructs by monitoring fluorescent protein expression in bacterial colonies. Protein expression was examined on bacterial plates under a fluorescence dissecting microscope equipped with filters for the four fluorescent proteins we used; namely GFP, YFP, mCherry and CFP (Figure 11).

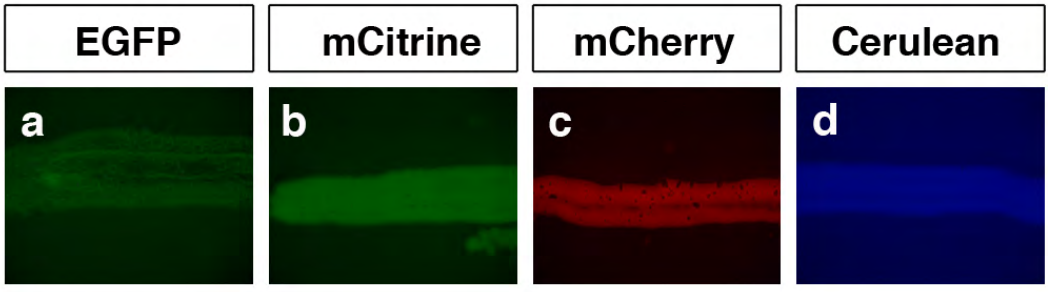

Figure 11. Direct screening for fluorescent protein expression in bacterial colonies.
Bacterial strains (TOP10, Invitrogen™) were cultured on agar plates in the presence of IPTG. In all cases, (a-d) fluorescence was observed using suitable filters: a) EGFP b) YFP c) mCherry and d) CFP. Images were acquired using a camera fitted to the dissecting microscope (Leica).

To verify correct localization of fluorescent proteins at the membrane, we monitored their expression in a cell culture experiment. EGFP and mCitrine expressing modules were used as they both contain the Cd8a membrane anchor, but utilize different polyadenylation signals. Initially, the *cd8-EGFP-SV40* and *cd8-mCitrine-hsp70* sequences were subcloned into the *pMT/V5*-His vector (Invitrogen™) using KpnI and NotI restriction enzymes. Next, the two resulting vectors were used for transient transfection of Schneider 2 receptor plus (S2R+) *Drosophila* cells. Inducible expression of these transgenes was achieved after exposure of the culture to $CuSO_4$. In this way, dosage dependent control of expression yielded good survival rates of the transfected cells. S2R+ cells are able to adhere to the cultured surface (Yanagawa et al., 1998) and are therefore easy to use in preparations suited for confocal imaging. In conclusion, we observed fluorescence localized to the membrane for both constructs (Figure 12). Importantly, the fluorescence was maintained in the fine cellular protrusions confirming that our recombinant proteins were suitable for use when reconstructing cells with complex cellular architecture.

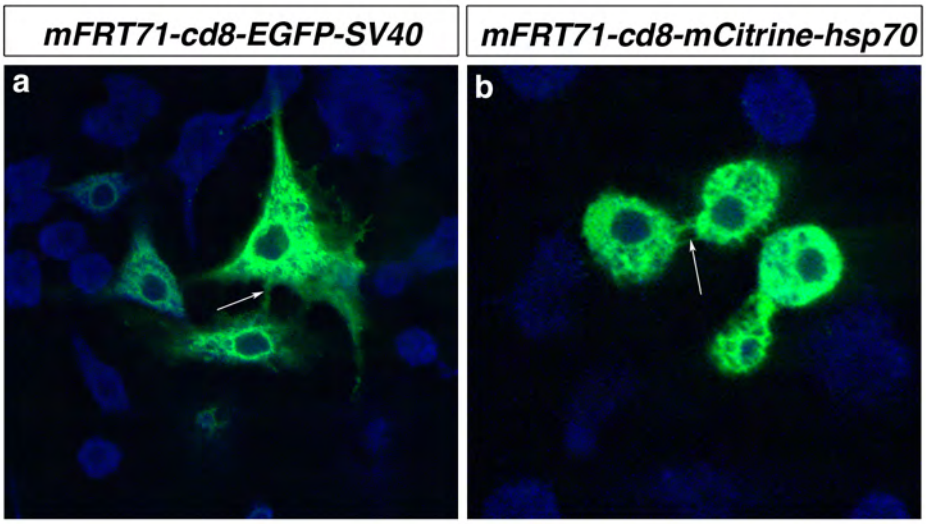

Figure 12. Membrane localization of recombinant fluorescent proteins in Schneider 2 R+ cells.
(a, b) S2R+ cells were transfected with vectors encoding recombinant EGFP (a) and mCitrine (b) proteins. Fluorescence was detected in the membrane of cells. Expression was maintained in fine cellular protrusions (arrows). Nuclei shown in blue were stained with TOPO3 (Invitrogen™).

3.7 Pilot transgenesis using *UAS-cd8-mCherry*

To confirm that all the components used in building our system were functional *in vivo*, another set of experiments was performed. The *mFRT71-cd8-mCherry-SV40* module was subcloned using KpnI and NotI into the *pKC26-mMCS* vector. The resulting *pKC26-mMCS-mFRT71-cd8-mCherry-SV40* plasmid included an *attB* site and was used for injections. Two different lines containing *attP* landing sites were employed (Groth et al., 2004). The first line bears an *attP* insertion on the left arm of the second chromosome (*VIE-260b*, 2L) at the 5' end of the *CG33987* locus, whereas in the second line the *attP* site is located on the right arm of the third chromosome (*VIE-57b*, 3R) in a not further characterized location. Males from these lines were crossed with *ϕC31* integrase expressing females. The latter bear an insertion of *vas-ϕC31* on the X chromosome, which serves as an endogenous germ line source of the integrase (Bischof et al., 2007). The progeny of this cross was injected with the *pKC26-mMCS-mFRT71-cd8-mCherry-SV40* vector and independent transformant lines were established for the 3R insertion (Line 5_1) and for the 2L insertion (Lines 4 and 60). Finally, transformants were crossed with

elav-Gal4^{c155} to evaluate the expression of the transgene in all neurons, and with *pGMR-Gal4* to visualize the expression selectively in R-cells**.** Expression of mCherry was observed in all neurons of the first instar larval ventral nerve cord using *elav-Gal4*^{c155} and specifically in all R-cells in the third instar larval brain when using *pGMR-Gal4*. Strong staining was detected both in third instar larvae and adults in the membrane of fine neuronal processes (Figure 13).

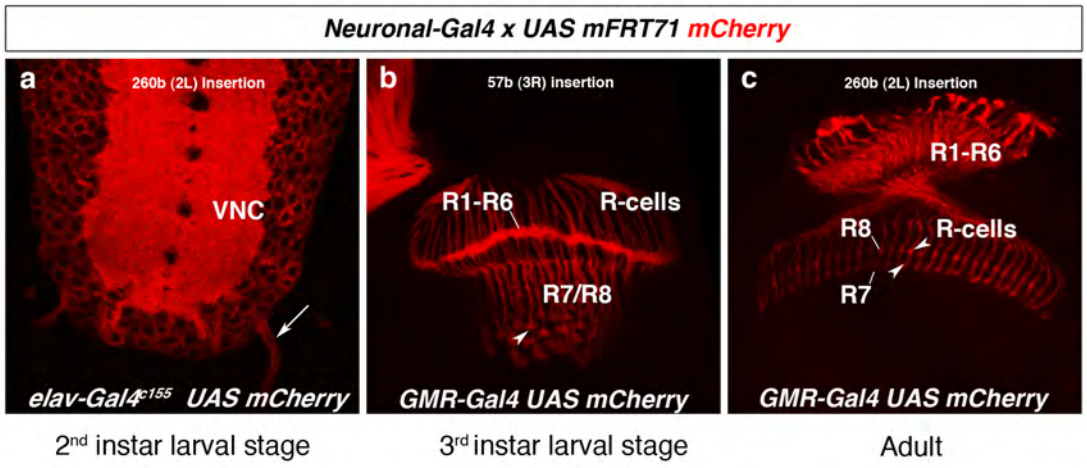

Figure 13. Visualizing mCherry expression in the developing fly nervous system.

Newly generated transgenic flies carrying the *UAS-mFTR71-cd8-mCherry* fragment on either the 2nd (2L, 260b) or 3rd (3R, 57b) chromosome were crossed with *Gal4* expressing lines specific for the neurons (*elav-Gal4*^{c155}) or photoreceptors (*GMR-Gal4*) (a-c). Expression of mCherry was monitored at larval and adult stages. (a) Abdominal segments of the ventral nerve cord (VNC) and peripheral axon bundles (white arrow) show no abnormalities in their morphology following to overexpression of the mCherry variant in the entirety of the nervous system. *elav-Gal4*^{c155}*/+ or Y ; UAS-mFRT71-cd8-mCherry* ^{260b}*/+*. (b-c) Photoreceptor cells (R-cells, R1-R8) in eye brain complexes of third instar larvae (b) and adult optic lobes (c) were visualized employing *GMR-Gal4* for mCherry expression. mCherry was evenly localized in the membranes of axonal processes and able to label fine cellular structures in the developing and adult R-cell target field (arrowheads, b-c). *yw/+ or Y*; *GMR-Gal4/+;UAS-mFRT71-cd8-mCherry*^{57b}*/+*, *yw/+ or Y*; *GMR-Gal4 UAS-mFRT71-cd8-mCherry*^{260b}*/+*.

3.8 Assembling Flybow variants

The completed modules were then sequentially inserted into the *pKC26-mMCS* vector. Making use of the new MCS (Figures 7b and 14), each of the four modules was subcloned into the modified vector in a specific order (Figure 14). The *Flybow 1.0* (*FB1.0)* variant was generated in two cloning steps. First, the *Cerulean*-containing module was inserted into the modified

pKC26-mMCS vector in a 3'-5' orientation using XhoI and NotI restriction enzymes. Next, the *mCherry*-expressing module was subcloned in a 5'-3' orientation by using KpnI and NotI.

To generate *FB1.1,* next the *mCitrine*-bearing fragment needed to be subcloned into the *FB1.0* transgene using KpnI and SacI in a 3' to 5' orientation. This proved to be particularly challenging due to the occurring bacterial recombination. Opposing *mCherry* and *mCitrine* modules contain highly similar sequences. As all modules, they bear an *mFRT71-cd8* sequence on their 5' end followed by the cDNA of their respective fluorescent protein. Additionally, the encoding sequences for EGFP, mCitrine and Cerulean are very similar (approximately 98% identical), as they are all derivatives of the original GFP. mCherry is a derivative of a different fluorescent protein (DsRed) but shares sequence fragments with the GFP-derived proteins, in its 5' and 3' termini (7 N- and C- terminal aa). These terminal sequences were artificially added to mCherry by protein engineering to enhance its fluorescence properties (Shaner et al., 2004). Thus, attempts to subclone the *mCitrine* module created an inverted repeat positioned face-to-face. To circumvent the potential problem of bacterial recombination, several approaches were undertaken. Different strains of bacteria (TOP10, DH5α, Stbl2, SURE, IVaF') were tested for cloning. The various bacteria strains were mutant for distinct recombinases. In addition, we tried to improve the bacterial culture conditions. Both plate and liquid cultures were grown at lower temperatures (30 °C instead of 37 ºC) and for a shorter time period (4-7 hours) to reduce the activity of the existing recombinases. Furthermore, different media were used since poor media are reported to contribute to a reduction in recombination (Wood, 1973). None of these strategies made a substantial difference. After screening of hundreds of colonies, we moved to alternative strategies.

Firstly, we aimed to build a *pKC26* construct containing the *EGFP* and *mCitrine* modules in a face-to-face orientation. These would then be excised as one cassette, making use of two KpnI sites found 5'and 3'. The *mCitrine* module was successfully subcloned in a 3' to 5' orientation into the *pKC26-mMCS* vector using KpnI and NotI. Subsequently, the resulting vector was used for cloning of the EGFP containing module with NotI and BglII in a 5' to 3' orientation. Upon completion, the cassette was excised using KpnI for further subcloning into

the *FB1.0* vector. Nevertheless, recombination was still taking place and it was not possible to recover correct colonies. Different bacterial strains and growing conditions were equally tested for this approach, but none of them was able to suppress recombination. Consequently, new methodologies were employed aiming to reduce the level of similarity between the sequences of the respective modules.

An initial strategy included the subcloning of a spacer sequence at the 5' end of the *mFRT71* site. The chosen fragment comprised 282 bp of the Ret kinase genomic sequence that has previously been used as a spacer in RNAi constructs. Newly designed *FB36*, *FB37* and *FB38* primers (Table 3) were used to PCR amplify the spacer sequence from the UAS *pR57* vector (Pili-Floury et al., 2004). We generated PCR products differing on their 5' ends by using two primer pair combinations (*FB36*/*FB38* and *FB37*/*FB38*). Subsequently, the amplicons were inserted into a TOPO vector by TA cloning. The fragment was excised using XhoI and SalI (*FB36*/*FB38*) or solely SalI (*FB37*/*FB38*) restriction enzymes and subcloned into the *mCitrine* module, in which the original *mFRT71* sequence has been removed. This strategy was carried out with the help of Lauren Ferreira.

In parallel, another approach aimed at replacing the sequence coding for the membrane localization tag of the *mCitrine* module with a different one. The Cd8 anchor is common in all four modules, thus exchanging it with an alternative membrane tag would result in a sequence arrangement including less similar neighboring fragments. A double myristoylation-palmitoylation (mp) membrane localization signal originating from the Lyn kinase (13 NH_2-terminal residues) has previously been used to successfully tag Citrine to the membrane (Zacharias et al., 2002). Initially new oligonucleotides were designed and used to PCR amplify the *2x-pm-mCitrine* sequence from the original *pCS-2xLyn-mCitrine* vector (*FB32*/*FB40*, Table 3). Similarly, using another pair of primers (*FB33*/*FB40*) a different amplicon was generated containing an XbaI restriction site (at the 5' end) followed by the 3' end of the *mFRT71* sequence and the *2x-pm-Citrine* (at the 3' end). TA cloning was used to clone the PCR products into a *pCR2.1-TOPO* vector. Subsequently, the *2x-pm-mCitrine* fragments were directionally cloned in a 5' to 3' orientation into a *pTRC-mMCS-hsp70* vector using AvrII and XbaI or SpeI respectively. Next, bacterial colonies were visualized under a fluorescence dissection

microscope and selected when found positive for mCitrine expression. However, digestion patterns for purified plasmids of Citrine fluorescing colonies appeared incorrect. This could be due to recombination occurring in the *2x-pm* fragment, since it consisted of two repeated sequences placed in tandem. Fluorescence could still be observed as recombination events did not lead to mutations in the ATG of *mCitrine*. Different strains of bacteria and culturing conditions were tested to overcome this limitation. Nevertheless this was unsuccessful and thus, modifications to this approach were attempted.

Subsequently, our efforts focused on subcloning solely the coding sequence of the new membrane anchor into the *pTRC-mCitrine* containing construct. All strategies employed included direct replacement of the *cd8* coding sequence with the *pm* fragments. Using new pairs of primers (*FB32*/*FB34, FB35, FB39*, *FB40***,** Table 3) a variety of PCR fragments were generated and cloned into the *pCR2.1-TOPO* vector. Next, the *2x-pm* sequence was subcloned in a 5'-3' orientation into the *pTRC-mMCS-cd8-mCitrine* module using SpeI and BamHI. This completed the new *mCitrine* module however; further cloning steps towards completing the *FB1.1* construct were compromised due to persistent bacterial recombination.

Thus, an alternative strategy was employed that included the design of two new oligonucleotides (*FB41*/*FB42*, Table 3) spanning a single myristoylation-palmitoylation sequence. The myristoylation signal requires N-terminal localization to direct localization of recombinant proteins to membrane lipids. Therefore, by using a single *pm* sequence, we depleted our methodology by only one membrane localization signal. These were annealed to generate a double stranded sequence that contained SpeI and BamHI compatible overhangs. The annealed sequence was cloned in a 5' to 3' orientation using SpeI and BamHI into the *pTRC-cd8-mCitrine-hsp70* construct to generate the new *pTRC-pm-mCitrine-hsp70* module. Monitoring of the fluorescence positive colonies under the dissection microscope showed increased numbers of positive clones. True positive clones were confirmed by sequencing results.

Next, the new *mCitrine*-containing module was subcloned into the *FB1.0* vector in a 3'-5' orientation using KpnI and SacI. The *EGFP*-containing module was inserted in a 5'-3' orientation using BglII and SacI. Finally, the *FB2.0* construct was generated by inserting the

PCR-amplified wild-type FRT stop cassette (*FRT lamin-2xHA hsp70Aa/hsp27 FRT*) into the *FB1.1* vector using NheI and BglII. To build this stop cassette, Shay Rotkopf, generated first the *lamin-2xHA* by inserting a PCR amplified *lamin* cDNA into an intermediate vector that contained two HA tags. Next, the *lamin-2xHA* fragment was inserted into a plasmid containing the *hsp70Aa* and *hsp27* polyadenylation sequences. Finally, the *lamin-2xHA hsp70Aa/hsp27* fragment was subcloned into a modified *pUAST* vector, containing two wild-type *FRT* sites in the same orientation using KpnI and SpeI.

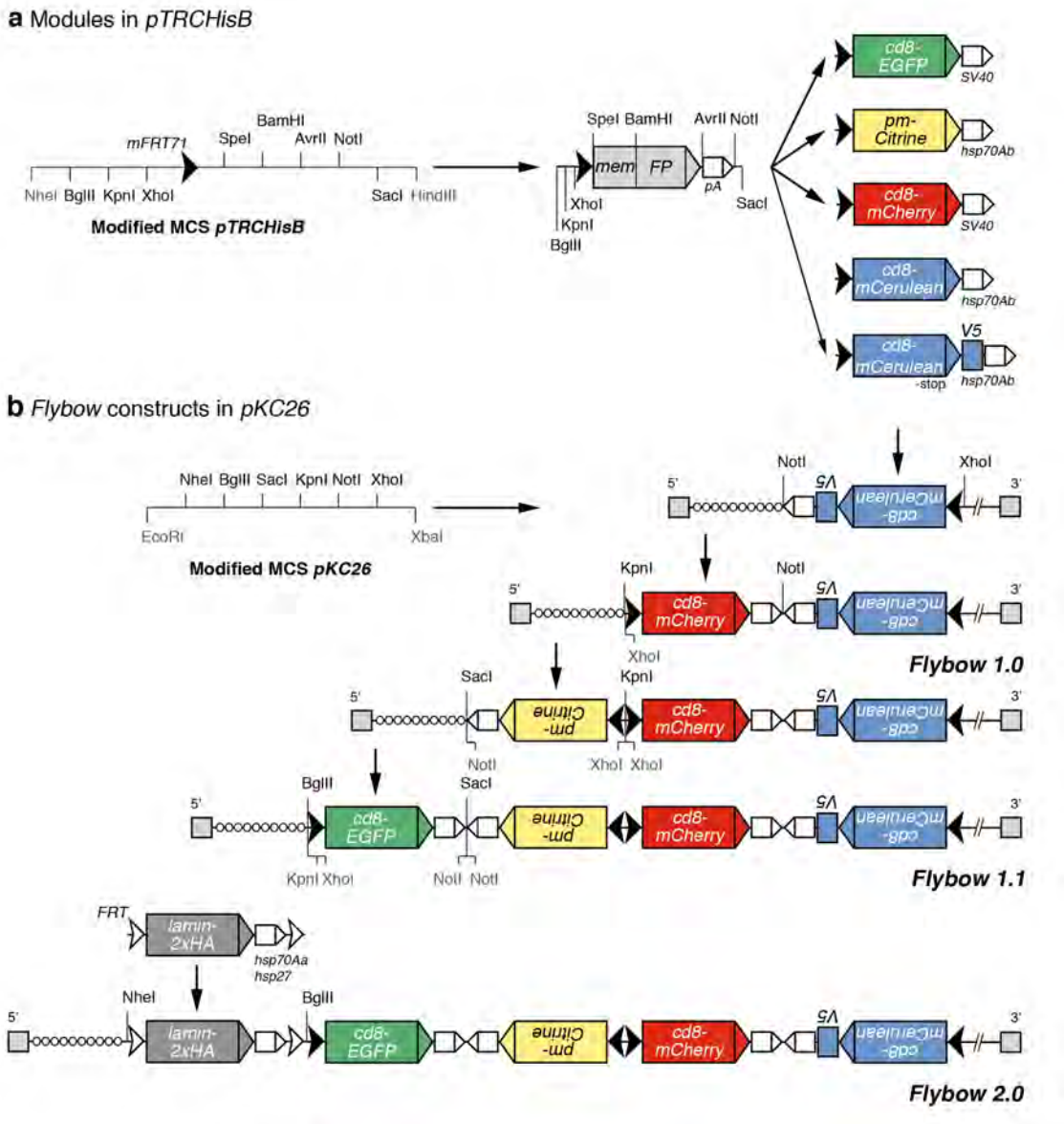

Figure 14. Details of stratagem used to build the three *Flybow* variants.

Flow diagram illustrating the two key steps used to build of *Flybow* constructs. (a) First, the four basic modules were generated. Each module contained a *mFRT71* sequence, a membrane-anchor, one of four

FP-encoding sequences and one of two polyadenylation signals. *Cerulean* was also tagged with a *V5* encoding sequence. (b) Second, the basic modules were subcloned sequentially into the modified *pKC26* to assemble the final constructs. Intermediate steps for the completion of all three variants are indicated by the down facing black arrows.

3.9 Generation of Flybow transgenic lines

Transgenic flies were generated using embryo injection protocols (discussed in sections 2.1.2 and 3.7). Constructs containing *attB-sites* (*FB1.0, FB1.1 FB2.0 and UAS-cd8-Citrine*) were inserted into specific *attP-site* containing loci on the second (*VIE-260b*, 2L) and third (*VIE-49b*, 3R) chromosomes using the *ϕC31* system (Bischof et al., 2007). For *FB1.0,* we prepared and injected 152 embryos for the second (2L) and 282 embryos for the third (3R) chromosomes. In the case of *FB1.1,* 246 (2L) and 123 (3R) embryos were injected for two genomic locations, respectively. 300 embryos were injected for the second (2L) and 131 for the third (3R) chromosomes with the *FB2.0* construct. Finally, injections for the *UAS-cd8-mCitrine* transgene included a group of 140 (2L) and 80 (3R) embryos correspondingly. We recovered approximately 30 or more transformants for each of the injected transgenes and at least two individual lines were established for each construct and chromosome (success rate 10-30%). The use of the *ϕC31* system for genetic transformation highly enhanced the recovery rate of successful transformants. Embryo injections were performed together with I. Salecker.

3.10 Discussion

3.10.1 Transfer to a Fly "bow"- Advantages and limitations

Brainbow has elegantly underlined the significance of genetic multicolor labeling of neighboring cells within a large cell population in studies of the mouse nervous system. With a main interest in understanding the development and function of relatively simpler, highly hardwired invertebrate connectomes we aimed to build a similar genetic tool. This chapter focused on the intricacies of planning and successfully generating the three FB variants.

Employing the power of fly genetics

Drosophilists have developed over the years an impressive array of genetic approaches enabling manipulations of individual genes (Brand AH, 1993; Dietzl et al., 2007; Golic and Lindquist, 1989; Lee and Luo, 1999). Importantly, instead of placing *FB* transgenes under the control of a single enhancer we employed the Gal4/*UAS* system (Brand AH, 1993) to tightly control their expression. The binary nature of this system translates into a sole necessity to generate three *UAS-FB* transgenic fly lines that can be employed for genetic crosses with any Gal4 expressing flies. This amplifies our possibilities for future experimental scenarios by taking advantage of the array of available Gal4 lines expressed in different subgroups of cells. FB would then be used to extract information on cell behavior within a given cellular group of interest by differentially labeling membranes of interacting cells, in which the *Gal4* elements are active. Combination of these two genetic approaches brings the "bow" technology a step further from its vertebrate versions (Livet et al., 2007; Snippert et al.) as it can offer stable expression of fluorescent proteins exclusively in desired cell groups throughout development and in adults. The use of the *pKC26* vector that includes a 10 instead of the commonly used 5 *UAS* elements offers the advantage of achieving strong expression of fluorescent proteins. This is essential in the case of weak Gal4 drivers especially since we aimed at visualizing fine neuronal processes including filopodia of growth cones without amplification by immunolabeling.

Switching to a new DNA recombination system

We aimed to avoid the use of the Cre/*loxP* system, since it has been reported to cause toxicity in proliferating cells when used in flies (Heidmann and Lehner, 2001). Toxicity can be correlated with high levels of expression of Cre leading to chromosomal aberrations and cell death. Inducible forms could help circumventing this problem. Nevertheless, all inducible tools generated to date bear problems either in terms of tight control of expression of the recombinase or poor inducibility (Heidmann and Lehner, 2001; Siegal and Hartl, 1996). These led to the limited application of Cre/*loxP* for fly manipulations, and thus, only a small number of specific Cre-expressing lines have been generated. In contrast, the Flp/*FRT* system has found

widespread use and served as a basis for tools aiming at the generation of genetic mosaics (Chalfie et al., 1994; Chotard et al., 2005; Lee and Luo, 1999)(Horn et al., 2005) (Evans et al., 2009). *Brainbow-1* uses pairs of heterospecific *loxP* sites recognized by Cre to excise individual cassettes. *Brainbow-2* employs both excisions and inversions of cassettes flanked by homotypic *loxP* sites to randomize color outcomes. To date a limited number of heterotypic *FRT* sites have been reported (Horn et al., 2005). We therefore sought to build Flybow based on the Brainbow-2 approach. Nevertheless, we still needed to employ a different Flp/*FRT* system to use for generating DNA rearrangements that would lead to varying color outcomes. Collaborating with Shay Rotkopf in the Dickson laboratory, different variants of Flp enzymes and modified *FRT* sites were tested for their function and specificity in vivo. The fruitful outcome was the identification of the new mFlp5/*mFRT71* combination as an alternative DNA recombination system for use in *Drosophila*. The new tool was placed under the control of a heat-shock responsive promoter to provide temporal control over recombination events. Importantly, Flp5 shows only low basal expression. Furthermore the modified Flp5 only minimally recognizes the canonical *FRT* sites. Consequently, the classical recombination system is available for use in genetic manipulations employing Flp/*FRT* based tools for clonal analysis approaches. Furthermore, FB variants can be combined with available Gal4- and *UAS*- techniques. Importantly, such analyses would directly provide insights of gene function at single cell level. *FB2.0* includes an additional stop cassette and can be used in intersectional studies facilitating sparse labeling (see Chapter 5).

3.10.2 Generating complex, yet adjustable DNA constructs

Thorough planning of the cloning strategy made the very complex task of generating a synthetic transgene comprised of highly similar repeated sequences possible. The basis of building the Flybow construct lies in its modular nature. This provides flexibility for future construct amendments. The advantages that this offers could already be exemplified when faced with the problem of replacing the V5 epitope, as well as the membrane anchor for the mCitrine module. In the same way, each of the components of the basic modules can in the future be replaced with more advanced variations.

Switching to a different membrane tag

Using different strategies and taking advantage of the construct versatility, we could successfully replace the membrane anchor. Concerns at this stage of the work included that in doing so we could have compromised the resolution offered by our tool in regards to imaging abilities. Our original strategy in using the same membrane tag would mean that all fluorescent proteins would have the same sub-cellular localization. Thus, when imaging cells in different colors fluorescence would be located in the same sub-cellular position. This could become crucial, especially in experimental settings in which one cell could express more than one fluorescent protein. Nevertheless, our results described in Chapter 5 show that for our purposes the use of palmitoylation/myristoylation membrane tag does not hamper imaging quality.

In conclusion, this effort led to the successful generation of three FB transgenes version. The next step constitutes their thorough testing *in vivo*.

Chapter 4

FB1.0 *in vivo*

Putting the approach to the test

4.1 Introduction

Studies in different organisms have demonstrated the ability of site-specific recombinases to catalyze inversions of DNA fragments flanked by inward facing recombination sites (Livet et al., 2007; Stark et al., 1992) (Branda and Dymecki, 2004). Flybow seeks to employ this ability of the yeast derived Flp recombinase for the generation of different color outcomes. However, the use of such recombination events had not been established in *Drosophila* in vivo studies.

4.2 Expression of mFlp5 leads to inversion of *FB1.0* cassette

To investigate the ability of the mFlp5/m*FRT71* system to mediate inversions, we used it in combination with the first Flybow variant that comprises a single, potentially invertible cassette. *FB1.0* transgenes were expressed in the nervous system using the pan-neuronal *elav-Gal4*^{c155} driver (Chalfie et al., 1994). A one-hour heat-shock pulse at 37 °C was applied at 48 hours AEL. This led to the transient expression of mFlp5 from a transgene placed under the control of the heat-shock sensitive promoter (*hs-mFlp5*). In turn, this triggered the random inversion of the *FB1.0* cassette. We assayed the recombination results in the developing visual system at the third instar larval stage. Confocal images from both eye discs and optic lobes show strong and largely mutually exclusive expression of *mCherry* and *Cerulean-V5* (Figure 15). This shows that the modified recombination system can efficiently induce inversions in vivo in *Drosophila*.

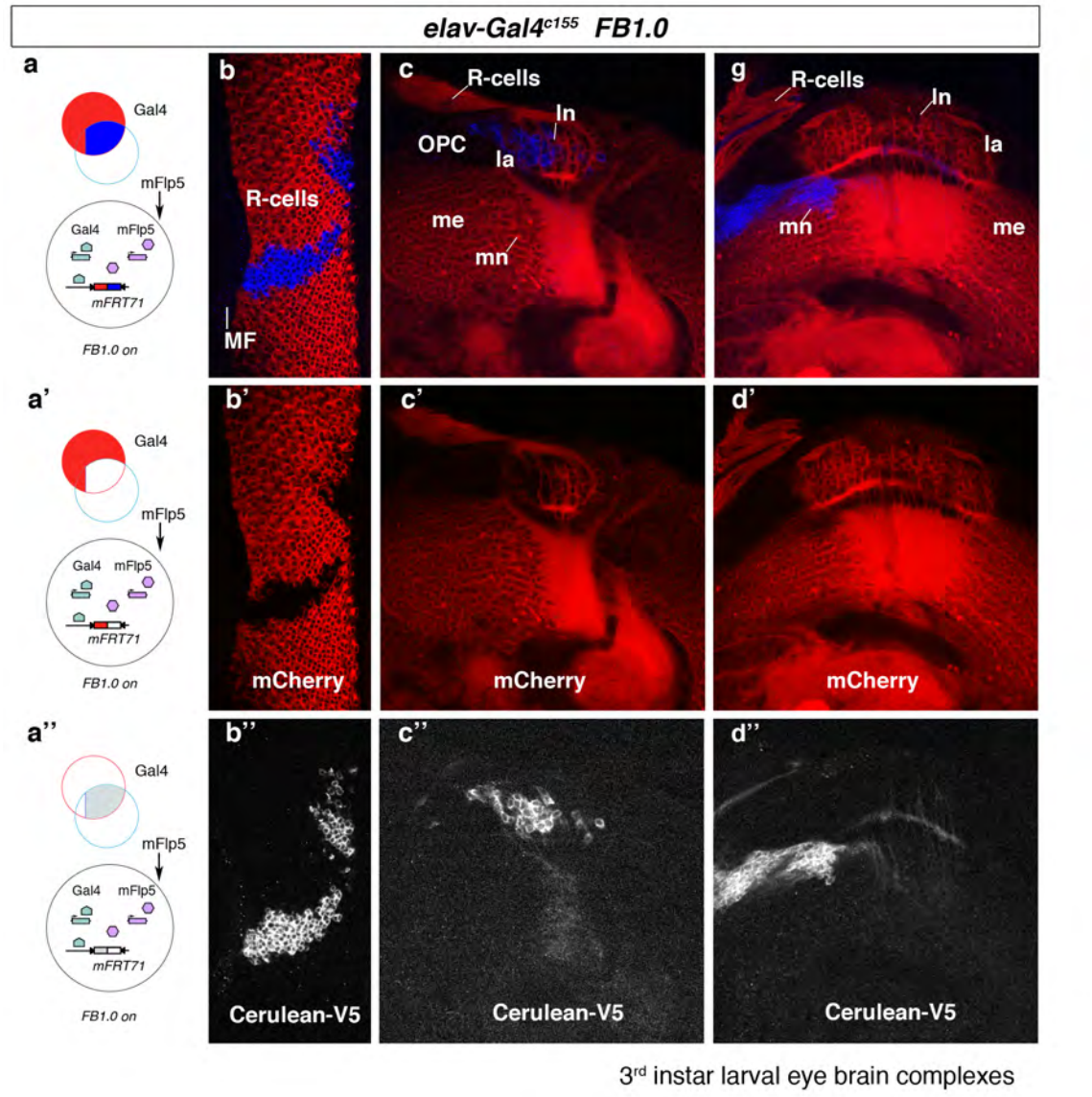

Figure 15. mFlp5 mediates inversion of the FP containing cassette in *FB1.0* transgene and leads to mutually exclusive expression of mCherry and Cerulean.

Gal4 expression labels the tissue of interest. mCherry prior to heat shock exposure. The modified mFlp5/*mFRT71* system is stochastically activated in a number of cells following to heat exposure and can lead to inversion of the *FB1.0* cassette. Within the Gal4-positive cell population, switch from *mCherry* to *Cerulean-V5* expression reports inversions. The pan-neuronal driver *elav* ^{c155}*-Gal4* was used to drive expression of *FB1.0* transgenes in the third instar larval visual system of *Drosophila*. Anti-V5 antibody was employed to visualize Cerulean-V5. Groups of photoreceptor cells (R-cells) in the eye imaginal disc differentiating posterior to the morphogenetic furrow (MF) express *Cerulean-V5* (b, b''). Similarly, lamina neurons (ln) in the developing lamina neuropil (la) as well as medulla neurons (mn) generated from the outer proliferation centre (OPC) in the medulla neuropil (mn) express *Cerulean-V5* in a mutually exclusive manner (c-d, c''-d''). *elav-Gal4*^{c155}*/+ or Y; hs-mFlp5/FB1.0*^{260b}. Confocal images collected a Zeiss / BioRad Radiance 2100 confocal microscope.

4.3 Suboptimal fluorescence levels of Cerulean

While conducting these experiments, we encountered a possible weakness in our approach. Samples that expressed *FB1.0* in the third instar larval visual system were visualized directly under the fluorescence dissecting microscope. We could readily detect mCherry fluorescence. Nevertheless, we could not observe a strong enough signal for Cerulean protein using this wide-field microscope. Thus, we next monitored endogenous fluorescence levels of Cerulean-V5 using confocal microscopy (Figure 16). Comparing the fluorescence intensity of the two fluorophores we could conclude that Cerulean is fluorescing at suboptimal endogenous levels when compared to mCherry. We thus decided to use immunolabeling of the V5 epitope to detect expression of Cerulean-V5 in all subsequent experiments.

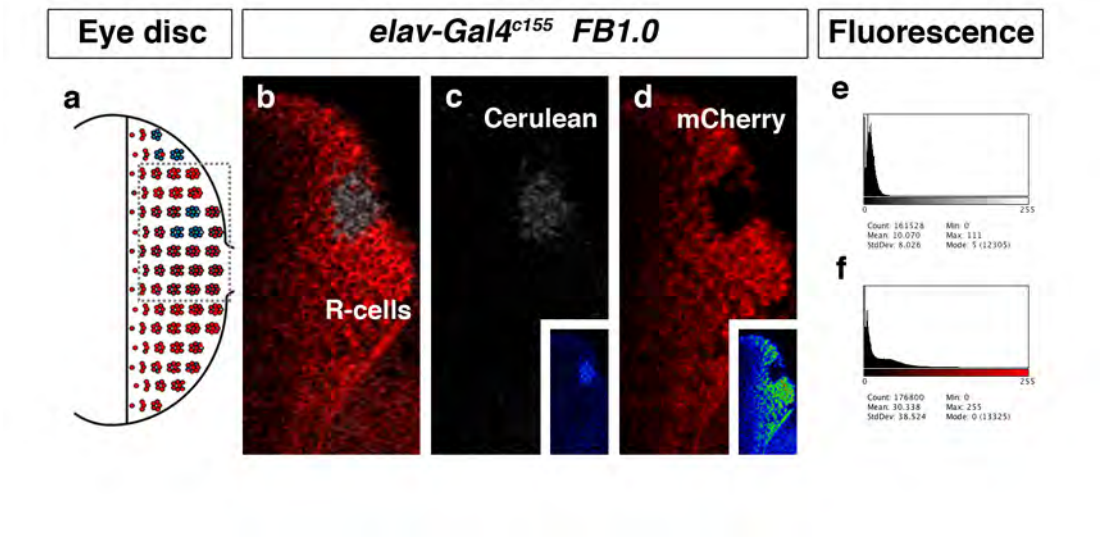

Figure 16. Endogenous Cerulean fluorescence levels are suboptimal for imaging in *Drosophila*
(a) Schematic drawing of ommatidial clusters within the developing eye imaginal disc at the third instar larval stage. (b-c) *elav^{c155}-Gal4* was used to drive expression of *FB1.0* transgenes. Fluorescence for both mCherry and Cerulean was detected using imaging conditions to match their optimal spectral properties. Endogenous fluorescent signal for Cerulean was detected and found to be mutually exclusive to the one obtained for mCherry (b-c, insets). Cerulean was found to fluoresce suboptimally. Use of high power of laser, as well as widening of the detection window were used to obtain larger amounts of detected signal. When compared to mCherry (e) the signal retrieved for Cerulean (f) was significantly lower. *elav-Gal4^{c155}/+ or Y; hs-mFlp5/FB1.0^{260b}*..Confocal images collected using a Leica MP-SP5 confocal microscope.

4.4 Discussion

4.4.1 Establishing inversions as an alternative recombination outcome available for use in *Drosophila* genetic manipulations

Using the *FB1.0* variant we could demonstrate that mFlp5 can successfully mediate inversions. It was crucial to evaluate the ability of Flp recombinases in inducing inversions of DNA elements flanked by oppositely oriented repeats of *FRT* sites in vivo. Based on the results of the Brainbow study we were optimistic that this could work in *Drosophila*. However, there were concerns regarding its feasibility since the two approaches differ in detail. Brainbow employs Cre that has been reported as being highly efficient in driving recombination mainly due to its inherent stability at physiological temperatures (Buchholz et al., 1996; Coates et al., 2005). Conversely, Flybow employs Flp for recombination that has been shown to be less stable at high temperatures (Buchholz et al., 1996). Furthermore, our approach uses a modified variant (mFlp5), for which no data are available in terms of thermostability properties. In his initial tests in eye imaginal discs, S. Rotkopf had previously shown that mFlp5 could readily induce excisions of cassettes flanked by direct *mFRT71* site repeats. Nevertheless, recombination efficiency was a concern since the task of inverting a cassette is thermodynamically less favourable to an excision event (Baer and Bode, 2001). This can be attributed to the fact that re-integration of the flanked DNA fragment is required. Employing this experimental set-up it is evident that one-hour exposure at 37 °C leads to sufficient levels of expression for the mFlp5 recombinase necessary to mediate inversion events.

4.4.2 Inversions result in predominantly exclusive fluorescent protein expression

We analyzed the expression profile of *FB1.0* transgenic flies 1-2 days after the heat-shock application. Importantly, we could show that inversion of the single cassette leads to primarily mutually exclusive expression of the two fluorescent proteins in use. We thus allowed at least

24 hours for the recombination events to occur, as well as subsequent expression of Cerulean-V5. This constitutes a relatively long time window. However, considering our limited knowledge in the kinetics of the different processes involved, we used it as a starting point. Further experiments discussed in the next chapter show that the time required for induction of mFlp5 expression that leads to subsequent color swaps within one cell could be significantly reduced. One of the key features of using inversions is that they are in essence reversible. However, a major concern was whether re-inversions could occur rapidly resulting in a fast switch between the two FPs. This could lead to the simultaneous expression the two FPs in a single cell ("purple" cells) or total loss of fluorescence respectively. Our data suggest that the inversion events are relatively stable and lead to expression of a single fluorophore at the time because of the transient heat-shock. It is crucial to note that the use of an inducible recombinase that is promptly removed following the heat-shock termination contributes to the observed stable outcome.

4.4.3 Immunolabeling is required for monitoring Cerulean expression

Strong fluorescence signals are crucial for acquiring data sets allowing for precise reconstruction of cells with elaborate morphologies. In accordance to this, we chose to use Cerulean (Rizzo et al., 2004) amongst the members of the Cyan fluorescent protein (CFP) family. At the time Cerulean was reported to be the best *Aquorea victoria* CFP derivative in terms of its brightness, quantum yield and oligomerization properties (Rizzo et al., 2004; Shaner et al., 2007; Shaner et al., 2005). Additionally, it was described to have surpassed its predecessor CFP derivatives by acquiring mono-exponential excitation and emission properties that could improve spectral unmixing in multicolored preparations. Nevertheless, our findings in agreement with work of others (Hampel et al., 2011) indicate that Cerulean is less suitable for *Drosophila* in vivo studies. The endogenous signal is significantly weaker when compared to mCherry. We needed to employ the argon 405 or 457 laser lines to their full capacity to maximise the amount of detected signal. Employing such strategy would compromise our multicolored imaging set up due to the requirement of sample exposure to high levels of laser power. This could then lead to an increase in the noise to signal ratio of our acquired images by

non-specific excitation of the spectrally neighbouring fluorophores (EGFP and mCitrine). Furthermore, it became clear that such an approach would not be optimal for live imaging as high laser power exposure could result in the damage of examined tissue. These observations are further supported by studies aiming to improve the existing palette of CFP variants. Interestingly, Shaner and Ai discuss that in typical photobleaching experiments Cerulean appears to contain a fast bleaching component leading to the decrease of its initial fluorescence up to 60% in a timescale of a few seconds (Ai et al., 2006; Shaner et al., 2005). Furthermore, it is becoming apparent that Cerulean as all the CFP variants, which employ tryptophan in their chromophores, face limitations in their fluorescence abilities due to dynamic interactions of the indole ring with the surrounding β-barrel structures (Ai et al., 2006; Lelimousin et al., 2009). Moreover, Cerulean has been reported to act as a weak dimer (Shaner et al., 2005) and recent reports indicate the existence of two peaks in its absorption and emission spectra (Chudakov et al., 2010; Goedhart et al., 2010; Lelimousin et al., 2009; Markwardt et al., 2011). This makes its excitability (by a single laser line) and detection of fluorescence (wide detection window) less optimal. Finally, a potential contributing factor to the insufficient endogenous fluorescence of Cerulean could be that it has been designed for use in mammalian systems by optimized codon usage as well as preferential folding at 37 °C (Rizzo et al., 2004). This constitutes a disadvantage for our experimental conditions, since our fly stocks are raised at a lower temperature (25 °C).

We thus reasoned to use anti-V5 antisera for monitoring the expression of Cerulean-V5 recombinant protein. Employing immunostaining protocols, we could establish an imaging set up using laser power levels and pixel dwell time for Cerulean-V5 similar to the other fluorescent proteins used in Flybow. Our data show that both neuronal cell bodies and fine axonal projections can be easily distinguished (Figure 15). The latter constitutes an improvement when compared to our results for samples with endogenously fluorescing Cerulean protein. Importantly, confocal images of samples visualizing endogenous fluorescence of Cerulean show that only shapes of large structures such as cell bodies could be recognized

(Figure 16). Nonetheless, we believe that monitoring expression of fluorescent proteins using antibody staining hampers their true potential in producing high-resolution data. Principally, this can be attributed to the increase of noise to signal ratio in even the cleanest of preparations. This becomes apparent when aiming to reconstruct intricate cellular processes of neurons at relatively long distances from their cell body in three-dimensional (3D) space of the tissue. In addition, live imaging paradigms would benefit from a more informative four-colored set up. Finally, monitoring the endogenous fluorescence of a CFP variant would allow us to use the far-red end of the spectrum to image other markers by immunolabeling, which could function as important landmarks to facilitate the identification of cells.

In the course of this study, more CFP variants have been generated and tested for their use in imaging from living tissues (Chudakov et al., 2010). Four variants - mTFP1 (Ai et al., 2006), mTurquoise (Goedhart et al., 2010), mTurquoise2 (Goedhart et al., 2012) and mCerulean3 (Markwardt et al., 2011) show significantly improved properties compared to Cerulean. The results discussed in this chapter are in agreement with the shared understanding in the fluorescent protein field that there is no single "star" fluorescent protein. Each experimental setting should test and make use of fluorescent proteins tailored to its specific needs. Ongoing work in the lab by a joint effort of Nana Shimosako and Iris Salecker demonstrates that mTurquoise (Goedhart et al., 2010) is suitable for use *Drosophila* studies. Thus, the obvious next step includes the replacement of Cerulean's coding sequence in all Flybow constructs with the one of mTurquoise and subsequent generation of the second group of transgenic flies.

Chapter 5

Using Flybow to visualize intricate cell morphologies

5.1 Introduction

Eukaryotic cells possess a highly advanced cytoskeleton consistent with their astonishing cell shape diversity (Wickstead and Gull, 2011). Their morphology provides insights into the current cellular states (e.g. division, migration, death), as well as their individual roles (e.g. border formation or information relay) within a multicellular organism. Moreover, uncovering interactions amongst cells of a specific tissue can therefore lead to a better understanding of the overall biological processes involved in its function. Specialized structures such as neuronal processes have been developed to serve as sensors of the cellular environment and transmit signals to cells, with which they interrelate. Neuronal cells have adopted the most elaborate cell shapes and thus, deciphering their interactions remains a highly challenging task. The ultimate goal is to generate complete physical circuitry maps, and further relate them with functional information. This chapter includes work aiming to gain more insights in the circuitry of the *Drosophila* nervous system using the Flybow approach to uncover cellular interactions. The fly nervous system is thought to comprise more than 150,000 neurons (Meinertzhagen and Sorra, 2001), which establish multiple connections with each other. We mainly focused on the visual system that consists of at least 70,000 neurons. This constitutes a good paradigm of a complex neural circuit. Morphological descriptions for distinct neuron classes innervating the four respective neuropils of the visual system together with some understanding concerning their first order connectivity in the lamina have been reported in detail (Gao et al., 2008; K.-F Fischbach, 1989; Sanes and Zipursky, 2010) (Meinertzhagen and Sorra, 2001; Morante and Desplan, 2008). However, the distribution of specific neuron subtypes within the visual neuropils is poorly understood, which particularly applies to the medulla, the largest and most common neuropil (Morante and Desplan, 2008). Thus, further investigation of single cell shapes in relation to the morphology of its neighbours within the medulla neuropil becomes an imperative need towards understanding circuit development and function in the *Drosophila* visual system.

We have shown that use of the modified mFlp5/*mFRT71* system leads to inversion of the *FB1.0* cassette and consequently to dual marker labeling of Gal4 positive cells. Ultimately, we aimed at multicolor cell labeling using the *FB1.1* and *FB2.0* transgenes for stochastic marker expression. Thus, combination of inversion events for sequences flanked by inward facing *mFRT71* sites together with excisions of sequences flanked by *mFRT71* sites facing in the same orientation is required to locate the coding sequences of fluorescent proteins closest to the *UAS* sites. Expression of mCitrine, mCherry and Cerulan-V5 instead of EGFP is the outcome of either: (a) an inversion of the first or both cassettes (mCitrine or Cerulean-V5, respectively), (b) an excision of the first cassette (mCherry), or (c) a combination of an excision and inversion event (Cerulean-V5)(Figure 17). Finally, for sparse multicolor labeling we have employed the *FB2.0* variant. Here, an additional recombination step is necessary for removal of a transcriptional block preventing the expression of the four fluorescent markers. This cassette flanked by a pair of wild-type *FRT* sites is placed upstream of the "core Flybow" transgene and can be removed upon Flp recombinase activity.

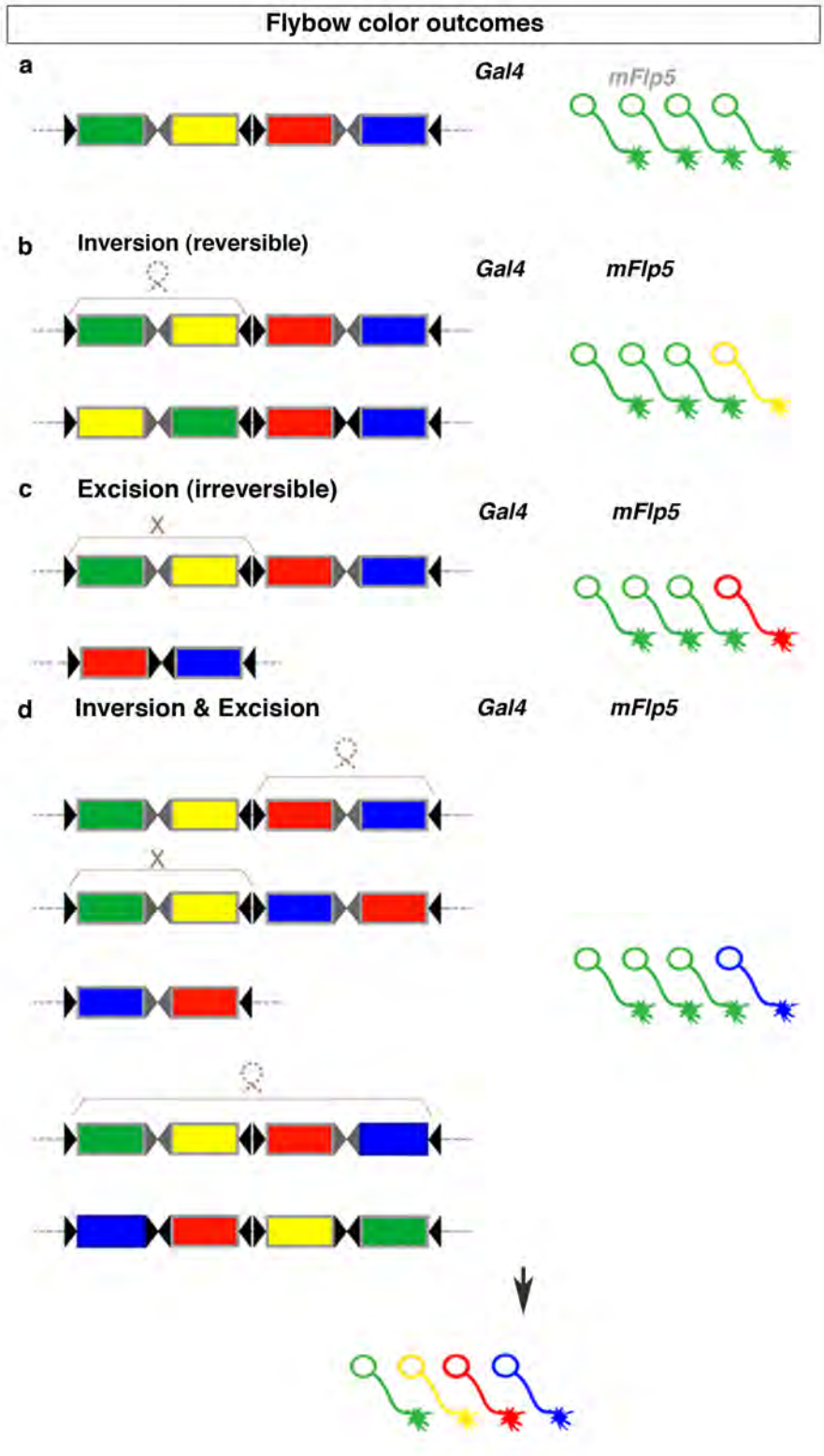

Figure 17. DNA re-arrangements mediated by mFlp5 result in four distinct color outcomes in a Gal4 expressing subset of cells.

Schematic diagram illustrates the potential fluorescent protein color outcomes visualized within a sample that employs the *FB1.1* approach. Upon activation, *FB1.1* transgenes label cells with four distinct colors

(color-coded cells). EGFP is located directly downstream of the UAS sites (green box) and, thus, is expressed by default. In the absence of mFlp5 (text, shaded grey) the entire Gal4-positive cell population is marked by EGFP expression (a, green cells). Following heat exposure, mFlp5 is expressed (text, black) and results in varying recombination events leading to the four outcomes (b-d). mFlp5 recognizes different pairs of *mFRT71* sites and can rearrange the sequences they flank accordingly. Recognition of the first inward facing *mFRT71* pair (b, black triangles) leads to the inversion of the first cassette and leads to the switch in position between the EGFP (green box) and mCitrine (yellow box) encoding sequences allowing for mCitrine expression (b, yellow cell). Alternatively mFlp5 can recognize *mFRT71* pairs facing tin the same direction (c, black triangles) mediating permanent excision of the first cassette. Exposing the mCherry coding sequence (red box) directly downstream of the *UAS* sites, leads to mCherry expression (c, red cell). Similarly, recognition of the second inward facing *mFRT71* leads to inversion of the second cassette. The Cerulean-V5 encoding sequence (d, blue box) is therefore located upstream. Subsequent recognition of the *mFRT71* pair oriented in the same direction and flanking the first cassette (d, black arrows) results in its permanent removal followed by the expression of Cerulean-V5 (blue cell). Finally, the inward facing *mFRT71* pair that flanks both cassettes within the *FB1.1* transgene (d, black triangles) can be inverted positioning the Cerulean-V5 coding sequence directly after the *UAS* sites and leading to its expression. These events occur stochastically and result in a multicolored cell population.

5.2 Using a pan-neuronal driver in combination with Flybow as a starting point

5.2.1 Optimization of experimental conditions

We chose to calibrate our experimental conditions using the nervous system-specific *elav*^{c155} regulatory element to drive expression of *Gal4* and consequently of *FB1.1* transgenes in all neurons. Firstly, the aim was to establish experimental conditions that could result in expression of all four fluorescent proteins within the examined tissue. This was achieved by testing various heat-shock regimes summarized in Table 2 and Figure 18. Both third instar larval eye-brain complexes and adult optic lobes were dissected and monitored for expression. We observed that repetitive heat-shocks induced all possible recombination events and consequently all color outcomes with equal probabilities (see also section 5.2.3).

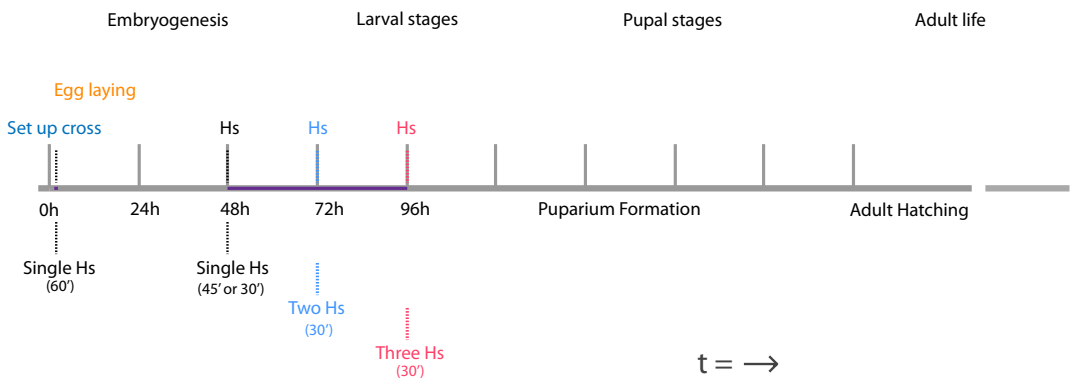

Figure 18. Heat-shock protocols to drive recombination in the nervous system using *FB1.1*. Crosses were set up (t = 0 hours). Following a 24-hour laying period (t = 24 hours after egg laying, AEL) the

cross was transferred to a new food vial for a further 24 hours. This was repeated for up to 7 days. Heat-shocks were performed using a water bath with set temperature of 37 °C. The earliest developmental point for inducing recombination events in the optic lobes was 48 hours AEL. When multiple heat-shock protocols were employed, heat shocks were repeated at 24-hour intervals (72 hours and 96 hours AEL). To generate clones in the embryonic nervous system, embryos were exposed to a single heat shock in a collection of embryos (approximately stages 1-14).

Next, using these conditions as a starting point, we employed the same *Gal4* driver line to test the expression of *FB2.0* transgenes in the nervous system. We reasoned that this would be harder to achieve since the expression of an additional Flp recombinase (Flp) was required for the removal of the "stop" cassette flanked by canonical *FRT* sites. Both Flp[1] and mFlp5 in our experimental setting were under the control of a heat-shock promoter. Thus, we performed longer heat-shocks as described in Table 2 and Figure 19. Allowing long heat exposure times (up to 90 minutes) proved sufficient for the expression of the two Flp recombinases, thus resulting in stochastic removal of the "stop" cassette and subsequent randomized expression of the four fluorescent markers and sparsely labeled multicolor samples. This served as a proof of principal and further experiments using different drivers (sections 5.3.3 and 5.4) showed that applying shorter heat-shock times is satisfactory for both recombinases to be expressed and mediate rearrangement events.

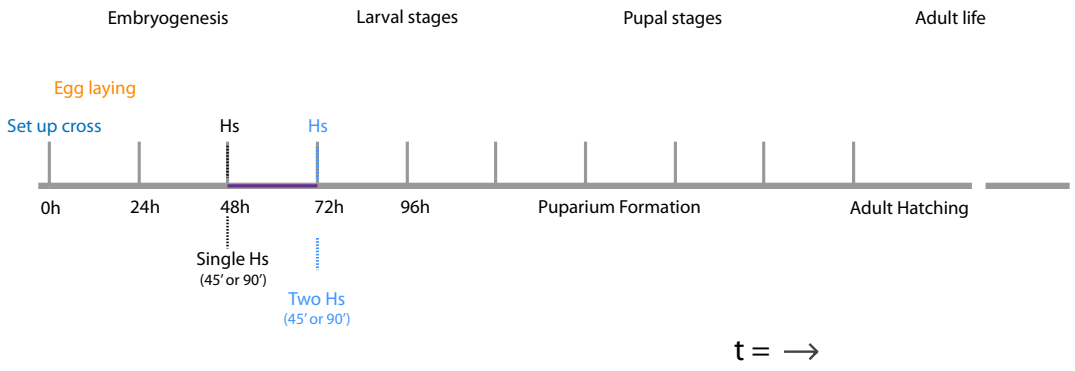

Figure 19. Heat-shock protocol for intersectional expression of two Flp recombinase systems in the fly nervous system.
elav-Gal4^{C155} was used to drive *FB2.0* transgene expression. Heat shocks (37 °C) were performed using a water bath. Two different protocols were followed. The first included a single heat pulse lasting 45 or 90 minutes and performed at 48 hours after egg laying (AEL). The second comprised two 90 minutes long heat shocks performed at 48 and 72 hours AEL, respectively. Both resulted in sufficient expression of the two Flp recombinase variants, as subsequently all possible color outcomes were observed.

5.2.2 Setting up image acquisition conditions

A fundamental difficulty of multicolor imaging lies in the separation of signals from fluorescent proteins with overlapping spectral properties. This holds true when imaging Flybow samples, specifically in the case of the EGFP and mCitrine fluorescent protein pair (cf. Figures 20 and 21). We thus needed to carefully determine the imaging settings for each marker to obtain optimally imaged samples. We imaged our experiments as described in detail in section 2.3.1. Using laser lines at wavelengths exactly (EGFP and Cy5) or very close (mCitrine and mCherry) to the theoretical excitation optima of the four fluorescent dyes, we aimed to recover strong emitted signals for the four respective proteins. More specifically, we employed: argon laser lines, 488 nm and 514 nm, to excite the EGFP and mCitrine fluorescent proteins respectively; a DPSS laser line, 561 nm, for mCherry excitation and a HeNe laser line, 633 nm, to excite the Cy5 coupled antibody. Subsequently, we could recover the emitted signal using detection windows very close to the theoretical emission peaks. Using narrow collection windows (Table 5, Figure 20), we aimed at increasing the true signal to background ratio. These varied depending on the fluorescent protein. Taking advantage of the narrow nature of the EGFP emission curve, as well as utilizing the powerful 488 laser line for excitation enabled us to collect a very high percentage of the EGFP fluorescence using a detection window as narrow as 25 nm (490-515 nm). Using these settings was crucial for our multicolor imaging approach, which also requires detection of mCitrine fluorescence, as it excluded detection of most of the non-specifically excited mCitrine signal. We used the same logic to select collection for windows for the other three markers. The main focus was to find a suitable balance between maximizing the percentage of detected signal for one specific fluorescent protein, whilst reducing the unspecific interference from the remaining markers within this region of the spectrum. Wider collection windows were thus used when detecting mCitrine (40 nm) mCherry (67 nm) and Cy5 (61 nm) fluorescent signals (Figure 20b).

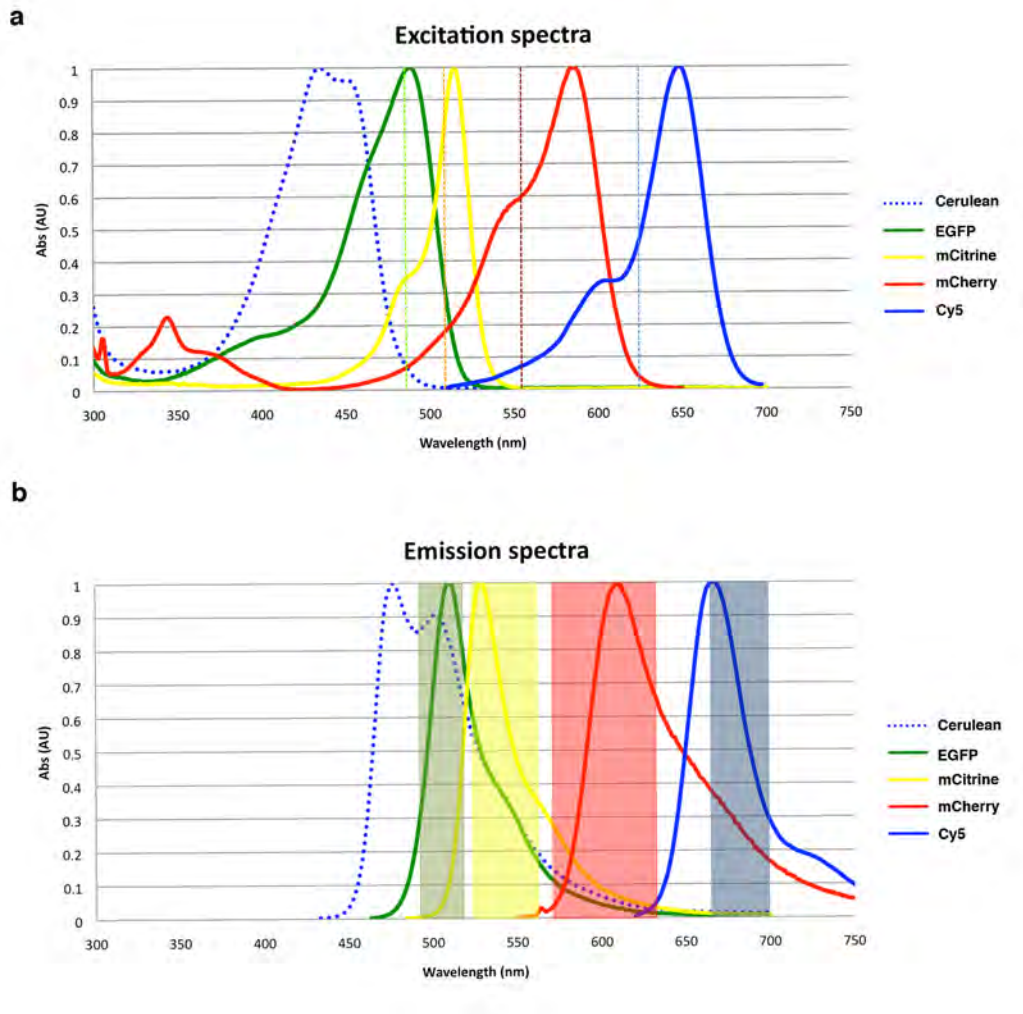

Figure 20. Spectral properties of fluorophores used in the Flybow approach imaged with a single-photon confocal microscope.
Excitation spectra of Cerulean (dotted blue line), EGFP (green line), mCitrine (yellow line), mCherry (red line) and Cy5-coupled secondary antibodies (blue line). The vertical dashed lines correspond to the laser lines used to excite the individual fluorophores (a). Namely, a 488 nm argon laser line (green dashed line), a 514 nm argon laser line (yellow dashed line), a 561 nm DPSS laser line (red dashed line) and a 633 nm HeNe laser line (blue dashed line). Emission spectra of Cerulean (dotted blue line), EGFP (green line), mCitrine (yellow line), mCherry (red line) and Cy5-coupled secondary antibodies (blue line). The shaded boxes correspond to the AOBS detection settings for each fluorophore. Specifically, 490-515 nm (green box), 525-565 nm (yellow box), 572-639 nm (red box) and 674-735 nm (blue box) (b). The spectral properties of Cerulean are included in this figure however were not used for imaging. Values in (a) provided by R. Tsien's lab (Tsien). Data have been normalized.

Next, we tested different scanning protocols. Theoretically, the different fluorescent markers could be scanned simultaneously to reduce the image acquisition times. However, the images acquired using this method showed high levels of unspecific signal due to cross channel excitation. Conversely, scanning of each of the four detection channels sequentially provided "clean" images but was considerably slower. Taking these points into consideration, we

combined both scanning modes by (a) simultaneously scanning pairs of spectrally well-separated fluorescent markers (EGFP:mCherry and mCitrine:Cy5, respectively) and (b) by using a two-step sequential scan protocol. This resulted in images with satisfactory quality in the case of mCitrine and Cy5 channels. However, we could still detect unspecific signal when imaging the EGFP and mCherry pair. We reasoned that this could be attributed to the use of the highly powerful 488 nm argon laser line included in our confocal set up, which resulted in unspecific excitation of the mCherry fluorescent marker. Therefore, we resolved this by using a three-scan sequential protocol that included detecting signal from: 1) mCitrine and Cerulean-V5 (detected with anti V5 primary antibody and Cy5 coupled secondary antibody), 2) EGFP and 3) mCherry (Table 5). Finally, to further shorten the image collection time, we employed the resonant scanner available in the SP5 confocal system. Using these tailored conditions we obtained images, in which true signals could be readily detected for all four channels. We observed in some cases that EGFP and mCitrine detected signals overlapped due to their inherent high emission spectral overlap. Therefore, the data we acquired from the EGFP and mCitrine emission signals required a further processing step. Reminiscent "cross-talk" between the two channels was eliminated using channel separation tools (Leica, LAS suite) (Figure 21). As illustrated in Figures 20 and 21, the detection window, recording emission of the mCitrine channel, also detects a significant proportion of the EGFP signal and *vice versa*. Therefore, we subjected images to a signal unmixing paradigm by determining "true signal" values for each of the respective florescent proteins. Initially, a region, in which detected signal for a given fluorescent dye was visibly evident, was manually allocated as region of interest (Rn, n=1-4 corresponding to the detection channel) for the respective marker. These regions were carefully selected aiming for the best intensity ratios amongst the emerging fluorescent protein pairs. Fully saturated regions of emitted signal were excluded from our selection and we instead tried to consistently allocate the regions of interest using values of approximately 60-80% signal intensity. Using the EGFP-mCitrine fluorescent protein pair as an example, this selection process is illustrated as follows: values of about 70% intensity for signals detected in the first part of the emission curve for EGFP (500 nm) are suitable for use, as this is only minimally

intermixed with low levels of mCitrine (less than 10% contribution). However, for mCitrine values of approximately 70% intensity detected in the first part of its emission (509 nm) curve cannot be used for unmixing, since this portion includes an almost equal contribution component from EGFP emission. However, values of similar intensity from signals collected at 550 nm can successfully be used to unmix our acquired data sets, since the EGFP component at this region is significantly reduced. The same approach was applied for the selection of all four regions of interest, to obtain sufficiently unmixed images (Figure 21).

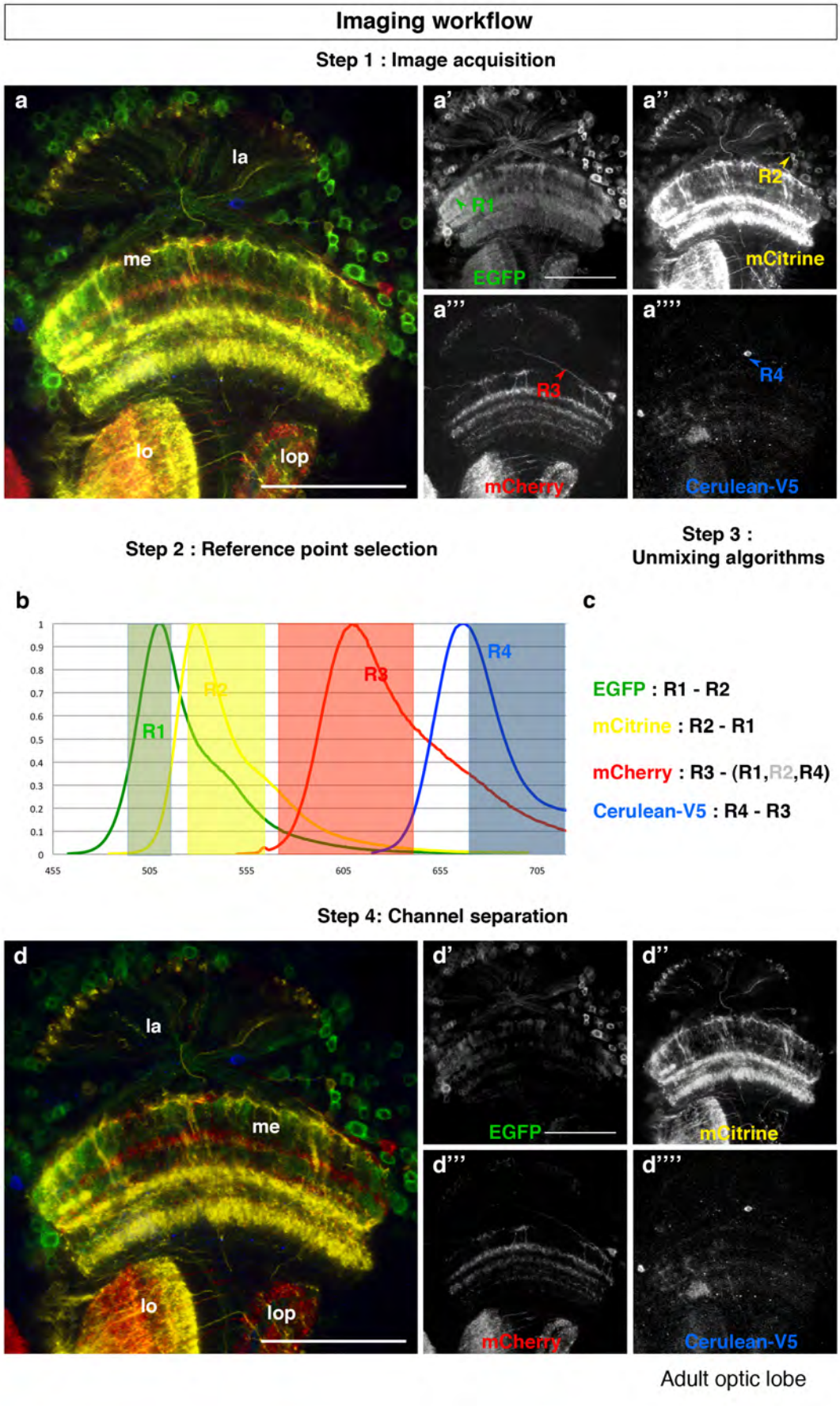
Imaging workflow
Step 1 : Image acquisition
a
la
me
lo
lop
a'
R1
EGFP
a''
R2
mCitrine
a'''
R3
mCherry
a''''
R4
Cerulean-V5
Step 2 : Reference point selection
Step 3 :
Unmixing algorithms
b
R1
R2
R3
R4
455
505
555
605
655
705
c
EGFP : R1 - R2
mCitrine : R2 - R1
mCherry : R3 - (R1,R2,R4)
Cerulean-V5 : R4 - R3
Step 4: Channel separation
d
la
me
lo
lop
d'
EGFP
d''
mCitrine
d'''
mCherry
d''''
Cerulean-V5
Adult optic lobe

Figure 21. Image acquisition protocol for samples expressing Flybow transgenes.
(a-a"") *elav-Gal4^{c155}* was used to drive expression of *FB2.0* in adult optic lobes. (a) Merged images of the four channels acquired. (a'-a"") Signal detected from three sequential scans mCitrine (a") and Cy5 (a""), mCherry (a'") EGFP (a'). Manually selected regions of interest (R1-4) are indicated with arrowheads for all channels. R1-4 was allocated as regions of the best signal to cross-talk ratio for every channel respectively **(b)**. Software algorithms (LAS suite) were employed to subtract the unspecific proportion of detected signal using manually allocated values (c). (d-d"") Unmixed images. (d) Overlayed and (d'-d"") individual images for true signal detected for (d') EGFP (d") mCitrine (d'") mCherry, (d"") Cy5. *elav-Gal4^{c155}/hs-Flp^{1}*; *hs-mFlp5/FB2.0*. Heat shocks 45' at 48 hours AEL. Scale bars, 50 μm.

In addition, we also tested two-photon confocal microscopy to image *FB1.1* transgene expression using the pan-neuronal driver *elav-Gal4^{c155}*. In all cases, we performed a series of lambda-scans (λ-scans) using a Mai Tai HP Deep Sea (680 nm-1040 nm spectral range, 100 fs pulse width) multiphoton laser for excitation. These were carried out using reference samples for the individual fluorophores. The newly generated lines *UAS-FB1.1^{260b}* (no heat-shock), *UAS-mCitrine^{260b}* and *UAS-mCherry^{260b}* were used to acquire the spectra for EGFP, mCitrine and mCherry respectively. We did not include a data set for Cerulean since we had previously observed suboptimal fluorescent properties. Interestingly, the emission spectra for the EGFP and mCitrine pair appeared to be overlapping to a greater extent (Figure 22) compared to the single photon conditions. In addition, mCitrine showed a weaker signal when compared to EGFP following two-photon excitation. Furthermore, we were able to retrieve emitted signal for mCherry, however due to the "blue-shift" in its excitation properties, it was sub-optimally excited, likely because of the Mai Tai laser limit at 1040 nm. These results are in agreement with previous reports confirming that spectral properties of fluorophores are substantially different when excited by two photons (Drobizhev et al., 2011). Our observations suggest that Flybow transgenes can in principle be used with two-photon microscopy. However, they need to be further optimized for such application by obtaining reference spectrum values for Cy5 and generating appropriate algorithms to unmix the signal obtained from all four channels. In conclusion, the current variants of the *Flybow* approach are better suited for single photon microscopy.

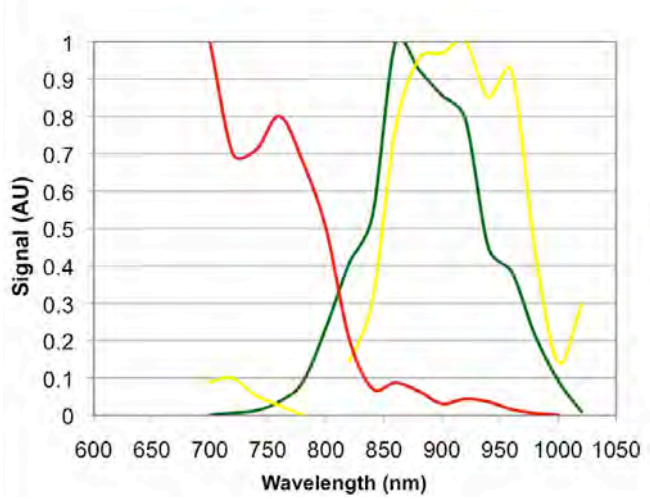

Figure 22. Spectral properties of fluorophores included in the Flybow approach using two-photon confocal microscopy.
Experimentally measured absorption spectra for mCherry (red line), EGFP (green line) and mCitrine (yellow line). Fluorophores were excited using a MaiTai HP Deep Sea Laser. Data have been normalized.

5.2.3 Evaluating the efficiency of the Flybow approach

Different transgenic lines yield similar transgene expression levels.

Position effects dramatically influence expression levels of non-native sequences inserted exogenously in the *Drosophila* genome (Schotta et al., 2003). This can be attributed to both the regional chromatin architecture, as well as the activity of locally acting regulatory elements. Using the *attP/attB* integration system, we inserted each of the Flybow transgene variants in two different genomic locations, one on the second (*VIE-260b, 2L*) and one on the third chromosome (*VIE-49b, 3R*) respectively (see section 3.9). These loci were selected based on observations indicating that they can serve as good landing positions for transgenes expressed using the Gal4/*UAS* system as they yield high expression levels and additionally show low background expression in absence of Gal4 (K. Keleman and B.J. Dickson, personal communication, (Dietzl et al., 2007)). Indeed, these loci yield low expression levels of transgenes under the control of defined enhancers and thus are less suitable for use in these experiments; e.g. a transgene driving expression of mCherry under a *Rhodopsin 6* (*Rh6*) enhancer element (*Rh6-mCherry*^{260b}) was not functional (W.Joly unpublished observations). Therefore, it was imperative to compare marker expression levels in animals, containing these different insertions. The use of *elav-Gal4*^{c155} resulted in expression of *FB1.1* in the nervous

system. We tested EGFP expression levels in third instar larval optic lobes of samples that corresponded to each of the two loci. We could confirm that there is no significance difference in fluorescence levels (Figure 23). We, thus, used both lines interchangeably in all subsequent experiments.

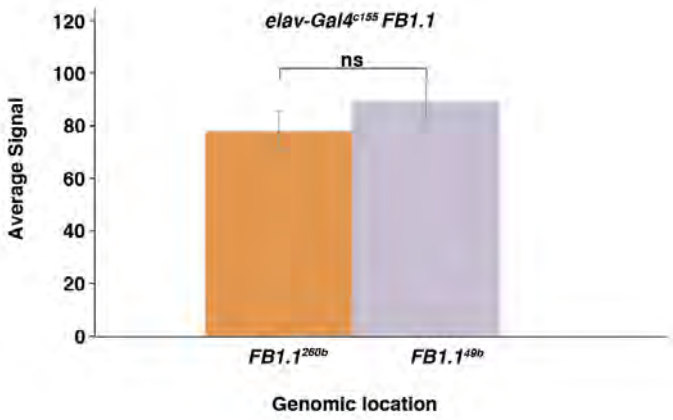

Figure 23. Quantification of EGFP fluorescence signal in *FB1.1*^{260b} and *FB1.1*^{49b} transgenic lines. The pan-neuronal *elav-Gal4*^{c155} driver was used for the expression of both the *FB1.1*^{260b} and *FB1.1*^{49b} transgenes in the visual system of *Drosophila*. Measurements indicating the amount of the detected fluorescence signal were obtained from cell bodies of neurons expressing EGFP at the third instar larval stage. Data for mean values of detected fluorescence across a cell body were considered for true signal estimation. True signal was calculated by subtracting the mean value for noise from the estimated mean value of detected signal per sample. Numbers indicate true signal averages for a total of 18 samples for both *FB1.1*^{260b} and *FB1.1*^{49b} used for quantifications. True signal averages from the two different genomic loci are not statistically different (*p=0.028*) indicating that the two transgenic lines can be used interchangeably. The histograms and error bars show averages and 95% confidence intervals. Unpaired two- tailed *t-tests* were performed for comparing data sets. Fiji measurement tools (line measuring tool) were used of measuring fluorescence levels. Values for detected signal ranged from 0-150 units, indicating no signal to fully saturated pixel, respectively. Statistical analysis was performed using Excel.

We next sought to compare the fluorescent signals from all the dyes employed. Individual fluorescent proteins used in our approach are inherently different with respect to their efficiency to fluoresce (Chudakov et al., 2010). Taking this into consideration we aimed to assess whether the acquired signal of each dye could be compared to each of the remaining three. *elav-Gal4*^{c155} was used to drive expression of *FB1.1* transgenes in the nervous system. Measurements from third instar larval optic lobes were performed to assess the relative range of

fluorescence intensity for each of the four dyes. These were taken from samples subjected to channel unmixing algorithms. Our results indicate that on average the signal detected in each channel is not significantly different when compared to each of the other three (Figure 24). We could thus be confident that the detected signals for all fluorescent proteins could be used to extract intricate cell shape information.

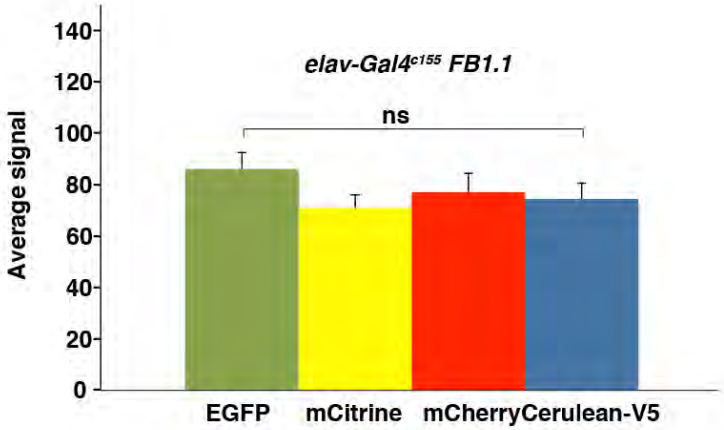

Figure 24. Signal from all four fluorescent dyes is detected at similar levels.
Employing *elav-Gal4*^{c155} in combination with the *FB1.1* approach on the second chromosome, optic lobes of third instar larvae were labeled with the expression of EGFP, mCitrine, mCherry and Cerulean-V5. We obtained data from 11 different samples. True signal values were estimated for four different measurements per sample for each of the four fluorescent markers. The average true signal values for each fluorescent dye are not statistically significant ($p > 0.05$). The histograms and error bars show averages and 95% confidence intervals. Unpaired two-tailed *t-tests* were performed for comparing data sets. Fiji measurement tools (line measuring tool) were used for measuring fluorescence levels. Values for detected signal ranged from 0-150 units, indicating no signal to fully saturated pixel, respectively. Statistical analysis was performed using Excel.

5.2.4. Recombination events occur in similar frequencies

We have established that *FB*^{260b} and *FB*^{49b} transgenic lines yield similar levels of fluorescent protein expression. Moreover, we have seen no significant difference in fluorescence levels regarding the four fluorescent proteins used. Next, we sought to examine the frequency, with which the modified mFlp5/*mFRT71* system induces the different recombination events and, thus, color outcomes. The *elav-Gal4*^{c155} driver line was used for expression of *FB1.1* and *FB2.0* in the

visual system at third instar larval stages. Sets of samples for both *FB1.1* and *FB2.0* were used for quantifications. We determined cell body numbers for the four channels within three different optical sections per sample. Sections, at least 10 µm apart within an individual sample, were selected to avoid double counting of single cells. Initial analysis of *FB1.1* expressing samples subjected to a single 45 minutes heat shock at 48 hours AEL showed that in addition to the abundantly expressed EGFP, 58% of samples expressed all the other three fluorescent proteins, 25% expressed two additional fluorescent proteins and 17% expressed one additional fluorescent protein. This showed that under these experimental conditions, mFlp5 induces all recombination events. Next, in a similar experiment, we exposed flies to three 30 minutes heat-shocks at 48, 72 and 96 hours AEL, respectively, aiming to increase the percentage of samples, in which all fluorescent dyes were expressed. In all samples, mFlp5 mediated color switches with 100% efficiency and we observed expression of all four markers. Overall, the default fluorescent protein, EGFP, was expressed in the majority of the cells counted. Nevertheless, the additionally expressed markers, mCitrine, mCherry and Cerulean-V5 were expressed at similar frequencies (Figure 25). Subsequently, we analysed *FB2.0* transgene expression in a cohort of samples exposed to 90 minutes heat-shocks at 48 and 72 hours AEL. As with *FB1.1*, samples similarly showed no significant difference in the occurrence of color events (mCitrine, mCherry and Cerulean-V5) (Figure 27). We can thus conclude that upon mFlp5 activity all recombination outcomes can occur and lead to a roughly even color distribution.

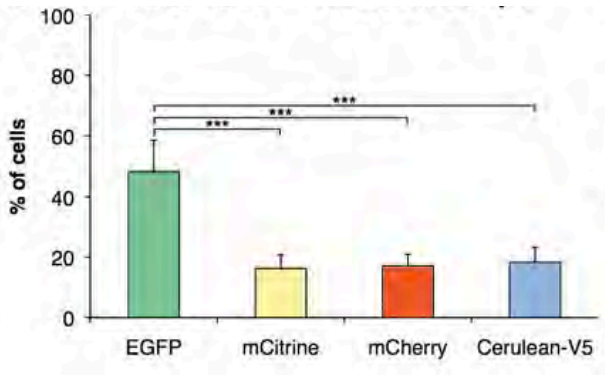

Figure 25. Quantification of mFlp5 mediated recombination events using the *FB1.1* transgene.
Recombination events induced by mFlp5 in the optic lobe of animals expressing *FB1.1* under the control of the pan-neuronal driver *elav-Gal4*^{c155} after exposure to three 30 minutes heat shocks at 48, 72 and 96

hours AEL. Numbers of neurons expressing the four FPs were obtained from three z sections of 10 optic lobes, corresponding to 3,367 ± 299.8 cells (mean and 95% confidence interval) per sample. Quantification of percentages indicated that an average of 48.2% of neurons expressed EGFP, 16.3% mCitrine, 17.2% mCherry and 18.3% Cerulean-V5. While EGFP is most abundantly expressed ($p < 0.0001$, unpaired two tailed *t*-test), the differences in percentages of mCitrine, mCherry and Cerulean-V5 expressing cells are not statistically significant ($P > 0.58$), indicating that these are expressed with similar probability. The histograms and error bars show mean percentages and 95% confidence intervals. Statistical analysis was performed using Excel.

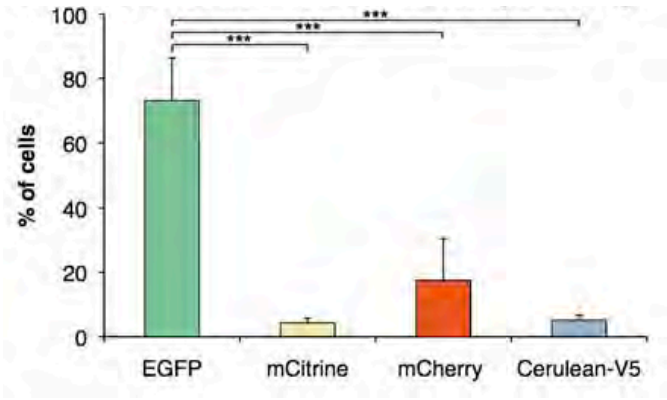

Figure 26. Quantification of mFlp5 mediated recombination events using the *FB2.0* transgene.
Recombination events in the optic lobe of animals expressing *FB2.0* under the control of *elav-Gal4*^{c155} after exposure to two 90 minutes heat shocks at 48 and 72 hours AEL. Numbers of neurons expressing the four fluorescent proteins were obtained from 10 optic lobes (three z sections, $n = 9$; two z sections $n = 1$), corresponding to 729.3 ± 268.5 labeled cells (mean and 95% confidence interval) per sample. This confirms that *FB2.0* in conjunction with Flp and mFlp5 leads to sparse labeling. An average of 73.1% of neurons expressed EGFP, 4.3% mCitrine, 17.5% mCherry and 5.1% Cerulean-V5. EGFP is most abundantly expressed ($p < 0.0001$, *t*-test). Frequencies of mCitrine, mCherry and Cerulean-V5 expressing cells are highly variable and differences are not statistically significant ($p > 0.06$, *t*-test). The histograms and error bars show mean percentages and 95% confidence intervals. Statistical analysis was performed using Excel.

5.2.5. Expression of the four fluorescent proteins was detected in a predominantly mutually exclusive manner

We sought to verify whether the *FB1.1* transgene is expressed in a mutually exclusive fashion similarly to the *FB1.0* approach. We chose the eye imaginal disc at the third instar larval stage to test *FB1.1* expression. The development of this epithelial structure is well characterized. Thus, assaying marker expression within this two-dimensional (2D) epithelium is much simpler in comparison to the complex 3D optic lobe structure. R-cells differentiate and assemble into clusters in a characteristic manner posterior of the morphogenetic furrow. This array allows monitoring as to whether single neurons express fluorescent proteins in a mutually exclusive

manner. Utilizing the *FB1.1* approach in combination with the *elav-Gal4^{c155}* driver we could label R-cells with the expression of EGFP, mCitrine, mCherrry and Cerulean-V5 in a randomized mutually exclusive manner. Flies subjected to as many as three heat shocks at early larval stages expressed sufficient levels of mFlp5 necessary for recombination (Figure 27).

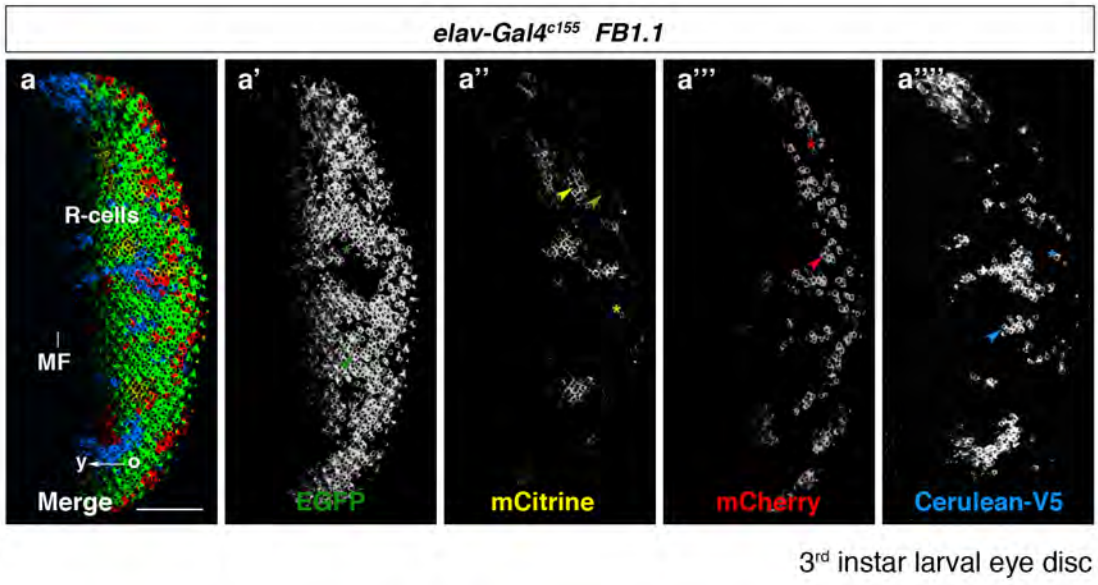

Figure 27. *FB1.1* transgene activation leads to mutually exclusive expression of the four FPs within the eye imaginal disc.
Photoreceptor cells (R-cells) within the third instar larval eye disc differentiate and assemble into ommatidial clusters behind the morphogenetic furrow (MF), in a posterior to anterior fashion (white arrow, a). The pan-neuronal driver *elav-Gal4^{c155}* was used to drive expression of *FB1.1* transgenes. Subsequent to heat shock pulses EGFP (a'), mCitrine (a''), mCherry (a''') and Cerulean-V5 (a'''') were expressed in a mutually exclusive manner (a-a''''). Expression of the same fluorescent protein was detected across several neighboring ommatidia (color-coded arrowheads) as well as individual R-cells within a single ommatidium (color-coded asterisks). EGFP is abundantly expressed, as it constitutes the default fluorescent protein for expression of the *FB1.1* transgene. Signals detected for all dyes were subjected to unmixing algorithms. Unspecific signal from EGFP expressing cells could still be detected following to unmixing in the mCitrine channel (a'', yellow-green arrowhead). *elav-Gal4^{c155}/+ or Y*; *hs-mFlp5/FB1.1^{260b}*. Heat shocks 90' at 48 h and 72 h AEL. Scale bar, 50 μm.

Next, using the same genetic scheme we tested expression in the optic lobe of third instar larvae (Figure 28). We could identify differentially labeled R-cell axons terminating within the emerging optic lobe neuropils; namely in the lamina, R1-R6 and the medulla, R7/R8 (Figure 28, a''). All color outcomes were observed. We could detect clusters of both lamina and medulla neurons stochastically labeled by the expression of four fluorescent markers. At the lateral edge

of the OPC, LPCs give rise to lamina neurons, L1-L5, which are subsequently recruited into lamina columns. Conversely, at the medial edge of the OPC, neuroblasts give rise to the different types of the medulla neurons. Early born medulla neurons, are displaced towards the neuropil and away from the OPC, by their newly generated siblings within the same lineage. Interestingly, we could identify lineage-related or non-related clusters for both lamina and medulla neurons. Single recombination events can mark the entire cluster with the same color in the younger part of the medulla (Figure 28a””). Nevertheless, older cells potentially exposed to sequential recombination events switch fluorescent marker expression multiple times and, thus, are differentially marked within their cluster (Figure 28a”’).

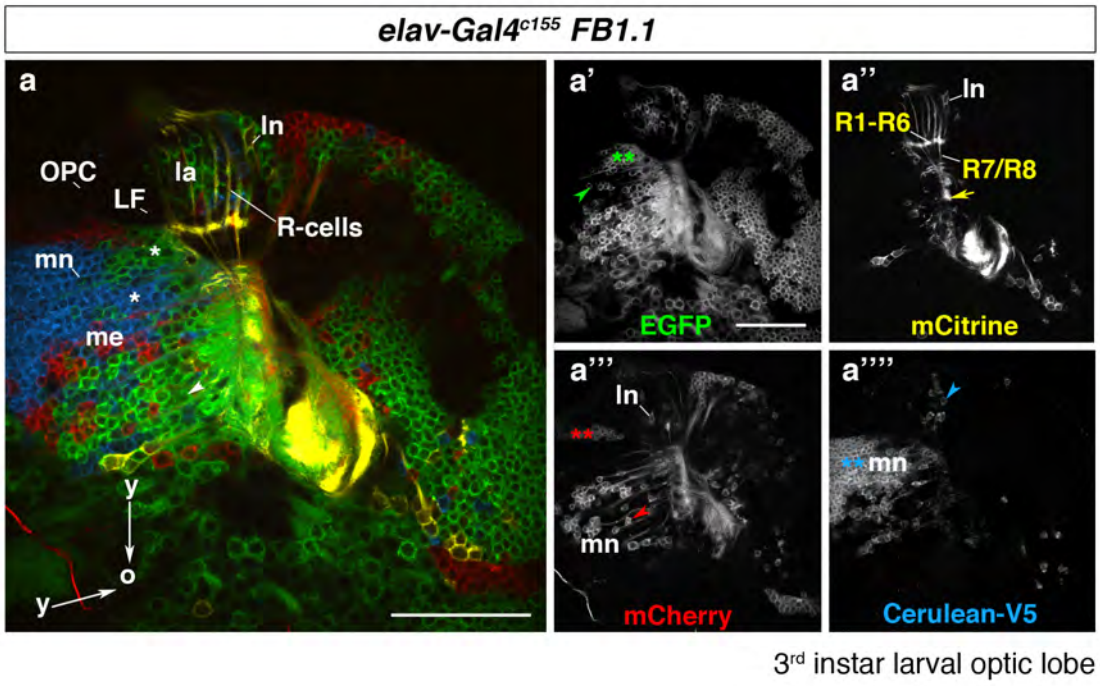

Figure 28. Expression of *FB1.1* transgenes in the developing optic lobe of *Drosophila*.
Photoreceptor cells (R-cells, R1-R8) extend their axons into the developing optic lobe. There, they release signals to promote the formation of the postsynaptic partners of R1-R6 axons in the lamina (la). R7 and R8 axons terminate in the medulla (me). Neuroepithelial cells in the outer proliferation center (OPC) generate lamina precursor cells that give rise to lamina neurons (ln) posterior to the lamina furrow (LF). Medially, the OPC generates neuroblasts (NB), which divide asymmetrically to produce ganglion mother cells and medulla neurons (mn). Older (o) neurons are located closest to the neuropil and away from the OPC (a, arrowhead), whereas younger (y) neurons are positioned proximal to the OPC (a, asterisks). *elav-Gal4*^{c155} was used for expression of *FB1.1* in third instar larval optic lobes. Activation of the *FB1.1* approach leads to expression of mCitrine (a”), mCherry (a”’) and Cerulean-V5 (a””) in addition to the default EGFP (a’). Distinct neuron subtypes within the optic lobes such as R-cells, lamina neurons (ln), medulla neurons (mn) express all four fluorescent proteins. Membrane expression of fluorescent proteins can be detected in clusters, single neuron cell bodies and axonal extensions (a-a””) as well as delicate

growth cone structures (a", arrow). Lineage-related clusters of cells were labeled with the same (double asterisks, color-coded) or distinct (arrowheads, color-coded) fluorescent proteins. *elav-Gal4^{c155}*/+ or *Y*; *hs-mFlp5/FB1.1^{260b}*. Heat shocks were 45 minutes at 48 hours, 72 hours and 96 hours AEL. Scale bar, 50 μm.

Subsequently, we sought to test the expression of the *FB1.1* variant in the adult to ensure that fluorescent protein expression is maintained throughout development and fine structures of individual neurons can be visualized within their positively labeled neuronal environment. Using the same genetic background we observed strong expression of the four markers in the entire neuronal population within the visual system (Figure 29a). Axonal and dendritic processes of individual lamina and medulla neurons were visualized (Figure 34). Owing to strong fluorescence, previously described neuron subtypes could be identified based on their characteristic morphologies that could be traced throughout the optical stack (Figure 34, 36 and 38). Moreover, aiming to better visualize branching patterns of single neurons we removed the GFP channel that was abundantly expressed (Figure 29a'). Consequently, we could readily recognize well known neuron morphologies: for instance in the lamina, the dendritic pattern of a lamina neuron L1, expressing mCherry, as well as an mCitrine expressing lamina neuron L5 terminating within the medulla was clearly identifiable.

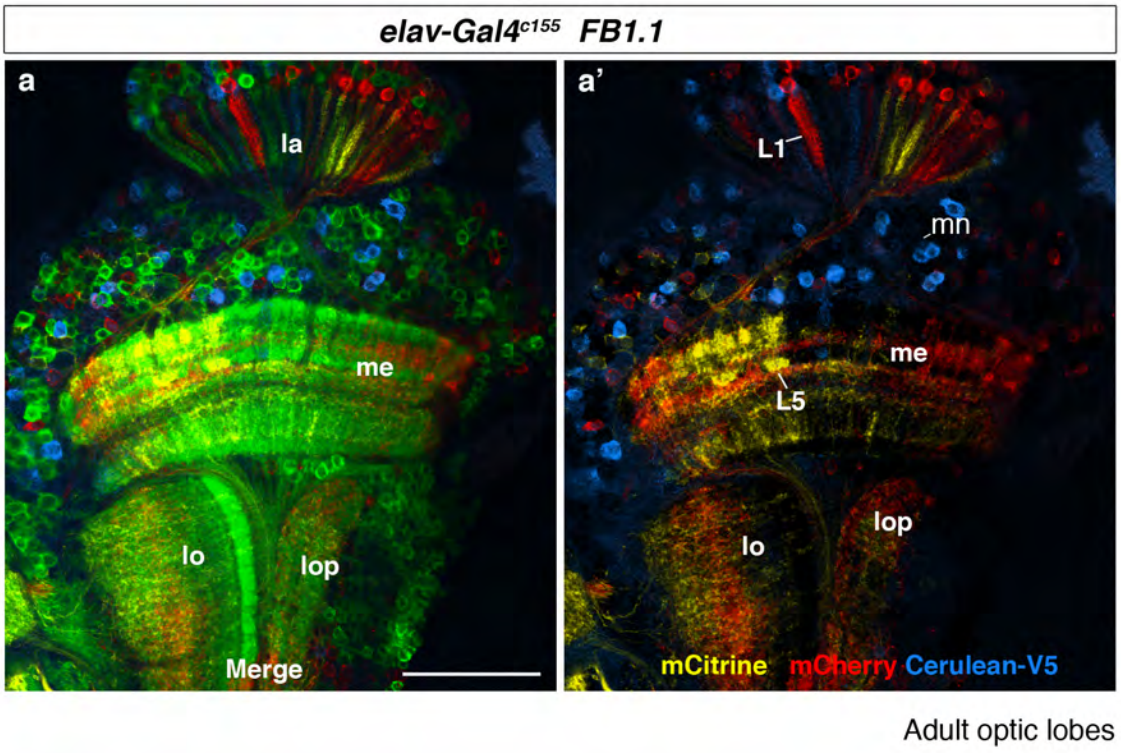

Figure 29. *FB1.1* transgene expressed in the adult visual system of *Drosophila*.
Adult optic lobes represent functional structures able to convey visual information to the brain for processing. *elav-Gal4*^{c155} was used for expression of *FB1.1* transgenes. Activation of the *FB1.1* approach leads to expression of mCitrine, mCherry and Cerulean-V5 in addition to the default EGFP (a-a'). *FB1.1* provides adequate resolution to identify neuron subtypes based on their arborizations. Lamina neurons L1 (mCherry) and L5 (mCitrine) could be identified in samples, in which all the neighboring neurons were also positively labeled. Arborization patterns were not affected by the expression of the fluorescent proteins. *elav-Gal4*^{c155}/+ or *Y*; *hs-mFlp5/FB1.1*^{260b}. Heat shocks 90 minutes at 48 and 72 hours AEL. Scale bar, 50 μm.

We have established heat-shock protocols that result in sufficient mFlp5 activity and consequently largely mutually exclusive expression of the four markers used in our approach, conferring single cell resolution within the visual system of the developing and adult flies. Next, we sought to test the scenario of repeated and prolonged exposure of samples from the same genetic background to elevated levels of mFlp5 activity. Prolonged time of heat exposure could be challenging for the flies used in our experiments. Moreover, we hypothesized that high levels of recombinase activity could potentially result in the detection of cells marked by the simultaneous expression of two fluorescent proteins as a result of continuous transgene rearrangements. Additionally, we tested as to whether this repeated exposure to mFlp5 could in some cases result in chromosomal aberrations due to unspecific recombination leading to cell

death and thus detection of "fragmented cells". We thus exposed *FB1.1* expressing flies to three long heat shocks during development of 90 minutes each. We could not detect any lethality caused by this prolonged exposure to heat. Interestingly, we observed the appearance of double-labeled cells; however, generally, expression remained predominantly mutually exclusive (Figure 30). Importantly, under these conditions we did not observe aberrations in cell morphology reminiscent of cell death occuring.

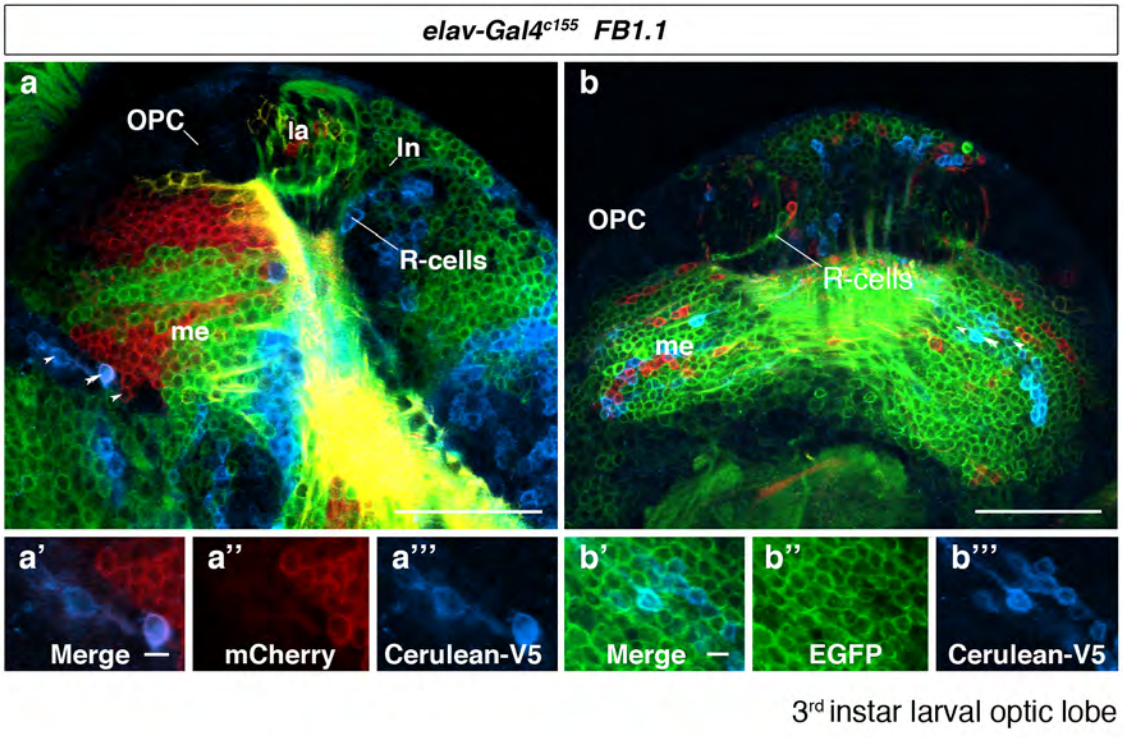

Figure 30. Inducible recombinase expression leads to mainly mutually exclusive expression of the four fluorescent proteins.
Flybow uses one transgene copy for the expression of the four fluorescent dyes within a single cell. Following mFlp5 expression, DNA rearrangements occur and lead to both reversible (inversions) and irreversible (excisions) events. mFlp5 is active throughout the length of the heat-shock pulse but likely becomes inactive soon after the end of the heat shock. Different recombination events can be monitored by the expression of the four different color outcomes. Expression is stable and largely mutually exclusive. *elav-Gal4^{c155}* was used for expression of *FB1.1* in third instar larval optic lobes (a-b'''). A three heat-shock protocol was performed to expose the samples to large amounts of mFlp5. Activation of the *FB1.1* approach leads to expression of mCitrine (a''), mCherry (a''') and Cerulean-V5 (a'''') in addition to the default EGFP. Photoreceptor cells (R-cells) and different lineages of the outer proliferation center (OPC) in the lamina (ln) and the medulla (me) were differentially labeled with the four dyes. (a-b''') A small number of double colored medulla neurons (mn) could be observed (a-b, double arrowheads and a'-b'''). The majority of mn express a single fluorescent protein, even the ones belonging to the same cluster (arrowheads). *elav-Gal4^{c155}*/+ or *Y*; *hs-mFlp5/FB1.1^{260b}*. Heat shocks 90 minutes at 48, 72 and 96 hours AEL. Scale bars, 50 μm (a, b) and 5 μm (a'-b''').

5.2.6. Constant mFlp5 activity increases the number of cells with overlapping fluorescent protein expression

The results described above showed that prolonged mFlp5 activity can lead to overlapping marker expression. Importantly in those experiments, we used repeated activation of *mFlp5* transcription leading to higher levels mFlp5 exposure compared to our standard protocol (Section 5.2.1). Placing its expression under the regulatory elements of specific genes of interest can provide an alternative source of mFlp5. In this case the recombinase will be expressed continuously within the gene expression domain. We thus sought to examine the outcome of a constitutively expressed recombinase in our system. We hypothesized that sequential recombination events would take place and result in double labeled cells. Since the *FB1.1* transgene contains both invertible and flip-out cassettes, we reasoned that constant mFlp5 activity would eventually lead to the excision of the one of the two cassettes in the majority of cells. The remaining single cassette would be continuously inverted and thus both of the marker coding sequences it includes would be interchangeably expressed. This could generate samples predominately containing "light-green" or "purple" cells. Additionally, we wanted to test if under constant expression we could detect cell death due to unspecific recombination. To test this, we chose to express mFlp5 under the control of *eyeless* (*ey*) regulatory elements, using 4 tandem repeats of a 258 bp sequence included in this enhancer (Newsome et al., 2000). This plasmid was provided by B. Dickson's laboratory. Because the original transgenic line had not been maintained, we re-injected the plasmid and recovered an insertion on the second chromosome. Embryo injections were performed together with I. Salecker. Using this new *ey-mFlp5* transgene, the recombinase was continuously expressed during eye development. We monitored *FB1.1* expression in the developing eye disc (Figure 31). As expected, double-labeled cells could be detected in abundance. Moreover, due to increased excision events that are irreversible samples were progressively labeled with either "light-green" or "purple" cells. This is indicative that a fine-tuned inducible system yields better results when aiming for the generation of samples labeled with all the four fluorescent proteins used in our approach.

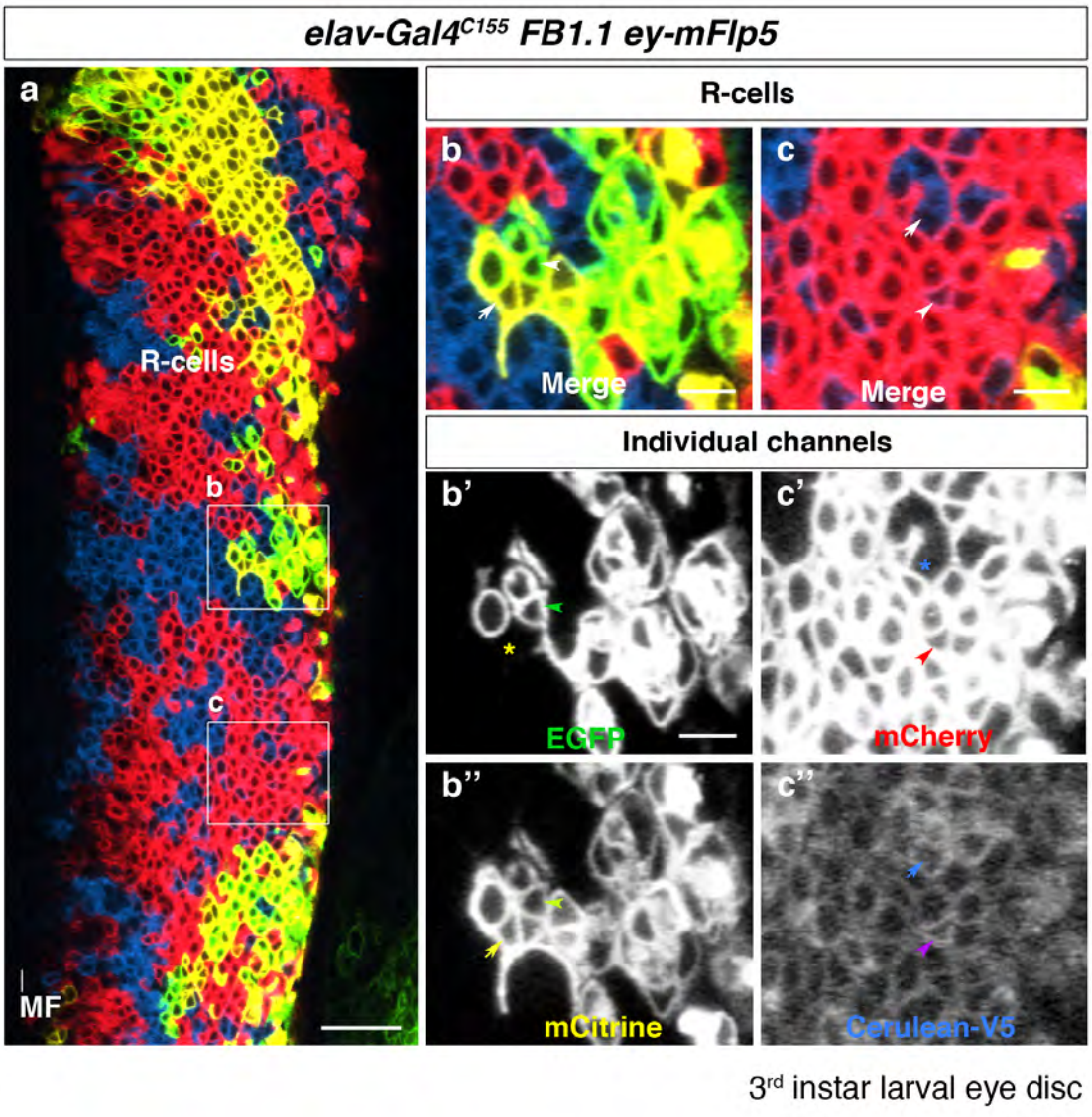

Figure 31. Continuous *mFlp5* activity increases the occurrence of overlapping expression of fluorescent proteins.

Photoreceptor cells (R-cells) differentiate within the eye disc posterior to the morphogenetic furrow (MF) at the third instar larval stage. *elav-Gal4^{c155}* was used to drive expression of *FB1.1* transgenes. The *eyeless* (*ey*) enhancer was employed to drive constitutive expression of mFlp5 recombinase. mCitrine, mCherry and Cerulean-V5 were observed in addition to default EGFP expression (a). Overlapping expression of two fluorescent proteins within single cells could be readily detected (a, b-c", arrowheads). Mutually exclusive expression could also be observed (b-c", arrows) but in lower numbers compared to samples generated using the inducible form of mFlp5. EGFP and Citrine expressing cells were reduced in numbers due to frequent excision of the first cassette. *elav-Gal4^{c155}/+ or Y*; *ey-mFlp5/FB1.1^{260b}*. Scale bars, 50 μm (a) 10 μm (b-c").

5.3 Expression of fluorescent proteins does not interfere with neuronal development

5.3.1 Assessment of shapes of growth cones and mature terminals

Recombinant fluorescent protein accumulation or its abnormal localization within a cell has been shown to interfere with normal development and function (Ito et al., 2003; Shaner et al., 2004; Shaner et al., 2007). To test if expression of the labeling agents used in our approach can cause defects we monitored fluorescent protein expression in the topographic array of R-cell axons in the developing and adult visual systems. Importantly, developing R-cell axons represent a very sensitive neuron population and, thus, provide a good system to uncover underlying toxicity due to marker expression. We used the *Glass Multimer Reporter* (*GMR)* driver, *GMR-Gal4,* to specifically express *FB1.1* transgenes in R-cells. We observed stochastic expression of all four fluorescent proteins in axonal projections at the third instar larval stage and in adult terminals (Figure 32). The characteristic morphology of R-cell axon terminals was not affected by the expression of membrane-anchored fluorescent proteins. In this experimental setting, we could monitor R7/R8 growth cone maturation in comparison to the previously reported morphological changes occurring during this process (Senti et al., 2003). Specifically, young growth cones display a spear-like shape; as they progress to a more mature state, they alter their structure to an inverted Y-like morphology. Importantly, this was easy to detect due to the fact that the entire R-cell array was positively marked by fluorescent protein expression, thus enabling direct comparison with neighboring cells. In the adult, R7 and R8 axons terminated normally in their M6 and M3 layers, respectively. Thus, pathfinding of R-cell axons was unaffected by expression of the four markers. R-cell axons innervating the same column in the medulla were labeled with either the same or a different fluorophore. Additionally, neighboring columns in accordance were either differentially labeled or marked with the same fluorescent protein color.

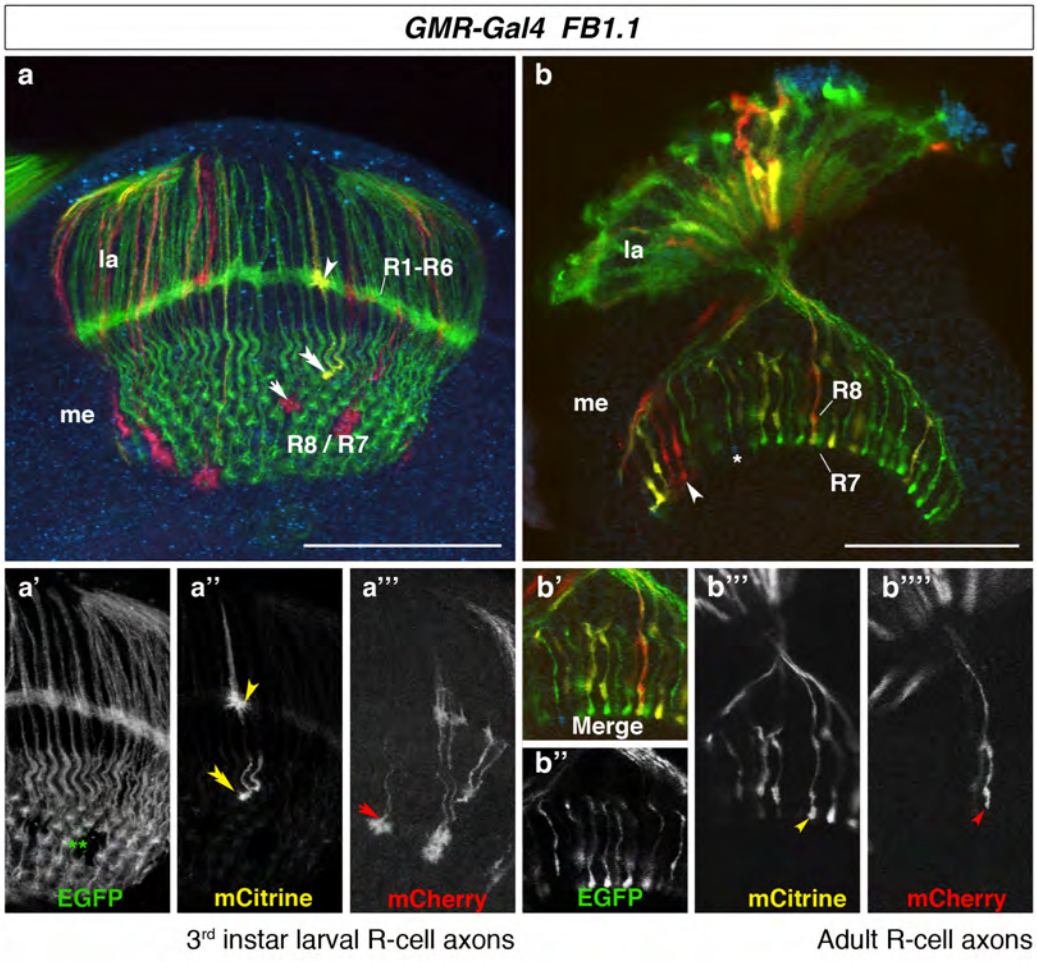

Figure 32. Labeling of R-cell projections with *FB1.1* does not disrupt growth cone guidance.
Photoreceptor subtypes R1-R8, expressed all four fluorescent proteins using *pGMR-Gal4* for *FB1.1* transgene expression. Individual R-cell projections in both the larval (a-a''') and adult (b-b'') brains extend normally into the lamina (la) and medulla (me). Activation of the *FB1.1* approach leads to expression of mCitrine, mCherry and Cerulean-V5 in addition to the default EGFP (a, b). Expression was mutually exclusive (a', double asterisks). Individual growth cones expressing different fluorescent proteins exhibit morphological changes during larval development (a-a'''). R1-R6 axons terminating in the lamina show elaborate growth cones (a, a'', arrowhead). Young R8 growth cones (double arrowhead) show a spear-like morphology. Mature R8 growth cones (a, a''', arrow) adopt an inverted Y shape. In adult brains, R8/R7 termini (b-b'''') innervating the same column can express the same (b, white arrowhead) or a combination of different fluorescent proteins (b, asterisk and b''', b'''' color coded arrowheads). *GMR-Gal4/FB1.1^{260b}; hs-mFlp5/+*. Heat shocks 30 minutes at 72 and 96 hours AEL. Scale bar, 50 µm.

5.3.2 Single cell clones allow identification of described neuron subtypes

An important application for our approach is to identify neuron subtypes based on their morphological characteristics. Having established that membrane-anchored expression of fluorescent proteins neither interferes with normal development of neurons nor alters their projections, we could further attempt to identify and reconstruct neuron subtypes within adult

optic lobes. Using *elav-Gal4*^{c155} in combination with the *FB1.1* transgene to label all neurons in the optic lobe, we focused our efforts on the densely innervated and thus more challenging medulla neuropil. We used a single heat shock of 45 minutes at 48 hours AEL, as at this developmental time, neurons innervating the medulla start to be generated. Interestingly, expression of *mFlp5* at this specific developmental time can uncover underlying biological processes within the medulla. For instance, a progenitor born at this point will be exposed to mFlp5 recombination that can result in a color swap. Since we only use one heat shock, these samples will not be further exposed to recombination. Thus, the entire lineage of this progenitor, which continues to divide, and will be stably marked with the newly acquired color outcome. In parallel, neighboring progenitors, and consequently their resulting offspring, could be labeled with the expression of a different fluorescent protein. We can thus examine individual neuron subtypes of cells marked with different colors in the adult and gain insights about their final positions or relative distribution within a neuropil. Furthermore, we could confirm that our experiments provide adequate resolution for neuron subtype identification. For instance, we obtained two different types of samples. First, we found lineage related cell clusters; we identified ascending T2-T5 neurons in groups labeled stochastically with the expression of mCitrine, mCherry and Cerulean-V5 in addition to the default EGFP (Figure 33). These lobula plate-derived neurons extensively innervate the medulla (K.-F Fischbach, 1989). Interestingly, differentially labeled clusters innervated neighboring columns within the neuropil. This indicated that progenitors generating this lineage are born at approximately at 48 hours AEL and produce their progeny at a later stage. These events occurred in the progenitors in the IPC, for which so far little is known about the modes of neurogenesis. Additionally, we could observe that neurons labeled with the same color remained in neigboring positions, thus indicating that unlike for medulla neuron types, there is limited mixing due to extensive cell body migration during metamorphosis within these individual lineage clusters in the lobula complex. Second, we frequently labeled single cells; in another example taken from the same set of experiments, we could identify distinct medulla neuron subtypes by extracting information solely from a single detection channel (Figure 34). While all three neurons

expressed mCherry they were located in different parts of the neuropil and their branches did not overlap (Figure 34a). Due to strong and homogeneous fluorescence of mCherry we could readily reconstruct their entire structure including fine dendritic arbors (Figure 34d-f), used the Single Neurite Tracer plug-in of the Fiji software suite (ImageJ). Reconstructions were then compared with the medulla neuron subtypes described in previous atlases (Figure 34b-d). We could thus identify an amacrine Dm3 neuron in the distal medulla (Figure 34c and e) and two transmedullary neuron subtypes, one projecting into the lobula, Tm18 (Figure 34d and f), and one projecting to both the lobula and the lobula plate, TmY5a (Figure 34b and d). Hence, we can confirm that our approach is suitable for studies aiming to characterize neuron subtypes included within a specific gene expression domain. Importantly in this example, we could reconstruct individual neurons using a pan-neuronal driver that results in the positive labeling of the entire tissue and thus constituted a very complicated task.

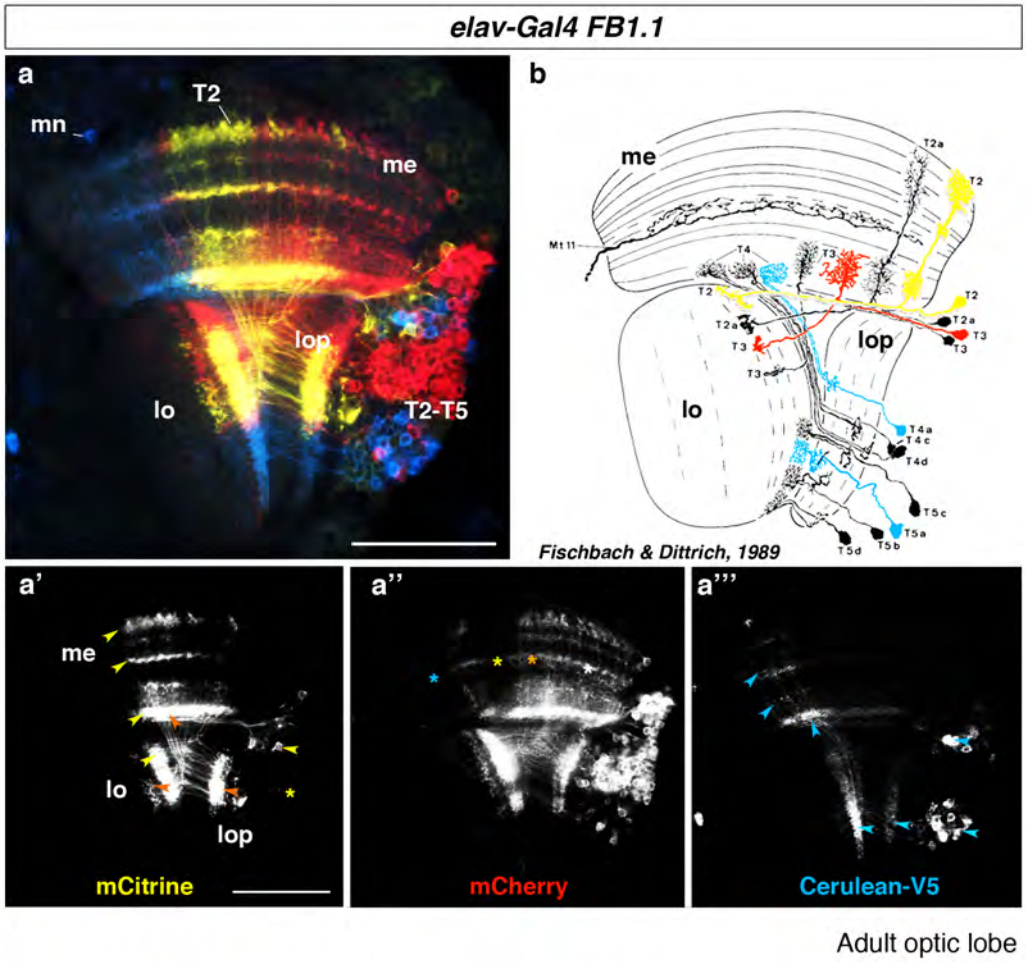

Figure 33. Expression of *FB1.1* transgenes can label clonally related neurons in the fly visual system

Flybow leads to stochastic expression of EGFP, mCitrine, mCherry and Cerulean-V5. Different color outcomes are consequent to DNA rearrangements mediated by to mFlp5 activity. *elav-Gal4*^{c155} was used for expression of *FB1.1* transgenes throughout development and visualized in adult stages (a-a'''). Schematic representation of ascending T2-T5 neurons (K.-F Fischbach, 1989) (b). Lineage-related T2-T5 neurons connecting the medulla (me) lobula (lo) and lobula plate (lop) were differentially labeled with mCitrine (a'), mCherry (a") and Cerulean-V5 (a"'). EGFP signals were removed. Clusters of T neurons were labeled with individual colors and both their cell bodies and axon and dendrite arborizations (color-coded arrowheads) are found to occupy neighboring areas (color-coded asterisks) within the adult visual system. *elav-Gal4*^{c155}/+ or *Y*; *hs-mFlp5/FB1.1*^{260b}. Heat shocks were 45 minutes at 48 hours AEL. Scale bar, 50 μm.

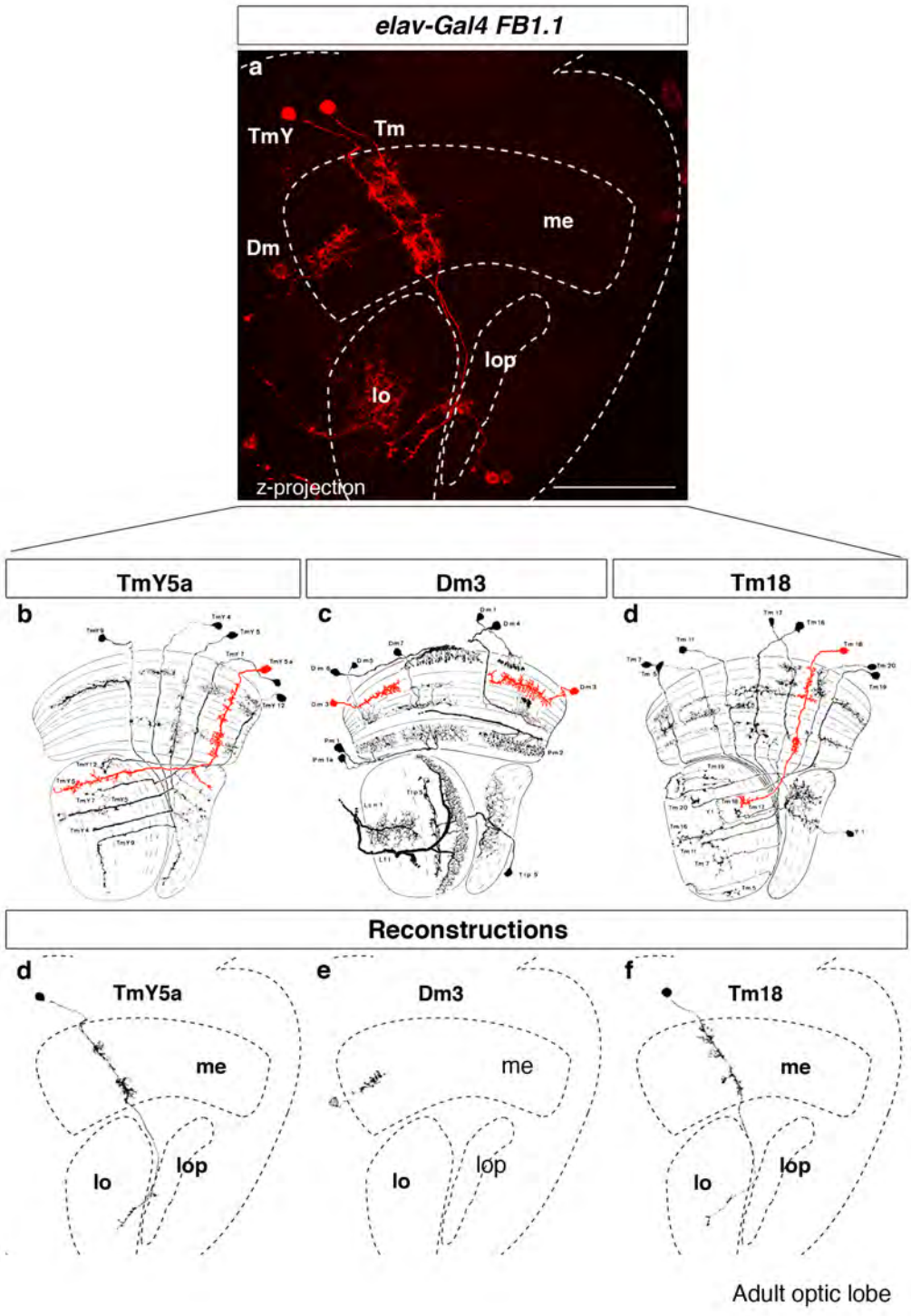

Figure 34. Subtype identity can be attributed to single cells within one sample using established anatomical maps

The medulla (me) comprises approximately 60 different medulla neuron subtypes, and thus constitutes the most complex of the visual system neuropils. Using the pan-neuronal driver *elav-Gal4*^{c155} for expression of *FB1.1* transgenes we could label the entire medulla neuron population in the adult optic lobe (a). Distinct medulla neuron subtypes were differentially labeled with the four fluorescent dyes. Using information from a single channel (mCherry) throughout a 36 µm portion of our z-stack, three medulla neurons could be identified. An amacrine (Dm) neuron in the distal medulla and two transmedullary neurons projecting to the lobula (Tm) or both the lobula and lobula plate (TmY) (a). Schematic representations of the adult visual system neuropils adapted from (K.-F Fischbach, 1989);

highlighted are the subtypes of medulla neuron types identified in our experiment (b). Reconstructions of the TmY5a, Dm3 and Tm18 neurons (c). *elav-Gal4^{c155}/+ or Y*; *hs-mFlp5/FB1.1^{260b}*. Heat shock:45 minutes at 48 hours AEL. Scale bar, 50 μm.

5.3.3 Employing Flybow to identify Vsx1 expressing neuron types in the adult visual system

We have so far examined the performance of Flybow in the context of positively labeling the entire neuron population using *elav-Gal4^{c155}*. However, the approach will be mostly used to discern neuron subtypes defined by the expression of genes in a more restricted fashion. In vertebrates, *vsx1* and *Chx10/vsx2* genes have been reported to play a crucial role in the development of the visual system (Burmeister et al., 1996; Ferda Percin et al., 2000; Liu et al., 1994). Homeodomain and CVC-domain containing transcription factors have been implicated in controlling the proliferation of retina progenitor cells and later the differentiation of bipolar cells (Burmeister et al., 1996; Liu et al., 1994). In *Drosophila,* the enhancer trap insertion *MzVum-Gal4* specifically reports the expression of Vsx1 and has been used to visualize the Ventral Unpaired Median (VUM) population in the ventral nerve cord (Erclik et al., 2008; Landgraf et al., 2003). Moreover in our laboratory, in the context of a genetic screen to uncover genetic markers expressed in subsets of cells within the optic lobe, *MzVum-Gal4,* was identified since it showed expression in the visual system. Thus, this driver has been previously characterized to drive strong expression specifically in the adult medulla (experiments performed by I. Salecker). Importantly, its expression is restricted to a high number of medulla neuron subtypes. We used *MzVum-Gal4* in combination with both *FB1.1* and *FB2.0* approaches and immunolabeling with the R-cell specific antibody mAb24B10. Using expression of a single marker, EGFP, we observed that innervation of the medulla neuropil layers M2 and M4 was particularly dense (Figure 35, a). However, we were not able to determine individual medulla neuron subtypes included in this population. On the contrary, when using *FB* in combination with the *MzVum-Gal4* driver, we could gather information leading to identification of specific subtypes. We used single detection channels that contain information from the expression of individual fluorescent proteins. We could determine the position and distribution of medulla neuron cell bodies, as well as the layered and columnar branching patterns of their neurites

(Figure 35b-b””). We observed gaps at layers M1, distal M2, M3 and M5 occurring in a reiterated manner (Figure 35). These correspond to characterized positions predominately occupied by lamina neuron axon terminals. Vsx1 positive medulla neurons highly innervate the proximal part of the M2 layer, as well as layers M4 and M6-M10. Interestingly, in this sample, cell bodies of neurons expressing mCherry were located more distally in comparison to the majority of subtypes marked by Cerulean-V5 expression (Figure 35b”’-b””, asterisks). This could perhaps indicate that a recombination event resulting in expression of either of the two markers within a specific linage marks selectively one medulla neuron subtype. Thus during metamorphosis, cell bodies of these neurons become located in a similar position on the proximal-distal axis and innervate the neuropil in a characteristic manner.

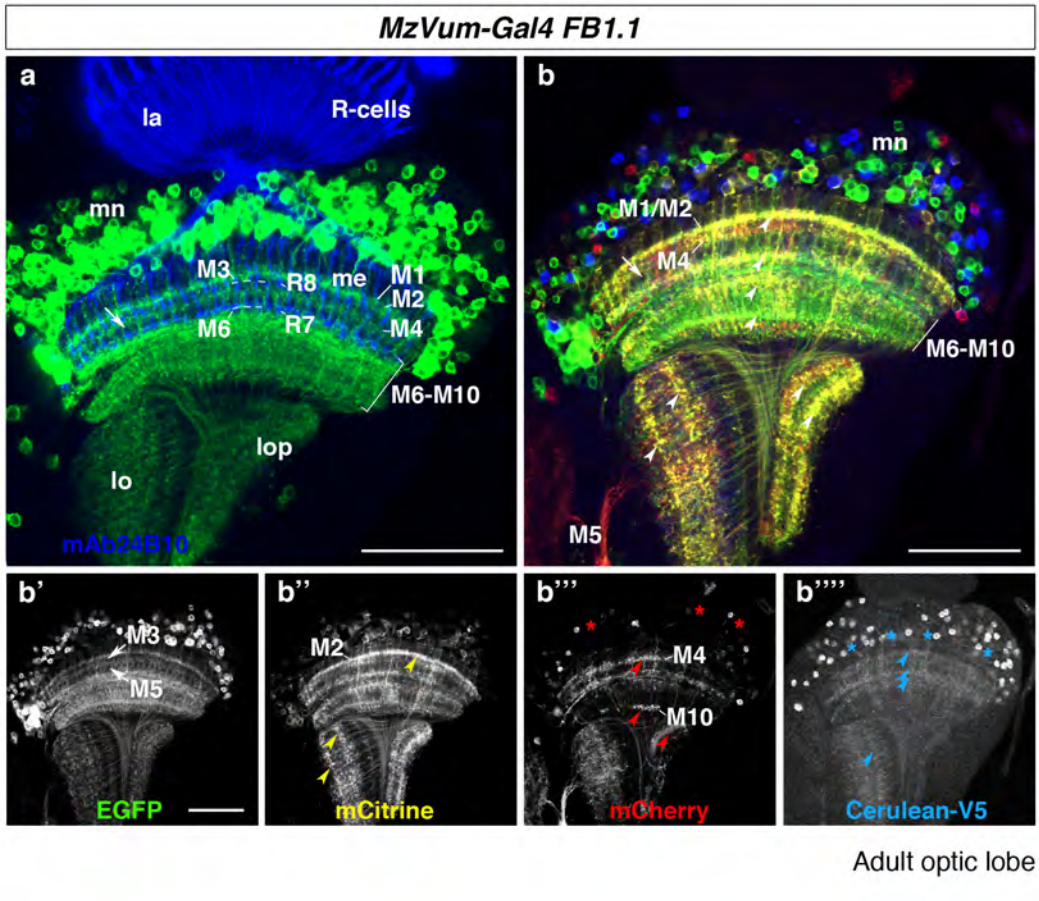

Figure 35. *FB1.1* transgenes active within the dVsx1 expression domain uncover a complex array of medulla neuron subtypes.
MzVum-Gal4 reports expression of the Vsx1 transcription factor in *Drosophila*. In the adult visual system, *MzVum-Gal4* used in combination with the *FB1.1* approach labels a subpopulation of neurons in the medulla (me) (a-b””). In the absence of mFlp5 recombinase *MzVum-Gal4* results in the expression of the

default EGFP reporter (a). Photoreceptor cells (R-cells) were visualized with mAb24B10 antiserum (a, blue antibody). R7 and R8 terminate in their respective M6 and M3 layers and offer landmarks for further medulla layer identification (a). Upon mFlp5 activation mCitrine (b"), mCherry (b"') and Cerulean-V5 complementary to the default EGFP reporter stochastically label the *MzVum-Gal4* positive medulla neurons (mn) (b). The observed gaps in the *MzVum-Gal4* expression pattern in the M3 and M5 layers constitute characterized positions for lamina neuron terminals. Vsx1 positive medulla neurons densely innervate the lower M2 (a-b) and layers M4 and M6-M10. Fewer branches occupy layers M1, upper M2, M3 and M5. *MzVum-Gal4* positive medulla neurons include subtypes innervating the medulla, lobula (lo) and lobula plate (lop). *MzVum-Gal4*/+ or *Y*; *hs-mFlp5*/*FB1.1*^{260b}. Heat shocks: 90 minutes at 48 and 72 hours AEL. Scale bars, 50 μm.

Next, due to strong fluorescence signal that was largely maintained at the same levels throughout the axonal projections within the optic lobe, we could use such samples for single neuron reconstructions. This required manual or semi-automated annotation (using Single Neurite Tracer) of axonal and dendritic branches using successive confocal images from the four individual channels. We could identify at least three new transmedullary medulla neuron types TmY4-like, TmY5-like and Tm22-like (Figure 36a'-c'). These neurons share similarities with the previously described TmY4, TmY5 and Tm22 medulla neurons, respectively (K.-F Fischbach, 1989; Morante and Desplan, 2008). For instance, they arborize in the same layers of the medulla; nevertheless, they might include branches extending to additional layers or columns. In this sample, we classified a new TmY4-like subtype, since it shows the same medulla innervation as TmY4, but includes an additional branch in both the lobula and lobula plate, respectively. Similarly, the TmY5-like neuron we observed shares medulla innervation with the TmY5 subtype, however, its branches occupy more layers and columns of the lobula, and in addition significantly less layers of the lobula plate. Finally, the Tm22-like neuron innervates the same medulla layer but innervates fewer layers in the lobula. We thus classified them as different new subtypes. We can overall conclude that our approach is suitable for use in studies that aim to discern individual neuron subtypes within a complex population.

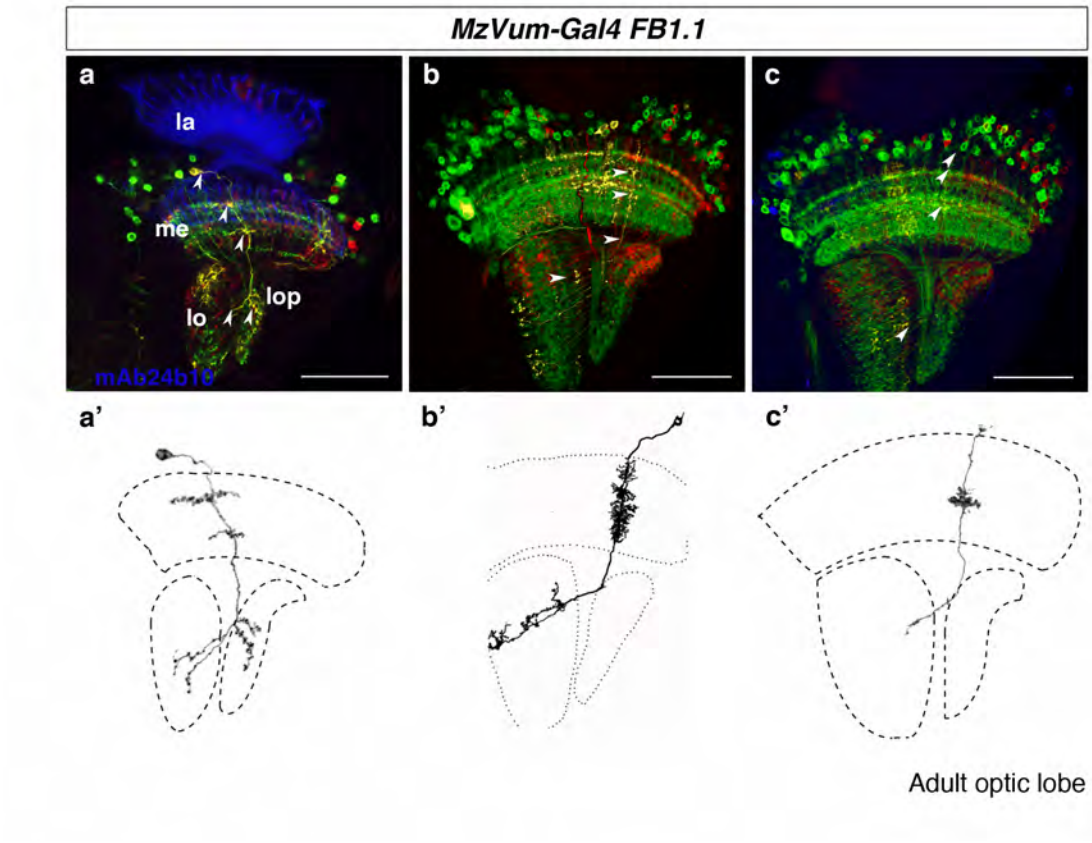

Figure 36. Medulla neuron subtypes identified using *FB* transgenes.
In the adult visual system dVsx1 positive neurons in the medulla (me) constitute a subset of medulla neuron (mn) subtypes. Using *MzVum-Gal4* for expression of *FB1.1* and *FB2.0* transgenes we could differentially label the dVsx1 positive population (a-c). Owing to strong expression of fluorescent markers single neurons could be traced from soma to axons and dendrites (arrowheads) when expressing a different fluorescent protein that of their neighboring cells fluorescent protein. Information from an individual channel (mCitrine) was used for neuron reconstructions (a'-c'). Identified subtypes include transmedullary neurons projecting solely to the lobula (lo) or both the lobula and the lobula plate (lop). Sharing features with TmY4, TmY5a and Tm22, the reconstructed neurons were identified as TmY4-like (a'), TmY5a-like (b') and Tm22-like (c'), respectively. (a) *MzVum-Gal4/hs-Flp*^{1}; *hs-mFlp5/FB2.0*^{260b} Heat shocks 25' at 48 h and 72 h AEL. (b-c) *MzVum-Gal4*/+ or *Y*; *hs-mFlp5/FB1.1*^{260b}. Heat shocks: 90 minutes at 48 and 72 hours AEL. Scale bars, 50 μm.

5.4 Flybow can be used to gain insights into local circuit assembly within a single layer

The medulla represents an excellent example of how circuits are organized into reiterated units to effectively integrate and transmit signals enabling correct visual information processing. This neuropil consists of approximately 800 columns, corresponding to innervation from R-cells within 800 ommatidia in the eye; each column is further divided into 10 synaptic medulla layers (M1-M10). Interconnected microcircuits are established within individual columns and across layers. These achieve local integration of information concerning object position in the visual

field, spectral sensitivity and motion detection (Borst, 2009; Morante and Desplan, 2008; Sanes and Zipursky, 2010). Layer formation occurs during metamorphosis as a multi-step process, in which different neuron subtypes employ distinct mechanisms to reach their target fields and precisely position their dendritic and axonal branches (Nern et al., 2008; Ting et al., 2005). Anatomical studies uncovered mature branch and axon terminal characteristics for neuron subtypes including R-cells, as well as target neurons within the medulla layers. R1-R6 axons form synaptic contacts with lamina neurons L1-L3 in the lamina (Meinertzhagen and Sorra, 2001), and relay motion information to their target neurons within the distal medulla layers M1, M2, M4 and M5 (K.-F Fischbach, 1989). Furthermore, R7 and R8 axons terminate in the layers M6 and M3 respectively, where they deliver color vision information to their synaptic partners. Thus, information from the visual field is delivered to the different medulla layers by synaptic pairing and further relayed to higher processing centers. Thus, it is key to understand how precise neuron pairing within specific layers occurs during development and how this results in the formation of fully functional networks.

Different studies have uncovered key molecular mechanisms employed in nervous system development, which control precise layer-specific targeting that finally results in pre- and post- synaptic neuron matching (Huberman et al., 2010). Neurons can selectively pair with their targets through homophilic interactions of a single cell adhesion molecule they express (Hakeda-Suzuki et al., 2011; Shinza-Kameda et al., 2006; Tomasi et al., 2008; Yamagata and Sanes, 2008, 2012). Additionally, a limited number of often abundantly expressed guidance molecules that are repeatedly employed in circuit assembly exist. Context-specific spatio-temporal regulation of their expression permits precise pairing of synaptic partners (Petrovic and Hummel, 2008). Furthermore, as aforementioned, neurons employ chemosensory guidance systems to navigate within neurite-rich environments (Dickson, 2002). Repellent signals released for instance from specific cells into the extracellular matrix could be recognized by axons expressing matching guidance receptors and lead to growth cone avoidance behavior thus forming exclusion zones for their neurites (Kidd et al., 1999; Kidd et al., 1998; Matsuoka et al., 2011). Attractant signals have similarly been used to effectively guide axons along specific

trajectories (Harris et al., 1996; Kolodziej et al., 1996); however, their role in layer-specific targeting was not known. Interestingly, some molecules can elicit attraction or repulsion in exploring axons depending on the guidance receptor they express (Dickson, 2002). In *Drosophila,* the secreted Netrin molecules (Netrin-A and Netrin-B) recognized by Frazzled (Fra) expressing neurons mediate attractive growth cone responses (Kolodziej et al., 1996). By contrast, Unc-5 expressing growth cones are repelled away from the Netrin source upon binding (Keleman and Dickson, 2001).

Despite the recent advances in our understanding of the mechanisms underlying axon pathfinding and targeting, strategies that instrruct pre- and postsynaptic pairing to selectively occur within a specific layer remain unexplored. Work by Katarina Timofeev and Willy Joly in our laboratory aimed at exploring this fundamental biological question using R8 axon targeting specifically to the M3 layer as an experimental paradigm. This study explores the role of the well-established Netrin/Frazzled chemoattractant guidance system in axon targeting within the *Drosophila* optic lobe. Their findings show that Fra is expressed in R8 growth cones at pupal stages and it is required during the second step of targeting in a cell autonomous manner. Strikingly, secreted Netrin ligands are solely localized within the M3 layer during metamorphosis, which importantly constitutes the recipient layer for R8 terminals. Joining forces with them, I conducted two different sets of experiments using the Flybow approach to extract morphological information about neurons with potential roles in the establishment of the M3 layer mini-circuit, as well as the dynamic morphological changes of R8 axons during metamorphosis

5.4.1 Uncovering the identity NetB expressing neuron subtypes

Our first aim was to identify neuron subtypes that could serve as Netrin source in the M3 layer. We hypothesized therefore that such neurons should either branch or terminate within or in close proximity to the M3 layer. Enhancer trap *Gal4* P-element lines with insertions close to *NetA* or *NetB* loci were combined with the Flybow approach to map Netrin expressing neuron

subtypes within the medulla. We selected the *NP4151-Gal4* driver (Hayashi et al., 2002) line for expression of the *FB2.0* transgenes. *NP4151-Gal4* reports expression of NetB, and positively labels a larger group of neurons within the adult optic lobe when combined with a single fluorescent marker (EGFP Figure 37a). Single marker analysis identified lamina neuron L3 amongst the NetB positive neuron subtypes. However, subtype identity in these samples could not be determined for any of the NetB positive medulla neurons due to the high number of neuronal branches labeled. Multicolor analysis in sparsely labeled samples conferred the required single cell resolution for swift mapping of neurons within the medulla (Figure 37b and 38).

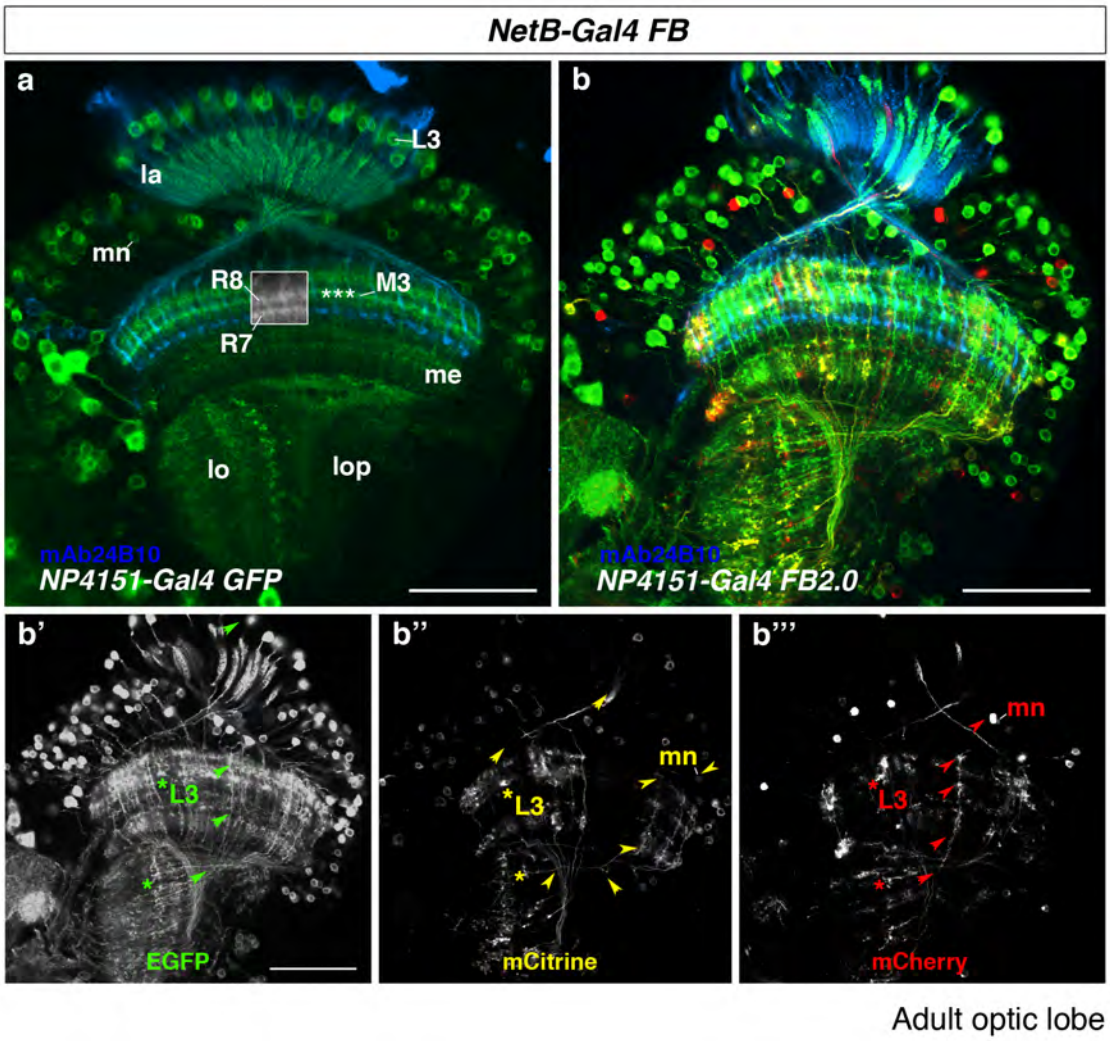

Figure 37. NetB expression in lamina and medulla neurons in the adult visual system
An enhancer trap Gal4 insertion located next to the *Netrin-B (Net-B)* locus generated the *NP4151-Gal4* driver line. *NP4151-Gal4* reports Net-B expression in the developing and adult visual system of *Drosophila*. *NP4151-Gal4* was used to drive EGFP expression in the adult visual system (a). Expression was detected in L3 neurons in the lamina (la) and in medulla neurons (mn) projecting to the lobula (lo) and/or the lobula plate (lop). Photoreceptor cells (R-cells) were labeled with mAb24B10 (blue) and used as medulla (me) layer landmarks. R8 terminate at layer M3 whereas R7 extend deeper and terminate at the M6 layer, boxed area indicates R7 and R8 terminals (a). L3 axons also arborize at the M3 layer (asterisks) and thus could serve as Netrin providers in this layer. Using *NP4151-Gal4* in combination with *FB2.0* transgenes we could label the Net-B positive population with the expression of EGFP, mCitrine and mCherry (b). Cerulean-V5 was not visualized in these experiments. Due to sparse labeling we could readily detect Net-B expressing subsets of neurons. Separating the individual channels (b'-b"') the L3 neuron and its characteristic arborization pattern could be easily detected (color-coded asterisks). Additionally transmedullary neurons extending arbors throughout the medulla to the lobula and/or lobula plate (color-coded arrowheads) could also be visualized. *NP4151-Gal4/+ or Y; UAS cd8-EGFP/+ NP4151-Gal4/+* or Y *; hs-Flp*^{1}; *hs-mFlp5/FB2.0*^{260b}. Heat shocks: 20 minutes at 48 hours and 72 hours AEL. Scale bars, 50 μm.

High levels of fluorescent signal allowed neuron tracing from the soma and along the dendritic and axonal arbors extending throughout the neuropil. Samples were immunostained with mAb24B10 to identify positions of layers M3 and M6. Comparing our reconstructions to published morphological descriptions (K.-F Fischbach, 1989; Morante and Desplan, 2008), we could show that NetB positive neurons include amongst others, lamina neurons L3, and transmedullary neurons Tm2, Tm3, Tm7 and Tm21 (Figure 38). These neurons potentially could release the diffusible Netrin molecules and Fra expressing cells could upon binding localize them specifically within the M3 layer. However, we observed that the lamina neuron L3 within this population were the only neuron subtype, which extended axons into the M3 layer, whereas all other neuron subtypes primarily had dendritic branches in this layer (Timofeev et al., 2012). This led us to propose that the precise localization of Netrins within the M3 layer could be accredited to local release by axon terminals of lamina neurons L3 (Timofeev et al., 2012). In conclusion, these findings illustrate that Flybow is highly useful to both map neuron subtypes in a genetic population defined by the production of a guidance molecule and to understand aspects of cell biology, for instance site of Netrin release.

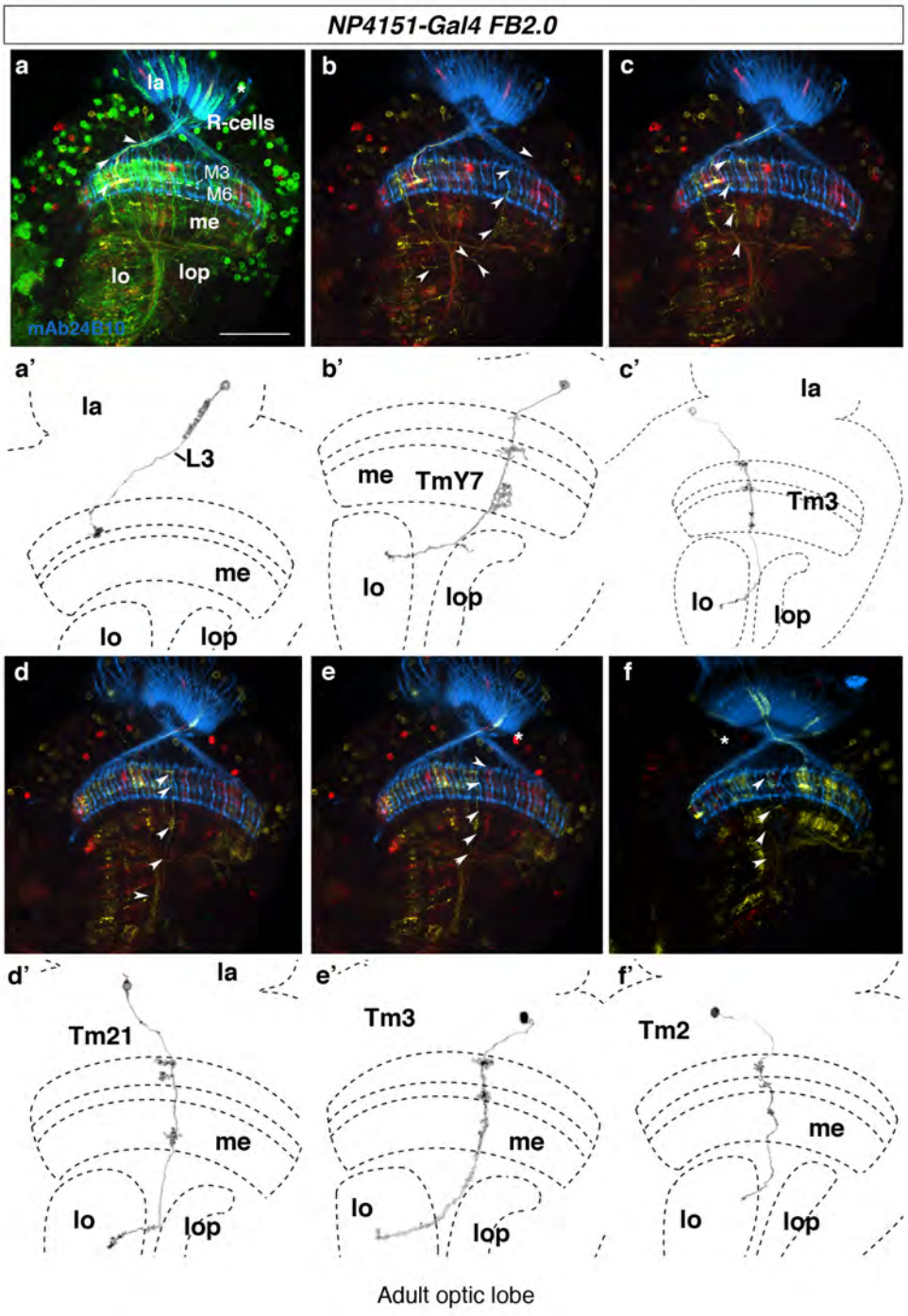

Figure 38. Neuron subtypes identified within the Net-B expression domain in the adult visual system of *Drosophila*

The *FB2.0* approach was used in conjunction with the *NP4151-Gal4* driver line for transgene expression in the adult visual system (a-f). Samples were sparsely labeled with EGFP, mCitrine and mCherry fluorescent proteins. Cerulean-V5 expression was not visualized in these experiments. Photoreceptor cells (R-cells) were stained with mAb24B10 (blue) and R7 and R8 terminals were used as landmarks for medulla layer M6 and M3, respectively. Strong marker expression allowed tracing of individual neurons from their cell body to their axonal and dendritic extensions (a-f, arrowheads). Data from individual channels were analyzed for the identification and reconstruction of *NetB* producing neuron subtypes (a-d'). Lamina neuron L3 was identified and reconstructed (a-a') by its characteristic axonal arborization pattern in the medulla layer M3 that makes it a key candidate for having a Netrin provider role within this

layer. Additionally, transmedullary neuron subtypes within the NetB expression domain in the medulla include TmY7 (b-b'), Tm3 (c-c', e-e'), Tm21 (d-d') and Tm2 (f-f') subtypes. *NP4151-Gal4/hs-Flp[1]; hs-mFlp5/FB2.0[260b]*. Heat shocks: 20 minutes at 48 hours AEL. Scale bar, 50 μm.

5.4.2 Filopodia of R8 growth cones bridge the distance between the medulla neuropil border and the M3 layer.

Netrins can mediate both long- and short-range growth cone attraction behaviors (Brankatschk and Dickson, 2006; Dickson, 2002; Tessier-Lavigne and Goodman, 1996). Findings by K. Timofeev and W. Joly show that layer-specific expression of Netrins within the medulla can be detected already at 42 hours after puparium formation (APF) before R8 axons proceed to their final layer. NetB accumulation peaks at approximately 55 hours APF and is reduced in adult optic lobe. Local Netrin release close or within the M3 layer suggests that R8 growth cones must sense the Netrin source at long range as they are positioned at the medulla neuropil border before the second step of their targeting is initiated. However, genetic analysis using a recombinant membrane-tethered version of Netrin in an otherwise Netrin mutant animal can fully replace Netrin function (Brankatschk and Dickson, 2006). Importantly, this finding indicates that Netrins within the medulla may act at short range. We therefore aimed at describing R8 growth cone morphologies during pupal development and match these with the dynamic expression of *NetB*. For this purpose, we employed the R-cell specific *GMR-Gal4* line for expression of the *FB1.1* transgene. Differential expression of the four markers within the R-cell array lead to single cell resolution and allowed us to monitor growth cone shape changes. We could observe that at the end of the third instar larval stage, R7/R8 growth cones contain elaborate filopodial extensions (Figure 39a). At 42-44 hours APF, R8 growth cone morphology changes to a broad "foot-like" shape as they pause at the medulla neuropil border (Figure 39b). Strikingly, at 48-50 hours APF, we observed the extension of a fine filopodium within the neuropil towards the emerging M3 layer (Figure 39c). Finally at 52-55 hours APF, the extension thickens and the filopodium gradually thickens into a mature R8 terminal stopping in the recipient M3 layer (Figure 39d). This suggests that NetB could act as a short-range signal within the medulla as the growth cone extends a filopodium towards the source of the attractive guidance factor.

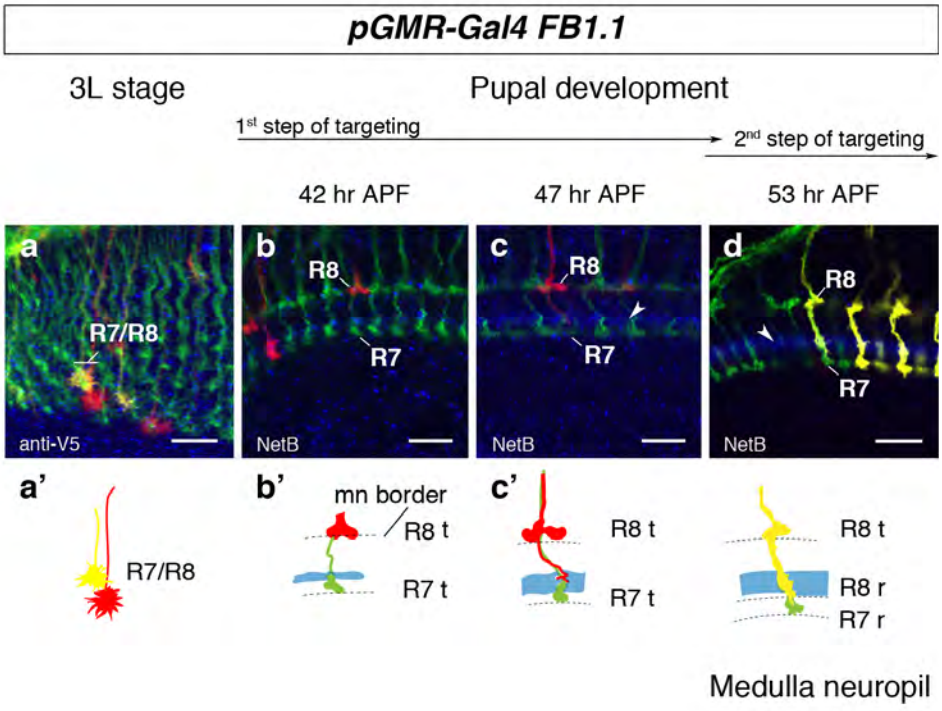

Figure 39. Flybow allows visualization of dynamic R7 and R8 shape changes as they explore their target field during development.
Photoreceptor cells (R-cells) R7 and R8 at the third instar larval stage extend axons in evenly distributed bundles within the medulla neuropil (mn) (a). Using *GMR-Gal4* to drive expression of *FB1.1* transgenes, samples were differentially labeled with mCitrine and mCherry in addition to EGFP. R7 and R8 growth cones could simultaneously be visualized within a single sample. At this stage they adopt elaborate morphologies with an extended number of filopodial protrusions (a-a'). At pupal stages, R7 and R8 target to their recipient layers (r) in a two step process (b-d). At 42 hoursAPF, R8 axons terminate at the medulla neuropil border, whereas R7 axons project deeper and terminate in a temporary (t) medulla layer (b). Growth cone morphology changes to a foot-like shape (b-b'). In parallel, a Netrin layer can be visualized using Net-B immunolabeling (blue). Using the *FB1.1* approach at 47 hours APF, we could uncover morphological changes at the single cell level. R8 growth cones form a fine filopodial extension that reaches the deeper Netrin positive layer (c-c'). During the second step of targeting at 53 hours APF, the R8 growth cone moves down to its recipient target layer (d-d'). In parallel, R7 terminals target from their temporary to their recipient medulla layer M6. Netrin is still localized in a sharply formed layer. Cerulean-V5 expression was not visualized in c-d. R-cells were marked with mAb24B10 staining (c-d). Optic lobes, in frontal (a) and horizontal (c-d) views. *GMR-Gal4/FB1.1*^{260b}*; hs-mFlp5*/+. Heat shocks: 30' at 72 and 96 hours AEL. Scale bars, 5 μm.

5.5 Clone formation in the embryonic nervous system

Mosaic analysis experiments at embryonic stages have so far been hindered by the lack of genetic tools active within this short time window (Brewster and Bodmer, 1995; Pearson and Doe, 2003). Thus, recombination events occurring at late embryogenesis could be monitored only at larval stages. Moreover, in addition to attempts of generating genetically labelled clones within the embryonic nervous system, the most commonly used technique to sparsely label

neurons at these early stages included DiI injections (Rickert et al., 2011). Using this method individual neuron morphologies can be uncovered; however, it is an extremely labor intensive approach. We therefore tested the new modified mFlp5/*mFRT71* system together with the *FB1.1* approach during embryogenesis to see if we could recover differentially labeled embryonic clones. We exposed a 14-hour overnight collection of eggs to a 60 minutes heat shock. Next, allowing a 7-11 hours gap, stage 15-16 embryos were selected and prepared for imaging. Two different sets of experiments were performed. Live embryos were imaged using confocal microscopy. Expression of EGFP, mCitrine and mCherry could be readily detected (Figure 40). Importantly, fluorescence decay was not observed at least at detectable levels in these experiments rendering the Flybow approach appropriate for live imaging and possibly time-lapse studies. Additionally, fixed embryo preparations of samples in combination with immunostaining using an anti-V5 antibody showed expression of EGFP, mCitrine, mCherry and Cerulean-V5 in both lineage related clones or single neurons (Figure 41). In both sets of experiments, we were able to visualize exploring growth cones during their pathfinding process along axonal tracts within the central and peripheral nervous systems.

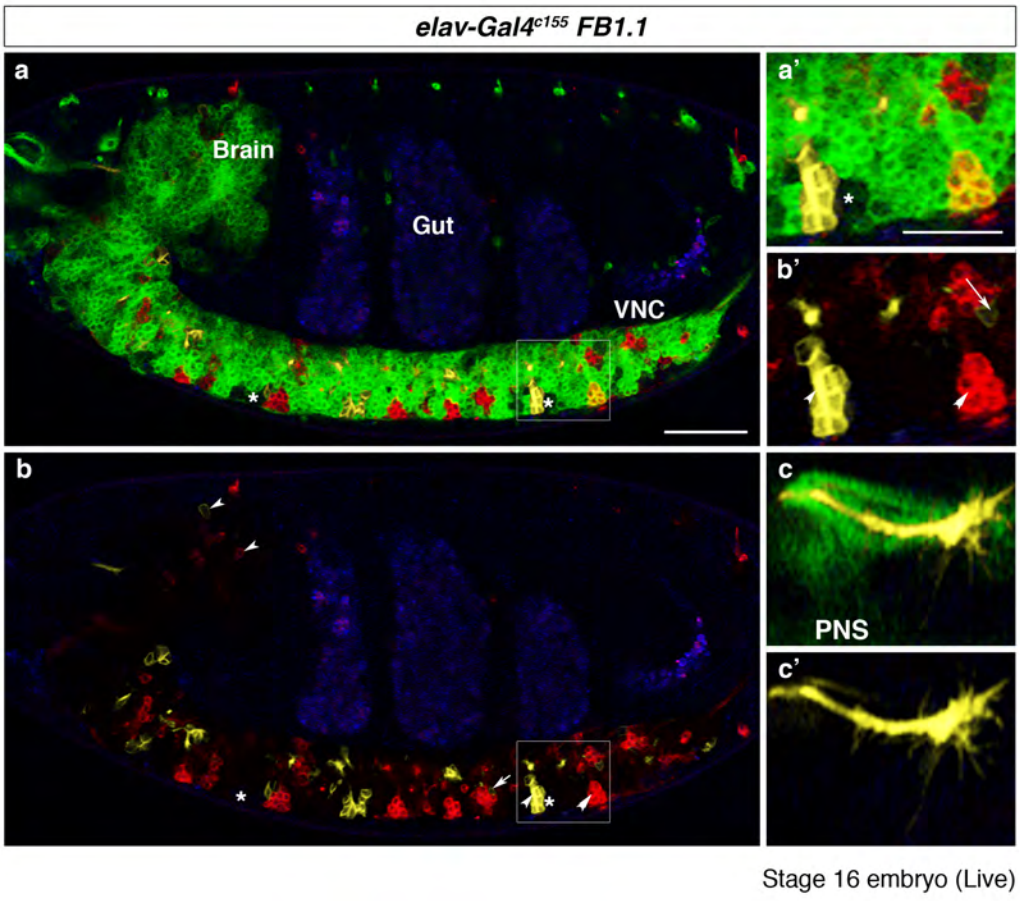

Figure 40. Flybow can be utilized to monitor embryonic nervous system development using live imaging.

Shown is a live preparation of a stage 16 embryo (a, sagittal view). *elav-Gal4^{c155}* was used for expression of *FB1.1* transgenes. Clusters (a, asterisks) and single neurons (a', arrows) in the brain and the ventral nerve cord (VNC) express mCitrine and mCherry. Boxed area shows a single cell cluster that expresses both mCitrine and mCherry due to perdurance (b, double arrowheads). Unlabeled clusters (a-b', asterisks) consist of Cerulean-V5 expressing neurons that cannot be visualized in this experiment. mCitrine expressing growth cone in the peripheral nervous system (PNS) can be visualized as it exits from the VNC. Expression is detected in the fine cellular structures of its exploring growth cone (c). *elav-Gal4^{c155}*/+ or *Y*; *hs-mFlp5*/*FB1.1^{260b}*. Heat shock: 60 minutes of a 14 hour embryo collection. Scale bars, 50 μm (a) and 20 μm (b -c').

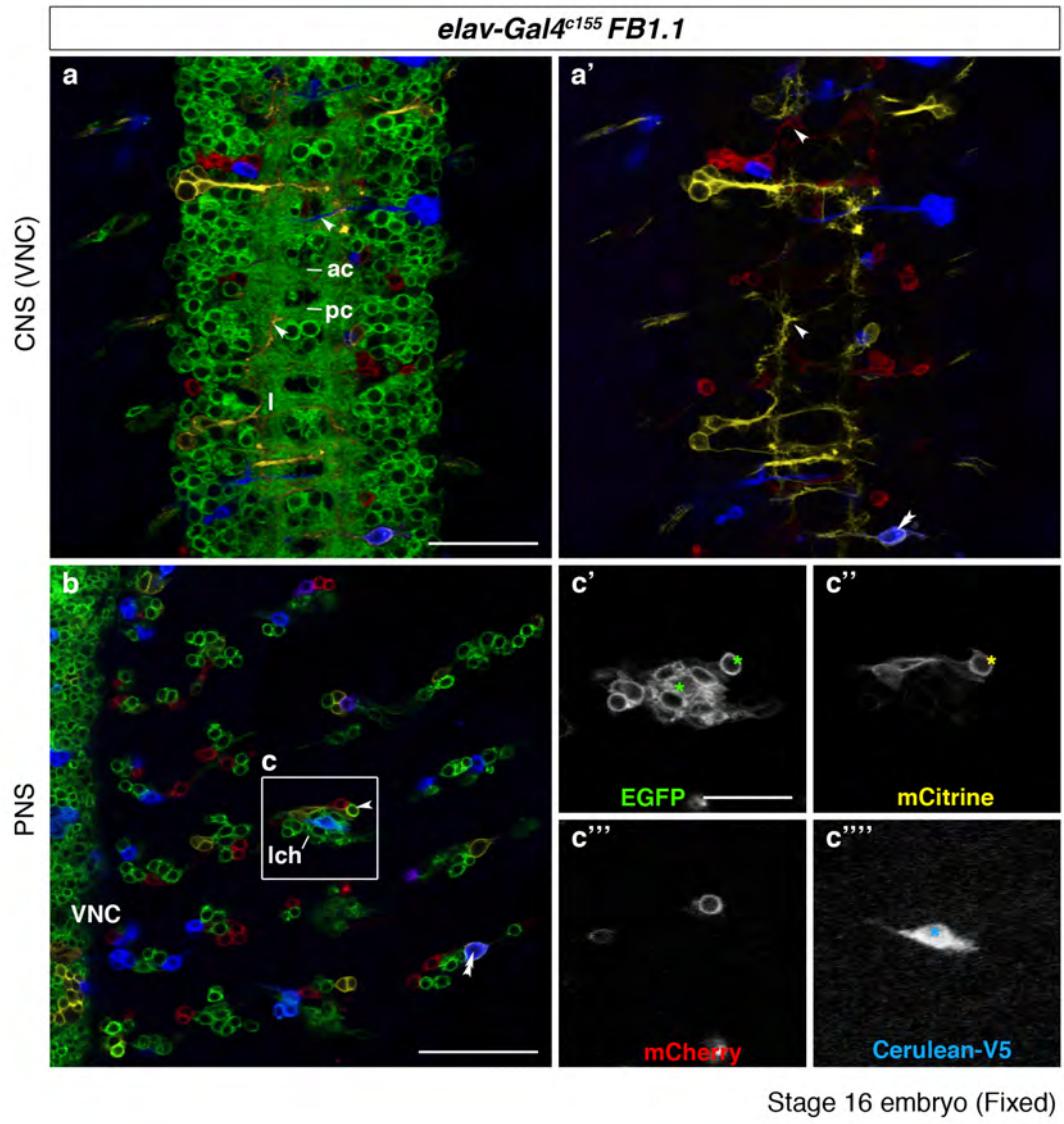

Figure 41. Expression of *FB1.1* transgenes in the embryonic nervous system of *Drosophila*.
The central (CNS) and peripheral nervous system (PNS) consist of neurons generated at early embryonic stages. *elav-Gal4^{c155}* was used to drive expression of *FB1.1* transgenes in the nervous system (a-c). In flat preparations of the ventral nerve cord (VNC), clones (double asterisks) or single neurons (single asterisk) were marked by the expression of mCitrine, mCherry and Cerulean-V5 in addition to the default EGFP (a,a'). Expression was visualized in cell bodies (a, asterisks), axons (a, arrowheads) as well as growth cones (a', arrowheads) navigating through the lateral (l) tracts and anterior (ac) or posterior (pc) commissures. Neurons of the PNS expressed all four fluorescent proteins (b). Boxed area indicates the lateral chordotonal organ (lch) (c). Higher magnification of the lch shows that all different fluorescent proteins were expressed (c'-c'''') and in at least two cases in an overlapping manner (color coded asterisks). Double arrowheads indicate cells expressing both mCitrine and Cerulean-V5 (a', b). *elav-Gal4^{c155}*/+ or *Y*; *hs-mFlp5*/*FB1.1^{260b}*. Heat shock: 60 minutes of a 14 hour embryo collection. Scale bars, 50 µm (a-b) and 20 µm (c'-c'''').

5.6 Flybow can be used to visualize the morphology of glial cells

So far, our efforts concentrated on the visualization of neurons. However, neural circuit assembly and function is dependent on fine-tuned interactions amongst neurons and between neurons and glia (Chotard and Salecker, 2004, 2007). In *Drosophila,* glial cells are categorized based on both their position and shape. Across species their role is evident in various steps required for wiring including axon guidance, formation of physical boundaries and homeostasis of synaptic function (Freeman and Doherty, 2006). Until recently, glial cell morphology within the adult visual system has not been well characterized (Edwards and Meinertzhagen, 2010). However, distinct glial cell populations have been already described at the third instar larval optic lobe (Chotard and Salecker, 2007). We thus aimed to label glial cells in our system and visualize individual cell morphologies both in the developing and adult visual system. Using the pan-glial *repo-Gal4* driver in combination with the *FB1.1* transgenes, we could differentially mark individual glial cells with the expression of the four fluorescent proteins. Importantly, we could not observe any distortion in the morphology of individual glial cells by the expression of the fluorescent markers at the third instar larval stage (Figure 42). We readily identified surface glia, consisting of perineurial and subperineurial glial cells surrounding the developing optic lobes to form the blood-brain barrier. Furthermore, we labeled epithelial and marginal glia in the lamina, as well as medulla glia (meg) and medulla neuropil glia (mng) associated with the medulla neuropil.

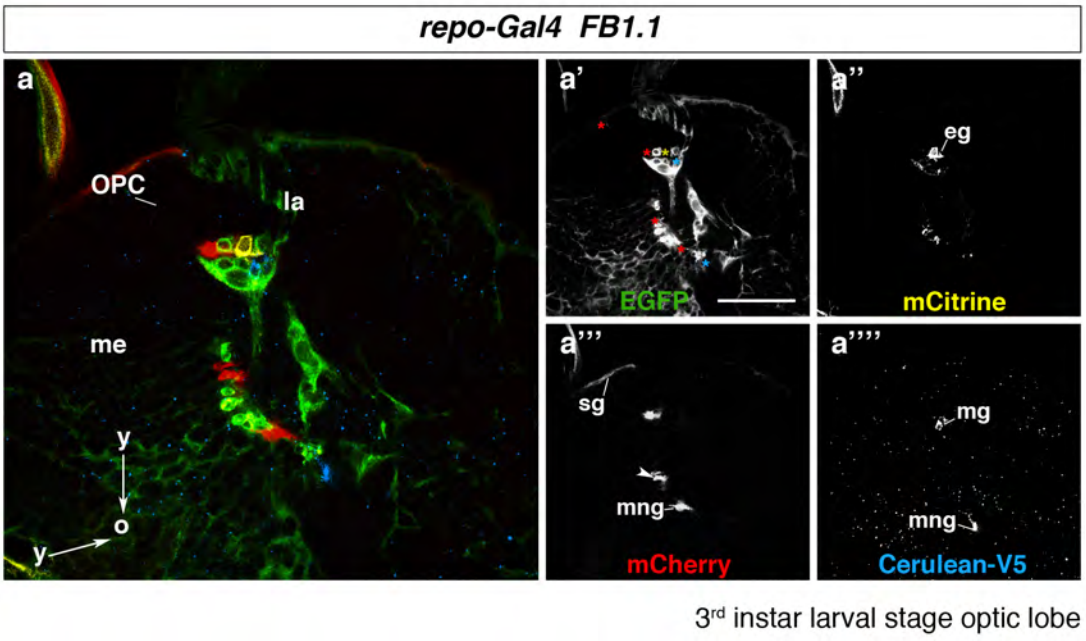

Figure 42. Visualizing distinct glial subtypes in the third instar larval optic lobe.
Glial cells represent a distinct cell population within the nervous system. Within the visual system, glia develop in parallel to neurons. The pan-glial *repo-Gal4* line was used to drive expression of *FB1.1* transgenes in all glial subtypes at the third instar larval stage (a-a''''). mCitrine (a''), mCherry (a''') and Cerulean-V5 (a'''') were expressed in addition to the default EGFP in a mutually exclusive manner (a', asterisks color-coded, a'). In the lamina (la), R1-R6 axons terminate between two rows of glia: the epithelial (eg) and marginal glia (mg) (a'' and a''''). Older (o) medulla neuropil glia (mng) are found closest to the neuropil and away from the outer proliferation center (OPC), whereas younger (y) mng are located proximal to the OPC (a'''). Surface glia (sg) are located in the periphery (a'''). Medulla (me). *hs-mFlp5/FB1.1*^{260b}*; repo-Gal4/+*. Heat shocks: 45 minutes at 48 hours AEL. Scale bars, 50 µm.

The medulla neuropil is densely packed with cellular processes and is assembled into complex columnar and layered units. We hypothesized that glia extending processes within this neuropil could play roles initially in the formation of neuronal connections, as well as later when they mature in network homeostasis, for instance by providing nutrients or regulation neurotransmitter uptake. As a first step, we thus sought to visualize distinct morphologies of potential different subtypes within a glial subpopulation associated with this neuropil - the medulla neuropil glia - in adults. At the instar larval stage, their cell bodies are positioned at the border of the emerging medulla neuropil (Figure 42). During subsequent steps of development, they extend processes into this neuropil. Our experiments in the adult uncovered how different glial cell subtypes adopt intricate morphologies in their mature form resembling the complexity of their neuronal counterparts (Figure 43). First, we could visualize the previously described

epithelia glial cells in the lamina, associated with individual lamina cartridges, along whose axes, they extend processes (Figure 43,a'). Next, we could detect the highly diverse cell shapes of different medulla neuropil glial cell subtypes. From our preliminary analysis, we could determine that variants include cells that extend: (a) multiple branches into the distal layers of the neuropil, while their cell body is located at the medulla neuropil border (Figure 43a-a"), (b) a single main branch extending within distal layers of the neuropil, while their cell body is similarly located at the medulla neuropil border (Figure 43a-a"'), (c) long processes along the serpentine layer, while their cell body is located laterally, (d) long multiple processes projecting into proximal layers of the neuropil, while their cell body is located distally (Figure 43b-b"'), (e) thick processes along the border of the neuropil, while their cell body is located laterally, and (f) short multiple processes at the border of the proximal medulla neuropil border together with a fine process that extends along the second chiasm and further thickens at its terminus within the lobula plate, while the cell body is located proximally (Figure 43 b''). We thus can conclude that medulla neuropil glia represents a highly divergent population that can be readily characterized in terms of its anatomy using Flybow.

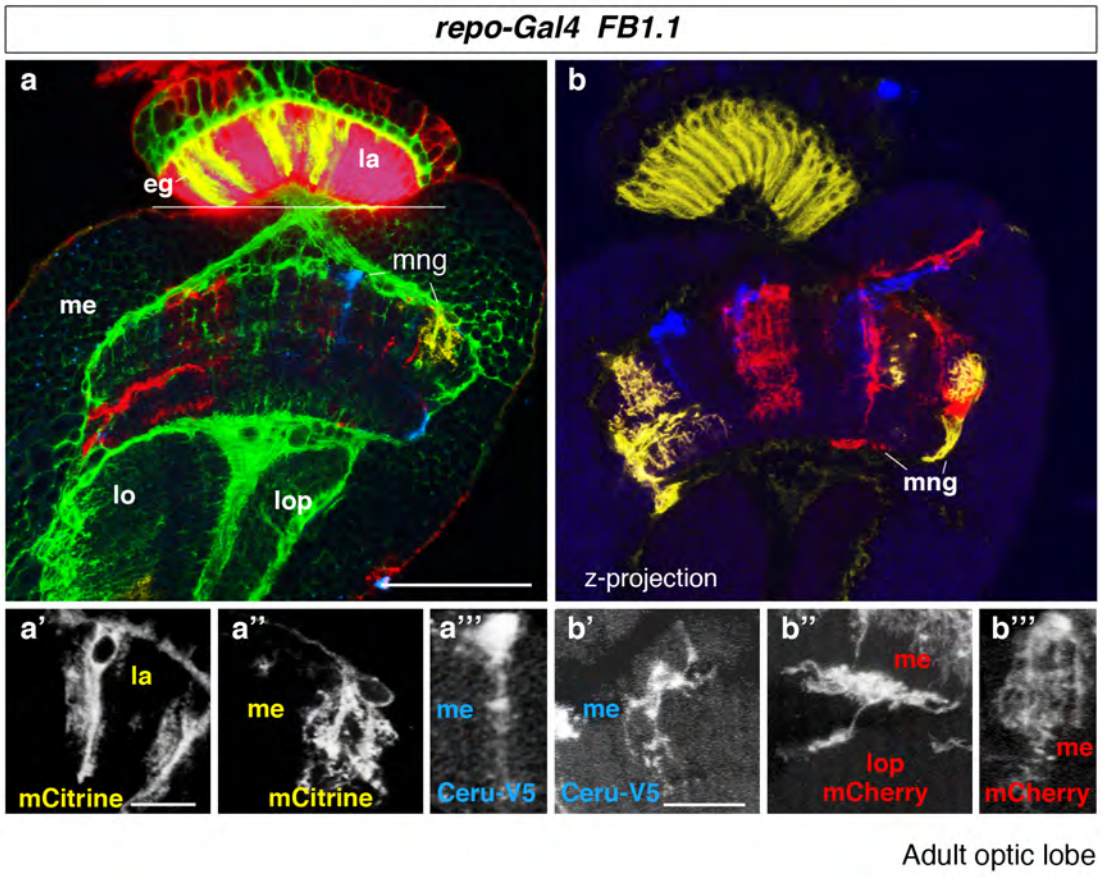

Figure 43. Expression of *FB1.1* transgenes reveals the intricate morphology of glial cells in the adult fly visual system.
Glial cells within the adult visual system are located within the lamina (la), the medulla (me), the lobula (lo) and lobula complex (lop) as well as the borders of the optic lobes. *repo-Gal4* was used to label the entirety of the glial population by expression of *FB1.1* transgenes. Distinct glial subtypes were differentially labeled with the four fluorescent proteins (a-b), revealing the elaborate morphologies of adult glia in the lamina, epithelial glia (eg), and the medulla, medulla neuropil glia (mng). Magnifications of samples (a-b) show the complex morphology of epithelial and medulla neuropil glia (a'-b"'). Fluorescence signals in the lamina above the white line have been reduced relative to the medulla (a-b). *hs-mFlp5/FB1.1*^{260b}*; repo-Gal4/+*. Heat shocks: 30 minutes at 48 and 72 hours AEL. Scale bars, 50 μm (a-b) and 10 μm (a'-b"').

Having discovered the shape diversity within this population, we next sought to assess the manner, by which their processes populate the neuropil. Specific glial subtypes within the vertebrate brain, the astrocytes, have been reported to occupy exclusively non-overlapping territories (Bushong et al., 2002; Livet et al., 2007). Thus, to test if medulla neuropil glia show astrocyte-like properties, we visualized the medulla neuropil from a different angle (transverse view). We could observe that processes from individual cells both occupy exclusive territories or overlap with neighboring processes (Figure 44). This difference could potentially be

attributed to distinct medulla neuropil glial subtypes. Therefore focusing on the ones that are exclusively occupying individual territories, specific subtypes could be identified that perhaps function similarly to vertebrate astrocytes. In summary, using the *FB1.1* approach we could differentially label neighboring glial cells that present highly complex shapes and retrieve information about single cells in relation to their direct neighbors.

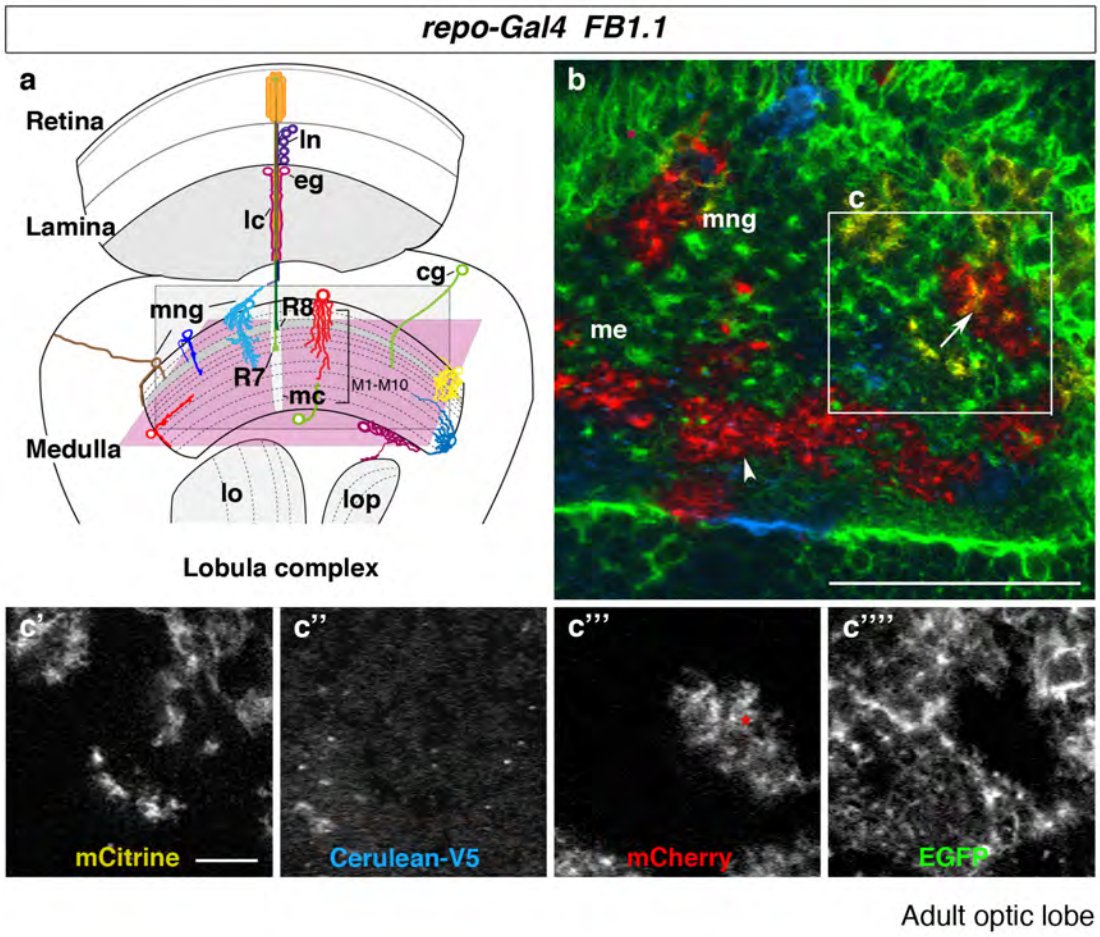

Figure 44. Glial cells associated with the medulla neuropil form processes to cover territories of varying size and shape in the adult visual system.
Schematic diagram of the adult visual system (a). Shown in the retina is an ommatidium consisting of eight photoreceptor cell bodies (R-cells). R1-R6 axons terminate in the lamina (la) and together with R7, R8, lamina neurons (ln) and epithelial glial cells (eg) form organizing units called lamina cartridges (lc). R7 and R8 project into the medulla (me) neuropil and innervate their respective medulla columns (mc, light gray shaded area). Medulla columns are further subdivided into ten layers (M1-M10). Rectangles indicate the sectioning plane through the medulla neuropil. Purple-shaded rectangle indicates the transverse section plane shown in (b). Glial cells in adult optic lobes were labeled by expression of *FB1.1* transgenes (b-c''') using the *repo-Gal4* driver. mCitrine, mCherry and Cerulean-V5 were expressed in addition to the default EGFP. Transverse cross-section through the medulla neuropil (b), showing territories occupied by medulla neuropil glial cell (mng) branches. Higher magnification of glial processes within the boxed area (c). Overlapping mng branches (arrow, red asterisk) are visualized by the

expression of mCitrine and mCherry within the same territory. Cortex glia (cg), lobula (lo) and lobula plate (lop). *hs-mFlp5/FB1.1*^{260b}*; repo-Gal4/+*. Heat shocks: 30 minutes at 48 and 72 hours AEL. Scale bars, 50 μm (b) and 10 μm (c'-c'''').

5.7 Flybow can be used for studies beyond the nervous system

Flybow uses the Gal4/*UAS* system for expression of fluorescent markers, thus rendering the approach available for studies in tissues other than the nervous system. Therefore, this tool can be employed to study cell behavior in tissues, in which the cells for example in the digestive system get constantly renewed or are even phenotypically static to maintain tissue structure as in different epithelia. To validate that Flybow could be employed beyond the nervous system, we used *engrailed (en)-Gal4* for expression of *FB1.1* transgenes in the posterior compartment of the wing imaginal disc, at the third instar larval stage. Epithelial cells within the Gal4 positive population were successfully marked by the differential expression of the four fluorescent proteins (Figure 45). This confirmed the functionality of our system in tissues different from the nervous system.

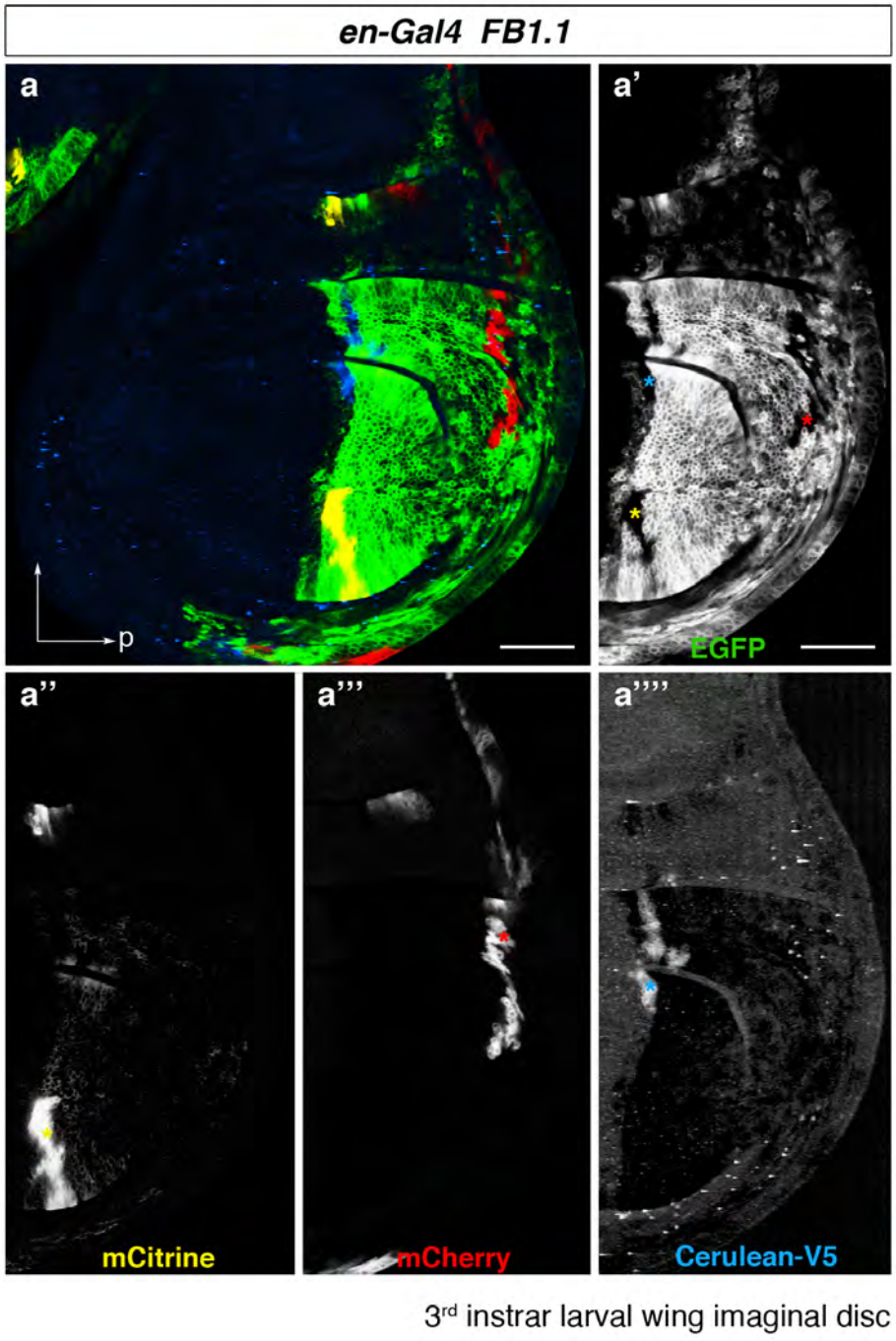

Figure 45. Expression of *FB1.1* transgenes in developing *Drosophila* tissues.
At the third instar larval stage, clones of epithelial cells within wing imaginal discs were differentially labeled by the expression of *FB1.1* transgenes. *en-Gal4* was used to drive expression in the posterior (p) compartment of the discs (a). mCitrine (a''), mCherry (a''') and Cerulean-V5 (a'''') were expressed in addition to the default EGFP in a mutually exclusive manner (color coded asterisks). *en-Gal4/FB1.1*^{260b}*; repo- hs-mFlp5*/+. Heat shock: 45 minutes at 72 hours AEL. Scale bar, 50 µm.

5.8 Multiple transgene insertions lead to combinatorial expression of fluorescent markers within a single cell

Our results have so far demonstrated that *Flybow* can be used for identification of cell shape morphology by tracing fluorescence signals from the cell body to distant cellular protrusions. *Brainbow* mice with multiple tandem insertions of the transgene have shown that expression of multiple markers within a single cell can become advantageous in providing unique color identity to neighboring cells. We thus decided to apply the same logic in experiments for the *Drosophila* nervous system. Using genetic crosses, new lines were generated that combined the transgenes inserted at positions *VIE260b (2L)* and *VIE49b (3R*) on the second and third chromosomes into one stock. Gal4 activation can therefore lead to expression of two fluorescent proteins within a single cell. *elav-Gal4^{c155}* was used for expression of *FB1.1* transgenes in optic lobes at the third instar larval stage (Figure 46). This can lead to the generation of 10 different hues (4 basic colors and 6 new color combinations) depending on the pair of fluorescent proteins expressed. Overlapping expression of fluorescent proteins was evident in all cells across the optic lobe in these samples. Cells expressing both EGFP and mCherry were easy to detect (Figure 46). The signal from either EGFP or mCherry in the double-labeled cells appeared less intense when compared to signal detected in neighboring single-labeled cells. The latter confirms that single labeled cells express the same fluorescent protein from the different transgene copies leading to higher fluorescence signal (Figure 46). Further data analysis is required to confirm that all 10 hues can be recognized. Nonetheless, these experiments constitute a proof of principal that increasing the number of Flybow transgene copies can lead to the expression of multiple markers in a single cell without disrupting its development.

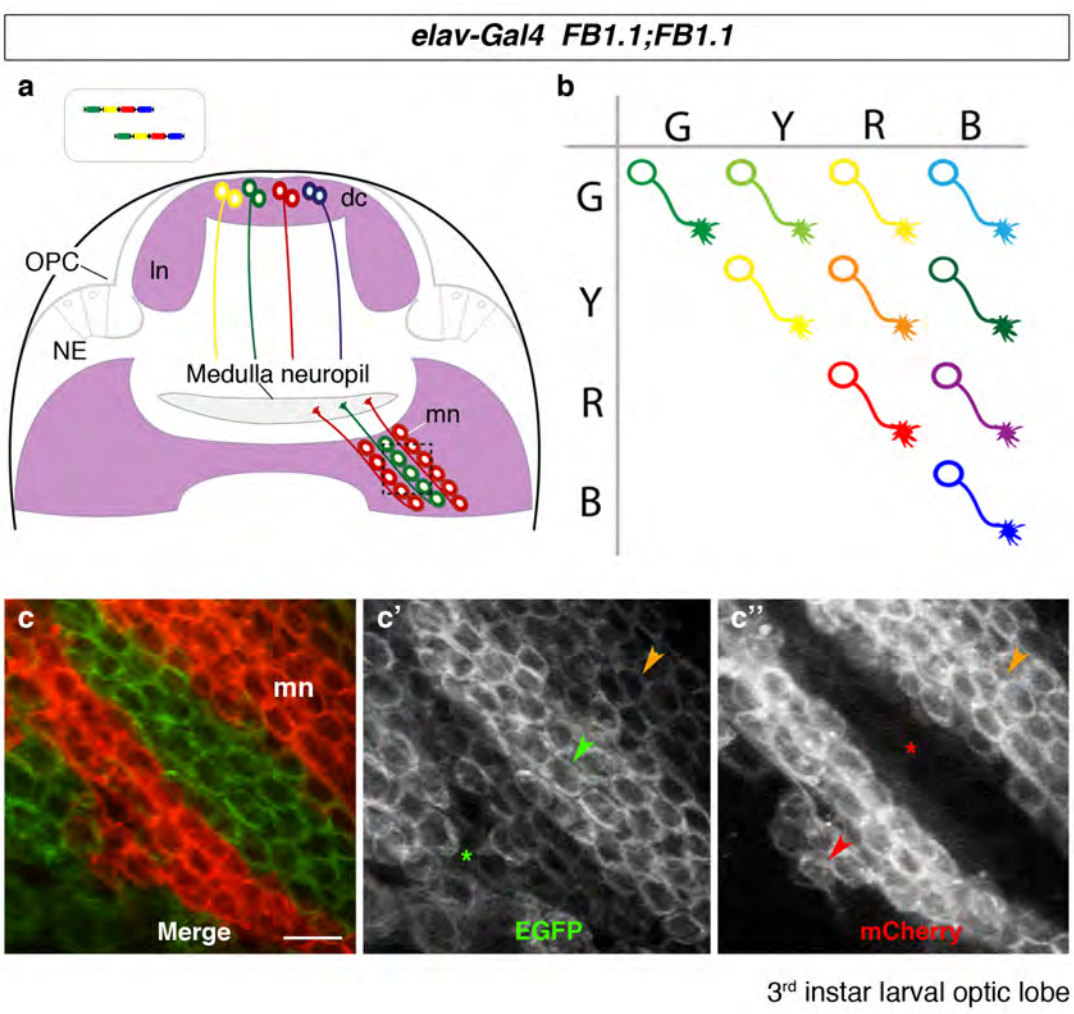

Figure 46. Expression of two copies of *FB1.1* transgenes.
Flybow lines were generated by insertion of a single transgene copy to a known genomic position on either the second or the third chromosomes. Activation of the *FB1.1* approach within an individual cell leads to expression of one of the four fluorescent markers, EGFP, mCitrine, mCherry or Cerulean-V5. Standard genetic crosses between lines that carry the transgene on different chromosomal locations generated flies bearing two transgene copies. Rounded rectangular shape indicates a single cell with two *FB1.1* transgene copies (a). Increasing the transgene copy number to two can theoretically lead to ten different color outcomes (b). Schematic diagram of an optic lobe at the third instar larval stage (a). Neuroepithelial (NE) cells in the outer proliferation center (OPC) give rise to both lamina (ln) and medulla (mn) neurons. Box (dashed-line) indicates the area shown in (c). *elav-Gal4*^{c155} was used for expression of the *FB1.1* transgenes. mCitrine, mCherry and Cerulean-V5 were expressed in addition to the default EGFP reporter. Expression of both EGFP and mCherry within the same cell could be readily detected (c-c", orange arrowheads). Sole EGFP or mCherry expression from individual cells was also detected in these experiments (color-coded arrowheads). *elav-Gal4*^{c155}/+ or *Y*; *hs-mFlp5/FB1.1*^{260b}*;FB1.1*^{49b}/+. Heat shocks: 45 minutes at 48 hours AEL. Scale bar 5 μm (a).

5.9 *FB2.0* facilitates single cell analysis

Using the *FB1.1* approach, we have demonstrated that stochastic expression of four fluorescent proteins confers single cell resolution even when using Gal4 drivers with highly broad expression domains. Focusing on the identification of well-studied morphologies of dendritic and axonal arborization patterns, we could readily detect lamina neuron projections. Nevertheless, characterization of medulla neuron subtypes tightly packed within the medulla neuropil was more difficult. We thus reasoned that sparse labeling of such cellular populations could significantly facilitate analysis. This could be made possible by employing the *FB2.0* approach. The *FB2.0* transgene contains a cassette flanked by canonical *FRT* sites upstream of the Flybow "core" cassette. Removal of this cassette by canonical Flp recombinase is permissive for reporter expression and overlapping mFlp5 activity leads to stochastic fluorescent protein expression. We used *elav-Gal4*^{c155} to drive *FB2.0* transgene expression in the developing visual system and in the adult. Following to Flp and mFlp5 activation, we could readily detect labeling within eye-brain complexes (Figures 47 and 48) and adult optic lobes (Figure 49). Importantly in these experiments, EGFP expression was restricted to fewer numbers of cells, thus, similarly to the other three markers, EGFP could be readily used to extract single cell information. Crucially, stochastic expression of the two Flp recombinase variants using a single heat shock protocol was sufficient to sparsely label cells distributed in different areas of the visual system. Together, these experiments confirm that *FB2.0* is more suitable for use in combination with broadly expressed Gal4 drivers and can speed up the data analysis process.

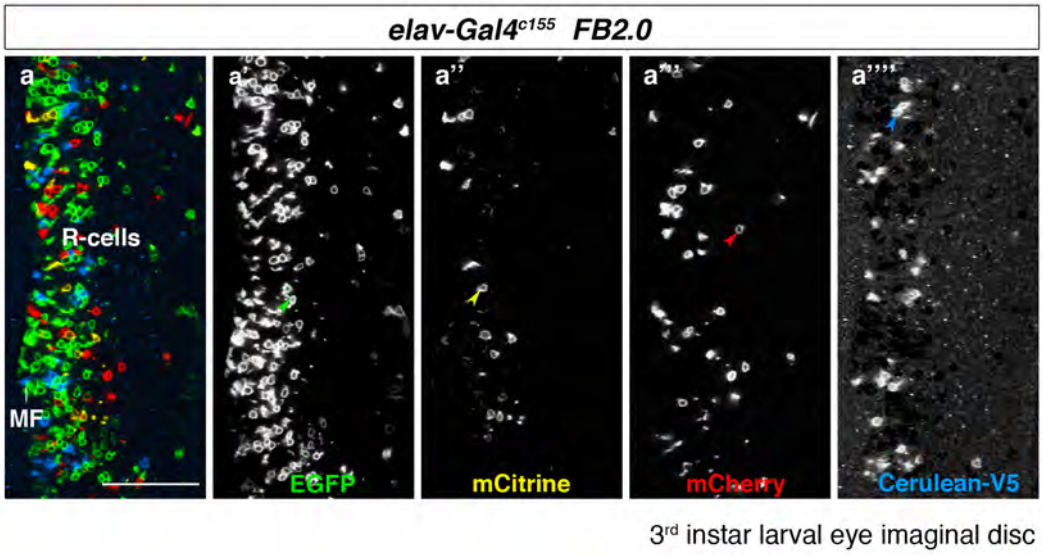

Figure 47. Activation of the *FB2.0* approach leads to sparse multicolor labeling of neurons in the developing eye imaginal disc.

FB2.0 transgenes contain an additional stop-cassette, compared to *FB1.1,* flanked by wild-type *FRT* sites facing in the same direction. This cassette is downstream of the *UAS* sites and, thus, blocks fluorescent protein expression. Overlapping activation of the *hs-Flp*^{1} and *hs-mFlp5* recombinases within the same cell is required for the removal of the stop cassette and the stochastic expression of the four fluorescent proteins. *elav-Gal4*^{c155} was used for expression of the *FB2.0* transgene within the eye imaginal disc at the third instar larval stage (a). EGFP (a'), mCitrine (a''), mCherry (a''') and Cerulean-V5 (a'''') were expressed in a subset of photoreceptor cells (R-cells) posterior of the morphogenetic furrow (MF). Expression was predominantly mutually exclusive (color-coded arrowheads). *elav-Gal4*^{c155} */hs-Flp*^{1}; *hs-mFlp5*/*FB2.0*^{260b}. Heat shock: 45' at 72 hours AEL. Scale bar, 50 µm.

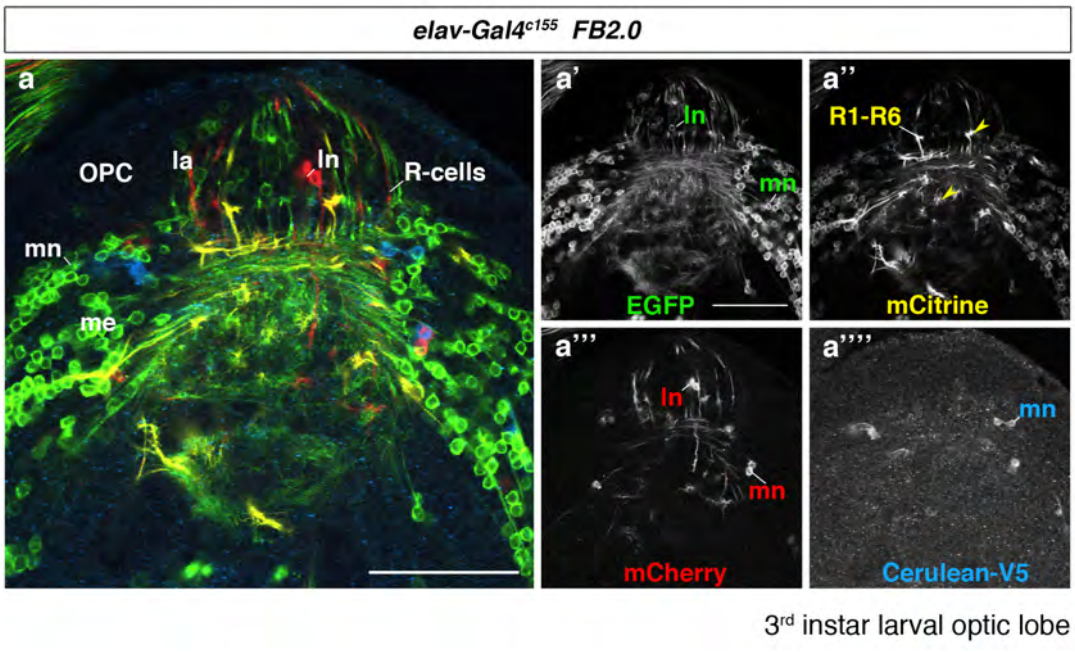

Figure 48. The *FB2.0* approach labels a small number of optic lobe neurons in the developing visual system.

In samples carrying the *FB2.0* transgenes, following heat exposure Flp and mFlp5 recombinases were expressed within developing *Drosophila* tissues. Recombination outcomes can be monitored in only those cells positive for the pan-neuronal *elav-Gal4*^{c155} driver, leading to expression of EGFP (a') mCitrine (a"), mCherry (a"') and Cerulean-V5 (a""). A small subset of photoreceptor cells (R-cells, R1-R8) and lamina neurons (ln) in the lamina (la) and medulla neurons (mn) in the medulla were marked by fluorescent protein expression. OPC, outer proliferation center. *elav-Gal4*^{c155} */hs-Flp*^{1}; *hs-mFlp5/FB2.0*^{260b}. Heat shocks: 45 minutes at 48 and 72 hours AEL. Scale bars, 50 μm.

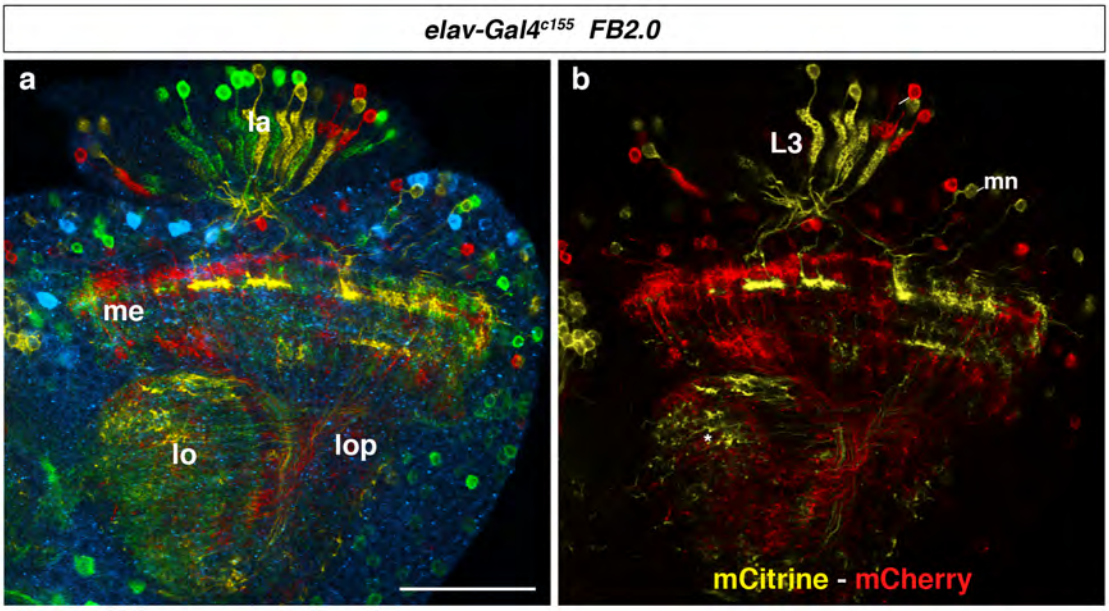

Figure 49. Sparse labeling using the *FB2.0* approach facilitates subtype neuron identification in the adult visual system.

(a, b) The pan-neuronal *elav-Gal4*^{c155} driver was used to drive expression of a *FB2.0* transgene in the adult visual system. A restricted number of neurons were labeled with EGFP, mCitrine, mCherry and Cerulean-V5. Subtypes of neurons in the lamina (la), medulla (me), lobula (lo) and lobula plate (lop) could be easily identified. Lamina neuron L3 terminals (mCitrine) could be easily recognized due to the characteristic morphology of their terminals in the M3 layer of the medulla. Neighboring cells with overlapping branches were also positively labeled with mCherry (b). *elav-Gal4*^{c155}*/hs-Flp*^{1}; *hs-mFlp5/FB2.0*^{260b}. Heat shocks: 45 minutes at 48 and 72 hours AEL. Scale bar, 50 μm.

5.10 Discussion

We used multicolor cell labeling to extract single cell morphologies from tissues, in which numerous cell types are positively marked by the expression of distinct fluorescent proteins. The new mFlp5/*mFRT71* recombination system has been efficiently utilized to induce all possible color outcomes derived from rearrangements within the *Flybow* transgenes. Aspiring to gain insights into the processes involved in neural circuit formation within the medulla, we used the Flybow approach to visualize the intricate morphology of neurons and glial cells. Furthermore, Flybow transgenes were successfully used to label neural lineages in the embryonic nervous system, rendering the approach suitable for studies at these early stages of development. Finally, experiments in the wing imaginal disc indicate that the approach is functional in tissues other than the nervous system. Consequently, experimental analyses included in this chapter demonstrate that randomized and sparse labeling provided by *FB1.1* and *FB2.0* approaches is sufficient for resolving shapes of tightly packed insect cells.

5.10.1 Flybow combined with light microscopy imaging provides data suitable for single cell reconstructions

Ramón y Cajal revolutionized the field of neuroscience by methodically reconstructing neurons of different origin in remarkable detail to produce anatomical atlases of neural circuitry. His work illustrated the significance of extracting morphological information at a single cell level using sparse labeling. We aimed in essence to achieve a similar goal by employing novel tools including genetically encoded fluorescent markers and confocal light microscopy. *FB1.1* and *FB2.0* transgenes can lead to the expression of up to four fluorophores; namely EGFP, mCitrine, mCherry and Cerulean-V5. Using our imaging conditions, we could retrieve fluorescent signals of all four markers. This further allowed us to discern true signal by subtracting “cross-talk” derived fluorescence, mainly in the case of the EGFP and mCitrine pair. Importantly, using dye separation algorithms we could quantify and compare the acquired signal for each of the four fluorophores and found that the levels, at which they fluoresce are overall similar. This mainly constitutes proof that our settings are suitable for the detection of sufficient amounts of

fluorescent signal from all channels for endogenous fluorescent protein expression and immunolabeling of Cerulean-V5. We could thus resolve overlapping branches of neighboring cells that express distinct fluorescent protein pairs. However, fluorescence levels from the four dyes appear dynamic. This can be illustrated when looking at the different measurements of an individual fluorescent protein within one or across a range of different samples. Contributing factors for this variability include position of a cell within the structure, fluctuation of laser line power, dynamic range of detector sensitivity and variability in the preparation of the samples to be imaged. Overall, cell localization within the tissue of interest is crucial in imaging experiments like ours, which use whole mount tissues as opposed to tissue sections. Our imaging paradigms typically run through a distance of 65-80 μm acquiring an image for three sequential scans every 1 μm. Thus, sample exposure to laser emission is relatively high and photobleaching occurs at least to a certain amount. Such photobleaching has not prohibited us from successfully tracing and reconstructing neurons in our four-color experiments. Nonetheless, it becomes a concern for experiments involving expression of more than one fluorescent protein within a single cell. Algorithms devised for data analysis of this kind must take into consideration the factor of photobleaching that differs across different fluorescent proteins (Chudakov et al., 2010; Shaner et al., 2007; Shaner et al., 2005) and it is inherently very dynamic. This is essential for studies that require tracing of the entire axonal and dendritic branching structures of a neuron, which can span several "cell-body diameters" away from its soma position. Moreover, considering that we need to make use of immunohistochemistry to visualize the Cerulean protein, we must also take into account that antibody penetration could differ in the innermost parts of a heavily populated tissue. Therefore, in our view the use of endogenous expression of a fluorescent protein by replacing Cerulean with a different strongly fluorescent cyan variant such as the newly generated mTurquoise or mTurquoise2 (Goedhart et al., 2010) (Goedhart et al., 2012) will further enhance our abilities to extract neuron structure information. This would in parallel make it possible to use immunostaining for "landmark" proteins, such as neuropil markers, and their detection with secondary antibodies emitting in the far-red portion of the spectrum. Importantly, immunostaining of landmark structures is not

affected by photobleaching phenomena, as its location and morphology is well characterized and normally spatially restricted.

We have demonstrated that fluorescence levels of EGFP expressed from *FB1.1* transgenes inserted in locations *260b(2L)* and *49b(3R),* on the second and third chromosomes, respectively, were not significantly different. Importantly, we included mainly unsaturated pixels for true signal measurements in this analysis. Signal to noise dynamic ranges for measurements of the two data showed similar values, thus further indicating true similarities amongst the two data cohorts. Future experiments could potentially make use of similar acceptor sites within the X chromosome for integration of Flybow transgenes facilitating genetic schemes with heavy requirement of transgenes on the second and third chromosomes. Such potential sites could directly be validated for fluorescent marker expression levels using the analyzed values for signal detection included in this chapter. Finally, alternative strategies placing the transgene under a specific promoter of choice (e.g. *fruitless-FB1.1*) would need to be validated for their ability to drive similar fluorescent protein expression levels when compared to the reported *UAS*-counterparts.

Scientists with a wide range of scientific focus routinely use single-photon confocal microscopy, particularly in laboratories studying cellular interactions. We have demonstrated that our approach is fully compatible with such light microscopy set-ups and thus can be easily incorporated in the daily toolbox of a *Drosophila* scientist. Furthermore, we have shown that the approach can in essence be utilized in two-photon confocal microscopy experiments. However, the selected fluorescent proteins have shortcomings in multicolor analysis using a two-photon microscope. Experiments conducted by Emily Richardson in our laboratory have shown that Flybow can be utilized as a single marker tool (EGFP or mCitrine) in time-lapse two-photon confocal imaging experiments of live pupae. In these specialized imaging paradigms, acquisition occurs in great tissue depth and crucially in a living animal. Flybow has proved to be suitable for use in these settings due to strong expression provided by the use of 10 *UAS* sites. Consequently, this reduces the amount of laser power required for excitation that is imperative for maintaining the animal alive throughout the imaging procedure. Hence, we reasoned that a

new set of fluorescent proteins should be incorporated in novel versions of the Flybow transgenes making it suitable for two-photon multicolor imaging. Given the modular character of our transgenes replacing the coding sequences with a new set is relatively uncomplicated. Taking advantage of the newly built *UAS-mTurquoise*^{260b} transgenic lines (courtesy Nana Shimosako and Iris Salecker) generated in our laboratory, we could directly test how this fluorescent protein performs when used in combination two-photon microscopy. These results show that mTurquoise yields very high amounts of fluorescence following excitation by the Mai-Tai laser. Fluorescence detected is, however, so high that it may yet hamper a multicolor imaging experiment, as it seems to saturate regions of the spectrum that overlap with EGFP emission (I. Salecker and D. Bell, unpublished observations). Nevertheless, linear unmixing algorithms could be applied and possibly overcome this obstacle. Furthermore, a different multiphoton laser line could be added to the existing confocal set-up to broaden the range of the spectrum that can be imaged. During the course of this study, Nana Shimosako in our laboratory has successfully generated a second set of transgenic Flybow lines, namely *FB1.0B*, *FB1.1B* and *FB2.0B* that include a palm /myr membrane anchored version of mTurquoise (Shimosako, 2013)

A potential new set of fluorescent proteins could include mTFP1.0 (Ai et al., 2006), mAmetrine (Ai et al., 2008), DsRed2 (Yanushevich et al., 2002) and tdKatuska (Shcherbo et al., 2009). Choosing the correct fluorescent protein for a two-photon experiment is a specifically difficult task; particularly due to published inconsistencies regarding values of two-photon cross section emissions that vary a great deal in the literature (Drobizhev et al., 2011). For instance, the suggested set of fluorescent proteins has been reported to yield similar brightness values. When excited by neodymium and ytterbium laser lines, the respective distances of each spectrally neighboring pair is at least 50 nm apart, thus rendering their combination suitable for simultaneous use in the same experiment. Technological progress in both fluorescent protein engineering, as well as in advanced microscopy methodologies promise to provide us with additional tools to fine tune our approach and achieve multicolor labeling in time lapse experiments. Such approaches would for example allow us to directly visualize neurons, as they

leave their birth location, and migrate or project their axons to populate the medulla neuropil during metamorphosis (Bazigou et al., 2007). Thus, retrieving such information could be indicative of the kinetics employed during the medulla circuit set up and could lead to precise temporal dissection of the involvement of specific genes during this process.

5.10.2 The mFlp5/*mFRT71* system effectively catalyzes a combination of inversion and excision events in *Flybow* transgenes

We analyzed the frequency, with which different color outcomes occur following mFlp5 activity in the developing optic lobes of animals at the third instar larval stage. Our results for both *FB1.1* and *FB2.0* approaches indicate that color switches happen at similar frequencies. Our results are consistent with a recent study using the Brainbow approach, which demonstrates that after exposure to large amounts of Cre activity all the sequence outcomes that can be produced, are generated with equal probability (Wei and Koulakov, 2012). Importantly, our measurements show an even distribution of recombination outcomes across a series of samples. This was mainly a concern for *Cerulean-V5,* whose expression requires either a combination of excision of the first cassette followed by the inversion of the second cassette, or an inversion of the two fluorescent protein coding cassettes together. We have not characterized, which of the two theoretical possibilities occurs more frequently or in effect if both can take place. Our reasoning is that both events can happen; however, we have no data to support that a large, approximately 8 kb, sequence can be efficiently inverted. To systematically investigate this possibility and as the investigated sequence codes for fluorescent protein expression, fluorescence activated cell sorting (FACS) methodologies could be utilized for analysis. However, it is important to note that our approach is based on both stochastic expression, as well as distribution of the four-color outcomes. Thus, our experiments are not negatively affected by the random infrequent representation of one color outcome. On the contrary, we could use such a tendency to our benefit for extracting morphological information from a restricted number of labeled cells.

These analyses additionally show that in experiments using either the *FB1.1* or *FB2.0* approach, EGFP remains the most frequently expressed fluorescent protein. This largely indicates absence of recombination events occurring within these cells. We could see, however, that in *FB2.0* experiments, EGFP expression occurs more frequently when compared to the *FB1.1* data sets (73.1% and 48.2%, respectively). This difference could potentially be attributed to the different heat exposure protocols performed in these two experiments. Repeated shorter heat-shocks at additional developmental stages might attenuate the mFlp5 expression level requirement for generation of more equally emerging color outcomes. This interpretation highlights two additional aspects important for future investigation. First, a thorough assessment of mFlp5 recombination efficiency in independently generating inversions or excisions, following to heat exposure of varying lengths would be highly informative. Such analysis could identify the minimum time required for mFlp5 to be expressed and deliver individual enzymatic reactions at saturated levels. Such experiments could be designed similarly to the ones described Section 3.3 using the eye imaginal disc for read out. Furthermore, our initial analysis (data not quantified) showed that mFlp5 is less efficient in generating cassette excisions when compared to the canonical Flp variant. This observation together with the elegant work in site-specific recombinase engineering by Nern *et al*. (Nern et al., 2011), led to ongoing work by Nana Shimosako in our laboratory aiming at generating a new variant of mFlp5 recombinase. Using optimized codon sequences for *Drosophila,* the newly generated version of mFlp5 could potentially prove to be more efficient in generating recombination events. However, a possible limitation of its use could be the cross reactivity with canonical *FRT* recognition sites. As a result, experiments similar to the ones performed by Shay Rotkopf (Section 3.3) will be required to ensure that this further modified recombinase can be combined with the canonical Flp^{1}/*FRT* system for use in intersectional studies. Finally, experiments showing the efficiency of this new variant in mediating inversion and excision could be performed as discussed for the initial mFlp5 transgene.

Second, the increase in occurring color swaps observed in the *FB1.1* sample cohort could be also attributed to additional heat exposure of samples at 96 hours AEL. Moreover, our

experiments have demonstrated that developmental time and length of heat exposure must be adjusted for each Gal4 line used to drive transgene expression. We believe that such timing coincides with the time of generation of this genetically defined group of cells. Nevertheless, recombination events using our approach could in theory happen within cells at any stage of their development. Therefore, both dividing and postmitotic cells should be competent to swap the fluorescent protein they express upon mFlp5 activation. Our current analysis provides evidence in support of this notion. First, we have observed higher numbers of differentially labeled medulla neurons in the older part of the medulla as compared with the newly generated neurons at the third instar larval stage (see Figure 27, data not quantified). The younger part of the medulla shows a relatively uniform expression of fluorescent protein (largely Cerulean-V5 and mCherry). It is possible that this originates from a recombination event carried out in the parental (neuroepithelium) cell. This was consequently stably conveyed to its entire progeny that was not exposed to further mFlp5 activity. By contrast, the older part of the medulla shows rather an intermixed expression mode of the different fluorescent proteins, which could indicate recombination events that have occurred in neuroblasts or ganglion mother cells, but also individual postmitotic neurons. We thus believe that mFlp5-mediated recombination can occur at different stages of cell development following cell-cycle exit. This interpretation, however, must be considered with caution, as it plausible to assume that to a certain extent color scattering is due the initiation of cellular migration in this older part of the medulla (Bazigou et al., 2007; Morante et al., 2011). Nevertheless, it is easy to assume that recombination can occur more frequently in dividing cells, in which chromatin oscillates between condensed and uncondensed states. We thus hypothesized that uncondensed chromatin is relatively more accessible to successful recombination reactions and such processes are less energy demanding. It is clear, however, that future experiments should address this issue in a more methodical manner. Heat exposure at developmental stages following to neurogenesis termination (mid pupal development) should confirm, that these events are feasible and in addition enable us to determine the frequency at which they can occur. Interestingly, similar experiments performed

in parallel for the codon optimized mFlp5 variant could test if higher efficiency of the enzyme yields more frequent recombination events in these experimental scenarios.

Overall, our experiments clearly profit from the tight temporal control of recombinase expression. Precise developmental timing for heat shocks application together with heat exposure titration offer the choice of selectively generating large or smaller labeled clones. Finally, a further level of refinement comprises the use of *FB2.0* transgenes for labeling only within cells, in which mFlp5 and Flp expression domains overlap.

5.10.3 Flybow marks cell populations by differential fluorescent protein expression and helps to resolves their respective morphology at the single cell level

Evidently, a milestone in the field of *Drosophila* genetics constitutes the use of the dually natured Gal4/*UAS* system for selective control of transgene expression within genetically defined cell groups. Thereafter, a great wealth of gene regulatory elements was used to generate transgenic driver lines, a high proportion of which is openly shared within the fly community (e.g. the NP collection from the Kyoto *Drosophila* genomics resource center (DGRC), the Bloomington stock center, and most recently, the Janelia farm and VDRC collections). Crucially, experiments elucidating cell behavior within gene expression domains throughout development and within adult tissues are now routinely performed. Hence, we employed different Gal4 driver lines for specific expression of the *Flybow* transgenes within cell populations important for our experiments. These included previously described subgroups of neurons found in the fly visual system; namely, R-cells, lamina neurons, and distinct medulla neuron classes, as well glial cell subpopulations at the third instar larva stage and in the adult. Additionally, we could identify previously unknown neuron subtypes innervating the medulla, as well as the highly divergent cell shapes of the medulla neuropil glia in the adult. We could perform reconstructions of single cell morphologies using samples, in which the entire tissue was positively labeled. Additionally in these experiments, we could uncover information relating birth time and final localization of a specific lobula plate derived neuronal population. Furthermore, using the well-studied R-cell array, that is easy to score because of its repetitive

and characterized pattern, we verified that fluorescent protein expression does not interfere with neuron development or axon targeting. Importantly, studies using mutant analyses for molecules that interfere with the correct development of this group of cells have identified disrupted morphologies, thus making them a well-suited system to score for even subtle defects.

Next our analyses showed that the novel mFlp5/*mFRT71* system could be used successfully to generate clones in the embryo. Specifically, we have shown that multicolor labeling in the embryonic nervous system, at least at late stages, could be readily achieved. This is an exciting application for Flybow, as it could potentially be used to monitor the effects of upregulation or loss of function of a specific gene at the level of individual neurons, in a whole animal mutant background for functional analyses in embryos. In addition, as we had anticipated, Flybow could be successfully used for multicolor labeling of tissues other than the nervous system. This offers the possibility to study for instance the morphological changes that an epithelium undergoes in cell ablation experiments. Multicolor labeling would facilitate monitoring of kinetics between differentially labeled cells that are tightly packed within the epithelia.

Importantly, most of the work described in this chapter aimed to confirm the functionality of our approach in different experimental paradigms. We have confirmed that single cell shapes can be uncovered using the *FB1.1* variant in a tissue that is labeled by fluorescent protein expression in its entirety. This comprised a highly complex situation that could benefit from sparse labeling. Thus, we believe that when using broadly expressed drivers, *FB2.0* transgenes are better suited to raise the information content per sample. Nonetheless, using both *FB1.1* and *FB2.0* approaches can empower analysis as they both offer different advantages for circuit studies. FB1.1 marks positively all neighboring cells and thus provides information about individual neuron interactions within its environment. This becomes even more obvious when combined with the MARCM approach for gene function studies (see Chapter 6). Conversely, *FB2.0* facilitates sparse labeling and importantly can be directly used as an intersectional tool by the expression of the canonical Flp recombinase under the control of specific regulatory elements. In conclusion, experiments employing Flybow for multicolor

labeling can be tailored to the needs of different experiments. Using a combination of the different Flybow approaches available can facilitate analysis.

5.10.4 Employing Flybow in circuit formation studies

As proof of principle, we combined Flybow with the *MzVum-Gal4* driver to gain insights into the identity of Vsx1 expressing neuron types in the adult visual system. Interestingly, complementing earlier descriptions (Erclik et al., 2008), we identified three novel transmedullary neuron subtypes, TmY4-like, TmY5-like, and Tm22-like. The branching patterns of these neurons share similarities to their previously described counterparts - TmY4, TmY5, and Tm22, respectively. Nevertheless, there are clear differences in their morphology to the description of Fischbach and Dittrich, 1989. Importantly, beyond the highly hardwired mechanisms that govern circuit assembly in the lamina (Hiesinger et al., 2006), it remains unclear to what extent network formation in other parts of the *Drosophila* brain is similarly stereotyped. Variations in the morphology of previously described subtypes that belong to the same group have been described both in the antennal lobe (Chou et al., 2010; Jenett et al., 2012) and in the visual system (K.-F Fischbach, 1989). So far, it is unclear whether these differences reflect distinct neuron subtypes or plasticity in the development of the same subtype. Flybow can be employed to address this important question in the future (also see section 7.2). Identification of Gal4 drivers expressed in single neuron subtypes (e.g. Janelia farm and VDRC collections) will help to express Flybow only in a particular neuron type. Therefore, comparing single cells in different colors within a single sample can easily reveal the presence of variation in the branching patterns of these neurons. For instance, if all neurons occupy precisely the same layers and columns, and their branching pattern is indistinguishable; it is plausible to conclude their connectivity is genetically determined. In a similar experiment, we applied Flybow to reveal the identity of Netrin expressing neurons, and identified amongst others Tm2, Tm3, TmY7 and Tm21 medulla neurons (Timofeev et al., 2012).

Importantly, while these neurons have branches in the M3 layer, lamina neurons L3 are the only neuron subtype with axonal terminals in the M3 layer. While we cannot entirely exclude the

contribution of NetB expressing medulla neurons, our findings support the model that local release of Netrins by lamina neurons L3 is central for the enrichment of this attractive guidance cue in the M3 layer. Moreover, to study the dynamic morphology of R8 axon growth cones during the targeting to their final M3 layer, we performed Flybow experiments using the *GMR-Gal4* driver line. Importantly, these studies exemplify that we are able to gain novel insights into long studied phenomena. We observed that R8 growth cones extend thin filopodia towards the M3 layer prior to their regrowth revealing a possible novel mechanism for the precise steps during R8 axon targeting. To explore the precise dynamics of R8 axon targeting in further detail it is possible to use the advantages of our tool in live imaging experiment, since studies of Emily Richardson demonstrated that cell morphology can be robustly visualized in vivo. It is noteworthy that a similar approach using MARCM would be hugely laborious since it relatively hard to identify single cell clones as R7 and R8 axonal projections within a single column overlap.

Chapter 6

Employing Flybow in gene function studies

6.1 Introduction

Morphological information provides identity to groups or individual cells within a multicellular environment. Similarly, gene expression domains offer an alternative way to characterize these cells within an organism. Thus, relating cell shape information to gene function can lead to a more comprehensive understanding of the role of an individual cell within a neural circuit, viewed as a "single-player" in the "multi-player" game of organism homeostasis. Numerous methodologies for cell labeling, as well as genetic tools for studying gene function have been developed and can provide information for individual cell behavior within a given network (see section 1.3). These can be grouped into categories and can elucidate roles of specific genes at different levels. Relevant to our interest in understanding the biology of circuit formation in *Drosophila,* one can classify three levels of cell manipulation. First, studies in the embryo are used to appreciate the effects of loss of gene function on the specific neuronal network of interest, in the generic background of a whole mutant animal. Within the embryo, individual cell morphologies of all interneurons were described in a laborious approach using DiI single cell injections (Rickert et al., 2011). Such comprehensive efforts are of great importance, because they can provide the basis for identification of morphological abnormalities in specific interneuron subtypes in this case in a mutant background. However, such studies could have been greatly accelerated by the use of genetic clonal cell labeling, which is not commonly used in the embryo. Flybow could be introduced in a mutant background for studies in the embryo. Second, using a binary system for expression, such as the Gal4/*UAS* system, it is possible to manipulate groups of cells i.e. neuron subtypes within a network of interest. This includes both gain of function studies of a gene of interest and knock down of its expression using the RNAi defined approach. *FB* transgenes could be co-expressed in these experiments and serve as multicolor reporters to facilitate singe cell resolution. Examining both whole mutant animals and entire mutant subpopulations of cells can be problematic due to early lethality. Thus thirdly, to overcome this and to truly study cell-autonomous roles of a neuron within a circuit, mosaic analyses must be employed. These elegant approaches can be used to switch off gene function

in subsets of cells leaving their neighbors wild type. Such tools are important for circuit studies, as neighbouring cells are known to directly communicate and depend on each other. Flybow uses the modified mFlp5/*mFRT71* recombination system for clone induction and, thus, is compatible with available approaches using the canonical system for recombination such as MARCM and Flp-out based approaches. Therefore an advantageous feature of Flybow compared to the vertebrate Brainbow system is that in principle, it can be readily combined with tools for functional analyses. This chapter focuses on demonstrating that Flybow and MARCM approaches can be combined to perform gene function studies.

6.2 Flybow in combination with MARCM to conduct functional studies

The MARCM approach employs the canonical Flp/*FRT* system for the generation of homozygous mutant or wild-type clones with a limited number or individual cells, that are positively marked by the expression of a reporter in an otherwise non-labeled tissue (Lee and Luo, 1999). This is achieved by homologous recombination, mediated by the Flp recombinase between *FRT* sites located on sister chromosomes *in trans* during mitosis. We have chosen the modified mFlp5/*mFRT71* system for Flybow as it does shows only limited cross-reactivity with the Flp/*FRT* system. mFlp5 can induce inversions and/or excisions leading to the four color outcomes within the same chromosome (*in cis*) (Figure 50). In this set of experiments, we combined the *FB1.1* approach with MARCM by generating stocks that combine the two methodologies.

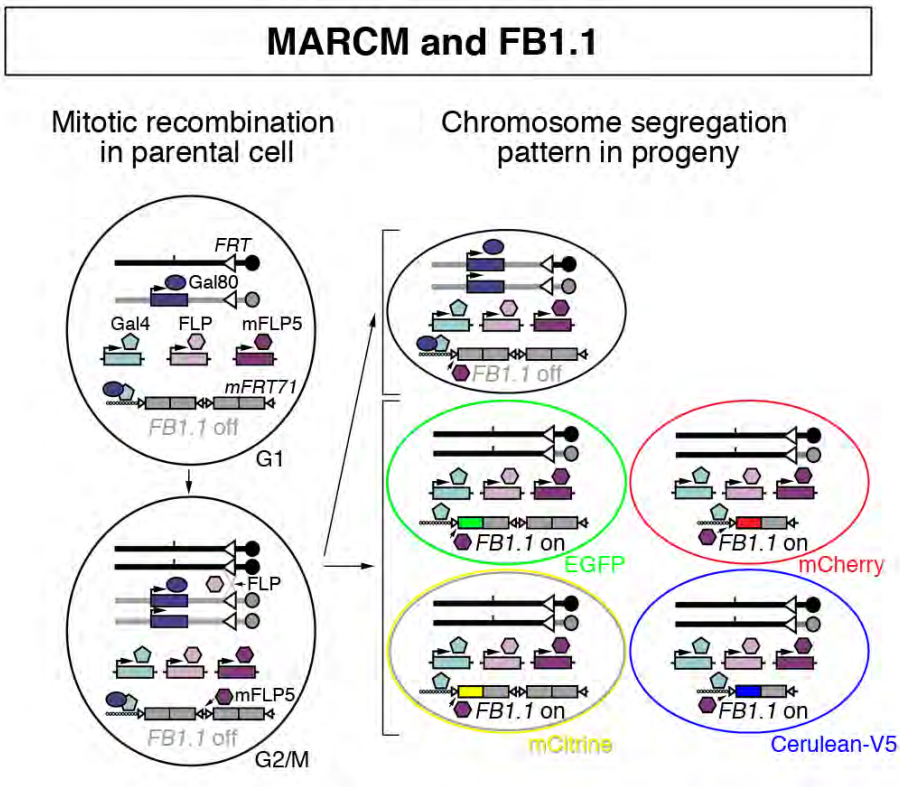

Figure 50. Combining MARCM with Flybow facilitates single cell labeling in gene function studies. Flybow used together with MARCM in mosaic analysis experiments of gene function can facilitate single cell labeling within one sample. Schematic diagram illustrates the processes a cell undergoes when combining the two approaches. During the G2 phase of the cell cycle, recombination occurs in *trans* upon activity of the Flp/*FRT* system. Subsequent chromosome segregation leads to the loss of the Gal80 repressor in one of the daughter cells, allowing reporter gene expression. This cell will be homozygous for any mutation located on the homologous chromosome carries arm (vertical bar on black chromosome). In addition within this cell, the mFlp5/*mFRT71* system mediates recombination *in cis* and leads to the expression of mCitrine, mCherry and Cerulean-V5 in addition to the default EGFP marker.

N-Cadherin (CadN), a calcium dependent homophilic cell adhesion molecule, is expressed in the growth cones of R-cells and in target neurons. Previous studies have uncovered a role of *CadN* in layer-specific axon targeting of lamina neurons ((Nern et al., 2008); see section 1.2) in the *Drosophila* visual system. Loss of function of *CadN* using the mutant $CadN^{M19}$ allele causes mistargeting and abnormal branching phenotypes within different lamina neuron subtypes. This study benefited from the availability of a *dac*-Flp recombinase transgenic line. Using this line, $CadN^{M19}$ mutant clones were solely induced in lamina neurons. Therefore, the analysis of lamina neuron morphology was not hindered by possible overlay of labeled medulla neurons and single cell clones were readily obtained.

Similarly to these results, we could generate *CadN*^{M19} mutant lamina neurons in our FB-MARCM approach using *hs-FLP*^{1} and *elav-Gal4*^{c155}. *FB1.1* transgene expression was observed in R-cells, lamina and medulla neurons. A significant number of these different neuron subtypes was differentially labeled by the expression of EGFP, mCitrine and mCherry (Cerulean-V5 was not visualized in these experiments). Immunostaining with mAb24B10 marked the R-cell terminals and provided layer landmarks in the medulla (Figure 51). Notably, multicolor cell labeling mediated by the *FB1.1* approach led to the unambiguous identification of wild-type and mutant lamina neuron subtypes based on their dendritic arborization pattern and cell body position in the lamina. In wild-type brains, monopolar lamina neuron 1 (L1) arborize in layers M1 and M5. Lamina neuron L5 extend branches into layers M1/M2 and M5 (K.-F Fischbach, 1989). We could therefore identify both L1 and L5 terminating in these layers in our wild-type experiments. *CadN* loss of function (*CadN*^{M19}) has been previously shown to lead to mistargeting of axonal processes to the proximal M10 layer for L1 neurons, while L5 mutant neurons fail to properly innervate the layer M2, lose their restricted columnar branching pattern, and extend ectopic branches to neighbouring columns (Nern et al., 2008). The penetrance of the mutant phenotypes ranged from 22-100% thus requiring high numbers samples to be analyzed; in the case of L1, 189 single cells. L5 neurons requires CadN for accurate interstitial branching in layer M2, in an L2 dependent manner. Thus, in this case more than 900 single cell clones for L5 were scored (Nern et al., 2008). In our FB-MARCM mutant samples, we could successfully recover phenotypes for these two lamina neuron subtypes. Crucially, the mistargeting of *CadN*^{M19} mutant lamina neurons was clearly visible even in the background of the neighboring medulla neuron branches, positively labeled with distinct colors. These results show that the two tools can be combined successfully together.

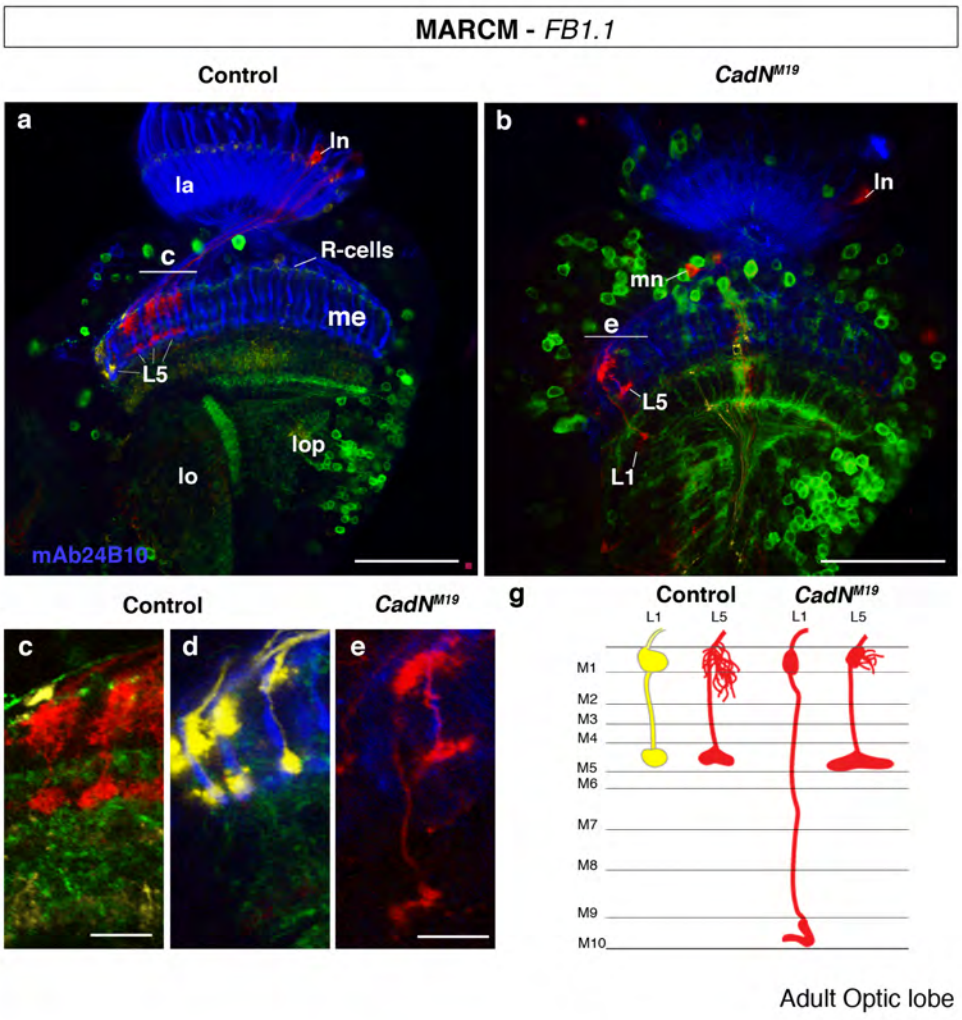

Figure 51. Flybow and MARCM used together to monitor lamina neuron targeting in the visual system of *Drosophila*.

Lamina neurons (ln) L1-L5, have characteristic dendritic and axonal arborization patterns and terminate in distinct layers of the medulla (me). N-Cadherin (*CadN*) is known to play a pivotal role in the correct layer targeting of lamina neuron subtypes. $CadN^{M19}$ mutation is known to cause lamina neuron targeting phenotypes. Overlapping activity of $hs\text{-}Flp^{1}$ and *hs-mFlp5* induced recombination events and enabled reporter expression in both wild-type control (a, c, d) and $CadN^{M19}$ homozygous mutant neurons (b and e). $elav^{c155}$*-Gal4* was used to drive *FB1.1* transgene expression. Expression was monitored in adult optic lobes. We used immunostaining with mAb24B10 (blue) to label photoreceptor cells (R-cells) that served as layer and column landmarks (a-e). mCitrine, mCherry and EGFP were expressed in neurons in the the lamina (la), medulla (me), lobula (lo) and lobula plate (lop). Differential labeling of cells within the optic lobe lead to the identification of neuron subtypes even in cases of neighboring cells with overlapping branches (c). L1 neurons arborize in the M1 and M5 layers in wild-type controls (a, d, g) and incorrectly extend deeper to the M10 layer in the absence of CadN (b, e, g). L5 neurons terminate in the M1/M2 and M5 layers in controls (b, c, g), but fail to form branches in M2 and abnormally project into neighboring columns when $CadN^{M19}$ mutants (b, e, g). (a, c, d) $elav\text{-}Gal4^{c155}$ $hs\text{-}Flp^{1}$/+ or *Y*; *tubP-Gal80 FRT40A/ FRT40A*; $FB1.1^{49b}$/+, (b, e) $elav\text{-}Gal4^{c155}$ $hs\text{-}Flp^{1}$/+ or *Y*; *tubP-Gal80 FRT40A/*$CadN^{M19}$ *FRT40A*; $FB1.1^{49b}$/+. Heat shocks: 90 minutes at 48 hours AEL. Scale bars, 50 µm (a, b) and 10 µm (c-e).

6.3 Discussion

A breakthrough for studies of neural circuit formation in *Drosophila* has been the development of the MARCM approach (Lee and Luo, 1999). By the expression of membrane-anchored GFP (*UAS-cd8-GFP*) this genetic method allowed visualization at a single cell level of wild-type neurons in exceptional detail. In addition, this genetic stratagem allows the generation of labeled homozygous mutant neurons in a heterozygous background and thus tremendously facilitates analysis of mutant cell morphology. MARCM has been very successfully applied to reveal the connectivity of the *Drosophila* olfactory system (Jefferis et al., 2001; Jefferis et al., 2007). The fly visual system is organized in highly repetitive fashion, making use of anatomical entities such as the medulla columns, which is an useful asset in clonal analysis studies. In this manner, abnormal morphologies or functions of a single mutant neuron subtype can be easily scored by direct comparison to cells of the same subtype that innervate neighboring columns. However, studies in the medulla neuropil are challenging since it is comprised of a large number of neuron subtypes that are very densely packed within these reiterated columns (Morante and Desplan, 2008). The identification of Gal4 drivers leading to *UAS-cd8-GFP* expression in restricted neural populations facilitates the visualization and mutant analysis of single cell morphologies (Hasegawa et al., 2011). Similarly, restricting the activity of the Flp/*FRT* system to a neural subpopulation provides advantages, by lowering the sample numbers required to identify single cell clones of particular neuron subtypes (Nern et al., 2008). For many studies, the lack of specific Gal4 transgenic lines combined with the lack of lines expressing the Flp recombinase under a specific promoter, for particular neuronal subtypes has been a limiting factor. We have shown in wild-type experiments that Flybow confers single cell resolution even when used with abundantly expressed drivers (section 5.2.4). Therefore, its application in mutant analysis of the aforementioned context can become highly advantageous similar to its facilitation in the visualization of wild-type neuron morphology.

Using *CadN* in our MARCM-FB experiments demonstrated that the two approaches are compatible for combinatorial use. FB can clearly increase the efficiency in comparison to a typical single-marker MARCM experiment. Samples generated solely with MARCM frequently

label the projections of overlapping wild-type or mutant cells. Thus, four color labeling significantly increases the possibility of retrieval of individual cell morphology information from simply one sample. This possibility is elevated since even cells within the same cluster can undergo individual mFlp5 mediated recombination events, leading to their differential expression of fluorescent markers. Nevertheless, it is important to emphasize that Flybow does not offer a golden solution to the reality of mosaic analyses that requires high numbers of experimental samples. In the aforementioned MARCM-FB experiment, we examined an already reported array of mistargeting phenotypes of lamina neurons and our sample numbers to recapitulate these were notably low (approximately 30 imaged samples); indicative is however that we have obtained the shown phenotypes in . Also the time to build the required stocks is not negligible, as this involves several generation of crosses. One can easily understand, therefore, that undertaking a similar effort for higher-order neurons for instance in the medulla, would still remain a daunting task even with the application of a multicolored reporter. Medulla connectivity is significantly more complex with more neurons innervating each column and layer. Thus, to assess mutant cell morphology for a general player in neural circuit formation, such as a cell adhesion molecule employed repeatedly by different cell types, these approaches would benefit from the generation of additional genetic tools. Individual medulla neuron subtypes could for instance be manipulated and labeled by the use of Flp recombinase under the regulatory elements of a transcription factor known to be active in specific lineages in combination with restricted Gal4 drivers for transgene expression. Overall however, we strongly believe that Flybow can significantly accelerate mosaic analyses, as well as other functional studies. For instance, experimental data by Benjamin Richier and Stefanie Schrettenbrunner in our laboratory have shown that Flybow can be successfully combined with RNAi approaches to gain insights into the mechanisms that control glial morphology in the visual system.

Chapter 7

Conclusions and future directions

7.1 Comprehending neural circuit structure constitutes a leap forward in understanding its function

As highly visual animals, a reiterated theme underlying our interactions within our habitat is the use of our sense of vision to assess the structure of unfamiliar organisms or engineered objects and predict their function capabilities. Consequently, it is easy for us to comprehend the notion that retrieval of detailed structural information from a system, which we aim to examine, represents the key first move on the chessboard of elucidating its functional aspects. Venturing into understanding such unknown biological systems, scientists over the centuries engineered ingenious methodologies to be able to study their structure. These were centered upon a main theme: enabling the human eye to analyze structures of ecosystems, organisms, internal organs cells and molecules. Using such visual representations of unknown systems, scientists could successfully combine information, hypothesize, test and finally uncover their individual functions. A recent triumph in technological innovation for biological sciences that exemplifies the aforementioned concept was the successful combination of serial block-face electron microscopy and two-photon calcium imaging to study the nervous system (Briggman et al., 2011). Using this approach, Briggman *et al*. have uncovered interesting features of a motion detection circuit within the mammalian retina. Their results showed that starburst amacrine cells wire asymmetrically with direction-selective ganglion cells, constituting an intuitive physical substrate to explain the computation of direction selectivity.

Importantly however, in stark contrast to other organ systems, the structure of the nervous system remains still poorly understood in the majority of model organisms and in humans (Lichtman and Denk, 2011). As discussed in Chapter 1, this can be attributed to its inherent complexity, which spans different anatomical scales (Sporns, 2011). This intricate structure is energetically very costly for the animal to maintain, indicating its crucial role in function. Thus, several substructures, microscopic and macroscopic, such as reiterated columns in the visual system of invertebrates or cortical folds in mammals have been developed to minimize its metabolic costs (Bullmore and Sporns, 2012). Importantly, in cases of neurodegeneration, the animal can fail to support these energy requirements, and structure deteriorates resulting in

erroneous functional outputs. Nonetheless, it is clear that neural circuits are not simply built using the most energy efficient means as that would likely mean that they could only communicate with their immediate synaptic partners as their next door neighbors. This would reduce the system's processing and functional adaptability capacities to much smaller scale ranges. Experimental data support the notion that the network architecture is built using a balanced wiring economy to volume exclusions ratio (Bullmore and Sporns, 2012; Rivera-Alba et al., 2011). Thus structural features at microstructure levels can be telling of network specializations that reflect function. Overall, it is important to remember that neurons are cells with axons that could extent the entire length of the animal and are thus often visible with the human eye. Nevertheless, their specialized arbors are many levels of magnitude smaller and predominantly require confocal light microscopy to be imaged. Finally, these cells communicate through synapses that can only be detected using electron microscopy preparations.

It thus remains a formidable task to create complete physical maps of connectivity in the nervous system, especially those of higher vertebrates. However, provided an initial map has been established that will include coarse ends, one can start by looking for obvious structural differences, which can be informative of function. In this manner for example, structural properties of visual systems differ greatly from those in place to perform executive tasks, such as memory recollection in regards to their respective structural distributions. This is consistent with their functional differences, since visual processing benefits from high levels of clustering information amongst neighboring cells in contrast to executive control, which requires large-scale information transfer (Bullmore and Sporns, 2012). With constant information flow from distinct neuroscience fields, these maps can be further refined and less obvious structural differences can be identified and used to hypothesize novel modes of circuit function. This clearly also requires incisive thinking and as H. D. Thoreau has stated, "*It is not what you look at that matters, it's what you see*". Thus, scientists are in addition expected to look beyond the obvious structural assets portrayed on pre-existing map descriptions. In my view, a fascinating recent example of this constitutes the ingenious findings from Su *et al*., which show that

neurons highly packed within a single sensillum in *Drosophila* influence each other via a synapse independent mechanism (Su et al., 2012). In this case a macroscopic structure constricts the space and provides the means, by which neighboring neurons that are not synaptically coupled can influence robustly each other via a direct electrical transmission signal.

Throughout this thesis, the reasoning that clarifying links between structure and function is key in biological studies has been repeatedly highlighted. In addition, the clear correlation between achieving leaps forward in understanding basic biology and the use of novel technology was discussed in detail. The work entailed in this thesis resulted in the successful generation of a new approach for studies in *Drosophila*, named Flybow. This tool allocates genetically tags on individual cells by randomized expression of four different fluorescent markers.

7.2 Multicolor cell labeling approaches augment information load within a given data set

Anatomical approaches to study neuron circuitry

Cell labeling approaches provide the means for constructing maps of cell content and have played a pivotal role in expanding our knowledge within the field of neurobiology. As previously discussed, strategies employed in the study of the nervous system can be divided into two main categories; namely anatomical and functional mapping approaches. This section focuses on the anatomical circuit mapping strategies and has the aim to position the multicolor "bow" approaches within this category. Many of the intricacies of the original Brainbow approach, such as advantages and limitations in its use, apply to the subsequently generated variants including Flybow.

Anatomical circuit mapping strategies aim to uncover entire neuron morphologies and their relative synapse distributions to ultimately reveal directly connected neurons. Thus, such experimental preparations can be assessed using light or electron microscopy, respectively (Dhawale and Bhalla, 2008). Altogether, these approaches make use of various labeling vectors such as intracellular injections of chemical reagents or application of diffusible/transportable

tracers, and expression of genetically encoded exogenous proteins under the control of endogenous regulatory elements. These can be visualized as scattered photons or electrons (Lichtman et al., 2008). Importantly, taking advantage of the blossoming array of molecular biology tools, labeling agents such as fluorescent proteins, can be placed under the control of desired genetic elements for expression. The latter innovation dramatically increased the speed of acquiring meaningful data by a) increasing reproducibility amongst samples, b) elevating the information content per sample, by for instance providing access to rare neuron subtypes, and crucially c) by lowering the requirements of manual skills proficiency (Luo et al., 2008). Linking genes to neuronal subtypes could concomitantly lead to distinct ways of circuit mapping. Forward mapping approaches set out to identify morphological profiles of different neurons within a gene expression domain. In contrast, backward mapping strategies aim to identify individual neuron morphologies and subsequently identify their gene expression profiles (Takemura et al., 2011).

A key difference between light and electron microscopy based mapping strategies lies within the extent of tissue labeling they rely on (Seung, 2009). Light microscopy depends on sparsely labeled samples for accurate reconstructions of neurons in contrast to densely labeled samples required for electron microscopy. Neurons lie densely packed within neuropils and thus resolving delicate structures such as overlapping dendritic arbors of neighboring cells labeled with the same marking agent becomes impossible using light microscopy. This can be attributed to the limits in spatial resolution of light microscopy that ranges between 50-100 nm and is determined by the wavelength range of visible light. Importantly for us, neurons in *Drosophila* are much smaller than their average vertebrate counterparts making analysis of overlapping structures an even more difficult task. Indicative is that the cell body of neurons in the fly visual system is on average 2-5 μm in diameter in comparison to a rodent pyramidal neuron that has a soma diameter of 10-30 μm (Tuthill, 2009). Despite these limitations, because of the larger field of view when compared with electron microscopy, the much faster processing times and the option of imaging from live tissue, the use of optical mapping tools remains central to a neurobiologist.

Cell labeling using single markers

Labeling of neuron subsets via directed use of a single marker within gene expression domains in sparsely labeled samples consisted a turning point in neurobiology practice the last two decades. Nevertheless, gene expression domains often involve a large number of neurons, which would simultaneously be labeled with the same marker. Even though such samples provide insights of the cell subgroup properties of neurons, for instance information about migration modes of GABAergic interneurons (Denaxa et al., 2012; Wonders and Anderson, 2006) they remain of limited use for single cell reconstructions. A clever way to limit the number of labeled cells in such paradigms is the use of intersectional approaches that would provide a second level of genetic control for positive cell marking. Such approaches make use of restricted expression of DNA recombinases to achieve intra- and inter- chromosomal recombination (Branda and Dymecki, 2004; Golic and Lindquist, 1989; Ito et al., 1997; Lee and Luo, 1999; Struhl and Basler, 1993; Wong et al., 2002; Zong et al., 2005). They can for example remove a DNA sequence placed as a "barrier" to prevent expression of the marker within the desired subpopulation. Thus controlled recombinase activation can remove this "barrier" for refined expression of transgenes containing the marker coding sequence. In this manner and specifically with the use of the MARCM approach, neurons in different parts of the fly nervous system have been successfully reconstructed (Jefferis et al., 2007; Morante and Desplan, 2008) Importantly, pre-existing atlases mainly were used as reference to identify neuron types within specific gene domains or uncover novel ones. Methodical analysis of the structure of these reconstructed neurons provided interesting insights into the mechanisms that govern circuit assembly in *Drosophila*. A fine paradigm comprises the understanding that a high level of hardwiring exists in the processes directing the innervation high olfactory centers by projection neuron arbors (Jefferis et al., 2007). In contrast, a different neuron class, the local interneurons in the antennal lobe, shows extensive morphological variability in the branching patterns of their dendritic arbors amongst different flies or even the two brain hemispheres of the same individual (Chou et al., 2010; Jenett et al., 2012). Thus, genetically identifiable subsets of cells that can be morphologically reconstructed provide the ground for understanding wiring

mechanisms and potential functions. These studies illustrate also how labor-intensive the task is to retrieve information for single neuron morphologies using these techniques; e.g. >1500 local interneurons assayed by Chou *et al.,* were required to draw these conclusions, and likely thus many more were dissected and prepared for imaging. In the *Drosophila* visual system, the transmedullary Tm5 neuron type has so far been described to present highly variable branching morphologies (K.-F Fischbach, 1989). Nevertheless, to date it is not clear which other neuron types in the visual system show morphological variability. Thus detailed analyses including information from more samples towards this direction would be extremely helpful to assemble more reference maps and uncover such underlying events.

Multicolor cell labeling

How could the high requirement of sample numbers be overcome? Conducting experiments, in which multiple markers are employed in parallel, was the apparent next step. Initially, it was achieved by combination of labeling agents and techniques in a single experiment. For example, a genetically encoded marker, such as GFP, together with immunohistochemistry using an antibody coupled with a fluorophore in a different part of the spectrum. However, the conception of the "rainbow" approaches would bring a fresh set of possibilities in this field. Originally introduced as DiOlistics, this approach delivered the uptake of beads covered with different combinations of lipophilic dyes presented to the tissue with a "gene gun" (Gan et al., 2000). This approach provided rapid multicolor labeling of tissue, thus achieving visualization of interacting cells. Importantly, this staining technique could be used for both light and electron microscopy. Nevertheless, its shortcomings included differential diffusion of dyes resulting in a heterogeneous color outcome and inefficient labeling of entire axon tracks as it is mostly applied *ex vivo*. Gero Miesenböck has stated that biology itself and not other scientific disciplines such as physics, chemistry or engineering offers the best-suited means for the study of biological systems (Miesenbock, 2004). A perspicacious thought that definitely suits the employment of molecular genetic tools in combination with fluorescent proteins for tissue labeling. Making use of the availability of spectrally distinct fluorescent protein members and

the availability of the Cre/*lox* system, Jean Livet together with Jeff W. Lichtman and Joshua R. Sanes transformed the "rainbow" logic to the Brainbow technology in the mouse nervous system (Livet et al., 2007). In this approach, DNA recombination is used to "shuffle" the coding sequences of fluorescent proteins within individual Brainbow transgenes. The additive result of marker expression creates a color identity that based on probabilities differs amongst neighboring cells. The two approach variants resulted in the randomized expression of up to four fluorescent proteins; following to Cre mediated DNA rearrangement by a) excision of cassettes between pairs of incompatible *lox* sequences or b) excisions or inversions of cassettes flanked by the repeated use of the same *lox* site. Cells within the expression domain of the *Thy1* gene were differentially labeled with up to 89 color shades. This was achieved by the combinatorial expression of distinct fluorescent proteins within a single cell. Using fluorescent dyes that are continuously expressed and specifically localized, axonal and dendritic arbors positioned distant to the cell body were homogeneously labeled. Consequently, reconstructions of entire cell morphology were performed more easily since unchanged color identity greatly assisted in tracking individual cell profiles through different tissue slices. It is important to mention that approaches using sparsely expressed single markers typically yield cell shape information for one cell per sample that can often be restricted to a certain part of the entire cell. Based on the neural circuit structure stereotypy, such information from a large number of samples is subsequently required and piecing it together results in entire cellular structure representations. However, using multicolor labeling, the structure of more than one cell can be resolved per experimental preparation. Considering the effort and cost required to generate a single sample using transgenic mouse lines, for example from a single brain, this constitutes a significant improvement for neural circuit analysis. Importantly, in Brainbow samples cells within the *thy1* expression domain were all positively labeled. Thus, Brainbow can overcome at least to a certain extent, the requirement for sparse labeling. Nevertheless there are limitations in the use of this elegant approach. The original lines labeled only a subpopulation of neural cells. Thus, these lines can only partially be used in connectome studies. Subsequently, the generation of the *R26R-Confetti* lines placed under the *CAGG* promoter could circumvent this drawback

and achieve ubiquitous labeling (Snippert et al., 2010). Importantly in this example, the use of a promoter element that is broadly expressed, labeled stochastically a large number of cells. The study investigated cellular homeostasis within a specific structural element of the gut, the intestinal crypt. Thus this offered a physical limit to the numerous cellular interactions under study that would need to be elucidated using a ubiquitous promoter. Moreover, the use of a transcriptional "barrier", similar to our *FB2.0* approach, offers additional control over tissue labeling. It is apparent, however, that the generation of new transgenic lines is required each time a specific gene expression domain is used for investigation of cell morphology. Therefore, this makes such experiments significantly time consuming and costly.

Notably, using Brainbow, neighboring neuron morphologies can be reconstructed with high accuracy. Nonetheless, overlap is only indicative of contact amongst pairs of neurons and conclusions can be drawn exclusively using electron microscopy. Combining Brainbow with the use of synaptic markers can to a certain extent overcome this limitation as such markers can reveal the structural trace of synapses. Nonetheless, even these approaches cannot prove that these synapses are active or provide information about their strength or properties. Finally, future application of super resolution microscopy together with advances in the accompanying technology for imaging and data analysis could further enforce the use of Brainbow in circuit studies. This requires the preparation of extremely thin tissue sections that are significantly thinner than optical sections, utilizing motorized stations for precise imaging and data stitching, and development of simple and user friendly software for data analysis (Lichtman et al., 2008).

Brainbow applications

Brainbow was introduced in 2007 and its application aspired to accelerate the pace, by which the connectome of mouse nervous system can be resolved. This has yet to be achieved, and untangling the wiring of the highly complex networks within mouse brain remains extremely challenging. Crucially, as discussed above this task requires tremendous human effort across various laboratories. Mapping is a painstaking process, and since its results are often appreciated years after the generation of initial wiring diagrams, scientists require correct

incentives for commitment on such undertakings. Thus, the best motivation is that they can directly link it to their tailored scientific interests. However, this requires an array of Brainbow lines that would label cells within numerous gene expression domains. The relatively long time required for an experiment using transgenic lines has been an additional limiting factor. The most accessible connectome within the mouse nervous system is the innervation of muscles by motor neurons. This model shows stereotypic connectivity and consists of a small number of cells. Thus, efforts in understanding its connectivity have been performed using single marker approaches in previous years. However, these attempts proved very labor intensive and demanded sophisticated imaging methodologies. Brainbow was used for the same task and proved to significantly accelerate the mapping process (Lichtman and Sanes, 2008). Importantly, making use of their discrete color characteristics motor neurons could be identified visualizing only their cell body location and their final axon destination at the skeletal muscle field. Thus, this example nicely illustrates the power of multicolor cell labeling in network studies. Nevertheless, this truly constitutes a simple connectome with a relatively small number of neurons labeled, which are easily discriminated by their color identity. In contrast, neuropils of the mouse cortex are densely packed and contain fine cellular processes that often are highly overlapping. In such tissues using high numbers of color hues is less advantageous. Color shades are the result of the additive expression of fluorescent proteins included in the Brainbow transgenes. Depending on the transgene copy number incorporated in the genome varying hues can be generated. In the scenario of mouse lines carrying 3 transgene copies of *Brainbow-2* up to 21 hues can be produced. Amongst them are for instance shades of purple, light purple and magenta that are relatively similar. When imaging big cellular structures such as the soma these can be separated in a straightforward manner, using reference spectra for automated color identity attribution. However, when imaging fine dendritic arbors this becomes more difficult. Moreover, it is obvious that this difficulty significantly increases with more copies inserted and hues becoming even more similar. Additionally, analysis is complicated when tracing over long distances due to inevitably occurring photobleaching. Distinct fluorescent proteins have inherently different photobleaching properties and perhaps even more importantly, the range of

bleaching differs significantly amongst samples. These factors must all be considered for data analysis, rendering it a highly time consuming task. Researchers now sometimes favor the use of fewer colors per experiment and new Brainbow lines carrying a single copy are currently available (personal communication, J. Sanes and T. Jessell). Nevertheless, Brainbow and Confetti approaches have been successfully used to study a variety of cell interactions in mice, for example linage tracing studies within the intestinal crypt(Snippert et al., 2010). More recently, a study aiming to understand the contribution of phenotypically equivalent cleavage stage blastomeres in generating the embryonic inner cell mass and the trophectoderm has employed Brainbow for cell labeling (Tabansky et al., 2012). The *Brainbow-1* transgene was placed under the control of the ubiquitous *CAGGS* promoter for expression in the entire animal. These new constructs were used for transgenesis of a new set of mouse lines named Rainbow. Amongst them the most useful for this study was the *Rainbow-2* transgenic line that yields up to 27 color shades. Importantly, in this study substantial cell mixing occurs throughout the different developmental stages, in contrast to previous studies in the gut and the regenerated digits of mice (Rinkevich et al., 2011; Snippert et al., 2010). Considering that the cells evaluated are sizable and can easily be assessed by light microscopy, the use of multiple shades to color-tag and trace their migration in the developing animal was a great advantage. Importantly, all these applications constitute another proof on how tools designed for studies in basic research can be of great use for advances in clinical research and practice. Acquired knowledge using "bow" approaches can be for example informative for neurological disorders now categorized as "connectopathies", regenerative medicine or help improve the outcome of patients undergoing fertility treatments (Tabansky et al., 2012). In conclusion, despite the existing drawbacks the multicolor "bow" technology offers an elegant solution to the laborious assembly of information, when studying cellular interactions in the nervous system and beyond.

Brainbow technology transferred to *Drosophila*

Brainbow was received in the scientific community with great enthusiasm and similar applications in simpler model organisms were anticipated to uncover conserved mechanisms

that govern wiring. These comparatively simpler systems, similar to the connectome of neuromuscular junction, could serve as "keys for locked doors" and bring solving vertebrate connectomes a step closer. In *Drosophila* two different "bow" systems have been generated synchronously. *Drosophila* Brainbow (dBrainbow) (Hampel et al., 2011) and Flybow (Hadjieconomou et al., 2011) were based on *Brainbow-1* and *Brainbow-2,* respectively. The two approaches share common features. Nevertheless, each displays distinct characteristics, thus creating a complementary genetic multicolor toolbox. They both make use of the binary Gal4/*UAS* system for transgene expression. Hence, they can be expressed in every genetically defined cell population of interest within the fly given the vast number of Gal4 driver lines shared within the community. However, they utilize different systems for intrachromosomal recombination. dBrainbow uses Cre to achieve the excision of cassettes flanked by incompatible *lox* sequences. Importantly, a modification of the original *Brainbow-1* transgene is the exchange of the first fluorescent protein with a sequence used as transcriptional barrier. Thus following recombination, tissues can be labeled with up to three different color outcomes. Flybow relies on the novel mFlp5 for recombination between identical *mFRT71* sites and the subsequent generation of different color outcomes. These include both excisions and inversions of two cassettes positioned in tandem. Each cassette contains a pair of fluorescent proteins placed in a face-to-face orientation and can lead to cell labeling with of up to four different colors. Moreover, *FB2.0* carries a stop cassette flanked by canonical *FRT* sites, thus, labeling can only occur following expression of Flp recombinase. *FB2.0* may directly serve as a tool for intersectional studies. If Flp is placed under the control of cell type specific regulatory elements, labeling will be restricted to cells exclusively within their respective expression domains; in parallel, mFlp5 expression will control the production of the different color outcomes. The use of the newly generated mFlp5/*mFRT71* approach clearly invigorated our approach, as it largely does not cross-react with the widely used canonical Flp/*FRT* recombination system. Consequently, Flybow can be combined with all the already available tools that are based on the use of original version of the Flp/*FRT* system. The same is true for dBrainbow, in which Cre is employed for recombination. Nevertheless, the use of mFlp5 overcomes the high toxicity

problems associated with the use of Cre recombinase in flies. Moreover, both approaches can offer temporal control over recombinase expression by taking advantage of inducible fly lines, in which the recombinase coding sequence is placed under the control of a heat-activated promoter. Importantly using *hs-Flp5*, this control is tightly regulated. Depending on the time of the exposure to high temperature, we could retrieve samples that include labeling of large neuroblast clones (early heat shock) or single cell clones (late heat shock). In contrast, due to high baseline activity observed using *hs-Cre* transgenic line, the vast majority of the clones retrieved are neuroblast clones. Another difference of the two approaches is that dBrainbow includes epitope tags for each of the fluorescent proteins it employs and was optimized for its use with antibody labeling. As a result samples can be imaged for both endogenous fluorescence as well as immunostaining. In contrast, Flybow includes a single epitope tag that was included to overcome the difficulties of imaging the Cerulean fluorescent protein. The use of antibodies to enhance weak fluorescent signals, especially in cases of weak Gal4 expression, can certainly be advantageous. Nevertheless, I believe that the presence of 10 *UAS* sites in the Flybow constructs together with appropriate tissue-handling protocols can in most cases avoid this need. The strong endogenous signals we could retrieve in our experiments from all the fluorescent markers, we used, with the exception of Cerulean, indicate that in most cases immunostaining is unnecessary. Consequently as aforementioned, to overcome this limitation in new Flybow transgenic variants generated in our laboratory, Cerulan-V5 has been replaced by mTurquoise that is a much brighter cyan variant (Goedhart et al., 2010). Using such strong endogenous expression can have certain advantages. First, multicolor labeling can be used in time-lapse live imaging experiments where cell interactions can be assayed in real time. Second, overcoming the requirement for enhancing the FP signal, immunolabeling can be reserved for neuropil markers that serve as positional landmarks invaluable for correct analysis. Third, images acquired do not suffer from unspecific background staining due to immunolabeling. The initial versions of both these approaches, as with every piece of technological advances have set the premise for new improved versions to be generated, with the hope that various scientists can make good use of them and eventually amend them to their specific needs.

Flybow applications

Flybow has now found applications in various ongoing projects in our laboratory and elsewhere. Initially, I used Flybow to reconstruct and identify different types of Netrin expressing neurons within the medulla neuropil. Working towards understanding the role of the Netrin/Frazzled guidance system within the visual system of *Drosophila,* R-cell behavior was assayed using Flybow during pupal development. Unexpectedly, this analysis led to the discovery that R8 growth cones extend filopodia at the right time-point to bridge the physical distance from the border of the medulla neuropil to their final target area. In this manner, they can possibly sense sufficient levels of Netrin and subsequently proceed to their second step of targeting (Timofeev et al., 2012) In continuation of this project, Nana Shimosako is currently mapping different Frazzled expressing target neurons. These could potentially employ the same guidance system for targeting within the medulla or the lobula complex. In this case, Flybow will be combined with both broad drivers that mark the entire *fra* expressing population, as well as the recently available *fra*-Gal4 lines (Pfeiffer et al., 2008) with refined expression patterns. These can be used together with tools for gene function studies; i.e. to analyze the effects of upregulation or knockdown of genes interacting with the Netrin/Frazzled guidance system in specific neuron subtypes of interest. In a different scenario, Emily Richardson, in our laboratory has employed Flybow in her study of developmental processes involved in circuit formation in the medulla. Using *islet* expressing medulla neurons as her model system, she focused on assaying remodeling of neuron structures predominantly as part of their axon targeting processes. Emily has used Flybow in both fixed tissue preparations as well as in live imaging set ups. Thus, in the latter experiments individual neuron behavior could be visualized in real-time with the added benefit of having neighboring neurons also positively labeled by the expression of a different fluorescent protein. However, perhaps the most elegant application that Flybow has found to date is its use in the project led by Benjamin Richier, aiming to uncover the morphologies of glia associated with the medulla neuropil. Benjamin has shown how Flybow can invigorate studies aspiring to understand the biology of uncharacterized groups of cells with limited

availability of genetic tools and with highly complex structures. Initially Benjamin used Flybow to map individual morphologies of medulla neuropil glia. Next, once subtypes could be identified, he moved on to combine Flybow with gene function tools to interfere with the canonical function of specific genes within this glia population. Using Flybow, Benjamin could employ broad drivers and uncover how removal of specific genes, encoding secreted and membrane-bound molecules, affects general aspects of glial cell morphogenesis that could affect the entire population or interfere with subtype-specific features.

Limitations and future improvements

The original variants of our approach generated in the course of this study present limitations in their use. The first limitation concerned the suboptimal fluorescence capacity of the cyan fluorescent protein Cerulean, which has now been overcome by its replacement with mTurquoise. Moreover, the sample numbers required for each Flybow experiment remained relatively high. A contributing factor to the latter was the use of the available *hs-mFlp5* transgenic lines that I have employed in these experiments. None of these were homozygous viable, thus half of the samples dissected would not have mFlp5 expressed and consequently would lack multiple color labeling. Nonetheless, in continuation of my work Nana Shimosako has now generated additional *hs-mFlp5* fly stocks; through re-injection the same transgene owing to random insertion, was placed into different genomic locations. These lines include homozygous viable insertions on the X, second and third chromosomes and an additional line that is homozygous lethal on the second, but has shown elevated levels of recombination efficiency (Shimosako et al., submitted). Therefore, these lines enrich our toolkit by making the existing genetic schemes more efficient due to the homozygous viable insertions and in addition open possibilities for additional genetic crosses with the new insertion on the X chromosome. Furthermore, the control over the size of clones, we achieve depends on the tailored heat exposure protocols applied in our experiments. A different level of control for both the temporal and spatial expression of mFlp5 can be provided using the confocal microscope as part of the experimental platform. Using the laser beam of the multiphoton laser, single cells could be

exposed to sufficient heat to activate expression of the *hs-mFlp5* transgene. Using dechorionated fly embryos, we have performed preliminary experiments in collaboration with Donald Bell. These show that such set-ups could be used for successful single cell heat-shocks.

Our results show that in studies where many color hues are desirable they could be obtained using genetic crosses of the currently available Flybow lines. Nevertheless, to make such experiments more efficient, an alterative way would be to generate new transgenes that contain additional copies of the original Flybow constructs positioned in tandem. This would potentially be easy to achieve, as the assembly of the original construct would need to be simply duplicated. Nonetheless, the recurring occurrence of unspecific bacterial recombination that was a significant drawback during this process could be a limiting factor in this undertaking. Thus, using synthesized DNA sequences covering the entire length of the repeated transgenes could be an alternative solution.

The modular nature of Flybow transgenes renders them accessible to amendments, as illustrated by the ease in switching the coding sequences of fluorescent protein variants included in the original versions with new improved ones. However, more substantial improvements could be attempted. Future constructs could for example include epitope tags for all fluorescent proteins thus complementing the Flybow array with a tool designed for use with weak Gal4 drivers. Moreover, the increasing availability of transgenic lines for the newly developed binary expression systems, Q and LexA allow more possibilities for their combined use with our approach. Notably, new Flybow variants could be also adapted to directly perform functional studies. These can be applied for studying neural circuit formation during development as well as manipulation of neural activity in networks under scrutiny. An example of such adaptation can additionally make use of the "2A peptide system", that delivers stoichiometric production of different protein products expressed from single open reading frame and has been successfully applied in *Drosophila* (Gonzalez et al., 2011). Thus, the 2A system can be employed to link the expression of one fluorescent protein to the expression of QF or LexA-VP16. This will allow the removal or ectopic activation of gene function in single neurons that will be identified by the expression of the designated fluorescent marker. Crucially, the consequences of gene function

alterations can be easily assessed when comparing the morphology of the manipulated neurons with their counterparts expressing the other three fluorescent proteins; especially when restricted Gal4 driver lines are employed. In addition, possible non-autonomous effects on neighbouring neurons that could influence connectivity can be easily observed. Another elegant example for future adaptation would be to link Flybow with available genetic tools for manipulating neural activity. For example, in the olfactory system we could make use of a Gal4 driver line active in a single glomerulus. Thus this driver in combination with Flybow would label the finite number of projection neurons included within this structure with different colors. New Flybow tools could be adapted to link expression of one fluorescent protein with a *Shibire^{ts1}* transgene, i.e. *mCherry-2A-Shibire^{ts1}* for specific silencing of the mCherry expressing neurons by an inducible block in vesicle recycling (Kitamoto, 2001). Similarly, we could make use of the temperature-sensitive cation channel dTrpA1 for elevation in neural activity. Thus, new transgenes with *cherry-2A-dTrpA1* could be generated. Making use of these Flybow variants to label the limited number of projection neurons with the aforementioned glomerulus specific driver we could examine effects following to silencing or activation of the "mCherry" neurons. This in combination with live imaging or simply by assaying connectivity at a later stage following the manipulation could be informative of the role of these neurons within this system. Similarly, we could imagine an experiment in the visual system with a driver that would be specific to a small subgroup of medulla neurons i.e. tangential neurons. Using these novel Flybow tools to label subsets of cells and in parallel to manipulate activity of individual cells within this subgroup; these could be used in combination with behavioral paradigms to provide information about color vision or motion detection processes. Finally, inspired by an elegant approach applied in *C. elegans* we could combine Flybow and Grasp approaches (Mishchenko, 2008). In our case split-GFP on the presynaptic site would be linked with the expression of one marker, i.e. sGFPPre-2A-mCherry. Similarly, the postsynaptically expressed split-GFP will be linked with a different fluorescent marker; e.g. sGFPPost-2A-mTurquoise. Thus expression of the membrane-tethered fluorescent proteins could mark the entire morphology and thus identify single neuron types and the reconstruction of GFP would reveal synaptic contacts amongst

neighboring neurons. This constitutes a nice example for a genetic approach that can allow simultaneous mapping together with gaining evidence about structural connectivity. In conclusion, many more possibilities exist to create novel useful Flybow adaptations and one could not get tired thinking about new variants tailored to specific scientific questions.

7.3 One step beyond constructing a wiring diagram

It is important to step back and ask as to whether Flybow combined with the aforementioned tools can resolve circuitry within the complex neural networks within the nervous system of *Drosophila*. The answer is certainly negative; nevertheless, it is clear that it can be utilized and greatly contributes towards the mad/necessary endeavor of generating several interrelated wiring maps. Currently, a neuroscientist can be paralleled with a car mechanic requested to understand how a sophisticated spaceship engine has been constructed and how it functions. Mapping of each individual neuron type and locating all its synaptic partners can theoretically provide a connectome and uncover how individual behaviors are propagated. Nevertheless, this is still not the entire picture of understanding how the nervous system functions. Anatomical wiring diagrams comprise a static image of the different versions of connectivity that can be extremely plastic within a given network. Indicative is that wiring maps cannot determine the response of single elements they include. It is thus critical to: 1) perform electrophysiological studies on single elements of a particular circuit using different experimental contexts and 2) reveal the composition of neurotransmitter and receptor expression of such single components. These can be altered by the context of behavior and internal status of the animal and thus differentially direct information flow. Furthermore, specific circuit elements can be electrically coupled via gap junctions. These might even link distinct circuits to each other, hidden in a connectome map, as has been recently described for the first elements in the color and motion processing circuits in *Drosophila* (Wardill et al., 2012). Additionally, the role of neuromodulation, mainly through G protein coupled receptors, has been shown to modify neuronal dynamics, synaptic efficiency and excitability ranges across model organisms (Bargmann, 2012). In summary, anatomical studies can provide information about subtypes of paired neurons and at the ultrastructural level can establish rules that govern synaptic coupling.

Functional studies using electrophysiological tools can confer information about the examined connectivity between individual neurons, but are limited by the context under which the experiment was conducted. Additionally, extrasynaptic inputs that can act at short or very long distances such as electrical coupling and neuromodulation play an important role in determining how the nervous system works. Thus, understanding precisely how the nervous system operates is a herculean labor, as new challenges come up when the current ones are tackled. Nonetheless science has always been based on herculean efforts by enthusiasts aiming defeat such *Lernea hydras*.

Abbasi, R., Abdou, Y., Abu-Zayyad, T., Ackermann, M., Adams, J., Aguilar, J.A., Ahlers, M., Allen, M.M., Altmann, D., Andeen, K., *et al*. (2012). Searches for Periodic Neutrino Emission from Binary Systems with 22 and 40 Strings of Icecube. Astrophys J *748*.

Adams, R.H., and Eichmann, A. (2010). Axon guidance molecules in vascular patterning. Cold Spring Harbor perspectives in biology *2*, a001875.

Agnati, L.F., Genedani, S., Leo, G., Rivera, A., Guidolin, D., and Fuxe, K. (2007). One century of progress in neuroscience founded on Golgi and Cajal's outstanding experimental and theoretical contributions. Brain research reviews *55*, 167-189.

Ai, H.W., Henderson, J.N., Remington, S.J., and Campbell, R.E. (2006). Directed evolution of a monomeric, bright and photostable version of Clavularia cyan fluorescent protein: structural characterization and applications in fluorescence imaging. Biochem J *400*, 531-540.

Ai, H.W., Olenych, S.G., Wong, P., Davidson, M.W., and Campbell, R.E. (2008). Hue-shifted monomeric variants of Clavularia cyan fluorescent protein: identification of the molecular determinants of color and applications in fluorescence imaging. BMC biology *6*, 13.

Anastassiadis, K., Glaser, S., Kranz, A., Berhardt, K., and Stewart, A.F. (2010). A practical summary of site-specific recombination, conditional mutagenesis, and tamoxifen induction of CreERT2. In Meth Enzymol, pp. 109-123.

Anderson, K.V., and Nusslein-Volhard, C. (1984). Information for the dorsal--ventral pattern of the Drosophila embryo is stored as maternal mRNA. Nature *311*, 223-227.

Andrews, G.L., Tanglao, S., Farmer, W.T., Morin, S., Brotman, S., Berberoglu, M.A., Price, H., Fernandez, G.C., Mastick, G.S., Charron, F., *et al*. (2008). Dscam guides embryonic axons by Netrin-dependent and -independent functions. Development *135*, 3839-3848.

Angelo, K., Rancz, E.A., Pimentel, D., Hundahl, C., Hannibal, J., Fleischmann, A., Pichler, B., and Margrie, T.W. (2012). A biophysical signature of network affiliation and sensory processing in mitral cells. Nature *488*, 375-378.

Astigarraga, S., Hofmeyer, K., and Treisman, J.E. (2010). Missed connections: photoreceptor axon seeks target neuron for synaptogenesis. Current opinion in genetics & development *20*, 400-407.

Baer, A., and Bode, J. (2001). Coping with kinetic and thermodynamic barriers: RMCE, an efficient strategy for the targeted integration of transgenes. Curr Opin Biotechnol *12*, 473-480.

Bargmann, C.I. (2012). Beyond the connectome: how neuromodulators shape neural circuits. BioEssays : news and reviews in molecular, cellular and developmental biology *34*, 458-465.

Bate, C.M. (1976a). Embryogenesis of an insect nervous system. I. A map of the thoracic and abdominal neuroblasts in Locusta migratoria. Journal of embryology and experimental morphology *35*, 107-123.

Bate, C.M. (1976b). Pioneer neurones in an insect embryo. Nature, 54-55.

Battye, R., Stevens, A., and Jacobs, J.R. (1999). Axon repulsion from the midline of the Drosophila CNS requires slit function. Development *126*, 2475-2481.

Bazigou, E., Apitz, H., Johansson, J., Loren, C.E., Hirst, E.M., Chen, P.L., Palmer, R.H., and Salecker, I. (2007). Anterograde Jelly belly and Alk receptor tyrosine kinase signaling mediates retinal axon targeting in Drosophila. Cell *128*, 961-975.

Bello, B., Resendez-Perez, D., and Gehring, W.J. (1998). Spatial and temporal targeting of gene expression in Drosophila by means of a tetracycline-dependent transactivator system. Development *125*, 2193-2202.

Bieschke, E.T., Wheeler, J.C., and Tower, J. (1998). Doxycycline-induced transgene expression during Drosophila development and aging. Molecular & general genetics : MGG *258*, 571-579.

Bischof, J., and Basler, K. (2008). Recombinases and their use in gene activation, gene inactivation, and transgenesis. Methods Mol Biol *420*, 175-195.

Bischof, J., Maeda, R.K., Hediger, M., Karch, F., and Basler, K. (2007). An optimized transgenesis system for Drosophila using germ-line-specific phiC31 integrases. In Proc Natl Acad Sci USA, pp. 3312-3317.

Borst, A. (2009). Drosophila's view on insect vision. Curr Biol *19*, R36-47.

Bossing, T., and Brand, A.H. (2002). Dephrin, a transmembrane ephrin with a unique structure, prevents interneuronal axons from exiting the Drosophila embryonic CNS. Development *129*, 4205-4218.

Boyle, M., Nighorn, A., and Thomas, J.B. (2006). Drosophila Eph receptor guides specific axon branches of mushroom body neurons. Development *133*, 1845-1854.

Brand, A.H., and Dormand, E.L. (1995). The GAL4 system as a tool for unravelling the mysteries of the Drosophila nervous system. Curr Opin Neurobiol *5*, 572-578.

Brand, A.H., and Livesey, F.J. (2011). Neural stem cell biology in vertebrates and invertebrates: more alike than different? Neuron *70*, 719-729.

Brand AH, P.N. (1993). Targeted gene expression as a means of altering cell fates and generating dominant phenotypes. Development 401-415.

Branda, C.S., and Dymecki, S.M. (2004). Talking about a revolution: The impact of site-specific recombinases on genetic analyses in mice. In Developmental Cell, pp. 7-28.

Brankatschk, M., and Dickson, B.J. (2006). Netrins guide Drosophila commissural axons at short range. Nat Neurosci *9*, 188-194.

Brenner, S. (1974). The genetics of Caenorhabditis elegans. Genetics *77*, 71-94.

Brewster, R., and Bodmer, R. (1995). Origin and specification of type II sensory neurons in Drosophila. Development *121*, 2923-2936.

Brierley, D.J., Blanc, E., Reddy, O.V., Vijayraghavan, K., and Williams, D.W. (2009). Dendritic targeting in the leg neuropil of Drosophila: the role of midline signalling molecules in generating a myotopic map. PLoS biology *7*, e1000199.

Briggman, K.L., Helmstaedter, M., and Denk, W. (2011). Wiring specificity in the direction-selectivity circuit of the retina. Nature *471*, 183-188.

Brose, K., Bland, K.S., Wang, K.H., Arnott, D., Henzel, W., Goodman, C.S., Tessier-Lavigne, M., and Kidd, T. (1999). Slit proteins bind Robo receptors and have an evolutionarily conserved role in repulsive axon guidance. Cell *96*, 795-806.

Buchholz, F., Ringrose, L., Angrand, P.O., Rossi, F., and Stewart, A.F. (1996). Different thermostabilities of FLP and Cre recombinases: implications for applied site-specific recombination. Nucleic Acids Res *24*, 4256-4262.

Bullmore, E., and Sporns, O. (2012). The economy of brain network organization. Nature reviews Neuroscience *13*, 336-349.

Burmeister, M., Novak, J., Liang, M.Y., Basu, S., Ploder, L., Hawes, N.L., Vidgen, D., Hoover, F., Goldman, D., Kalnins, V.I., *et al*. (1996). Ocular retardation mouse caused by Chx10 homeobox null allele: impaired retinal progenitor proliferation and bipolar cell differentiation. Nature genetics *12*, 376-384.

Bushong, E.A., Martone, M.E., Jones, Y.Z., and Ellisman, M.H. (2002). Protoplasmic astrocytes in CA1 stratum radiatum occupy separate anatomical domains. The Journal of neuroscience : the official journal of the Society for Neuroscience *22*, 183-192.

Cachero, S., and Jefferis, G.S. (2011). Double brainbow. Nat Methods *8*, 217-218.

Cajal, S.R.a.S., D. (1915). Contribucion al conocimiento de los centros nerviosos del los insectos. Lab Invest Biol *13*, 1-167.

Canty, A.J., and Murphy, M. (2008). Molecular mechanisms of axon guidance in the developing corticospinal tract. Progress in neurobiology *85*, 214-235.

Chalfie, M., Tu, Y., Euskirchen, G., Ward, W.W., and Prasher, D.C. (1994). Green fluorescent protein as a marker for gene expression. Science *263*, 802-805.

Chan, S.S., Zheng, H., Su, M.W., Wilk, R., Killeen, M.T., Hedgecock, E.M., and Culotti, J.G. (1996). UNC-40, a C. elegans homolog of DCC (Deleted in Colorectal Cancer), is required in motile cells responding to UNC-6 netrin cues. Cell *87*, 187-195.

Chao, D.L., Ma, L., and Shen, K. (2009). Transient cell-cell interactions in neural circuit formation. Nature reviews Neuroscience *10*, 262-271.

Chisholm, A., and Tessier-Lavigne, M. (1999). Conservation and divergence of axon guidance mechanisms. Curr Opin Neurobiol *9*, 603-615.

Chotard, C., Leung, W., and Salecker, I. (2005). glial cells missing and gcm2 cell autonomously regulate both glial and neuronal development in the visual system of Drosophila. Neuron *48*, 237-251.

Chotard, C., and Salecker, I. (2004). Neurons and glia: team players in axon guidance. Trends Neurosci *27*, 655-661.

Chotard, C., and Salecker, I. (2007). Glial cell development and function in the Drosophila visual system. Neuron Glia Biol *3*, 17-25.

Chotard, C., and Salecker, I. (2009). Screening for potential regulators of glial development in the Drosophila visual system. J Neurogenet *23*, S25-S25.

Chou, Y.H., Spletter, M.L., Yaksi, E., Leong, J.C., Wilson, R.I., and Luo, L. (2010). Diversity and wiring variability of olfactory local interneurons in the Drosophila antennal lobe. Nat Neurosci *13*, 439-449.

Chudakov, D.M., Matz, M.V., Lukyanov, S., and Lukyanov, K.A. (2010). Fluorescent proteins and their applications in imaging living cells and tissues. Physiol Rev *90*, 1103-1163.

Clandinin, T.R., and Feldheim, D.A. (2009). Making a visual map: mechanisms and molecules. Curr Opin Neurobiol *19*, 174-180.

Clandinin, T.R., and Zipursky, S.L. (2002). Making connections in the fly visual system. Neuron *35*, 827-841.

Coates, C.J., Kaminski, J.M., Summers, J.B., Segal, D.J., Miller, A.D., and Kolb, A.F. (2005). Site-directed genome modification: derivatives of DNA-modifying enzymes as targeting tools. In Trends Biotechnol, pp. 407-419.

Colon-Ramos, D.A. (2009). Synapse formation in developing neural circuits. Current topics in developmental biology *87*, 53-79.

Colon-Ramos, D.A., Margeta, M.A., and Shen, K. (2007). Glia promote local synaptogenesis through UNC-6 (netrin) signaling in C. elegans. Science *318*, 103-106.

Dacey, D.M., and Packer, O.S. (2003). Colour coding in the primate retina: diverse cell types and cone-specific circuitry. Curr Opin Neurobiol *13*, 421-427.

Datta, S.R., Vasconcelos, M.L., Ruta, V., Luo, S., Wong, A., Demir, E., Flores, J., Balonze, K., Dickson, B.J., and Axel, R. (2008). The Drosophila pheromone cVA activates a sexually dimorphic neural circuit. Nature *452*, 473-477.

Davidson, E.H., and Levine, M.S. (2008). Properties of developmental gene regulatory networks. Proc Natl Acad Sci U S A *105*, 20063-20066.

De Carlos, J.A., and Borrell, J. (2007). A historical reflection of the contributions of Cajal and Golgi to the foundations of neuroscience. Brain research reviews *55*, 8-16.

de Castro, F., Lopez-Mascaraque, L., and De Carlos, J.A. (2007). Cajal: lessons on brain development. Brain research reviews *55*, 481-489.

Dearborn, R., Jr., He, Q., Kunes, S., and Dai, Y. (2002). Eph receptor tyrosine kinase-mediated formation of a topographic map in the Drosophila visual system. The Journal of neuroscience : the official journal of the Society for Neuroscience *22*, 1338-1349.

DeFelipe, J. (2010). From the connectome to the synaptome: an epic love story. Science *330*, 1198-1201.

Denaxa, M., Kalaitzidou, M., Garefalaki, A., Achimastou, A., Lasrado, R., Maes, T., and Pachnis, V. (2012). Maturation-Promoting Activity of SATB1 in MGE-Derived Cortical Interneurons. Cell reports *2*, 1351-1362.

Denk, W., Briggman, K.L., and Helmstaedter, M. (2012). Structural neurobiology: missing link to a mechanistic understanding of neural computation. Nature reviews Neuroscience *13*, 351-358.

Denk, W., and Horstmann, H. (2004). Serial block-face scanning electron microscopy to reconstruct three-dimensional tissue nanostructure. PLoS biology *2*, e329.

Dent, E.W., and Gertler, F.B. (2003). Cytoskeletal dynamics and transport in growth cone motility and axon guidance. Neuron *40*, 209-227.

Dent, E.W., Gupton, S.L., and Gertler, F.B. (2011). The growth cone cytoskeleton in axon outgrowth and guidance. Cold Spring Harbor perspectives in biology *3*.

Dhawale, A., and Bhalla, U.S. (2008). The network and the synapse: 100 years after Cajal. HFSP journal *2*, 12-16.

Dickson, B.J. (2002). Molecular mechanisms of axon guidance. Science *298*, 1959-1964.

Dietzl, G., Chen, D., Schnorrer, F., Su, K., Barinova, Y., Fellner, M., Gasser, B., Kinsey, K., Oppel, S., Scheiblauer, S., *et al*. (2007). A genome-wide transgenic RNAi library for conditional gene inactivation in Drosophila. In Nature, pp. 151-156.

Douglas, R.J., and Martin, K.A. (2007). The butterfly and the loom. Brain research reviews *55*, 314-328.

Drobizhev, M., Makarov, N.S., Tillo, S.E., Hughes, T.E., and Rebane, A. Two-photon absorption properties of fluorescent proteins. Nat Methods *8*, 393-399.

Edwards, T.N., and Meinertzhagen, I.A. (2010). The functional organisation of glia in the adult brain of Drosophila and other insects. Progress in neurobiology *90*, 471-497.

Egger, B., Boone, J.Q., Stevens, N.R., Brand, A.H., and Doe, C.Q. (2007). Regulation of spindle orientation and neural stem cell fate in the Drosophila optic lobe. Neural development *2*, 1.

Egger, B., Chell, J.M., and Brand, A.H. (2008). Insights into neural stem cell biology from flies. Philosophical transactions of the Royal Society of London Series B, Biological sciences *363*, 39-56.

Ekstrand, M.I., Enquist, L.W., and Pomeranz, L.E. (2008). The alpha-herpesviruses: molecular pathfinders in nervous system circuits. Trends in molecular medicine *14*, 134-140.

Elliott, D.A., and Brand, A.H. (2008). The GAL4 system : a versatile system for the expression of genes. Methods Mol Biol *420*, 79-95.

Englund, C., Steneberg, P., Falileeva, L., Xylourgidis, N., and Samakovlis, C. (2002). Attractive and repulsive functions of Slit are mediated by different receptors in the Drosophila trachea. Development *129*, 4941-4951.

Erclik, T., Hartenstein, V., Lipshitz, H.D., and McInnes, R.R. (2008). Conserved role of the Vsx genes supports a monophyletic origin for bilaterian visual systems. Curr Biol *18*, 1278-1287.

Erickson, L. Ortho's All About Wiring Basics (Meredith Books).

Evans, C.J., Olson, J.M., Ngo, K.T., Kim, E., Lee, N.E., Kuoy, E., Patananan, A.N., Sitz, D., Tran, P., Do, M.T.*, et al*. (2009). G-TRACE: rapid Gal4-based cell lineage analysis in Drosophila. Nat Methods *6*, 603-605.

Fan, Y., Soller, M., Flister, S., Hollmann, M., Muller, M., Bello, B., Egger, B., White, K., Schafer, M.A., and Reichert, H. (2005). The egghead gene is required for compartmentalization in Drosophila optic lobe development. Dev Biol *287*, 61-73.

Farazi, T.A., Waksman, G., and Gordon, J.I. (2001). The biology and enzymology of protein N-myristoylation. The Journal of biological chemistry *276*, 39501-39504.

Fazeli, A., Dickinson, S.L., Hermiston, M.L., Tighe, R.V., Steen, R.G., Small, C.G., Stoeckli, E.T., Keino-Masu, K., Masu, M., Rayburn, H.*, et al*. (1997). Phenotype of mice lacking functional Deleted in colorectal cancer (Dcc) gene. Nature *386*, 796-804.

Feinberg, E.H., Vanhoven, M.K., Bendesky, A., Wang, G., Fetter, R.D., Shen, K., and Bargmann, C.I. (2008). GFP Reconstitution Across Synaptic Partners (GRASP) defines cell contacts and synapses in living nervous systems. Neuron *57*, 353-363.

Ferda Percin, E., Ploder, L.A., Yu, J.J., Arici, K., Horsford, D.J., Rutherford, A., Bapat, B., Cox, D.W., Duncan, A.M., Kalnins, V.I., *et al*. (2000). Human microphthalmia associated with mutations in the retinal homeobox gene CHX10. Nature genetics *25*, 397-401.

Fischer, J.A., Giniger, E., Maniatis, T., and Ptashne, M. (1988). GAL4 activates transcription in Drosophila. Nature *332*, 853-856.

Freeman, M.R., and Doherty, J. (2006). Glial cell biology in Drosophila and vertebrates. Trends Neurosci *29*, 82-90.

Gan, W.B., Grutzendler, J., Wong, W.T., Wong, R.O., and Lichtman, J.W. (2000). Multicolor "DiOlistic" labeling of the nervous system using lipophilic dye combinations. Neuron *27*, 219-225.

Gao, S., Takemura, S.Y., Ting, C.Y., Huang, S., Lu, Z., Luan, H., Rister, J., Thum, A.S., Yang, M., Hong, S.T., *et al*. (2008). The neural substrate of spectral preference in Drosophila. Neuron *60*, 328-342.

Geisbrecht, B.V., Dowd, K.A., Barfield, R.W., Longo, P.A., and Leahy, D.J. (2003). Netrin binds discrete subdomains of DCC and UNC5 and mediates interactions between DCC and heparin. The Journal of biological chemistry *278*, 32561-32568.

Georgiou, M., and Tear, G. (2002). Commissureless is required both in commissural neurones and midline cells for axon guidance across the midline. Development *129*, 2947-2956.

Georgiou, M., and Tear, G. (2003). The N-terminal and transmembrane domains of Commissureless are necessary for its function and trafficking within neurons. Mechanisms of development *120*, 1009-1019.

Godenschwege, T.A., Simpson, J.H., Shan, X., Bashaw, G.J., Goodman, C.S., and Murphey, R.K. (2002). Ectopic expression in the giant fiber system of Drosophila reveals distinct roles for roundabout (Robo), Robo2, and Robo3 in dendritic guidance and synaptic connectivity. The Journal of neuroscience : the official journal of the Society for Neuroscience *22*, 3117-3129.

Goedhart, J., van Weeren, L., Hink, M.A., Vischer, N.O., Jalink, K., and Gadella, T.W., Jr. (2010). Bright cyan fluorescent protein variants identified by fluorescence lifetime screening. Nat Methods *7*, 137-139.

Goedhart, J., von Stetten, D., Noirclerc-Savoye, M., Lelimousin, M., Joosen, L., Hink, M.A., van Weeren, L., Gadella, T.W., Jr., and Royant, A. (2012). Structure-guided evolution of cyan fluorescent proteins towards a quantum yield of 93%. Nature communications *3*, 751.

Golic, K.G., and Lindquist, S. (1989). The FLP recombinase of yeast catalyzes site-specific recombination in the Drosophila genome. Cell *59*, 499-509.

Gonzalez, M., Martin-Ruiz, I., Jimenez, S., Pirone, L., Barrio, R., and Sutherland, J.D. (2011). Generation of stable Drosophila cell lines using multicistronic vectors. Scientific reports *1*, 75.

Gordon, M.D., and Scott, K. (2009). Motor control in a Drosophila taste circuit. Neuron *61*, 373-384.

Green, P., Hartenstein, A.Y., and Hartenstein, V. (1993). The embryonic development of the Drosophila visual system. Cell and tissue research *273*, 583-598.

Griesbeck, O., Baird, G.S., Campbell, R.E., Zacharias, D.A., and Tsien, R.Y. (2001). Reducing the environmental sensitivity of yellow fluorescent protein. Mechanism and applications. The Journal of biological chemistry *276*, 29188-29194.

Groth, A.C., Fish, M., Nusse, R., and Calos, M.P. (2004). Construction of transgenic Drosophila by using the site-specific integrase from phage phiC31. In Genetics, pp. 1775-1782.

Guillemot, F. (2007). Spatial and temporal specification of neural fates by transcription factor codes. Development *134*, 3771-3780.

Gupta, V., and Poss, K.D. (2012). Clonally dominant cardiomyocytes direct heart morphogenesis. Nature *484*, 479-484.

Hadjieconomou, D., Rotkopf, S., Alexandre, C., Bell, D.M., Dickson, B.J., and Salecker, I. (2010). Flybow: genetic multicolor cell labeling for neural circuit analysis in Drosophila melanogaster. Nat Methods *8*, 260-266.

Hadjieconomou, D., Timofeev, K., and Salecker, I. (2011). A step-by-step guide to visual circuit assembly in Drosophila. Curr Opin Neurobiol *21*, 76-84.

Hakeda-Suzuki, S., Berger-Muller, S., Tomasi, T., Usui, T., Horiuchi, S.Y., Uemura, T., and Suzuki, T. (2011). Golden Goal collaborates with Flamingo in conferring synaptic-layer specificity in the visual system. Nat Neurosci *14*, 314-323.

Hall, D.H., and Russell, R.L. (1991). The posterior nervous system of the nematode Caenorhabditis elegans: serial reconstruction of identified neurons and complete pattern of synaptic interactions. The Journal of neuroscience : the official journal of the Society for Neuroscience *11*, 1-22.

Hampel, S., Chung, P., McKellar, C.E., Hall, D., Looger, L.L., and Simpson, J.H. (2010). Drosophila Brainbow: a recombinase-based fluorescence labeling technique to subdivide neural expression patterns. Nat Methods *8*, 253-259.

Han, D.D., Stein, D., and Stevens, L.M. (2000). Investigating the function of follicular subpopulations during Drosophila oogenesis through hormone-dependent enhancer-targeted cell ablation. Development *127*, 573-583.

Harris, R., Sabatelli, L.M., and Seeger, M.A. (1996). Guidance cues at the Drosophila CNS midline: identification and characterization of two Drosophila Netrin/UNC-6 homologs. Neuron *17*, 217-228.

Hartenstein, V. (2011). Morphological diversity and development of glia in Drosophila. Glia *59*, 1237-1252.

Hasegawa, E., Kitada, Y., Kaido, M., Takayama, R., Awasaki, T., Tabata, T., and Sato, M. (2011). Concentric zones, cell migration and neuronal circuits in the Drosophila visual center. Development *138*, 983-993.

Hayashi, S., Ito, K., Sado, Y., Taniguchi, M., Akimoto, A., Takeuchi, H., Aigaki, T., Matsuzaki, F., Nakagoshi, H., Tanimura, T., *et al*. (2002). GETDB, a database compiling expression patterns and molecular locations of a collection of Gal4 enhancer traps. Genesis *34*, 58-61.

Hedgecock, E.M., Culotti, J.G., and Hall, D.H. (1990). The unc-5, unc-6, and unc-40 genes guide circumferential migrations of pioneer axons and mesodermal cells on the epidermis in C. elegans. Neuron *4*, 61-85.

Heidmann, D., and Lehner, C.F. (2001). Reduction of Cre recombinase toxicity in proliferating Drosophila cells by estrogen-dependent activity regulation. Development genes and evolution *211*, 458-465.

Hidalgo, A., and Brand, A.H. (1997). Targeted neuronal ablation: the role of pioneer neurons in guidance and fasciculation in the CNS of Drosophila. Development *124*, 3253-3262.

Hiesinger, P.R., Zhai, R.G., Zhou, Y., Koh, T.W., Mehta, S.Q., Schulze, K.L., Cao, Y., Verstreken, P., Clandinin, T.R., Fischbach, K.F., *et al*. (2006). Activity-independent prespecification of synaptic partners in the visual map of Drosophila. Curr Biol *16*, 1835-1843.

Hiramoto, M., Hiromi, Y., Giniger, E., and Hotta, Y. (2000). The Drosophila Netrin receptor Frazzled guides axons by controlling Netrin distribution. Nature *406*, 886-889.

Hong, K., Hinck, L., Nishiyama, M., Poo, M.M., Tessier-Lavigne, M., and Stein, E. (1999). A ligand-gated association between cytoplasmic domains of UNC5 and DCC family receptors converts netrin-induced growth cone attraction to repulsion. Cell *97*, 927-941.

Huang, Z., and Kunes, S. (1996). Hedgehog, transmitted along retinal axons, triggers neurogenesis in the developing visual centers of the Drosophila brain. Cell *86*, 411-422.

Huang, Z., and Kunes, S. (1998). Signals transmitted along retinal axons in Drosophila: Hedgehog signal reception and the cell circuitry of lamina cartridge assembly. Development *125*, 3753-3764.

Huber, A.B., Kolodkin, A.L., Ginty, D.D., and Cloutier, J.F. (2003). Signaling at the growth cone: ligand-receptor complexes and the control of axon growth and guidance. Annual review of neuroscience *26*, 509-563.

Huberman, A.D., Clandinin, T.R., and Baier, H. (2010). Molecular and cellular mechanisms of lamina-specific axon targeting. Cold Spring Harbor perspectives in biology *2*, a001743.

Ishii, N., Wadsworth, W.G., Stern, B.D., Culotti, J.G., and Hedgecock, E.M. (1992). UNC-6, a laminin-related protein, guides cell and pioneer axon migrations in C. elegans. Neuron *9*, 873-881.

Ito, K., Okada, R., Tanaka, N.K., and Awasaki, T. (2003). Cautionary observations on preparing and interpreting brain images using molecular biology-based staining techniques. Microscopy research and technique *62*, 170-186.

Ito, K., Sass, H., Urban, J., Hofbauer, A., and Schneuwly, S. (1997). GAL4-responsive UAS-tau as a tool for studying the anatomy and development of the Drosophila central nervous system. Cell and tissue research *290*, 1-10.

Jefferis, G.S., Marin, E.C., Stocker, R.F., and Luo, L. (2001). Target neuron prespecification in the olfactory map of Drosophila. Nature *414*, 204-208.

Jefferis, G.S., Potter, C.J., Chan, A.M., Marin, E.C., Rohlfing, T., Maurer, C.R., Jr., and Luo, L. (2007). Comprehensive maps of Drosophila higher olfactory centers: spatially segregated fruit and pheromone representation. Cell *128*, 1187-1203.

Jenett, A., Rubin, G.M., Ngo, T.T., Shepherd, D., Murphy, C., Dionne, H., Pfeiffer, B.D., Cavallaro, A., Hall, D., Jeter, J., *et al*. (2012). A GAL4-Driver Line Resource for Drosophila Neurobiology. Cell reports *2*, 991-1001.

Jessell, T.M. (2000). Neuronal specification in the spinal cord: inductive signals and transcriptional codes. Nature reviews Genetics *1*, 20-29.

Jhaveri, D., Saharan, S., Sen, A., and Rodrigues, V. (2004). Positioning sensory terminals in the olfactory lobe of Drosophila by Robo signaling. Development *131*, 1903-1912.

Jin, P., Zarnescu, D.C., Zhang, F.P., Pearson, C.E., Lucchesi, J.C., Moses, K., and Warren, S.T. (2003). RNA-mediated neurodegeneration caused by the fragile X premutation rCGG repeats in Drosophila. Neuron *39*, 739-747.

K.-F Fischbach, A.P.M. Dittrich (1989). The optic lobe of Drosophila melanogaster. I. A Golgi analysis of wild-type structure. Cell Tissue and Research, 441-475.

Kaiser, M. (2011). A tutorial in connectome analysis: topological and spatial features of brain networks. NeuroImage *57*, 892-907.

Keino-Masu, K., Masu, M., Hinck, L., Leonardo, E.D., Chan, S.S., Culotti, J.G., and Tessier-Lavigne, M. (1996). Deleted in Colorectal Cancer (DCC) encodes a netrin receptor. Cell *87*, 175-185.

Keleman, K., and Dickson, B.J. (2001). Short- and long-range repulsion by the Drosophila Unc5 netrin receptor. Neuron *32*, 605-617.

Keleman, K., Rajagopalan, S., Cleppien, D., Teis, D., Paiha, K., Huber, L.A., Technau, G.M., and Dickson, B.J. (2002). Comm sorts robo to control axon guidance at the Drosophila midline. Cell *110*, 415-427.

Keleman, K., Ribeiro, C., and Dickson, B.J. (2005). Comm function in commissural axon guidance: cell-autonomous sorting of Robo in vivo. Nat Neurosci *8*, 156-163.

Kennedy, T.E., Serafini, T., de la Torre, J.R., and Tessier-Lavigne, M. (1994). Netrins are diffusible chemotropic factors for commissural axons in the embryonic spinal cord. Cell *78*, 425-435.

Kidd, T., Bland, K.S., and Goodman, C.S. (1999). Slit is the midline repellent for the robo receptor in Drosophila. Cell *96*, 785-794.

Kidd, T., Brose, K., Mitchell, K.J., Fetter, R.D., Tessier-Lavigne, M., Goodman, C.S., and Tear, G. (1998). Roundabout controls axon crossing of the CNS midline and defines a novel subfamily of evolutionarily conserved guidance receptors. Cell *92*, 205-215.

Killeen, M.T., and Sybingco, S.S. (2008). Netrin, Slit and Wnt receptors allow axons to choose the axis of migration. Dev Biol *323*, 143-151.

Kim, S., and Chiba, A. (2004). Dendritic guidance. Trends Neurosci *27*, 194-202.

Kitamoto, T. (2001). Conditional modification of behavior in Drosophila by targeted expression of a temperature-sensitive shibire allele in defined neurons. Journal of neurobiology *47*, 81-92.

Klein, R. (2012). Eph/ephrin signalling during development. Development *139*, 4105-4109.

Kleinfeld, D., Bharioke, A., Blinder, P., Bock, D.D., Briggman, K.L., Chklovskii, D.B., Denk, W., Helmstaedter, M., Kaufhold, J.P., Lee, W.C., *et al*. (2011). Large-scale automated histology in the pursuit of connectomes. The Journal of neuroscience : the official journal of the Society for Neuroscience *31*, 16125-16138.

Kohl, J., and Jefferis, G.S. (2011). Neuroanatomy: decoding the fly brain. Curr Biol *21*, R19-20.

Kolodziej, P.A., Timpe, L.C., Mitchell, K.J., Fried, S.R., Goodman, C.S., Jan, L.Y., and Jan, Y.N. (1996). frazzled encodes a Drosophila member of the DCC immunoglobulin subfamily and is required for CNS and motor axon guidance. Cell *87*, 197-204.

Kramer, S.G., Kidd, T., Simpson, J.H., and Goodman, C.S. (2001). Switching repulsion to attraction: changing responses to slit during transition in mesoderm migration. Science *292*, 737-740.

Kraut, R., and Zinn, K. (2004). Roundabout 2 regulates migration of sensory neurons by signaling in trans. Curr Biol *14*, 1319-1329.

Kruger, R.P., Lee, J., Li, W., and Guan, K.L. (2004). Mapping netrin receptor binding reveals domains of Unc5 regulating its tyrosine phosphorylation. The Journal of neuroscience : the official journal of the Society for Neuroscience *24*, 10826-10834.

Lai, S.L., and Lee, T. (2006). Genetic mosaic with dual binary transcriptional systems in Drosophila. Nat Neurosci *9*, 703-709.

Lai Wing Sun, K., Correia, J.P., and Kennedy, T.E. (2011). Netrins: versatile extracellular cues with diverse functions. Development *138*, 2153-2169.

Landgraf, M., Sanchez-Soriano, N., Technau, G.M., Urban, J., and Prokop, A. (2003). Charting the Drosophila neuropile: a strategy for the standardised characterisation of genetically amenable neurites. Dev Biol *260*, 207-225.

Lee, C.H., Herman, T., Clandinin, T.R., Lee, R., and Zipursky, S.L. (2001). N-cadherin regulates target specificity in the Drosophila visual system. Neuron *30*, 437-450.

Lee, T., and Luo, L. (1999). Mosaic analysis with a repressible cell marker for studies of gene function in neuronal morphogenesis. Neuron *22*, 451-461.

Lelimousin, M., Noirclerc-Savoye, M., Lazareno-Saez, C., Paetzold, B., Le Vot, S., Chazal, R., Macheboeuf, P., Field, M.J., Bourgeois, D., and Royant, A. (2009). Intrinsic dynamics in ECFP and Cerulean control fluorescence quantum yield. Biochemistry *48*, 10038-10046.

Leonardo, E.D., Hinck, L., Masu, M., Keino-Masu, K., Ackerman, S.L., and Tessier-Lavigne, M. (1997). Vertebrate homologues of C. elegans UNC-5 are candidate netrin receptors. Nature *386*, 833-838.

Leung-Hagesteijn, C., Spence, A.M., Stern, B.D., Zhou, Y., Su, M.W., Hedgecock, E.M., and Culotti, J.G. (1992). UNC-5, a transmembrane protein with immunoglobulin and thrombospondin type 1 domains, guides cell and pioneer axon migrations in C. elegans. Cell *71*, 289-299.

Li, E., and Davidson, E.H. (2009). Building developmental gene regulatory networks. Birth defects research Part C, Embryo today : reviews *87*, 123-130.

Liaw, C.W., Zamoyska, R., and Parnes, J.R. (1986). Structure, sequence, and polymorphism of the Lyt-2 T cell differentiation antigen gene. J Immunol *137*, 1037-1043.

Lichtman, J.W., and Denk, W. (2011). The big and the small: challenges of imaging the brain's circuits. Science *334*, 618-623.

Lichtman, J.W., Livet, J., and Sanes, J.R. (2008). A technicolour approach to the connectome. Nature reviews Neuroscience *9*, 417-422.

Lichtman, J.W., and Sanes, J.R. (2008). Ome sweet ome: what can the genome tell us about the connectome? Curr Opin Neurobiol *18*, 346-353.

Lichtman, J.W., and Smith, S.J. (2008). Seeing circuits assemble. Neuron *60*, 441-448.

Lim, Y.S., and Wadsworth, W.G. (2002). Identification of domains of netrin UNC-6 that mediate attractive and repulsive guidance and responses from cells and growth cones. The Journal of neuroscience : the official journal of the Society for Neuroscience *22*, 7080-7087.

Lin, D.M., and Goodman, C.S. (1994). Ectopic and increased expression of Fasciclin II alters motoneuron growth cone guidance. Neuron *13*, 507-523.

Liu, G., Li, W., Wang, L., Kar, A., Guan, K.L., Rao, Y., and Wu, J.Y. (2009). DSCAM functions as a netrin receptor in commissural axon pathfinding. Proc Natl Acad Sci U S A *106*, 2951-2956.

Liu, I.S., Chen, J.D., Ploder, L., Vidgen, D., van der Kooy, D., Kalnins, V.I., and McInnes, R.R. (1994). Developmental expression of a novel murine homeobox gene (Chx10): evidence for roles in determination of the neuroretina and inner nuclear layer. Neuron *13*, 377-393.

Liu, Y., Stein, E., Oliver, T., Li, Y., Brunken, W.J., Koch, M., Tessier-Lavigne, M., and Hogan, B.L. (2004). Novel role for Netrins in regulating epithelial behavior during lung branching morphogenesis. Curr Biol *14*, 897-905.

Livet, J., Weissman, T., Kang, H., Draft, R., Lu, J., Bennis, R., Sanes, J., and Lichtman, J. (2007). Transgenic strategies for combinatorial expression of fluorescent proteins in the nervous system. In Nature, pp. 56-62.

Llinas, R.R. (2003). The contribution of Santiago Ramon y Cajal to functional neuroscience. Nature reviews Neuroscience *4*, 77-80.

Long, H., Sabatier, C., Ma, L., Plump, A., Yuan, W., Ornitz, D.M., Tamada, A., Murakami, F., Goodman, C.S., and Tessier-Lavigne, M. (2004). Conserved roles for Slit and Robo proteins in midline commissural axon guidance. Neuron *42*, 213-223.

Lopez-Munoz, F., Boya, J., and Alamo, C. (2006). Neuron theory, the cornerstone of neuroscience, on the centenary of the Nobel Prize award to Santiago Ramon y Cajal. Brain Res Bull *70*, 391-405.

Lowery, L.A., and Van Vactor, D. (2009). The trip of the tip: understanding the growth cone machinery. Nature reviews Molecular cell biology *10*, 332-343.

Luan, H., Peabody, N.C., Vinson, C.R., and White, B.H. (2006). Refined spatial manipulation of neuronal function by combinatorial restriction of transgene expression. Neuron *52*, 425-436.

Luo, L., Callaway, E.M., and Svoboda, K. (2008). Genetic dissection of neural circuits. Neuron *57*, 634-660.

Luo, L., and Flanagan, J.G. (2007). Development of continuous and discrete neural maps. Neuron *56*, 284-300.

Ly, A., Nikolaev, A., Suresh, G., Zheng, Y., Tessier-Lavigne, M., and Stein, E. (2008). DSCAM is a netrin receptor that collaborates with DCC in mediating turning responses to netrin-1. Cell *133*, 1241-1254.

Macagno, E.R., Lopresti, V., and Levinthal, C. (1973). Structure and development of neuronal connections in isogenic organisms: variations and similarities in the optic system of Daphnia magna. Proc Natl Acad Sci U S A *70*, 57-61.

Mao, H., Lv, Z., and Ho, M.S. (2012). Gcm proteins function in the developing nervous system. Dev Biol *370*, 63-70.

Markwardt, M.L., Kremers, G.J., Kraft, C.A., Ray, K., Cranfill, P.J., Wilson, K.A., Day, R.N., Wachter, R.M., Davidson, M.W., and Rizzo, M.A. (2011). An improved cerulean fluorescent protein with enhanced brightness and reduced reversible photoswitching. PloS one *6*, e17896.

Mast, J.D., Prakash, S., Chen, P.L., and Clandinin, T.R. (2006). The mechanisms and molecules that connect photoreceptor axons to their targets in Drosophila. Semin Cell Dev Biol *17*, 42-49.

Matsuoka, R.L., Nguyen-Ba-Charvet, K.T., Parray, A., Badea, T.C., Chedotal, A., and Kolodkin, A.L. (2011). Transmembrane semaphorin signalling controls laminar stratification in the mammalian retina. Nature *470*, 259-263.

Matz, M.V., Fradkov, A.F., Labas, Y.A., Savitsky, A.P., Zaraisky, A.G., Markelov, M.L., and Lukyanov, S.A. (1999). Fluorescent proteins from nonbioluminescent Anthozoa species. Nature biotechnology *17*, 969-973.

McGuire, S.E., Le, P.T., Osborn, A.J., Matsumoto, K., and Davis, R.L. (2003). Spatiotemporal rescue of memory dysfunction in Drosophila. Science *302*, 1765-1768.

Meinertzhagen, I.A., and Lee, C.H. (2012). The genetic analysis of functional connectomics in Drosophila. Advances in genetics *80*, 99-151.

Meinertzhagen, I.A., and O'Neil, S.D. (1991). Synaptic organization of columnar elements in the lamina of the wild type in Drosophila melanogaster. J Comp Neurol *305*, 232-263.

Meinertzhagen, I.A., and Sorra, K.E. (2001). Synaptic organization in the fly's optic lamina: few cells, many synapses and divergent microcircuits. Prog Brain Res *131*, 53-69.

Meinertzhagen, I.A.H., T.E. (1993). The development of the optic lobe. Bate, Martinez Arias: The development of Drosophila melanogaster Cold Spring Laboratory Press, 1363-1491.

Meunier, D., Achard, S., Morcom, A., and Bullmore, E. (2009). Age-related changes in modular organization of human brain functional networks. NeuroImage *44*, 715-723.

Miesenbock, G. (2004). Genetic methods for illuminating the function of neural circuits. Curr Opin Neurobiol *14*, 395-402.

Mishchenko, Y. (2008). Strategies for identifying exact structure of neural circuits with broad light microscopy connectivity probes. Nature Precedings.

Mitchell, K.J., Doyle, J.L., Serafini, T., Kennedy, T.E., Tessier-Lavigne, M., Goodman, C.S., and Dickson, B.J. (1996). Genetic analysis of Netrin genes in Drosophila: Netrins guide CNS commissural axons and peripheral motor axons. Neuron *17*, 203-215.

Montell, C., Jones, K., Zuker, C., and Rubin, G. (1987). A second opsin gene expressed in the ultraviolet-sensitive R7 photoreceptor cells of Drosophila melanogaster. The Journal of neuroscience : the official journal of the Society for Neuroscience *7*, 1558-1566.

Morante, J., and Desplan, C. (2008). The color-vision circuit in the medulla of Drosophila. In Curr Biol, pp. 553-565.

Morante, J., Erclik, T., and Desplan, C. (2011). Cell migration in Drosophila optic lobe neurons is controlled by eyeless/Pax6. Development *138*, 687-693.

Myat, A., Henry, P., McCabe, V., Flintoft, L., Rotin, D., and Tear, G. (2002). Drosophila Nedd4, a ubiquitin ligase, is recruited by Commissureless to control cell surface levels of the roundabout receptor. Neuron *35*, 447-459.

Nern, A., Pfeiffer, B.D., Svoboda, K., and Rubin, G.M. (2011). Multiple new site-specific recombinases for use in manipulating animal genomes. Proc Natl Acad Sci U S A *108*, 14198-14203.

Nern, A., Zhu, Y., and Zipursky, S.L. (2008). Local N-cadherin interactions mediate distinct steps in the targeting of lamina neurons. In Neuron, pp. 34-41.

Newsome, T.P., Asling, B., and Dickson, B.J. (2000). Analysis of Drosophila photoreceptor axon guidance in eye-specific mosaics. Development *127*, 851-860.

Ni, J.Q., Liu, L.P., Binari, R., Hardy, R., Shim, H.S., Cavallaro, A., Booker, M., Pfeiffer, B.D., Markstein, M., Wang, H., *et al*. (2009). A Drosophila resource of transgenic RNAi lines for neurogenetics. Genetics *182*, 1089-1100.

Ni, J.Q., Zhou, R., Czech, B., Liu, L.P., Holderbaum, L., Yang-Zhou, D., Shim, H.S., Tao, R., Handler, D., Karpowicz, P., *et al*. (2011). A genome-scale shRNA resource for transgenic RNAi in Drosophila. Nat Methods *8*, 405-407.

Ogura, K., Asakura, T., and Goshima, Y. (2012). Localization mechanisms of the axon guidance molecule UNC-6/Netrin and its receptors, UNC-5 and UNC-40, in Caenorhabditis elegans. Development, growth & differentiation *54*, 390-397.

Osterwalder, T., Yoon, K.S., White, B.H., and Keshishian, H. (2001). A conditional tissue-specific transgene expression system using inducible GAL4. Proc Natl Acad Sci U S A *98*, 12596-12601.

Ostroy, S.E., Wilson, M., and Pak, W.L. (1974). Drosophila rhodopsin: photochemistry, extraction and differences in the norp AP12 phototransduction mutant. Biochemical and biophysical research communications *59*, 960-966.

Papatsenko, D., Nazina, A., and Desplan, C. (2001). A conserved regulatory element present in all Drosophila rhodopsin genes mediates Pax6 functions and participates in the fine-tuning of cell-specific expression. Mechanisms of development *101*, 143-153.

Park, K.W., Urness, L.D., Senchuk, M.M., Colvin, C.J., Wythe, J.D., Chien, C.B., and Li, D.Y. (2005). Identification of new netrin family members in zebrafish: developmental expression of netrin 2 and netrin 4. Developmental dynamics : an official publication of the American Association of Anatomists *234*, 726-731.

Pasterkamp, R.J. (2012). Getting neural circuits into shape with semaphorins. Nature reviews Neuroscience *13*, 605-618.

Pearson, A.M., Baksa, K., Ramet, M., Protas, M., McKee, M., Brown, D., and Ezekowitz, R.A.B. (2003). Identification of cytoskeletal regulatory proteins required for efficient phagocytosis in Drosophila. Microbes Infect *5*, 815-824.

Pearson, B.J., and Doe, C.Q. (2003). Regulation of neuroblast competence in Drosophila. Nature *425*, 624-628.

Peng, H., Chung, P., Long, F., Qu, L., Jenett, A., Seeds, A.M., Myers, E.W., and Simpson, J.H. (2011). BrainAligner: 3D registration atlases of Drosophila brains. Nat Methods *8*, 493-500.

Petrovic, M., and Hummel, T. (2008). Temporal identity in axonal target layer recognition. In Nature, pp. 800-803.

Pfeiffer, B.D., Jenett, A., Hammonds, A.S., Ngo, T.T., Misra, S., Murphy, C., Scully, A., Carlson, J.W., Wan, K.H., Laverty, T.R., *et al*. (2008). Tools for neuroanatomy and neurogenetics in Drosophila. Proc Natl Acad Sci U S A *105*, 9715-9720.

Pfeiffer, B.D., Ngo, T.T., Hibbard, K.L., Murphy, C., Jenett, A., Truman, J.W., and Rubin, G.M. (2010). Refinement of tools for targeted gene expression in Drosophila. Genetics *186*, 735-755.

Pfeiffer, S., Ricardo, S., Manneville, J.B., Alexandre, C., and Vincent, J.P. (2002). Producing cells retain and recycle Wingless in Drosophila embryos. Curr Biol *12*, 957-962.

Phelps, C.B., and Brand, A.H. (1998). Ectopic gene expression in Drosophila using GAL4 system. Methods *14*, 367-379.

Pili-Floury, S., Leulier, F., Takahashi, K., Saigo, K., Samain, E., Ueda, R., and Lemaitre, B. (2004). In vivo RNA interference analysis reveals an unexpected role for GNBP1 in the defense against Gram-positive bacterial infection in *Drosophila* adults. The Journal of biological chemistry *279*, 12848-12853

Poeck, B., Fischer, S., Gunning, D., Zipursky, S.L., and Salecker, I. (2001). Glial cells mediate target layer selection of retinal axons in the developing visual system of *Drosophila*. Neuron *29*, 99-113.

Potter, C.J., Tasic, B., Russler, E.V., Liang, L., and Luo, L. (2010). The Q system: a repressible binary system for transgene expression, lineage tracing, and mosaic analysis. Cell *141*, 536-548.

Prakash, S., Caldwell, J.C., Eberl, D.F., and Clandinin, T.R. (2005). Drosophila N-cadherin mediates an attractive interaction between photoreceptor axons and their targets. Nat Neurosci *8*, 443-450.

Prasher, D.C., Eckenrode, V.K., Ward, W.W., Prendergast, F.G., and Cormier, M.J. (1992). Primary structure of the Aequorea victoria green-fluorescent protein. Gene *111*, 229-233.

Prieto-Godino, L.L., Diegelmann, S., and Bate, M. (2012). Embryonic origin of olfactory circuitry in Drosophila: contact and activity-mediated interactions pattern connectivity in the antennal lobe. PLoS biology *10*, e1001400.

Prokop, A., and Meinertzhagen, I.A. (2006). Development and structure of synaptic contacts in Drosophila. Semin Cell Dev Biol *17*, 20-30.

Rajagopalan, S., Nicolas, E., Vivancos, V., Berger, J., and Dickson, B.J. (2000a). Crossing the midline: roles and regulation of Robo receptors. Neuron *28*, 767-777.

Rajagopalan, S., Vivancos, V., Nicolas, E., and Dickson, B.J. (2000b). Selecting a longitudinal pathway: Robo receptors specify the lateral position of axons in the Drosophila CNS. Cell *103*, 1033-1045.

Ribchester, R.R. (2009). Mammalian neuromuscular junctions: modern tools to monitor synaptic form and function. Current opinion in pharmacology *9*, 297-305.

Rickert, C., Kunz, T., Harris, K.L., Whitington, P.M., and Technau, G.M. (2011). Morphological characterization of the entire interneuron population reveals principles of neuromere organization in the ventral nerve cord of Drosophila. The Journal of neuroscience : the official journal of the Society for Neuroscience *31*, 15870-15883.

Rinkevich, Y., Lindau, P., Ueno, H., Longaker, M.T., and Weissman, I.L. (2011). Germ-layer and lineage-restricted stem/progenitors regenerate the mouse digit tip. Nature *476*, 409-413.

Rister, J., Pauls, D., Schnell, B., Ting, C.Y., Lee, C.H., Sinakevitch, I., Morante, J., Strausfeld, N.J., Ito, K., and Heisenberg, M. (2007). Dissection of the peripheral motion channel in the visual system of Drosophila melanogaster. Neuron *56*, 155-170.

Rivera-Alba, M., Vitaladevuni, S.N., Mishchenko, Y., Lu, Z., Takemura, S.Y., Scheffer, L., Meinertzhagen, I.A., Chklovskii, D.B., and de Polavieja, G.G. (2011). Wiring economy and volume exclusion determine neuronal placement in the Drosophila brain. Curr Biol *21*, 2000-2005.

Rizzo, M.A., Springer, G.H., Granada, B., and Piston, D.W. (2004). An improved cyan fluorescent protein variant useful for FRET. Nature biotechnology *22*, 445-449.

Roman, G., Endo, K., Zong, L., and Davis, R.L. (2001). P[Switch], a system for spatial and temporal control of gene expression in Drosophila melanogaster. Proc Natl Acad Sci U S A *98*, 12602-12607.

Rothberg, J.M., Hartley, D.A., Walther, Z., and Artavanis-Tsakonas, S. (1988). slit: an EGF-homologous locus of D. melanogaster involved in the development of the embryonic central nervous system. Cell *55*, 1047-1059.

Ruta, V., Datta, S.R., Vasconcelos, M.L., Freeland, J., Looger, L.L., and Axel, R. (2010). A dimorphic pheromone circuit in Drosophila from sensory input to descending output. Nature *468*, 686-690.

Salcedo, E., Huber, A., Henrich, S., Chadwell, L.V., Chou, W.H., Paulsen, R., and Britt, S.G. (1999). Blue- and green-absorbing visual pigments of Drosophila: ectopic expression and physiological characterization of the R8 photoreceptor cell-specific Rh5 and Rh6 rhodopsins. The Journal of neuroscience : the official journal of the Society for Neuroscience *19*, 10716-10726.

Sanchez-Soriano, N., Tear, G., Whitington, P., and Prokop, A. (2007). Drosophila as a genetic and cellular model for studies on axonal growth. Neural development *2*, 9.

Sanes, J.R., and Zipursky, S.L. (2010). Design principles of insect and vertebrate visual systems. In Neuron, pp. 15-36.

Schimmelpfeng, K., Gogel, S., and Klambt, C. (2001). The function of leak and kuzbanian during growth cone and cell migration. Mechanisms of development *106*, 25-36.

Schotta, G., Ebert, A., Dorn, R., and Reuter, G. (2003). Position-effect variegation and the genetic dissection of chromatin regulation in Drosophila. Semin Cell Dev Biol *14*, 67-75.

Senti, K.A., Usui, T., Boucke, K., Greber, U., Uemura, T., and Dickson, B.J. (2003). Flamingo regulates R8 axon-axon and axon-target interactions in the Drosophila visual system. Curr Biol *13*, 828-832.

Serafini, T., Colamarino, S.A., Leonardo, E.D., Wang, H., Beddington, R., Skarnes, W.C., and Tessier-Lavigne, M. (1996). Netrin-1 is required for commissural axon guidance in the developing vertebrate nervous system. Cell *87*, 1001-1014.

Serafini, T., Kennedy, T.E., Galko, M.J., Mirzayan, C., Jessell, T.M., and Tessier-Lavigne, M. (1994). The netrins define a family of axon outgrowth-promoting proteins homologous to C. elegans UNC-6. Cell *78*, 409-424.

Seung, H.S. (2009). Reading the book of memory: sparse sampling versus dense mapping of connectomes. Neuron *62*, 17-29.

Shaner, N.C., Campbell, R.E., Steinbach, P.A., Giepmans, B.N., Palmer, A.E., and Tsien, R.Y. (2004). Improved monomeric red, orange and yellow fluorescent proteins derived from Discosoma sp. red fluorescent protein. Nature biotechnology *22*, 1567-1572.

Shaner, N.C., Patterson, G.H., and Davidson, M.W. (2007). Advances in fluorescent protein technology. J Cell Sci *120*, 4247-4260.

Shaner, N.C., Steinbach, P.A., and Tsien, R.Y. (2005). A guide to choosing fluorescent proteins. Nat Methods *2*, 905-909.

Shatz, C.J. (1996). Emergence of order in visual system development. Proc Natl Acad Sci U S A *93*, 602-608.

Shcherbo, D., Murphy, C.S., Ermakova, G.V., Solovieva, E.A., Chepurnykh, T.V., Shcheglov, A.S., Verkhusha, V.V., Pletnev, V.Z., Hazelwood, K.L., Roche, P.M., *et al*. (2009). Far-red fluorescent tags for protein imaging in living tissues. Biochem J *418*, 567-574.

Shimomura, O., Johnson, F.H., and Saiga, Y. (1962). Extraction, purification and properties of aequorin, a bioluminescent protein from the luminous hydromedusan, Aequorea. Journal of cellular and comparative physiology *59*, 223-239.

Shimosako, N., Hadjieconomou, D., Salecker, I. (2013). Flybow to dissect circuit assembly in the Drosophila brain.

Shinza-Kameda, M., Takasu, E., Sakurai, K., Hayashi, S., and Nose, A. (2006). Regulation of layer-specific targeting by reciprocal expression of a cell adhesion molecule, capricious. In Neuron, pp. 205-213.

Siegal, M.L., and Hartl, D.L. (1996). Transgene Coplacement and high efficiency site-specific recombination with the Cre/loxP system in Drosophila. Genetics *144*, 715-726.

Simpson, J.H., Bland, K.S., Fetter, R.D., and Goodman, C.S. (2000a). Short-range and long-range guidance by Slit and its Robo receptors: a combinatorial code of Robo receptors controls lateral position. Cell *103*, 1019-1032.

Simpson, J.H., Kidd, T., Bland, K.S., and Goodman, C.S. (2000b). Short-range and long-range guidance by slit and its Robo receptors. Robo and Robo2 play distinct roles in midline guidance. Neuron *28*, 753-766.

Snippert, H.J., van der Flier, L.G., Sato, T., van Es, J.H., van den Born, M., Kroon-Veenboer, C., Barker, N., Klein, A.M., van Rheenen, J., Simons, B.D., *et al*. Intestinal crypt homeostasis results from neutral competition between symmetrically dividing Lgr5 stem cells. Cell *143*, 134-144.

Southall, T.D., and Brand, A.H. (2008). Generation of Driver and Reporter Constructs for the GAL4 Expression System in Drosophila. CSH Protoc *2008*, pdb prot5029.

Southall, T.D., Elliott, D.A., and Brand, A.H. (2008). The GAL4 System: A Versatile Toolkit for Gene Expression in Drosophila. CSH Protoc *2008*, pdb top49.

Sperry, R.W. (1963). Chemoaffinity in the Orderly Growth of Nerve Fiber Patterns and Connections. Proc Natl Acad Sci U S A *50*, 703-710.

Spitzweck, B., Brankatschk, M., and Dickson, B.J. (2010). Distinct protein domains and expression patterns confer divergent axon guidance functions for Drosophila Robo receptors. Cell *140*, 409-420.

Sporns, O. (2011). The human connectome: a complex network. Annals of the New York Academy of Sciences *1224*, 109-125.

Sporns, O., Tononi, G., and Kotter, R. (2005). The human connectome: A structural description of the human brain. PLoS computational biology *1*, e42.

Stark, W.M., Boocock, M.R., and Sherratt, D.J. (1992). Catalysis by site-specific recombinases. Trends Genet *8*, 432-439.

Stebbins, M.J., Urlinger, S., Byrne, G., Bello, B., Hillen, W., and Yin, J.C. (2001). Tetracycline-inducible systems for Drosophila. Proc Natl Acad Sci U S A *98*, 10775-10780.

Stebbins, M.J., and Yin, J.C. (2001). Adaptable doxycycline-regulated gene expression systems for Drosophila. Gene *270*, 103-111.

Struhl, G., and Basler, K. (1993). Organizing activity of wingless protein in Drosophila. Cell *72*, 527-540.

Su, C.Y., Menuz, K., Reisert, J., and Carlson, J.R. (2012). Non-synaptic inhibition between grouped neurons in an olfactory circuit. Nature.

Szuts, D., and Bienz, M. (2000). LexA chimeras reveal the function of Drosophila Fos as a context-dependent transcriptional activator. Proc Natl Acad Sci U S A *97*, 5351-5356.

Tabansky, I., Lenarcic, A., Draft, R.W., Loulier, K., Keskin, D.B., Rosains, J., Rivera-Feliciano, J., Lichtman, J.W., Livet, J., Stern, J.N.*, et al*. (2012). Developmental Bias in Cleavage-Stage Mouse Blastomeres. Curr Biol.

Takemura, S.Y., Karuppudurai, T., Ting, C.Y., Lu, Z., Lee, C.H., and Meinertzhagen, I.A. (2011). Cholinergic circuits integrate neighboring visual signals in a Drosophila motion detection pathway. Curr Biol *21*, 2077-2084.

Takemura, S.Y., Lu, Z., and Meinertzhagen, I.A. (2008). Synaptic circuits of the Drosophila optic lobe: the input terminals to the medulla. J Comp Neurol *509*, 493-513.

Tayler, T.D., Robichaux, M.B., and Garrity, P.A. (2004). Compartmentalization of visual centers in the Drosophila brain requires Slit and Robo proteins. Development *131*, 5935-5945.

Tessier-Lavigne, M., and Goodman, C.S. (1996). The molecular biology of axon guidance. Science *274*, 1123-1133.

Timofeev, K., Joly, W., Hadjieconomou, D., and Salecker, I. (2012). Localized netrins act as positional cues to control layer-specific targeting of photoreceptor axons in Drosophila. Neuron *75*, 80-93.

Ting, C.Y., Gu, S., Guttikonda, S., Lin, T.Y., White, B.H., and Lee, C.H. (2011). Focusing transgene expression in Drosophila by coupling Gal4 with a novel split-LexA expression system. Genetics *188*, 229-233.

Ting, C.Y., Yonekura, S., Chung, P., Hsu, S.N., Robertson, H.M., Chiba, A., and Lee, C.H. (2005). Drosophila N-cadherin functions in the first stage of the two-stage layer-selection process of R7 photoreceptor afferents. In Development, pp. 953-963.

Tomasi, T., Hakeda-Suzuki, S., Ohler, S., Schleiffer, A., and Suzuki, T. (2008). The transmembrane protein Golden goal regulates R8 photoreceptor axon-axon and axon-target interactions. In Neuron, pp. 691-704.

Triplett, J.W., and Feldheim, D.A. (2012). Eph and ephrin signaling in the formation of topographic maps. Semin Cell Dev Biol *23*, 7-15.

Tsien, R. http://www.tsienlab.ucsd.edu/Documents.htm

Tuthill, J.C. (2009). Lessons from a compartmental model of a Drosophila neuron. The Journal of neuroscience : the official journal of the Society for Neuroscience *29*, 12033-12034.

Urban, N., and Tripathy, S. (2012). Neuroscience: Circuits drive cell diversity. Nature *488*, 289-290.

Van Roessel, P., Hayward, N.M., Barros, C.S., and Brand, A.H. (2002). Two-color GFP imaging demonstrates cell-autonomy of GAL4-driven RNA interference in Drosophila. Genesis *34*, 170-173.

Varshney, L.R., Chen, B.L., Paniagua, E., Hall, D.H., and Chklovskii, D.B. (2011). Structural properties of the Caenorhabditis elegans neuronal network. PLoS computational biology *7*, e1001066.

Venken, K.J., Simpson, J.H., and Bellen, H.J. (2011). Genetic manipulation of genes and cells in the nervous system of the fruit fly. Neuron *72*, 202-230.

Voziyanov, Y., Konieczka, J.H., Stewart, A.F., and Jayaram, M. (2003). Stepwise manipulation of DNA specificity in Flp recombinase: progressively adapting Flp to individual and combinatorial mutations in its target site. In J Mol Biol, pp. 65-76.

Voziyanov, Y., Stewart, A.F., and Jayaram, M. (2002). A dual reporter screening system identifies the amino acid at position 82 in Flp site-specific recombinase as a determinant for target specificity. Nucleic Acids Res *30*, 1656-1663.

Wadsworth, W.G., Bhatt, H., and Hedgecock, E.M. (1996). Neuroglia and pioneer neurons express UNC-6 to provide global and local netrin cues for guiding migrations in C. elegans. Neuron *16*, 35-46.

Wardill, T.J., List, O., Li, X., Dongre, S., McCulloch, M., Ting, C.Y., O'Kane, C.J., Tang, S., Lee, C.H., Hardie, R.C.*, et al*. (2012). Multiple spectral inputs improve motion discrimination in the Drosophila visual system. Science *336*, 925-931.

Wedeen, V.J., Rosene, D.L., Wang, R., Dai, G., Mortazavi, F., Hagmann, P., Kaas, J.H., and Tseng, W.Y. (2012). The geometric structure of the brain fiber pathways. Science *335*, 1628-1634.

Wei, Y., and Koulakov, A.A. (2012). An exactly solvable model of random site-specific recombinations. Bulletin of mathematical biology *74*, 2897-2916.

White, J.G., Southgate, E., Thomson, J.N., and Brenner, S. (1986). The structure of the nervous system of the nematode Caenorhabditis elegans. Philosophical transactions of the Royal Society of London Series B, Biological sciences *314*, 1-340.

Wickersham, I.R., Lyon, D.C., Barnard, R.J., Mori, T., Finke, S., Conzelmann, K.K., Young, J.A., and Callaway, E.M. (2007). Monosynaptic restriction of transsynaptic tracing from single, genetically targeted neurons. Neuron *53*, 639-647.

Wickstead, B., and Gull, K. (2011). Evolution: The evolution of the cytoskeleton. J Cell Biol *194*, 513-525.

Wonders, C.P., and Anderson, S.A. (2006). The origin and specification of cortical interneurons. Nature reviews Neuroscience *7*, 687-696.

Wong, A.M., Wang, J.W., and Axel, R. (2002). Spatial representation of the glomerular map in the Drosophila protocerebrum. Cell *109*, 229-241.

Wood, J.T.O.a.T.H. (1973). Kinetics of genetic recombination in *Escherichia Coli* K-12: Competition between genetic integration and degradation. Genetics *75*, 579-592.

Xu, T., and Rubin, G.M. (1993). Analysis of genetic mosaics in developing and adult Drosophila tissues. Development *117*, 1223-1237.

Yagi, R., Mayer, F., and Basler, K. (2010). Refined LexA transactivators and their use in combination with the Drosophila Gal4 system. Proc Natl Acad Sci U S A *107*, 16166-16171.

Yamagata, M., and Sanes, J.R. (2008). Dscam and Sidekick proteins direct lamina-specific synaptic connections in vertebrate retina. Nature *451*, 465-469.

Yamagata, M., and Sanes, J.R. (2012). Expanding the Ig superfamily code for laminar specificity in retina: expression and role of contactins. The Journal of neuroscience : the official journal of the Society for Neuroscience *32*, 14402-14414.

Yamakawa, K., Huot, Y.K., Haendelt, M.A., Hubert, R., Chen, X.N., Lyons, G.E., and Korenberg, J.R. (1998). DSCAM: a novel member of the immunoglobulin superfamily maps in a Down syndrome region and is involved in the development of the nervous system. Human molecular genetics *7*, 227-237.

Yanagawa, S., Lee, J.S., and Ishimoto, A. (1998). Identification and characterization of a novel line of Drosophila Schneider S2 cells that respond to wingless signaling. The Journal of biological chemistry *273*, 32353-32359.

Yang, L., Garbe, D.S., and Bashaw, G.J. (2009). A frazzled/DCC-dependent transcriptional switch regulates midline axon guidance. Science *324*, 944-947.

Yanushevich, Y.G., Staroverov, D.B., Savitsky, A.P., Fradkov, A.F., Gurskaya, N.G., Bulina, M.E., Lukyanov, K.A., and Lukyanov, S.A. (2002). A strategy for the generation of non-aggregating mutants of Anthozoa fluorescent proteins. FEBS Lett *511*, 11-14.

Yoshida, T., Uchida, S., and Mishina, M. (2009). Regulation of synaptic vesicle accumulation and axon terminal remodeling during synapse formation by distinct Ca signaling. Journal of neurochemistry *111*, 160-170.

Yoshida, Y. (2012). Semaphorin signaling in vertebrate neural circuit assembly. Frontiers in molecular neuroscience *5*, 71.

Yu, C.R., Power, J., Barnea, G., O'Donnell, S., Brown, H.E., Osborne, J., Axel, R., and Gogos, J.A. (2004). Spontaneous neural activity is required for the establishment and maintenance of the olfactory sensory map. Neuron *42*, 553-566.

Yu, H.H., Chen, C.H., Shi, L., Huang, Y., and Lee, T. (2009). Twin-spot MARCM to reveal the developmental origin and identity of neurons. Nat Neurosci *12*, 947-953.

Yurchenco, P.D., and Wadsworth, W.G. (2004). Assembly and tissue functions of early embryonic laminins and netrins. Current opinion in cell biology *16*, 572-579.

Yuste, R. (2008). Circuit neuroscience: the road ahead. Frontiers in neuroscience *2*, 6-9.

Zacharias, D.A., and Tsien, R.Y. (2006). Molecular biology and mutation of green fluorescent protein. Methods of biochemical analysis *47*, 83-120.

Zador, A.M., Dubnau, J., Oyibo, H.K., Zhan, H., Cao, G., and Peikon, I.D. (2012). Sequencing the connectome. PLoS biology *10*, e1001411.

Zamoyska, R., Vollmer, A.C., Sizer, K.C., Liaw, C.W., and Parnes, J.R. (1985). Two Lyt-2 polypeptides arise from a single gene by alternative splicing patterns of mRNA. Cell *43*, 153-163.

Zong, H., Espinosa, J.S., Su, H.H., Muzumdar, M.D., and Luo, L. (2005). Mosaic analysis with double markers in mice. Cell *121*, 479-492.

Zuker, C.S., Montell, C., Jones, K., Laverty, T., and Rubin, G.M. (1987). A rhodopsin gene expressed in photoreceptor cell R7 of the Drosophila eye: homologies with other signal-transducing molecules. The Journal of neuroscience : the official journal of the Society for Neuroscience *7*, 1550-1557.

Name	Length	TM (°C)	Sequence	Aim
FB1	93 bp	73	5'-P CTAGCagAGATCTGGTACCCTCGAGGAAGTTTC TATACtttctagaGAATAGAAACTTCACTAGTGGAT CCCCTAGGGCGGCCGCaGAGCTCA	Generate mMCs for pTRCHisB
FB2	73 bp	73	5'-P AGCTTGAGCTCtGCGGCCGCCCTAGGGGATCCA CTAGTGAAGTTTCTATTCtctagaaaGTATAGAAAC TTCCTCGAGGGTACCAGATCTctG	Generate mMCs for pTRCHisB
FB3	44 bp	75	5'-P AATTCGCTAGCAGATCTGAGCTCGGTACCGCG GCCGCCTCGAGT	Generate mMCs for pKC26
FB4	44 bp	75	5'-P CTAGACTCGAGGCGGCCGCGGTACCGAGCTCA GATCTGCTAGCG	Generate mMCs for pKC26
FB5	28 bp	60	GATCGCTAGCCGAAGTTCCTATACTTTC	Amplify wtFRT cassette from pSR513
FB6	28 bp	60	TCACACCACAGAAGTAAGGTTCCTTCAC	Amplify wtFRT cassette from pSR513
FB7	28 bp	61	GATTACTAGTATGGCCTCACCGTTGACC	Amplify cd8 encoding sequence from pCd8a-EGFP
FB8	29bp	66	TCATGGATCCGCGGCTGTGGTAGCAGATG	Amplify cd8 encoding sequence from pCd8a-EGFP
FB9	28 bp	61	GTACCCTAGGGATCTTTGTGAAGGAACC	Amplify SV40 polyA from pUAST
FB10	29 bp	63	ATTAGCGGCCGCGATCCAGACATGATAAG	Amplify SV40 polyA from pUAST
FB11	37 bp	63	GATCCCTAGGTAAGGCCAAAGAGTCTAATTTT TGTTC	Amplify hsp70Ab polyA from pCasper-hs
FB12	38 bp	69	TAATGCGGCCGCTCCTGACCGTCCATCGCAAT AAAATG	Amplify hsp70Ab polyA from pCasper-hs
FB15	28 bp	63	TATTGGATCCATGGTGAGCAAGGGCGAG	Amplify

				mCherry, mCitrine, Cerulean & EGFP
FB16	28 bp	63	GACGCCTAGGTTACTTGTACAGCTCGTC	Amplify mCherry, mCitrine, Cerulean & EGFP
FB17	95 bp	84	5'-P GAATGGCAAGCCCATCCCCAACCCCCTGCTGG GCCTGGATTCCACCAATGGCAAGCCCATCCCC AACCCCCTGCTGGGCCTGGATTCCACCTAAC	Generate V5-V5 tag
FB18	103 bp	84	5'-P CTAGGTTAGGTGGAATCCAGGCCCAGCAGGGG GTTGGGGATGGGCTTGCCATTGGTGGAATCCA GGCCCAGCAGGGGGTTGGGGATGGGCTTGCCA TTCTGCA	To generate V5-V5 tag
FB19	37 bp	69	ATATGGATCCATGGTGAGCAAGGGCGAGGAGC TGTTC	Amplify Cerulean
FB20	37 bp	69	GATCCCTAGGATTCTGCAGGGACTTGTACAGC TCGTC	Amplify Cerulean
FB21	37 bp	64	CTAGCCTAGGATTCTGCAGGGACTTGTACAGC TCGTC	Amplify Cerulean-primer FB20 forming 2ndary structures
FB22	20 bp	54	CAGACAATCTGTGTGGGCAC	Sequence pTRCHisB mMCS
FB23	20 bp	54	ATCAGACCGCTTCTGCGTTC	Sequence pTRCHisB mMCS
FB24	20 bp	56	CAAGCGCAGCTGAACAAGCT	Sequence pKC26mM CS
FB25	20 bp	56	ACTGTCCTCCGAGCGGAGAC	Sequence pKC26mM CS
FB26	40 bp	63	5'-P TCGAGGAAGTTTCTATACTTTCTAGAGAATAG AAACTTCA	Generate ds-mFRT71
FB27	40 bp	60	5'-P CTAGTGAAGTTTCTATTCTCTAGAAAGTATAGA AACTTCC	Generate ds-mFRT71
FB28	79 bp	77	GATACCTAGGTTAGGTGGAATCCAGGCCCAGC AGGGGGTTGGGGATGGGCTTGCCCTTGTACAG CTCGTCCATGCCGAG	Amplify cerulean-1xV5
FB29	28 bp	61	CATACCTAGGGGACTTGTACAGCTCGTC	Amplify cerulean 3' AvrII without stop
FB30	57 bp	69	5'-P CTAGTGGTAAGCCTATCCCTAACCCTCTCCTCG GTCTCGATTCTACTGCAGGTTAAC	Generate 1x-V5 tag mutagenizing AvrII 5' site
FB31	58 bp	69	5'-P	Generate

			CTAGGTTAACCTGCAGTAGAATCGAGACCGAG GAGAGGGTTAGGGATAGGCTTACCA	1x-V5 tag mutagenizing AvrII 5' site
FB32	28 bp	61	GATGACTAGTATGGGCTGCATCAAGAGC	Amplify 5' 2x-mp-mCitrine
FB33	41 bp	69	ACTTTCTAGAGAATAGAAACTTCATGGGCTGC ATCAAGAG	Amplify XbaI 3' mFRT71-2x-mp-Citrine
FB34	28 bp	70	ATTACCTAGGCCACCGCTGGCCACGGAG	Amplify 3' 2x-mp-BamHI
FB35	29 bp	67	CAACCTGAACGACGACGAGGGATCCAATA	Amplify 3' 2x-mp-BamHI
FB36	28 bp	60	AGTCCTCGAGGAGTTAAAGGTGGGTAAG	Amplify XhoI 5' Ret spacer
FB37	28 bp	62	AGTCGTCGACGAGTTAAAGGTGGGTAAG	Amplify SalI 5' Ret spacer
FB38	28 bp	66	TATAGTCGACGATTCCGGAGCCATCCAC	Amplify SalI 3' Ret spacer
FB39	28 bp	62	TATTGGATCCGGTGGCGACCGGTGCCTC	Amplify BamHI 3' 2x-mp from lyn-cherry vector
FB40	28 bp	59	TATTGGATCCGGGATCTTCCGGTGCCTC	Amplify BamHI 3' 2x-mp from lyn-citrine vector
FB41	60 bp	71	5'-P CTAGTATGGGCTGCATCAAGAGCAAGCGCAAG GACAACCTGAACGACGACGAGGCAGCAG	Generate ds-1x-mp
FB42	60 bp	71	5'-P GATCCTGCTGCCTCGTCGTCGTTCAGGTTGTCC TTGCGCTTGCTCTTGATGCAGCCCATA	Generate ds-1x-mp
FB43	20 bp	59	GATAGGCTTACCACTAGGGG	Sequence Cerulean
FB44	19 bp		TTGGAGCCGTACATGAACT	Sequence 1x-mp-Citrine

Table 3 List of oligonucleotides used to generate the Flybow constructs.
DNA sequences were amplified by PCR or annealed in pairs to generate double stranded DNA (ds-DNA). The generation of FB1, FB2, FB3, FB4, FB17 and FB18 primers included an additional step of phosphorylation and HPLC purification.

Name	Application - Use	Manufacturer
pTRCHisB	Cloning vector-Build basic FB modules	Invitrogen™
pKC26	Cloning vector-Build final FB constructs	B. Dickson
pMT/V5-His A	Cloning Vector-Build vectors for cell transfections	Invitrogen™
pCRII-Topo	TA cloning kit-T4 ligase kit-Build intermediate steps of basic FB modules	Invitrogen™
pCR2.1-Topo	TA cloning kit-T4 ligase kit-Build intermediate steps of basic FB modules	Invitrogen™
pCR2.1-Topo	TA cloning kit- Topoisomerase kit-Build intermediate steps of basic FB modules	Invitrogen™
Subcloning Efficiency DH5α	Chemically Competent Bacteria-Used for all vectors apart from the *pTRCHisB* based ones	Invitrogen™
One shot TOP10	Chemically Competent Bacteria-Used for all *pTRCHisB* based vectors and *Cerulean* basic module and *Citrine* containing modules into final FB construct	Invitrogen™
One shot IVaF'	Chemically Competent Bacteria- Used when trying to clone Citrine basic module	Invitrogen™
Max Efficiency Stbl2	Chemically Competent Bacteria- Used when trying to clone *Cerulean* basic module and *Citrine* containing modules into final FB construct	Invitrogen™
SURE Competent Cells	Chemically Competent Bacteria- Used when trying to clone *Citrine* basic module	Stratagene™
Phosphatase, Alkaline	Cloning- Dephosphorylation	Roche™
T4 ligase	Cloning-Ligation	NEB™
TAKARA ligase	Cloning-Ligation	Takara™
Expand High Fidelity PCR kit	Cloning- Taq polymerase	Roche™
Platinum Taq DNA Polymerase High Fidelity	Cloning- Taq polymerase	Invitrogen™
1.1 Ready Mix PCR Master Mix	Cloning- Screening Bacterial Colonies	Thermo Scientific™
EcorI, XhoI, BamHI, KpnI, NotI. BglII, XbaI, Asp718, SpeI, BamHI, SacI, NheI, HindIII,	Cloning -Restriciton endonucleases of mMCSs	Roche™
AvrII	Cloning -Restriciton endonucleases of mMCSs	NEB™
Qiaprep Mini, Midi Kits	Cloning -Plasmid Purification	Qiagen™
PCR purification Kit	Cloning - PCR Purification	Qiagen™
Gel Extraction Kit	Cloning - Gel Extraction	Qiagen™
Effectine Transfection Reagent	Transfection of S2 Cells	Qiagen™
WH5 mcd8EGFP	Cloning - PCR amplification of cd8 membrane anchor	W. Joly
pCaSpeR-hs	Cloning - PCR amplification of hsp70 poly A	DGRC
pUAST	Cloning - PCR amplification of hsp70 poly A	(Brand and Perrimon, 1993)
tub-memb-mCherry	Cloning - PCR amplification of mCherry, and pm membrane tag	C. Alexandre, (Shaner et al. 2004)
pCS-memb-mCitrine	Cloning - PCR amplification of mCitrine 2pm membane tag and 2xpm-citrine	E. Ober, (Griesbeck et al., 2001)
pCS-memb-Cerulean	Cloning - PCR amplification of Cerulean	E. Ober, (Rizzo et al., 2004)
pEGFP-N1	Cloning - PCR amplification of EGFP	C. Alexandre, Clonetech
pSR513	Cloning - PCR amplification of wtFRT-lamin-HA-hsp70Ab/hsp27-wtFRT	B. Dickson
TOTO3	Transfection- Nuclear Staining	Invitrogen

Table 4. List of materials used to generate of Flybow constructs.